Cranfield

College of Aeronautics Report 8401
January 1984

Evolution of a Heave Control System for an Amphibious Hovercraft

by

P.A.T. Christopher, K.F. Man,
Y.N. Cheng and E.W. Osbourn

College of Aeronautics
Cranfield Institute of Technology
Cranfield, Bedford, UK.

Cranfield
College of Aeronautics Report 8401
January 1984

Evolution of a Heave Control System for an Amphibious Hovercraft

by

P.A.T. Christopher, K.F. Man,
Y.N. Cheng and E.W. Osbourn

College of Aeronautics
Cranfield Institute of Technology
Cranfield, Bedford, UK.

ISBN 0902937 97 9

£7.50

SUMMARY

A heave control system for amphibious hovercraft has been designed and tested. The central element in the system being an axial flow, lift-fan whose blade angles are continuously varied by means of feedback signals from a pressure transducer located in the front end of the hovercraft cushion and from an accelerometer measuring the heave acceleration. Results from experiments, conducted on the Cranfield Whirling-Arm facility, have shown that the system provides a rapid and effective means of controlling the heave acceleration, and, in addition, produces a valuable reduction in craft drag whilst traversing waves.

An extensive parameter identification programme, using a non-linear optimisation algorithm, was constructed and applied to the control sub-system, such that a full mathematical model of the controlled craft was obtained. This was then used to design an optimum control with particular reference to passenger ride comfort.

CONTENTS

LIST OF FIGURES

4.19 Cushion pressure simulator

4.20 Cushion pressure simulator, (close up)

4.21 Cushion pressure simulator, (general arrangement)

5.1 Pressure-flow rate characteristics at fan speed 5200 rpm (0,5 and 10 degrees)

5.2 Pressure-flow rate characteristics at fan speed 5200 rpm (15 and 20 degrees)

5.3a Lift vs cushion pressure characteristics

5.3b Lift vs cushion pressure characteristics

5.4 Nominal height and cushion pressure characteristics

5.5 Relationship between cushion pressure and hover gap

5.6 Relationship between hover gap and nominal height

5.7 Relationship between leakage flow rate and hover gap

5.8a Heave characteristics

5.8b Heave characteristics

6.1 Inner loop transient response

6.2 Inner loop behaviour due to step heave height changes

6.3 Responses over 10ft waves

6.4 Comparison of vertical acceleration between control system on and off over 10ft waves

9.5 Blade profile lift curve

9.6 Cushion pressure and blade angle characteristics

NOTATION

A, B, C	matrices
A_e	effective cushion area
A_o	total area of orifices
$a_1 \ldots . a_4$	coefficients, Eqn 8.18
C	constant, Eqn.8.1
C	damping force, Fig.2.4
C_B	adiabatic stiffness
C_h	capacitive component of flow impedence
C_D	discharge coefficient of orifices, Eqn.5.1
C_{DO}	equivalent discharge coefficient of leakage orifices
C_{DC}	drag coefficient
C_L	lift coefficient
$C(s)$	characteristic equation
$C(s)$	transfer function of controller
C_{drop}	damping force factor when dropping
C_{rise}	damping force factor when rising
D	total drag
D_i	ride discomfort index
D_{aero}	aerodynamic profile drag
D_{mon}	momentum drag
D_{sk}	skirt drag
D_{wave}	wave drag
$D(s)$	sea spectrum filter
d	command signal
d	differential operator
e	error
F	vertical force
Fr	Froude number
f	frequency, Hz
f_t	truncation frequency, Hz
G	leakage flow parameter, Eqn.7.9
$G_A(s)$	transfer function of accelerometer
$G(f)$	transmissibility at crew station
$G(s)$	transfer function
$G_c(s)$	transfer function of cushion pressure/blade angle
$G_{ch}(s)$	transfer function of cushion-craft dynamics
$G_{Fi}(s)$	filter
$G_{hc}(s)$	transfer function of cushion pressure/heave disturbance

$G_{LC}(s)$	transfer function of cushion/loop section
$G_T(s)$	transfer function of pressure transducer
$G_\alpha(s)$	transfer function of actuation system
$G_{\alpha L}(s)$	transfer function loop/blade angle
$G(j\omega)$	transfer function of overall system, Eqn.9.2
g	acceleration due to gravity
g	system output or system error
g(t)	forcing function
H(s)	overall closed loop transfer function
H(z)	Hessian matrix
h	heave displacement
h	hover gap
h_f	forward heave height
h_g	ground height
h_n	nominal height
h_r	rear heave height
h_w	wave amplitude
h_s	skirt height
J	cost function
j	$\sqrt{-1}$
K	constant
K	stiffness, Fig.2.4
K_s	constant of sea spectrum filter
k	step
L	cushion length
L_p	cushion perimeter
ℓ	number of experimental responses
ℓ_f	length of full scale craft
ℓ_m	length of model craft
M_H	mass of hull
M_s	mass of skirt
M(s)	transfer function of measurement noise
m	mass of total craft
n	integer
n	white noise of measurement disturbance
P_A	atmospheric pressure
$P_{c\alpha}$	cushion pressure due to blade angle changes
P_f	fan pressure
P_{hc}	cushion pressure due to heave height changes
P_L	loop pressure

$P(s)$	transfer function of process
Q	flow rate
Q	positive definite matrix, Eqn3.16
Q_i	inlet flow rate
Q_o	outlet rate
Re	real part of complex number
S_F	frontal area of craft
$S(\omega)$	Pierson-Moskowitz sea spectrum
$S_i(\omega)$	power spectral density of disturbance white noise
s_i, s_j	search direction
s	Laplace operator
T	total time
t	time
$U(s)$	input signal in Laplace form
u	input
V_c	cushion volumn
v	white noise
W	weight of craft
$W(f)$	weighting function of acceleration
$\underline{x}$	state vectors
$Y(s)$	output signal in Laplace form
y	output
y_e	experimental output
y_m	model output
$y(t)$	output time variable
z	vector
α	blade angle
$\alpha_1 \cdots \alpha_n$	coefficient of denominator
$\beta_1 \cdots \beta_n$	coefficient of numerator
γ	ratio of specific heat od gas
ζ	damping ratio
ε	error
ε_i	error signal to actuation system
ω	angular frequency
ω_i	weighting factor
ω_n	natural frequency
λ	Lagrange multiplier
λ_i	step size
ρ	air density

$\phi_q(\omega)$	spectral density of error signal
$\phi_u(\omega)$	spectral density of input signal
$\psi(s)$	function of error signal, e.g. $\overline{e^2} = \lvert\psi(s)\rvert^2$
$\Delta(s)$	error function
$\hat{}$	stimates
ξ	wave surface height
$\mathcal{L}^{-1}$	Inverse Laplace operator

Chapter 1

1.0 INTRODUCTION

1.1.1 HOVERCRAFT STABILITY

It is widely accepted that hovercraft heave motion is largely governed by the quantity variation of inlet and outlet leakage air flow within the cushion volume as the craft travels across the surface (sea). In order to minimise the vertical forces (acceleration) being exerted by the craft, balancing of these air flows is vitally important to the ride quality (1,2). One possible way to solve the problem is to use an active control system in which a constant cushion pressure is maintained.

However, the problem is far more complicated than the fundamental principle stated above. The heave dynamics are not the easiest subject to understand and require thorough investigation in order that this type of control system can operate effectively.

The state-of-the-art of current research is concentrated mainly on the area of cushion dynamics. These investigations include the fan characteristics, skirt movements, wave pumping effect, and most of all the unpredictable leakage air flow from the cushion. The development of ride control systems is rare despite the findings of the research, although a few designs have been under development in the United States. As in the U.K., the research on hovercraft is, in general, limited. It is therefore, the purpose of the present research to develop an automatic heave control system using the existing Cranfield Whirling Arm Facility.

1.1.2 CONTROL CONCEPT OF HEAVE MOTION

IN 1969, an elementary study of an heave acceleration

attenuation system (3) was carried out by NASA. It was based on a non-skirted plenum air cushion system. Two different approaches to the heave control problem were considered. The first one was a passive control method using a spring-loaded plate. Its motion would respond to positive increases of cushion pressure to open an orifice and allow additional air to escape from the cushion volume. The second idea was an active control valve. Its actuation was monitored by the plenum acceleration which was measured by an accelerometer from a predominant position. The idea was to modulate the input air flow in such a manner as to oppose or null the plenum acceleration response. Although the physical model was merely a simple plenum box, the approaches to the heave motion control concept is basically sound.

1.2 REVIEW OF CURRENT HEAVE CONTROL SYSTEMS

1.2.1 LOUVRE (VENTING) CONTROL SYSTEM

This technique is similar to the passive device described in (3), but now the louvre is actively controlled. The system controls the air leakage flow when the cushion pressure rises. Since the pressure itself cannot be increased by means of additional opening, the effective means of achieving a useful heave acceleration reduction is by allowing the venting area to change about a reference position. This control system (4,5) has been investigated and (6) describes the system. Its main disadvantage is the energy loss due to air vents out of the cushion, and thereby requires more power during operation. Thus it is necessary to limit the extent of the equilibrium louvre opening in order to reduce the power consumption due to control whilst still obtaining useful heave acceleration attenuation.

1.2.2 FAN INLET AREA CONTROL SYSTEM

The use of variable fan inlet area as a means of control of heave acceleration is possible, so that the fan output flow is then altered in order to change the resultant pressure in the cushion and the heave acceleration. This idea was mentioned in (5) and eventually implemented in (7). The control system comprises a fan speed (RPM) control which is monitored by a computer so that speed of the fan is maintained constant whilst the load changes. A pressure transducer senses the air pressure at the output of the blower fan and at the plenum chamber. The difference of these signals drives the servo mechanism of the inlet flow device which in turn regulates the volume of air flow into the cushion. This system automatically maintains a constant pressure in the plenum chamber which will limit the vertical acceleration. In addition, a second servo system, operating in conjunction with the first, provides a manual control.

1.2.3 VARIABLE GEOMETRY LIFT FAN CONTROL SYSTEM

This system has a variable geometry, double air-inlet, centrifugal-fan for heave motion control (8). The fan provides rapid response to heave motion with minimal actuating power requirement. The fan has a means of varying its volume of flow by changing the effective cross-section of the air passage. The control action is monitored by a signal coming from an accelerometer placed at a predetermined location on the craft. Details of this system can be obtained in (8).

1.2.4 ACTIVE SKIRT SYSTEM

In (13) another possible system, the active skirt, is described. The idea is to raise portions of the hemline at the command of sensors that detect wave characteristics and craft motions. However, from the investigation, it was

found that the power requirements were large and the system was very complicated mechanically.

1.3 ACTIVE-FAN SYSTEM —— PRESENT RESEARCH

An alternative to the systems described in section 1.2 is the active-fan system wherein the geometry of the fan itself is changed during operation. The basic idea has been described in (5,13) and it is the aim of the present research to design, test and develop a particular system having a variable pitch fan and, thereby, demonstrate that this type of heave control is both effective and practical.

1.3.1 HOVERCRAFT RESEARCH ON THE CRANFIELD WHIRLING ARM FACILITY

For some years the Whirling-Arm Facility at C.I.T., Cranfield, has been used for research into hovercraft dynamics, particular emphasis being given to the study of heave motion, see (9,12). The general arrangement of the facility is shown in Fig.1.1,1.2 and 1.4 whilst Fig.1.3 shows the disposition of the solid sinusoidal waves on the outer wall of the test chamber. It will be noted that Fig.1.1, which is a relatively old photograph, does not show the test annulus, illustrated in Fig.1.2 and Fig.1.4, which is now an essential part of the existing facility. As can be seen from Fig.1.2, the craft is mounted vertically on the end of the arm, and as this rotates the craft rides on its cushion over the waves. Whilst so doing measurements of cushion pressure and craft motion, in heave and pitch, can be made and these are used in studying the craft dynamics, particularly in establishing mathmetical models for both the un-controlled and controlled motion.

In the first investigations of hovercraft cushion dynamics (9) the model cushion was supplied with air, through a long duct, from a centrifugal fan mounted on the Whirling-Arm

structure. At this time some doubt existed (7), as to the part played by the duct in determining the overall heave response and subsequently, an experimental and theoretical analysis of the effect was published (10,11). In the light of this the centrifugal fan was replaced by an axial-flow fan mounted in the craft itself. The design, development and testing of the new fan-craft system is described in chapter five and a comparison of the static characteristics of the original centrifugal and the new axial flow fan is shown in Fig.1.5.

1.3.2 CONCEPT OF VARIABLE FAN PITCH ANGLE CONTROL SYSTEM

This idea, as a means of controlling the heave motion is discussed in (5,13), whereas the practical system has yet to be reported. Bearing in mind the basic concept of heave control, as stated in 1.1.1 and 1.1.2, here is a possible system which will capitalise on the idea of controlling the inlet air flow as a means of controlling the heave acceleration. The advantages of this system are that energy loss during the operation is not great as compared to the venting system mentioned in 1.2.1, and provides a direct control of air flow toward the cushion volume. The technique is to modify the fan characteristics dynamically by means of fan blades, whose pitch angle is continuously adjusted during the operation. The angular movement of the blades can be achieved by means of an hydraulic driven actuator and itself is controlled by a position feedback loop. This system is similar to that on the hub of a helicopter.

In order to operate this system effectively, such that the blade angle movement is adequately monitored to counteract the craft heave motion, some kind of feedback signals from the craft must be available. By and large, the forces in the vertical direction are the result of variations of

cushion pressure acting upon an effective cushion area, therefore, feedback of cushion pressure signals into the blade angle actuation system should provide a means of controlling the heave motion.

However, for an amphibious hovercraft the cushion pressure is greatly dependent on the hover gap (the height between the tip of skirt finger and the surface) and the power produced by the fan, i.e. the blade angle setting. Thus, when the loop is closed, the blade angle movement is conversely governed by the level of the cushion pressure. This feedback strategy may be justifiable if the external disturbance on the cushion region is regular and/or the hover gap is non-existent, i.e. similar to that of the sidewall hovercraft in which the sidewalls always submerged in water. But in the case of an amphibious craft, the cushion pressure and heave height relationship is much more complex and strongly coupled together, especially when the surface disturbance is irregular. To offset this condition, another signal which comes from the accelerometer at the c.g. position of the craft can also be utilised for feedback in order that the pre-trimmed blade angle condition is maintained. This, in turn, keeps the hover gap at an equilibrium position. This extra loop is necessary if the wear and tear of the cushion skirt as well as the craft performance in terms of drag forces are to be minimised.

1.3.3 SYSTEM IDENTIFICATION

Whenever possible the dynamic characteristics of a control system are analysed by means of a derived mathematical model, in order that proper control laws can be developed to improve the overall system performance. In some cases, such a model is not easy to develop due mainly to the complexity and lack of deep understanding of the physical processes involved. This is true for the hovercraft heave dynamics

concerned. Although research in this area has been in progress for some twenty years, a general mathematical model is still under development.

It is well known that the problem of modelling the heave dynamics is concerned principally with understanding the cushion behaviour. Although there are a number of models in existence, the difficulty with a generalised model is the problem of obtaining the values of the appropriate parameters in the model, through either theory or experiment. In particular, the quantity of escape air flow beneath the cushion and the movement of the skirt fingers is very difficult to determine in the dynamic, non-steady situation. It is hoped that more insight into these phenomena may be gained during the current research (14) at University College, London, where the wave belt facility is being used. At the present time these quantities can only be estimated approximately.

Having recognised these problems, a different approach to the matter is made. This is to apply the well-known parameter identification technique. Many algorithms have been devised for this purpose (15,16). Researches in this area are still very active, and better and more agile, algorithms are still expected. The basic idea is to use the record of an output(s) of a tested system with some knowledge of the input excitation, and then attempt to obtain the relevant parameters from the degree of matching between a model and system output. Of course, the goodness of the matching is dependent on the defined cost function of which an optimisation algorithm is devised in order to ensure a minimum value to be reached. Thereby, an optimum set of parameters can be obtained. A general identification procedure is shown in Fig.1.6.

1.3.4 FUTURE DESIGN AND SYSTEM SYNTHESIS

It is expected from the current research that a practical control system for hovercraft heave control will be possible and suitable for future development on a full-scale craft. Therefore, in this research, apart from developing the variable fan pitch-angle control system, and demonstrating its effectiveness over the waves (solid) in the Whirling Arm Facility, a theoretical study on an optimum heave control strategy is proposed. This study uses, as a basis, the results obtained from experiment as well as the parameter identification technique, and applies to a realistic sea state. The theoretical system is simulated on the Cranfield VAX/782 computer, and appropriate results will be presented.

The final part of this research is an outline of the implications of the heave control system on the ride quality.

Chapter 2

2.0 CONTROL PHILOSOPHY AND SYSTEM MODELLING

2.1 Basic Mechanism of Pressurised Skirted Cushion

The basic mechanism of a pressurised cushion can be understood from Fig. 2.1. The fluid flow Q_i is supplied to the cushion region from a fan. In the steady state (wave height h_w=0), the flow Q_o escapes through an hover gap h formed between the surface and the periphery of the cushion. The combination of the fluid restriction, the fan characteristics and any other restrictions or leakage paths determine an equilibrium cushion pressure P_c. This pressure acting over the cushion base area A_e provides the equilibrium force F. When the hover gap h is slowly decreased, the exit resistance increases and P_c increases, causing the force F to increase. Thus, the pressurised skirt has a spring-like relationship between load and hover gap h. In the actual dynamic case, a description of cushion behaviour must include the fluid compressibility, the mass, flexibility and damping of the skirt, the fan characteristics and the effects of parameter modulation by skirt and hover gap. An effective control system must take these quantities into consideration.

2.2 Inner-loop

As indicated in the introduction, the basic controlling action is by means of changes in cushion pressure, P_c, brought about by continuously controlled changes in α, the fan blade angle to the plane of rotation of the disc. On the basis of small perturbations, it is reasonable to expect that a net air flow can be maintained by shifting the P_c vs Q characteristics across according to the action of the blade angle, see Fig. 2.2. Since the primary forcing of the heave motion, by waves or other means, is through the medium of the cushion pressure acting on an effective lifting area of the cushion, then

the above means of controlling the cushion pressure offers a way of controlling the heaving motion. Thus, this feedback system is completed by measuring the cushion pressure by means of a suitable transducer, and it is called the inner-loop, see Fig. 2.3.

The capability of this system will depend greatly on the size of the changes in P_c brought about by the changes of α at a nominal fan speed, as a result, modifying the fan characteristics. Providing that the steady state value (stiffness) of (P_c/α) is large enough, and the associated time-constant is small enough, achieving these conditions is the major factor in the design of the inner-loop.

2.2.1 Mathematical Modelling of the Inner-loop

In order to justify this feedback system mathematically, it was thought that the multi-lumped-parameter technique (17) might be appropriate. In this method the air passage between the fan chamber and cushion, via the loop and fingers is treated as a series of inter-connected small lumps of flow impedence. As a result, the system transfer-function relating the cushion pressure P_c to fan pressure, P_f can be obtained. This is derived in (18) and shown in APPENDIX A. However, the difficulty of applying this model in practice arises from the problem of evaluating the overall bulk modulus of the material of the walls of the plenum, loop and skirt fingers. The reason is that, unlike the simple geometric situation of fluid in a pipe envisaged in (17), the loop and finger geometry is complicated and the effect on volume produced by elastic distortion of the wall material is unknown. Added to this is the fact that Young's modulus for the material (polyurethane coated nylon) under tension varies with direction (relative to warp or weft) by a factor of two.

From the literature (10, 11, 19, 20, 21, 22), the fluid transient model was also thought to be another means of modelling the system. However, this distributed parameter technique still requires an estimation of C_h and is therefore subject to the same shortcoming as the lumped parameter model. To show the inadequacy of the model, a first and second order model of (22) is used for trial. The results are shown in APPENDIX B. The associated time lags are found to be under-estimated as compared to that obtained from experiment. See chapter seven.

Strictly speaking, modelling of the inner-loop, should include the blade angle actuating dynamics, as the cushion pressure is directly dependent on its action. Although the frequency response characteristics of the servo valve used is given by the manufacturer, the modelling on the integral system of fan hub mechanism is not easily achieved. This is because of the complexity of the system which including the hydraulic actuator (piston), the linkages, the fan speed interference and the aerodynamic loading on the blades.

As a result of the above difficulties, it was decided to leave this work on mathematical modelling in abeyance and proceed on the basis of the experimentally determined transfer-function, via a parameter identification technique, (see chapters three and seven for details).

2.3 Cushion-Craft Dynamics

A simple analogy to the mechanism of a pressurised skirted cushion is to assume that the skirt is a rigid one and its footprint area remains unchanged. Then, the matter is amenable to solution by considering a point mass floating on a heaving surface, see Fig. 2.4. From (23, 24) a mathematical model is produced. In (25), the idea is

extended to include the pitching effect. In the case of sidewall hovercraft, in which the cushion is always submerged in water and the skirt vibration is considered to be negligible, this so called 'flat plate' model should be applicable and the capability of the inner-loop described previously would offer a means of heaving motion control. For an amphibious hovercraft, the state of the cushion pressure is not merely dependent on the inlet air flow, it is also strongly influenced by the outlet air flow Q_o and the hover gap h, see Fig. 2.1. Variation of h or Q_o causes the cushion pressure P_c to fluctuate. This situation happens often when the disturbance surface is irregular, has high frequency content and hence affects the direct proportionality relationship between F and P_c used in the model of the inner-loop. As a result, the credibility of the control system model is questionable.

2.3.1 Compressibility Effects

In view of the skirt dynamics, a further model (26,27) in which the condition of changes in cushion pressure due to isentropic compression or expansion is considered. A similar model is also derived in APPENDIX C. In (28) the dynamic system is modelled via Bond Graph technique (29, 30, 31) whereas (32) proposed a four element discrete model with the results presented in terms of spring and dashpot forces. These models are relevant from the point of view of mathematical derivation but their practical application may face some instrumentational problems. When the compressibility effect is being considered, the associated parameters are assumed to be obtained experimentally. For example, the measurements of flow rate, vertical movements of the skirt, the changes of cushion volume etc. are not easy to make and appropriate transducers may not be available.

Furthermore, if the derived model is applied to a scaled craft, the laws of dynamic similarity restricts the compressibility effects. This is indicated in (26) as the atmospheric pressure has to be scaled in order to accommodate the adiabatic stiffness term ($C_B = (P_C + P_A)\gamma / V_C$) to have a correct scaled value. It is found that when P_A is not scaled, C_B is $(\ell_f / \ell_m)^{-2}$ in error.

Another comment on this type of modelling is the contradiction between the theorem of compressible and incompressible flow. To be able to achieve the ultimate model, the incompressible Bernoulli relationship is applied to the outlet flow whereas compressible flow relationships are used inside the cushion. Maybe for practical purposes, this conflict is not important.

2.4 Model Analysis

In view of all the possible problems, it was decided to model and evaluate the flexible skirt system via the system identification technique. Since the purpose of the inner-loop is established and provides a significant insight into the rigid skirt dynamics, it is believed that the flexible skirt dynamics can be represented by a transfer-function $G_{ch}(s)$ as shown in Fig. 2.5. Obviously, the exact format of $G_{ch}(s)$ is not yet known but can be determined from the identification programme (chapter three) using both cushion pressure and acceleration signals. As matter of interest, if the skirt is said to be a rigid one, then, $G_{ch}(s)$ is merely a gain $(A_e/(M_H + M_S))$ which should be identical to the model of (23,24). Therefore, by placing different forms of $G_{ch}(s)$ and inspecting the degree of matching, it is possible to obtain a model to represent the flexible skirt system.

2.5 Overall Control System-Acceleration Feedback Loop

In order to accommodate all the possible interactions between the surface disturbance and skirt dynamics, as previously described, a single cushion pressure feedback loop, the inner-loop,is considered to be inadequate. Strictly speaking, the inner-loop is merely a controller which only serves the purpose of an input to the state of air flow in the cushion, whereas its influence on the heave dynamics is secondary. Therefore, the control system ought to be completed by feeding back the acceleration signal from an accelerometer at the craft c.g. position. Then, by pre-trimming the fan-blade angle to an equilibrium position, the heave acceleration, due to surface disturbance h_w is thus minimised by the action of the fan-blade angle. The degree of success of this system is greatly dependent on the dynamic behaviour described by the transfer-functions as shown in Fig. 2.6. Identification of these blocks will be discussed in a later chapter.

Chapter 3

3.0 PARAMETER IDENTIFICATION

3.1.1. BACKGROUND

In the topic of parameter identification, it is usual to divide the subject into (i) process identification and (ii) parameter estimation. An excellent review paper(33) describes the various techniques used and (34) emphasises the differences between them quite vividly.

In general, the first stage in the application of the technique is to classify the physical process into the following categories:

A. No available information-Black box. The structural configuration of the process is unknown and can only be determined experimentally. "Process identification" is usually applied here. Sometimes, it is used for procedures which consist of a series of parameter estimation problems with different assumed models. Then, it is followed by a model discrimination routine to select the "Best" model(33).

B. Partial information available-Grey box. Some information about the structural configuration of the model (including estimates, or the limits on some of the parameters) can be used to select a suitable functional form for the model. The identification procedure is thus simplified considerably. In some applications, a priori information is also used as the starting point for the selected techniques.

C. Complete information available. By definition, the process identification is completed at this point and all that remains is the parameter estimation problem.

This classification covers all the possible intended uses of the physical system model for identification. In the case of C, the model evaluation is based on the mathematical description of the physical behaviour of the system and relevant knowledge about the geometrical and physical system nature is available. Identification on this type of system is useful for model building and is an effective means of validating the mathematical-physical analysis.

In the case of A and B, it is sometimes possible to apply the same approach. Nevertheless, it is convenient to utilise fully the fact that an identified system is in operation and measurements are possible. In which case it is legitimate to expect that observation and experiment are the most favourable means of system understanding. Therefore, measuring input/output data is all that is required for identification purposes. However, it should be stressed that the final model obtained from the system identification will only represent the essential properties of the dynamic system and present the properties in a suitable form. An exact mathematical description of the physical reality cannot be expected. Nevertheless one would expect to have an identified model which will be useful for future applications. Fig.3.1. is a schematical diagram which illustrates most of the identification procedures.

3.1.2 DESIGN OF EXPERIMENTS

For the purpose of the identification, the available physical knowledge of the process plays an important role in the design of experiments. Even when "black box" techniques are used for identification, it is necessary to consider the physics of the process when designing the experiments. Experiments should be conducted when the process is in a mode of operation which is close to the desired one. In many cases preliminary experiments have to be carried out in order to achieve sufficient knowledge of the process so

that the best experiment can be designed. It is often preferred to use first a step and/or impulse response analysis from a perturbation because of the simplicity of these methods. The results should indicate:

1. major time constants
2. input size
3. nonlinearities and time variation of the process
4. noise levels
5. delays

These quantities can then be used for the design of identification experiments.

3.1.3 IDENTIFICATION TECHNIQUES

There are many techniques (15,16,33) available for the purpose of parameter identification. But, it is difficult to choose between them, mostly because so few comparisons have been made. Another difficulty is that even when comparisons are made the outcome may be dubious because the 'goodness' of a model must always be judged in relation to its intended uses. Which one to choose is often more a matter of convenience, as a good fit or a good prediction does not necessarily give a good model for the design of control strategies.

In general, the mathematical approach used in the identification process are either of the deterministic or stochastic type (34). The choice of method depends partly on data properties. For data with small disturbances, either method should work well. For very noisy processes, a more elaborate data analysis (stochastic) is required in order to give reasonable results. From the application point of view, it can be observed that as data become more corrupted more elaborate methods have to be tried in order to extract some information from the data. The other important factor is the suitability of a model. For a

system which has a very high-order model with few measurements available, the well known recursive maximum-likelihood estimation technique (35,44) is generally used. For these reasons it is difficult to define a "best" method. In practice, one must judge the purpose of the selected identification method and then weigh the attainable results and the cost (computing time) of obtaining them. Maybe, a more complex method will be used in future when the programme itself becomes available and that it can show the required computing time is shortened considerably, and of course a better result is achieved.

It is very important that the results obtained must not be taken for granted, but the advantage and disadvantage of the specific methods used must be clear. It is also important that the results are able to relate to the real process and achieve the aim of identification. The more understanding about the process, the better chance that a good model can be obtained from identification. In other words, good identification still requires a deep understanding of the process.

3.1.4 RELIABILITY ESTIMATES

It should be remembered that verification of a model cannot generally be made, especially when the process is classified as a 'black-box'. The only possibility of identifying a model is to investigate the one that is suitable for a specific purpose. For example, a closed-loop system design based on the identification of the open-loop dynamics. Then, the goodness of the model is assessed on the ultimate performance of the control system.

In many cases the identification results can be checked by different tests on the residuals (37,38), although the model error method is sometimes used (39,40,41). Frequently

the reliability of the output responses predicted from a model are of primary interest but not the parameters themselves. Therefore, a decision based upon subjective examination of residuals is often adequate (42).

In order to get a reliable model, more than one experiment is almost always necessary so that cross-checks between the sets of data can be made. In this way, a general idea about the goodness of the model (43) can be obtained. Of course, all the assumptions made on the model should also be checked whenever possible, e.g. the time invariance, linearity, model order and so on. However, because of the experimental limitation, these quantities cannot always be checked other than by the physical knowledge of the process and the information provided by the experiments. When the model has passed all diagnostic tests, it is then acceptable for its intended uses, i.e. control synthesis.

3.2.1. NONLINEAR OPTIMISATION ALGORITHM FOR PARAMETER IDENTIFICATION - PRESENT METHOD

Having gathered all the important features about techniques on identification, a direct and practical programme was developed for the use of parameter identification. Bearing in mind that the data obtained from the Whirling arm was not corrupted badly by noise, it was decided that a deterministic approach would be adequate to identify the relevant parameters of the heave dynamics and their associated systems. However, a more elaborate method will be required for the analysis of the trial data of a full scale craft dynamics in which the dynamics will almost certainly be influenced by the external disturbances. Therefore, parallel to the present programme, another programme using the well known stochastic Kalman Filtering technique was also developed. Although the initial phase of the development of this technique has been completed and tested successfully (at least to one system), considerable additional testing is required to

prove its reliability. It is therefore, only the present nonlinear optimisation programme which is reported in this thesis. The details of the Kalman Filtering programme can be obtained in (45).

3.2.2. CONCEPT OF THE PRESENT APPROACH

This approach is similar to all the other identification techniques in that the experiment on the process due to the input disturbance is possible and output measurements are available. Thus, the identification procedures are followed according to the steps as shown Fig.1.6 and 3.1. The model structure is assumed to be of a linear transfer-function type. A nonlinear optimisation programme is developed for estimating the best possible set of coefficients or poles/zeros of the model transfer function, such that the error between the measurement and model output is a minimum. See Fig.1.6. The error minimisation routine used is either the Powell or Davidon-Fletcher-Powell optimisation algorithm. See sections 3.2.5 and 3.2.6.

3.2.3 MODEL STRUCTURE

In general, a linear dynamic system can be represented by a transfer function of the form:

$$G(s) = \frac{Y(s)}{U(s)} = \frac{\beta_1 s^{n-1} + \beta_2 s^{n-2} + ... + \beta_n}{s^n + \alpha_1 s^{n-1} + ... + \alpha_n} \qquad (3.1)$$

where Y(s) and U(s) are the output and input in Laplace-transform form respectively, $\alpha_1 .... \alpha_n$ and $\beta_1 .... \beta_n$ are the coefficients and n is the order of the denominator.

From (46), it is possible to convert Eqn (3.1) into an equivalent time-variant, state matrix form:

$$\dot{\underline{x}} = A\underline{x} + B\underline{u},$$

$$y = C\underline{x} \qquad (3.2)$$

where $\underline{x}$ is the state vector, $\underline{u}$ is the input vector, y is the output vector and A,B,C are constant matrices.

Thus, Eqn(3.1) can be written in matrix form:

$$\begin{bmatrix} \dot{x}_1 \\ \dot{x}_2 \\ \cdot \\ \cdot \\ \cdot \\ \cdot \\ \cdot \\ x_n \end{bmatrix} = \begin{bmatrix} 0 & 0 & \cdots & 0 & -\alpha_n \\ 1 & 0 & \cdots & 0 & -\alpha_{n-1} \\ \cdot & \cdot & & \cdot & \cdot \\ \cdot & \cdot & & \cdot & \cdot \\ \cdot & \cdot & & \cdot & \cdot \\ \cdot & \cdot & & \cdot & \cdot \\ \cdot & \cdot & & \cdot & \cdot \\ 0 & 0 & \cdots & 1 & -\alpha_1 \end{bmatrix} \begin{bmatrix} x_1 \\ x_2 \\ \cdot \\ \cdot \\ \cdot \\ \cdot \\ \cdot \\ x_n \end{bmatrix} + \begin{bmatrix} \beta_n \\ \beta_{n-1} \\ \cdot \\ \cdot \\ \cdot \\ \cdot \\ \cdot \\ \beta_1 \end{bmatrix} u$$

and

$$y = \begin{bmatrix} 0 & 0 & \cdots & 0 & 1 \end{bmatrix} \underline{x} \qquad (3.3)$$

Generally speaking, Eqn(3.3) has sufficient information for all the numerical calculation required to produce time responses when a subroutine of Runge-Kutta integration step is employed. However, from experience, this tends to be a long and expensive process especially when a 4th-order mode is used and the system model-order is high. Therefore, in order to speed up the calculation with less cost, an analytical approach to obtain a time response is necessary. One way to solve Eqn(3.1) is to use the Inverse Laplace Transform (ILT), such that

$$y(t) = Y(s) = \mathcal{L}^{-1}\{ G(s).U(s)\} \qquad (3.4)$$

where $\mathcal{L}^{-1}$ is the ILT operator.

In theory, Eqn(3.4) should be applicable to all kinds of input signal if the appropriate form of U(s) is found. This would not be a problem as far as a step, impulse and sine function are concerned. However, with random input signals it is difficult, if not impossible, to generate an appropriate analytical function, and so the Runge-Kutta subroutine must be used. Both methods are described in detail in APPENDIX D.

3.2.4 COST FUNCTION

In order to develop a numerical estimation procedure such that the error between the experimental signal and the model output can reach a minimum value, statistical method may be used. Consider the experimental signal whose discrete output measurement has the form

$$y_e = [\, y_{eo}, y_{e1} \ldots\ldots y_{ei} \ldots . y_{eI} \,] \qquad (3.5)$$

$$y_{ei} = y_e(t_i) \qquad (3.6)$$

and the model discrete output

$$y_m = [\, y_{mo}, y_{m1} \ldots\ldots y_{mi} \ldots . y_{mI} \,] \qquad (3.7)$$

$$y_{mi} = y_m(t_i) \qquad (3.8)$$

over a suitable interval of time t=(O,T). Then the error ε between these outputs, see Fig.3.2, is

$$\varepsilon = y_e - y_m \qquad (3.9)$$

where

$$y_m = f(\alpha, \beta) \qquad (3.10)$$

and $f(\alpha,\beta)$ are the parameters (coefficients or poles/zeros) of the model defined in Eqn(3.1). Then, the classical parameter estimation problem is to determine an estimate $(\hat{\alpha},\hat{\beta})$ such that $f(\hat{\alpha},\hat{\beta})$ gives the "best fit" to the observed output as defined by some criterion of optimality, i.e. a cost function:

$$J = f(\omega_i, \varepsilon) \tag{3.11}$$

where ω_i is vector weight function attached at each sampling instant. A number of different criteria have been suggested namely the least-squares, maximum likelihood and Bayesian techniques. The most common one is the least-squares as stated in the following:

$$J = \sum_{i=o}^{I} \omega_i |\varepsilon|^2 \tag{3.12}$$

where $\omega_i = 1$

In some cases, ω_i is not equal to unity, as described in (47), or has some statistical properties (38,48,49).

If a number of experimental responses are to be fitted simultaneously, the cost function J can be written as

$$J = \sum_{j=1}^{\ell} \omega_j(\varepsilon_j) \tag{3.13}$$

where

$$\varepsilon_j = \sum_{i=1}^{I} \{ Y_{ej} - Y_{mi} \}^2 \tag{3.14}$$

ℓ is the number of the experimental responses

ω_j are the weighting factors, and

$j = 1,2, \ldots\ldots \ell$.

The ultimate residual value of J is dependent on the sampling interval (50) and the total number of I. When the model is selected correctly, it is reasonable to expect a good match when J is found to be the minimum by some optimisation algorithm.

3.2.5 POWELL OPTIMISATION ALGORITHM

The advantage of the Powell method (51,52) lies in the fact that the derivatives of the minimised function are not required. For a function which is defined to be quadratic and a sum of squares of a nonlinear function as stated in Eqn.(3.12) and (3.14), this algorithm is certainly a very attractive one to be used. Its principle rests essentially on that the minimum of the quadratic function J(z) is found along each of p conjugate directions in one stage of the search and a step is accordingly made in each direction. The overall step from the start to the p(th) step is then said to be a conjugate to all p subdirections of this search.

Thus, at each search stage, the transition from a point $z_o^{(k)}$ (superscripts denote stages, subscripts denote vectors) to points $z_m^{(k)}$ is given as

$$z_m^{(k)} = z_o^{(k)} + \sum_{i=0}^{m-1} \lambda_i^{(k)} s_i^{(k)} \qquad (3.15)$$

where λ_i is the computed step length for the minimisation of J(z) in each direction, and $s_i^{(k)}$ is the search direction at k(th) stage, such that s_i and s_j are conjugate if

$$(s_j)^T Q\ (s_i) = 0 \qquad i \neq j$$

$$(s_j)^T Q\ (s_i) \geq 0 \qquad i = j \qquad (3.16)$$

where Q is a positive definite matrix.

There are many algorithms available to calculate the value of step size λ_i. The advanced Coggins unidimensional search method (53) is chosen here because it has the ability to "bracket" a range of each search direction in which the position of the minimum of J(z) is located. In APPENDIX E, the required computational procedures are outlined while the complete computing subroutine including the Coggins search method are given in (54).

3.2.6 DAVIDON-FLETCHER-POWELL OPTIMISATION ALGORITHM

This is an alternative choice to that of the Powell method. It is an iterative descent algorithm for locating a minimum of J(z) by a defined or estimated gradient vector of the function. The essence of this method is that the Hessian matrix H(z), or its inverse $H^{-1}(z)$. of J(z) can be approximated from a knowledge of the first order derivatives. This idea was first originated in (55) and later improved in (56). Again, the computing subroutine is given in (54).

3.2.7 PARAMETER IDENTIFICATION PROCEDURES

From Fig.(3.3), the procedure for the present parameter identification technique is clearly illustrated, The computer programme is now stored in Cranfield VAX/782 computer. A programme listing is given in (57) and the results produced by this technique are reported in (58). This programme is now being used extensively to analyse the heave dynamics in the research, the results are presented in chapter seven of this thesis.

Chapter 4

4.0 DESCRIPTION OF HOVERCRAFT MODEL AND THE ASSOCIATED EXPERIMENTAL RIGS

4.1.1 DESIGN OF HOVERCRAFT MODEL

The hull of the model craft was constructed of plywood to a geometry representing the craft of Hovercraft Development Ltd,HD2,below the level of the outer loop attachment,to a scale of 0.19. The model is a single cell skirted one which is illustrated in Fig.4.1. The lines were curved longitudinally to conform to the curvature of the mean wave height. The length of the structure is 1.75m(5.74ft) and beam of 0.76m(2.5ft). The bare hull weights are 28.8kg(63.51b) and 69.4kg(1541b) which includes the mounting tube,skirt and the fan hub.

4.1.2 SKIRT DESIGN

The advantage of using the whirling arm over the conventional heave table or wave belt facility is to enable a full-scale type of fabric to be used for skirt construction. In ref.(59) it is shown that when the correct Froude number is maintained through the gravity field (centrifugal acceleration), the elastic scaling of the skirt can be achieved.

The skirt configuration used for this research is shown in Figs.4.2 and 4.3. It is a British Hovercraft Corp. skirt which was used in practice in about 1969 with a comparative high bag/cushion pressure ratio. The cushion area is measured as 1.039 m^2(11.18 ft^2) with a length of 1.435m(4.7ft.) and width of 0.722m(2.37ft). Details of this skirt are reported in (9).

4.1.3 MODEL INSTALLATION

The model craft is installed at the end of the arm by a

box structure, Fig.4.4. It is mounted on three tubes which are supported by the rollers. The centre of gravity of the model is arranged to be halfway between the aft tube and the two forward tubes. Adjustable stops engage flanges at the inner end (towards centre of the arm) of each mounting tube to restrict movement of the model to avoid model structural impact either with the box carriage, or the waves. Also this limits the large transient responses arising from certain waves conditions and provides a locking system for the model at a predetermined location if required. The other end of the tube is attached by a pivot at the forward end and a sliding link at the aft end to the strain gauge balances which are rigidly attached to the model for static investigation. Details of the installation can be seen in Fig.4.4.

4.2 INSTRUMENTATION

4.2.1 SLIP RINGS

Power supplies for the model are carried by the arm via 6 slip rings having rating of 15 amps at 250 volts. A further 23 Signal rings with precious metal contacts having rating of 0.2 amps at 50 volts are mounted on the top of the tower, while 4 more rings beneath the tower provide 440 volts 3-phase supply to the fan motor.

4.2.2 HEAVE DISPLACEMENT AND PITCH ANGLE MEASUREMENTS

The displacement of the forward and aft support tube is measured by two linear transducers one at each side. The difference of the two signals is proportional to the pitch angle.

4.2.3 PRESSURE TAPPINGS OF THE MODEL

A separate pressure transducer, Kulite XCQ-152-5,having

bandwidth of 70KHz is mounted in a robust holder at the plenum box and the loop, whereas in the cushion, although there are nine possible positions for pressure measurements, only station 3 and station 8 are used. See Fig.4.5. The swirl and turbulence generated by the arm motion, in the test chamber causes a pseudo-atmospheric reference pressure to be sensed by the device, and as a result, an incorrect gauge value is produced. This is rectified by placing a long tube from the reference hole extended to the centre of the whirling arm where the turbulence field is not so strong.

4.2.4 HEAVE ACCELERATION MEASUREMENTS

A Sunstrand servo accelerometer, Type 305B, is mounted on the c.g. position of the craft and is used for heave acceleration measurement. It has a wide bandwidth in 1MHz region which is sufficiently large for any required dynamic tests.

4.2.5 DRAG BALANCE

The original drag balance used in (9) was formed as an integral part of the lift and moment strain gauge balances. Serious vibration problems were encountered when measuring the drag. Therefore a new drag balance was designed for the purpose in which the drag balance is now isolated from the lift balance by interposing three links between the existing model attachment to the lift balances and the support tubes, as shown in Fig.4.6. These links were designed to withstand the lift (radial) and weight (vertical) loads on the model, simultaneously, with limited amounts of distortion. Low friction bearings were fitted at each end of the links, thereby permitting freedom of model movement in the fore and aft sense even when lift loads were being transmitted. An adjustable strain gauge web was fitted to the rear support tube, see Fig.4.7, and a point load from the rear of the model was imposed on this

web, via a miniature ball race whose careful positioning permitted the measurement of drag in both fixed and free heave as well as pitch cases. As a result of these changes, good drag records are obtained.

4.2.6 DATA ACQUISITION

A diagram of the signal conditioning and data acquisition is given in Fig.4.8. The main feature of the recording system is the SE3012 24-channel UVrecorder which is located in the control room. The communications between the model rig and the control room is transmitted electrically via the slip rings.

4.3.1 THE HYDRAULIC DRIVE SYSTEM

As a result of the installation of the axial flow fan in the model, instead of the centrifugal fan with ducted air-supply, a fan motor was required. After initial consideration of an electrical motor, which was eventually rejected on the grounds of possible interference with various measurement transducers within the model, an hydraulic motor was chosen. This has an additional attraction, in that it provides a ready source of power to the hydraulic servo-actuation system for blade pitch-angle changes (see later).

This system comprises an hydraulic pump of gear type which is driven by an electrical motor. The original 15 h.p. GEC electrical motor was replaced (after cut-outs and overheating problems) by a 20 h.p. BTH electrical motor with Lucas worm gear pump 3PA38. A flow control valve (Lucas PR3 -300/3P) was used in the hydraulic line to provide a simple low cost, fan-speed control rather than the motor speed control. Details of the hydraulic drive and lines are shown in Fig.4.9.

4.3.2 FAN SPEED CONTROL SYSTEM

The original fan speed control system using a flow control valve in the hydraulic line was able to keep the fan speed under control during the static test condition and various fan speed demands can be made. However, when a sudden loading on the fan was applied by actuating the blade angle in a step, a large fan speed transient appeared. This effect not only affected the cushion pressure, see fig.4.10, but stretched the blade excessively. On one occasion this caused the blade tip to touch the inner-wall of the air intake. As a result, all the fan blades and their associated linkages and bearings were stripped from the hub and scattered far and wide in the test chamber.

It was then decided that the hydraulic-line system had to be redesigned. At first a pressure compensated flow control valve supplied by Singlehurst Hydraulic Ltd. was tried. Subsequent transient tests showed that there was a significant drop, up to 10% of fan speed for a change of 10 degrees of blade angle. This result was undesirable for several reasons and in particular it reduced the effectiveness of the heave control and complicated the system analysis. Finally, another control flow valve, supplied by Mannamann Rexroth, was installed and fitted in the feedback path of the fan motor line. A series of dynamic tests has shown that the valve is capable of controlling the fan speed transient but the speed of the fan is limited to 5200 rpm instead of the original top speed 7000 rpm. Since the resultant cushion pressure from this speed is high enough for most of the investigation no further improvement on the system was made. Ideally, one would like to have an active fan speed control, similar to that used in blade angle actuation system, but this is out of the question because of limited funds. The subsequent hydraulic drive system, including the blade angle actuation system, is shown in fig.4.11.

4.3.3 MECHANICAL ARRANGEMENT OF THE VARIABLE PITCH FAN

An overall impression of the modified fan and actuating system can be seen from Fig.4.12 and 4.13, whilst details of the actuating linkages and associated bearings are shown in Fig.4.14 and Fig.4.15. In order to allow rotation of the fan blades, each blade root is modified to accept a precision roller bearing. A miniature thrust bearing is also used in order to minimise friction arising from the large centrifugal load. Accurate location of each blade in the root housing on the die-cast hub, is obtained by jig-boring the holes and fitting to give 0.0076cm(0.003 inch) end float, see Fig 4.15. Simultaneous rotation of the ten fan blades is obtained by means of an hydraulic actuator working through the linkage mechanism shown in Fig.4.14. This converts the linear motion of the actuator, via a high-speed ballrace, intermediate actuating hub, actuating arms and attachment links to a rotation about the blade longitudinal axis, i.e. the axis of the radial bearing on the blade root.

The hydraulic actuator is a double acting piston type, bore 1.78cm(0.7inch) and having a maximum stroke of 5.08cm(2.0inch). Its piston rod is clamped to the stationary outer ring of a high-speed ballrace, 12.065cm(4.75inch) diameter. The inner portion of the ballrace which is free to rotate, is fitted to a light-alloy hub (intermediate actuating hub) located by six hardened-steel guide pillars descending from the main fan hub. Movement of this intermediate hub is facilitated by a linear ballrace, Fig.4.14, around the guide pillars, allowing a maximum axial movement of 0.635cm(0.25inch). An annular groove is machined into the intermediate hub in which ten miniature roller bearings, 0.0953cm(0.375inch) diameter are located. Each of the rollers is attached to a light-alloy actuating arm, see Fig.4.13,4.14, and 4.15. These arms are pivoted on forks, machined into a support ring which is bolted to the main hub. The movement of the actuating arms is transmitted via the

linked attachment arms, which are themselves hinged to blade actuating legs, Fig.4.14, bolted directly to the nylon blade and offset from the axis of the blade rotation, Fig. 4.14. Maximum blade movement is from 0 to 20 degrees.

When operating at normal fan rotational speed (6000 to 7000 rpm) the centrifugal load on individual blades is approximately 2.86KN(630 lbf). This force generates a friction torque at the blade bearing surfaces, and in the early stages of the design it was considered essential to determine the influence of this torque on the performance of the system, in terms of both the angular response of the blade and the wear on the thrust bearing. For this purpose a temporary test rig was built which could apply this order of end load to a single blade and simultaneously apply an angular oscillation of $\pm$20 degrees at frequencies up to 50 Hz. These tests helped in the development of the design and its present configuration is such that friction torque does not cause serious deterioration of the angular response or excessive wear of the thrust bearing.

4.4 DESIGN AND DEVELOPMENT OF THE SERVO ACTUATION SYSTEM

The flow of oil to the actuator is controlled by a spool valve (Dowty series 4552) which is itself stroked by a pilot flapper valve driven by an electric torque motor.

In order to design the position control loop for the blade pitch angle defined by the transfer-function $G_{\alpha}(s)$ in Fig.2.3, an experimental bench-rig, Fig.4.16, was constructed in which the fan hub was replaced by an equivalent mass of 1.039Kg(2.29lbs). Such an arrangement is able to simulate the inertial load, which is the main one, on the actuator. The actuator piston displacement was measured by a linear transducer (poteniometer) and later this transducer was moved to its final position on the fan assembly shown in

Fig.4.13. It is assumed that the linear displacement of the piston is proportional to the angular movement of the blade. This assumption depends on the fact the angular travel is small, and the absence of "dead space" or "slop" in the linkage due to poor fitting or wear. Regular attention is required to maintain this situation.

4.4.1 OPEN-LOOP FREQUENCY RESPONSES

Initially an "open-loop" frequency response was conducted on the bench-rig using a frequency generator to provide a sinusoidal signal (voltage) to the torque motor. The resulting gain between the input signal and the output (linear transducer, measuring piston displacement), was plotted in the form of a Bode diagram and a typical curve is shown in Fig.4.17. From the bandwidth shown on this plot it was anticipated that the closed-loop system would not have a sufficiently fast transient response. To improve this situation a phase-advance filter, whose characteristics were obtained by trial, was placed in series with the torque motor. The modified open-loop frequency response is also shown in Fig.4.17 by the dashed line. Finally the loop was closed by a direct feedback from the linear displacement transducer. See Fig.4.18. A satisfactory transient response was obtained, as shown in Fig.4.10.

4.4.2 CUSHION PRESSURE SIMULATOR RIG

Having obtained a satisfactory position control of the fan blade, it was decided to expand the bench rig to include simulated cushion pressure signals from the pressure transducer used to measure mean cushion pressure, thereby allowing further development of the inner-loop prior to the full model assembly being available. The overall view and main components of this rig are shown in Figs.4.19, 4.20 and 4.21. It can be seen that a compressor provides a mean pressure (2.0kPa) to a chamber with a piston.

This piston was oscillated by means of a d.c. motor drive giving rise to pressure fluctuations in the chamber. A pressure tapping in the chamber allowed a tube to be taken to a manometer, to record mean chamber pressure, and to the pressure transducer, to measure the fluctuation about the mean. The output from the pressure transducer was then fed to the input of the actuation servo, Fig.4.18, effectively closing the inner-loop. This rig proved very useful during the development stage. Later, of course, the actuator was mounted on to the fan-motor assembly, Fig.4.12, and this was installed into the experimental hovercraft model, Fig.4.13, and the pressure transducer was then fitted into the cushion.

The dynamic characteristics of this actuation system are investigated in chapter seven using the parameter identification technique.

Chapter 5

5.0 STATIC MEASUREMENTS

5.1.1 TEST TECHNIQUE

Before conducting the dynamic tests to evaluate the heave control performance of the model, the parameters which govern the stability and control of the system must be known in order to achieve the required results. These parameters, for example, are the fan and heave characteristics, quantity of leakage flow, determination of equilibrium heave height, the fan and arm speed, etc. A way of finding these quantities is desirable and can be done by means of static tests on the hovercraft model.

These tests were conducted with the hovercraft model locked at various nominal heights h_n above the flat surface (the wall of the Whirling-Arm test chamber), and the fan rotational speed maintained constant at 5200 rpm. During the test runs, the fan blade angle was altered (by means of changing the offset voltage of the servo torque motor, see Fig.4.18), in steps of 5 degrees from 0 to 20 degrees. The lift force on the model was measured by means of the strain-gauge balance arrangement described in (60). Simultaneously the pressures at the plenum box, loop section and cushion region were recorded by means of Kulite XCQ-152-5 pressure transducers installed in these positions. The detailed description of the instrumentation can be seen in chapter four.

5.1.2 DETERMINATION OF FLOW-RATE

In the earlier experiment described in (60), the pressure versus flow-rate characteristics of the fan were determined by the use of a plenum box rig shown in Fig.10 of (60). Such an experiment has two main disadvantages:

(1) It can only simulate the fan characteristics, (see Fig.1.5).

(2) The pressure vs flow-rate characteristics at various positions of the model, namely, the loop section and cushion region cannot be obtained directly. Hence, the characteristics of loss between the plenum and cushion are indeterminate, and efficiency of the fan for this particular application is unknown.

Therefore, for the present tests, it was decided not to re-assemble this rig (which had been dismantled anyway), but to calculate the flow-rate, Q, on the basis of the steady Bernoulli equation applied to the flow from the loop to the cushion. Thus the flow-rate is given by

$$Q = Q_i = C_D A_o [2(P_L - P_C)]^{\frac{1}{2}} \qquad (5.1)$$

Where A is the area of flow-feed orifices from the loop to cushion, which can be measured from Fig.4.2 and 4.3, and C_D is the discharge coefficient of these orifices. In (13), a value of C_D=0.5 for such orifices is quoted and this figure was employed.

5.1.3 DETERMINATION OF FAN CHARACTERISTICS

The results of the tests measured at zero model pitch, as described in section 5.1.1, are tabulated in Table 5.1. The nominal height h_n is defined in (12) where h_n=0 is a distance of 8.89cm measured from the bottom of the hull to the flat surface of the chamber wall. The graphical form of the fan, loop and cushion characteristics are shown together in Figs.5.1 and 5.2 for a range of blade angle settings. As a check on the validity of the method of determining Q, using Eqn.5.1, a comparison was made, for the case α=20 degrees, with the previous tests described in (60). This comparison is shown in Fig.5.2 and can be seen to be a good one.

5.1.4 DETERMINATION OF EFFECTIVE AREA

It is generally accepted that under steady conditions, the lift force is equal to the mean cushion pressure times the effective area, A_e, of the cushion. It was shown in (60), that when the heave displacement is taken to extremes of its travel the effective cushion area, A_e, varies by $\pm 10\%$ from the mean. By plotting the lift versus cushion-pressure characteristics for different blade angle setting, as shown in Fig.5.3a, it is reasonable to construct a straight line fit to these data except at the lower pressure (lower heave heights), as can be seen in Fig.5.3b. Thus the effective cushion area, A_e, which is the slope of this curve, is constant for a large range of heave height, but tends to decrease at the lower cushion pressures. This would appear to agree with the expected behaviour arising from the "tucking-in" of the fingers under the craft (13).

5.1.5 DETERMINATION OF HOVER GAP

As indicated in section 2.3, the cushion pressure is not merely dependent on the fan characteristics, it is also governed by the leakage flow Q_o from the cushion region. As a result, the relationship between hover gap and cushion pressure becomes an important factor as far as stability and control is concerned. Although the characteristics of heave height h (defined in section 5.1.3) and cushion pressure are obtained and shown in Fig.5.4, strictly speaking, the value of hover gap,h, ought to be:

$$h = h_n - h_s \qquad (5.2)$$

where h_s is the height of the skirt.

Since h_s can be influenced by the skirt finger "tucking-in" behaviour, as described in section 5.1.4, the accuracy of h obtained from Eqn.5.2 is therefore questionable. Thus,

a means of determining h is required.

One way of finding h is to use the incompressible Bernoulli equation again for the leakage flow Q_o, in which case,

$$h = Q_o / [C_{DO} L_p (2P_c / \rho)]^{1/2} \qquad (5.3)$$

where C_{DO} is the equivalent orifice flow discharge coefficient. From (61), a value C_{DO}=0.61 is quoted, and L_p is the perimeter of the cushion.

Since the hovercraft model is stationary during the tests the flow inlet Q_i and outlet Q_o must equal Q, as tabulated in Table 5.1. Thus, the h in Eqn.5.3 is now amenable to solution. The characteristics of hover gap and cushion pressure are shown in Fig.5.5. The relationship between h_n and h is shown in Fig.5.6, whereas Fig.5.7 shows the characteristics of Q and h.

5.1.6 STATIC HEAVE CHARACTERISTICS

In ref.(60), the static heave characteristics were obtained by plotting the nominal height h_n against lift as indicated in Fig.5.8a. Since the actual heave characteristics are defined by the lift versus hover gap (27), the appropriate heave characteristics must then be represented as shown in Fig.5.8b.

Chapter 6

6.0 SYSTEM PERFORMANCE

In this chapter, both heave-control-system performance and drag measurements are presented. The experiment on the heave-control-system performance was conducted on the basis of the control concepts stated in chapter two, whilst the drag measurements were taken using the technique described in chapter four, In order to make a direct comparison between the system ON/OFF conditions, the experimental results for both open, and closed loop cases are presented.

6.1.1 INNER-LOOP RESPONSE

From previous research (23,24), the assumption of direct proportionality between cushion pressure, P_c, and vertical force, F, has been demonstrated. Indeed, a control system based on this concept, using the cushion pressure as the feedback signal has been developed (7). But the problem of heave-motion-control is not quite solved by this technique as described in section 2.3. In particular when similar analogy applies to the dynamics of a flexible skirted amphibious hovercraft, of which the characteristics of heave height and cushion pressure are important.

A clear way to prove its inadequacy is to perform step tests on the model craft using the purpose-built mechanical release unit (60). This unit permits the model to be held at a prescribed height, relative to the equilibrium heave height, and released whilst travelling over the flat wall section of the test chamber.

Two tests (inner-loop open and closed) were conducted at a nominal height above a predetermined equilibrium position and the transient responses are shown in Fig.6.1. From these responses, the inner-loop system obviously tends to alleviate the heave acceleration by altering the setting of fan blade angles, from 12 degrees to 7 degrees.

But a substantial loss in heave height is observed after the initial transient. As a result of the lower α setting resulting the hovercraft model is travelling at a new equilibrium position closer to the surface of the wall.

This phenomenon occurs for the P_c of the form,

$$P_c = f(\alpha,h) \qquad (6.1)$$

which means that P_c is also heave height dependent. The form of this function is validated further by the static test in which the characteristics of P_c/h are shown in Fig.5.5. From this figure, it is clearly shown that the cushion pressure is not only coupled strongly with the blade angle, but is governed by the level of the hover gap. Inner-loop behaviour shown in Fig.6.1 can, therefore, be explained on the basis of the characteristics shown in Fig.6.2.

When the open-loop test was done, a step change in heave height (h_A to h_E) was made resulting in the cushion pressure rising from a value P_{ca} to the equilibrium value P_{ce}. The transient vertical force (acceleration) resulting from this change behaves according to the characteristics of P_c/h at 12 degrees, i.e. along the curve from A to E in the graph, Fig.6.2. When the loop is closed, using the cushion pressure feedback technique, as shown in Fig.2.3, the changes in cushion pressure from P_{ca} to P_{ce} no longer proceed in the direction of A to E, but diverge towards B. This arises because the fan blade angle has been changed by the actuation system, to 7° and B is the appropriate point on the curve of 7°. The position of the blade angle will remain at B, since the equilibrium cushion pressure P_{ce} became a steady state value after the initial transient, the hover-craft model is thus settled down at a new hover-gap h_B instead of h_E. As a result, a height loss, h_L, is observed,

where $h_L = h_E - h_B$ (6.2)

This behaviour is for various reasons highly undesirable for an amphibious hovercraft and particularly because of the increased wave drag and skirt wear. Hence, the inner-loop control system is, by itself, not suitable for this application. Whereas, for a sidewall hovercraft, in which the hover gap is almost non-existent, the height loss phenomena will not be a problem. Therefore, the inner-loop system should be able to reduce the heave acceleration.

6.1.2 HEAVE CONTROL SYSTEM PERFORMANCE

Having understood the inner-loop responses and their shortcomings, the craft-cushion dynamics, see Fig.2.5, as described in section 2.3 and 2.4 must be considered. It would seem reasonable to assume that the heave control system should be completed by feedback of the signals from an accelerometer, see section 2.5. Then, following the overall heave control system layout, as shown in Fig.2.6, tests on this system can be pursued.

The test was conducted over the 10ft wave trains, and the appropriate measurements of various quantities were recorded. These are compared with the open-loop responses in Fig.6.3. It can be seen that the attenuation of the heave acceleration is considerable, in fact, up to 40% rms as compared with the open-loop system, and with the fan-blade-angle changing $\pm$5 degrees about a mean of 12 degrees, see Fig.6.4. Although the mean level of heave height is seen to have dropped, the overall peak to peak values are greatly reduced. The reason behind this drop in mean height is not fully understood, but it is possible that a non-linear damping effect may be a contributory factor to this problem, as will be discussed in chapter seven.

It should be stressed that the responses obtained from this

system are, so far, not viewed as the optimum, and improvements of the system may therefore be achieved when the overall control system is fully investigated. Nevertheless, the principle of using an active variable-pitch fan system to control the heave motion is demonstrated and the results are very encouraging.

6.1.3 DRAG PERFORMANCE

When the drag performance is being investigated the total drag, D, of the craft should be considered. It is given by,

$$D = D_{aero} + D_{mom} + D_{wave} + D_{sk} \qquad (6.3)$$

where D_{aero} is the aerodynamic profile drag,
D_{mom} is the momentum drag, which is a function of air flow through the cushion,
D_{wave} is the cushion wave drag, which is a function of cushion pressure and length-to-beam ratio of the craft, and
D_{sk} is the skirt drag, which influences the speed of the craft in rough water.

Much research on the individual drag components, as listed above, are reported in (4). It is believed that all the essential elements are included and considerable attention is given to each component. However, the problem of evaluating the drag is far from straightforward, and estimating the total drag is still difficult.

In this research, the evaluation of the total drag, D, is not attempted. This is because the hovercraft model runs over the solid waves, and will give un-realistic or non-existent values to some of the components defined in Eqn 6.3. Secondly, instrumentation poses another problem, especially when the skirt drag is considered. This is because measurements of the skirt (fingers) height and the cushion

depth are required (62), whilst the craft is travelling over the waves. Further from these, the amount of skirt wear has an important influence on the drag. It is shown in (4) that a great difference in forward speed is observed between a worn and a new skirt under the same test conditions.

In order to investigate the drag performance of the craft, despite the difficulties mentioned above, the only realistic drag component which can be deduced with confidence is the aerodynamic drag, D_{aero}, which is of the form

$$D_{aero} = WC_{DC}\left[\frac{S_F}{A_e}\right]K \qquad (6.4)$$

where

$$K = \frac{\rho g}{2}\,\frac{Fr^2}{P_c/L} \qquad (6.5)$$

and

	W	is the weight of the craft,
	C_{DC}	is the drag coefficient,
	S_F	is the frontal area of the craft,
	A_e	is the area of the cushion,
	ρ	is air density,
	g	is the gravity,
	Fr	is the Froude Number,
	P_c	is cushion pressure, and
	L	is the length of the craft.

It can be seen that D_{aero} is dependent on the cushion pressure, P_c. Hence, if the Froude Number, Fr, is maintained in both ON/OFF conditions, a direct comparison in drag measurement can be made. The measuring device used is the strain-gauge balance which has already been described in chapter four. The test runs were again conducted over the 10ft waves. The results are shown in Fig.6.5 for both

ON/OFF conditions and it can be seen that a significant drag reduction is obtained. Fig.6.6 shows the enlarged drag traces and a 22.4% reduction in drag is achieved.

It should be stressed that the results obtained from this drag balance do not represent the total drag, D, of an amphibious craft. Further detailed investigation into total drag performance is necessary, especially if this heave control system is being implemented on a full scale craft. At present, due to the lack of time and limited financial resource, only the current drag measurement can be presented. However, it is demonstrated that the drag performance can benefit from this heave control system.

Chapter 7

7.0 DYNAMIC ANALYSIS

The purpose of this chapter is to use the parameter identification technique described in chapter three to model the dynamics of the heave-control-system, and those of its sub-systems which may influence the overall performance. It is hoped that, through this exercise, the synthesis of the control system can be achieved and, possibly, improved designs of the systems obtained for future development.

7.1.1 ANALYSIS OF BLADE PITCH-ANGLE ACTUATION SYSTEM

In order that the modelling of the overall control system is successfully validated, the dynamics of the blade pitch-angle actuation system, which is an integral part of the heave control system, must be thoroughly investigated. Because of the complexity of the fan hub mechanism, the irregular geometry of the flow path inside the craft model and the elasticity of the skirt, mathematical modelling of such a system proved to be inadequate (see chapter two). As a result, the system had to be experimentally determined by using the parameter identification technique.

Since the servo-controlled actuation system, $G_{\alpha}(s)$, is the main input control, then $G_{\alpha}(s)$ must be the first transfer function to be identified, see Fig.7.1. The experiment was conducted by locking the craft model at a nominal height whilst the fan was running at a speed of 5200rpm. The angular movement of the blade was obtained by driving the servo system via a function generator and recording for identification purposes.

To be able to use the parameter identification procedure to identify the transfer-function, $G_{\alpha}(s)$, a representative model is required. This can be a problem since the physical nature of the system is not completely understood, in particular, the linkage mechanism of the fan hub and the

action of the actuator. However, it is assumed that under the normal operating conditions, the movement of the actuator is proportional to the angular changes of the fan-blade-pitch-angle. Therefore, a model which represents the servo torque motor is assumed to be reasonable. Research on this type of servo system has been extensively carried out at UWIST, Cardiff, (64,65,66). From which an 8th order theoretical model is found to be approximated by a 6th order model (64). Therefore on the basis of this model and using the parameter identification technique, the experimental trace is appropriately matched as shown in Fig.7.2. From this, $G_\alpha(s)$ is identified to be:

$$G_\alpha(s) = \frac{(s+19.6)}{(s+13.2)(s+156.2)(s^2+95.74s+135590)(s^2+102.7s+44799)} \qquad (7.1)$$

Having now successfully identified $G_\alpha(s)$, the next stage is to identify the complete control input system, i.e. the forward path of the inner-loop, see Fig.7.1. In order to obtain better accuracy, the cost function for the multi-trace case is used for the optimisation routine within the parameter identification programme. The experiment was done by applying a step function to the servo torque motor and recording the outputs of blade angle, loop pressure and cushion pressure for the optimisation procedure. Since the models of $G_{\alpha L}(s)$ and $G_{LC}(s)$ are not available, for the reasons described in chapter two, the models identified were as follows:

$$G_{\alpha L}(s) = \frac{(s+473.7)(s^2+8916.7s+250936.4)}{(s+12.3)(s^2+195.6s+15219.7)} \qquad (7.2)$$

and

$$G_{LC}(s) = \frac{(s+426.5)}{s^2+322.5s+9082.6} \qquad (7.3)$$

whereas $G_\alpha(s)$ is the same as that shown in Eqn.7.1. The identified traces are shown in Fig.7.3.

It should be emphasised that the numerical values in Eqns.7.1 to 7.3 have, so far, no significant meaning, other than their ability to match the experimental results. In practice, one would prefer a model which can be related to the physical characteristics of the system and yet appropriately match the experimental results. In this case, the lumped parameter model of APPENDIX A is employed to validate the response of the cushion pressure to step blade-angle changes. It can be seen from Fig.7.4, that the response of this model is too fast as compared with the test results (in fact, judging from the value of time constant, it is found that it has a value 10 times higher than that obtained by the parameter identification programme). In order to have a model which can practically represent the test result, the first order model (66) can be adapted. A typical response is also shown in Fig.7.4. The validation of any of these models can only be justified when the loop is closed and their time constants are found to be closely related to overall dynamics. This model will be justified further when the closed-loop response is examined. See section 7.1.4.

7.1.2 VALIDATION OF NON-LINEAR HEAVE DAMPING PHENOMENON

When an hovercraft travels across the waves, it will not, as in the flat surface case, be tangential to the ground, but contours along or rides over the waves dependent on the encounter frequency. Thus, the air inflow is generally at a different rate from the outflow of the cushion. This rate of air flow change is physically associated with the heave damping and therefore non-linear.

Analogue computer studies at Hovercraft Development Limited have shown that this non-linearity can lead to a loss of

hover height (67). Basically, this phenomenon can be represented by the equations of heave motion,

$$\ddot{h} + 2\zeta\omega_n(\dot{h}-\dot{h}_g) + \omega_n^2(h-h_g) = 0 \qquad (7.4)$$

or

$$(\ddot{h}-\ddot{h}_g) + 2\zeta\omega_n(\dot{h}-\dot{h}_g) + \omega_n(h-h_g) = -\ddot{h}_g \qquad (7.5)$$

where h_g is the ground height,
h is the craft heave height,
ζ is the damping coefficient having two discrete values according to the condition $0<\dot{h}-\dot{h}_g>0$,
ω_n is the natural frequency.

Eqn.7.5 can be simplified by letting $x=h-h_g$, thus,

$$\ddot{x} + f(\dot{x}) + \omega_n^2 x = g(t) \qquad (7.6)$$

where

$$f(\dot{x}) = 2\zeta\omega_n\dot{x}$$

$$f(\dot{x}) = C_{rise}\,\dot{x} \quad \text{for all } \dot{x}>0 \qquad (7.7)$$

$$f(\dot{x}) = C_{drop}\,\dot{x} \quad \text{for all } \dot{x}<0 \qquad (7.8)$$

$g(t)$ is the forcing function

By the same token, Eqn.7.6 can also be derived by considering the volume of air in the cushion and using the equation of air flow continuity (68).

It is clearly indicated that the damping force terms, C_{rise} and C_{drop}, defined in Eqns.7.7 and 7.8 respectively, are dependent on the direction of $\dot{x}$.

In order to validate this phenomenon experimentally, step tests on the hovercraft model were conducted. These were done by locking the craft model at hover heights, above or below the pre-determined equilibrium position whilst the arm was running. A release mechanism unit was used which enabled the model to be released rapidly when the model was traversing the flat section of the test chamber wall. As a result, the cushion pressure transient responses were obtained, Fig.7.6.

By applying the parameter identification technique to these responses, it is reasonable to expect the damping ratio, ζ, and natural frequency, ω_n, to be estimated. In Fig.7.5, ζ and ω_n are depicted for six different transient responses, from which, it is shown that the damping ratio obtained from the calculation of $C_{rise}/2\omega_n$ is almost twice the values of that $C_{drop}/2\omega_n$ whilst the natural frequency remains unchanged. Therefore, the assumption made by reference (67,68,69) is justified and it can be concluded that this non-linearity will lead to loss in heave height as the craft travels across the waves. Typical transient responses which are closely matched by the models via parameter identification technique, are shown in Fig.7.6.

7.1.3 ANALYSIS OF HEAVE DYNAMICS

As described in section 6.1.2, the basic concept of the heave control system has been demonstrated experimentally. It proved that the variable fan-pitch-angle control is a sound technique for the alleviation of the heave acceleration. However, since the performance shown in Fig.6.3 and Fig.6.4 is not optimum, it is possible that the system can be improved if the heave dynamics are properly analysed.

Before attempting to investigate the heave dynamics in more detail, a means of justifying the heave control system over the 10ft waves is necessary. Because of its versatility in

accepting various forms of disturbance, the parameter identification programme is applicable in this case once a model becomes available.

It is still a problem to select a model which describes that response. A direct approach to the possible solution is to use different trial models. The obvious model is that derived in APPENDIX C. A similar version is given in (26), which is modified and stated in APPENDIX F. Thus the model can be expressed as,

$$\frac{h}{h_w}(s) = \frac{\frac{C_B A_e}{m}(A_{es} + G)}{s^3 - C_B R s^2 + \frac{C_B A_e}{m} s + \frac{C_B A_e G}{m}} \qquad (7.9)$$

where h is the heave displacement,
h_w is the wave height.

By applying this model in the parameter identification programme, the heave displacement response is appropriately identified as shown in Fig.7.7a. The characteristic equation (denominator) of Eqn.7.9 is found to be,

$$C(s) = (s + 1000)(s^2 + 9.6s + 576) \qquad (7.10)$$

In order to validate this model further, the cushion pressure and heave acceleration responses are also used for optimisation. As a result, the same C(s) is predicted in both cases. The responses are shown in Fig.7.7b and 7.7c respectively. As far as the quality of the matching is concerned, this model seems to be justified. However, when the C(s) are carefully examined, the pole (s=-1000) which is situated far away from the origin in the s-plane, Fig.7.8, indicates that it has no significant effect. In the physical sense, this pole is directly associated with the

compressibility effect of the cushion. This tends to agree with the argument made in section 2.3.1.

Having now gained a little insight into the problem of modelling, the heave dynamics model can use the "flat plate" assumption by considering the skirt to be rigid (23). Applying the same procedure as before, the complex conjugate pair of Eqn.7.10 is estimated as,

$$C(s) = s^2 + 10.92s + 676 \qquad (7.11)$$

The resemblance of the complex pair between Eqn.7.10 and 7.11 proving that the "flat plate" model is an adequate representation and the prediction error is kept to a very small value, see Fig.7.9. From this experience of modelling and the result obtained, another interesting observation is made. That is the value of the damping ratio ζ calculated from Eqn.7.11 is 0.22. Comparing this with the values shown in Fig.7.5a, it can be seen that this is in the middle of the range, indicating that a mean value of damping ratio can be used for regular head sea conditions. Such a value has been used in the analogue computer studies (68).

7.1.4 IDENTIFICATION OF HEAVE CONTROL SYSTEM PERFORMANCE OVER THE 10FT WAVES

Having now gained more confidence in modelling the dynamic responses, in particular, the heave response, it is logical to use the same approach to identify the closed-loop system dynamics. Since the preliminary identifications have already been applied to the relevant sub-systems of the heave control system, for example, the input control dynamic loop and the heave dynamics, the models required for the complete heave control system are available for optimisation purpose.

Strictly speaking, the system which is shown in Fig.2.6

should be considered here. However, in the case of the 10ft wave responses, the craft-cushion dynamics described in section 2.4 have been proved to be insignificant. Thus, the heave control system has a simple form as shown in Fig.7.10, i.e. the "flat plate" model and the first order time-lag of the actuation system described in section 7.1.1 is required for the models to be identified.

In Fig.7.11 which shows the results from the parameter identification programme, the characteristic equation of the system is found to be

$$C(s) = (s + 10.0)(s^2 + 14s + 380) \qquad (7.12)$$

This can be depicted in a root locus plot, Fig.7.12, in which the open-loop characteristic mode has been modified. From this figure, the variable fan-pitch-angle control system does increase the stability margin by shifting the damping ratio from a value 0.22 to 0.36, while the natural frequency decreases from 26.0 rad/s to 19.5 rad/s. Since the ζ is strongly associated with the rate of air flow, an increase in this value would minimise the height loss and the heave acceleration can therefore be alleviated. As a result, the heave performance shown in Fig.6.3 is now justified.

7.1.5 ANALYSIS OF DYNAMIC RESPONSES OVER THE 3.3FT WAVES

Although a valid model which can adequately represent the heave dynamics, at least to the 10ft waves case, is obtained, to be able to justify this model for future development, a series of frequency responses tests, at least for a few decades, are desirable. Better still, by using the popular Pierson-Moskowitz sea spectrum analysis (4,69), the overall system dynamic characteristics can be thoroughly investigated. Unfortunately, this

approach is not cost effective as the cost of construction of the solid wave trains is expensive. Nevertheless since the 3.3ft wave trains have already been built and physically displayed in the test chamber wall, the dynamic responses over these waves are available for model identification.

Using the same procedure as above, the heave acceleration responses were obtained. The result is shown in Fig.7.13 which clearly indicates that the matching of this model is not good, especially at the beginning of the trace. This phenomenon may be caused by the pitching effect of the craft as it rides over the steeper slope of the waves as compared to the 10ft waves, resulting in an extra acceleration component being experienced by the accelerometer. This behaviour does not stop until the whole craft is physically on top of the waves, where the heave dynamics are properly excited without the pitching. This argument seems to be justified by examining the whole trace of the responses as shown in Fig.7.14. It is found that the distance, L, is about 4.125ft which approximates to the cushion length. Hence, to be able to use the "flat plate" model to the response of 3.3ft waves, the sampling point should start at the position A as shown in the graph. As a result, the matching of the model to this response, shown in Fig.7.15, proved that the assumption is justifiable.

7.1.6 ANALYSIS OF CUSHION-CRAFT DYNAMICS

In this particular section, the cushion-craft dynamics are investigated. A motion of this type happens when the skirt is no longer rigid and reacts to surface contact, via the fingers, resulting in a skirt "bounce" phenomenon (13). Therefore, when a mathematical model is developed for the hovercraft motion, this feature must be included.

Since the skirts always oscillate relative to the craft, it is possible to postulate the dynamics by a number of masses

that are attached to the rigid structure of the craft by springs and dashpots, see Fig.2.5. In this way, the associated stiffness and damping coefficients of this representative system can, in principle, be obtained via analysis on the test results using the parameter identification technique.

As indicated in Fig.2.5, the experiment can be conducted in two different ways:

(I) to oscillate the blade angle through the servo torque motor by a function generator while the craft is running over the flat section of the test chamber wall, or

(II) to perform heave height test by releasing the craft model from a nominal height.

As a result, the responses of the cushion pressure and vertical acceleration are obtained. Then, by choosing an appropriate model order for $G_{ch}(s)$, which is the main transfer function of this exercise, into the parameter identification programme, the corresponding stiffness and damping ratio of this system can be estimated.

Both experimental results of (I) and (II) were used for matching purposes. It is found that a 2nd order model would adequately represent the craft-cushion dynamics, and the natural frequency and damping ratio are estimated to be 75.0 rad/s and 0.7, respectively, by the programme. The results of the matching for both cases are shown in Figs.7.16 and 7.17.

Chapter 8

8.0 FUTURE DESIGN OF HEAVE CONTROL SYSTEM

The main objective of this chapter is to develop a realistic optimal control technique to design the heave control system for future application. The strategy is to use Wiener Filtering theory (70,71) for the control optimisation by considering the disturbance acting on the heave dynamics as white noise. Thereby, the mean-square error of the output (heave acceleration in this case) is minimised by a closed-form expression of a controller. This technique will be demonstrated by an example using the information from previous chapters.

It should be pointed out that the above technique is only one of the possible solutions to the problem of optimum control design. An alternative approach to the problem is to use the well known Kalman Filtering technique, to estimate the mean current state vector and then apply the separation principle (72) to the design of the optimal feedback loop. Since this technique is well documented (73,74), no attempt to explain this approach will be made. However, the practical application of this technique has been demonstrated (75,76).

8.1.1 SYSTEM OPTIMISATION

The system to be optimised is shown in Fig.2.6. For simplicity of mathematical description it is modified and depicted in Fig.8.1. Assuming the plant is linear, the time-invariant $g(t)$, $h_w(t)$ and $u(t)$ are scalar quantities and the command signal $d(t)$ is taken as zero, then the plant output $g(t)$ is the system error. The controller is said to be linear and time-invariant, and has noisy measurement $g + y$ of the system error g. The controller output u is subject to a power constraint:

$$\overline{u^2} \leq C \qquad (8.1)$$

where $\bar{u}^2$ is the ensemble-average of u^2. The design problem is to have a controller C(s) such that the mean-square-error $\bar{g}^2$ is minimised when the system is in stochastic steady state. The plant (heave dynamics) and the controller transfer function are designated respectively P(s) and C(s), where s is the Laplace transform variable. The wave disturbance is generated by passing white noise, with unit spectral density and zero mean, through a linear, time-invariant, element filter(sea spectrum) with transfer function D(s). The measurement noise is generated by passing an independant white noise, with unit spectral density and zero mean, through a linear, time-invariant, element transfer function M(s).

8.1.2 APPLICATION OF WIENER FILTERING THEORY TO CONTROL OPTIMISATION

The method by which the Wiener filtering theory is applied to the control problem is briefly describes in APPENDIX G. Further details can be obtained from reference (70,71). The aim of the theory is the minimisation of $\overline{g^2}$ subject to a constraint on $\overline{u^2}$, and this is treated by minimising

$$\overline{e^2} = \overline{g^2} + \lambda \overline{u^2}, \qquad (8.2)$$

where λ is a Lagrange multiplier, and adjusting λ so that the constraint on $\overline{u^2}$ is satisfied. Then G3 may be written

$$\overline{g^2} + \lambda \overline{u^2} = \frac{1}{2\pi} \int_{-\infty}^{\infty} [\, \phi_q(\omega) + \phi_u(\omega) \,]\, d\omega \qquad (8.3)$$

where ω is frequency (rad/s).

The closed-loop transfer function from v to g is found to be

$$\frac{g}{v}(s) = [\, 1 - H(s) \,]\, D(s) P(s), \qquad (8.4)$$

where H(s), the closed-loop transfer function from d to g, has the form

$$\frac{g}{d}(s) = H(s) = \frac{C(s)P(s)}{1+C(s)P(s)} \qquad (8.5)$$

Thus the spectral density of g from the contribution of v is

$$|1 - H(j\omega)|^2 \; |P(j\omega)D(j\omega)|^2, \qquad (8.6)$$

and, similarly, the contribution of n to the spectral density of g is

$$|-H(j\omega)M(j\omega)|^2 = |H(j\omega)|^2 \, |M(j\omega)|^2 \qquad (8.7)$$

Therefore, adding 8.6 and 8.7 gives

$$\overline{g^2} = \phi_q(\omega) = |1 - H(j\omega)|^2 |P(j\omega)D(j\omega)|^2 + |H(j\omega)|^2 |M(j\omega)|^2 \qquad (8.8)$$

Similarly, the spectral density of the controller signal $\overline{u^2}$ is

$$\overline{u^2} = \phi_u(\omega) = |H(j\omega)|^2 |D(j\omega)|^2 + |H(j\omega)|^2 \left|\frac{M(j\omega)}{P(j\omega)}\right|^2 \qquad (8.9)$$

Substituting for $\phi_q(\omega)$ and $\phi_u(\omega)$ in Eqn.8.3 then gives

$$\overline{g^2} + \lambda\overline{u^2} = \frac{1}{2\pi}\int_{-\infty}^{\infty}\Big[|1-H(j\omega)|^2 |P(j\omega)D(j\omega)|^2 + |H(j\omega)|^2\Big\{|M(j\omega)|^2 + \lambda|D(j\omega)|^2 + \left|\frac{M(j\omega)}{P(j\omega)}\right|\Big\}\Big] \, d\omega \qquad (8.10)$$

Comparing Eqn.8.10 with Eqn.G4 shows that the control

optimisation problem is equivalent to a filter optimisation problem. In this case, the signal spectral density is

$$\phi_p(\omega) = |P(j\omega)D(j\omega)|^2 \tag{8.11}$$

and the noise spectral density is

$$\phi_q(\omega) = |M(j\omega)|^2 + \lambda |D(j\omega)|^2 + \left|\frac{M(j\omega)}{P(j\omega)}\right|^2 \tag{8.12}$$

Consequently the optimal H(s) is given by Eqn.G6-G8 with $\phi_p(\omega)$ and $\phi_q(\omega)$ substituted from Eqn.8.11 and 8.12. It follows that

$$H(s) = \frac{P(s)P(-s)D(s)D(-s)}{\psi(s)\psi(-s)}$$

or

$$|H(j\omega)|^2 = \left|\frac{P(j\omega)D(j\omega)}{\psi(j\omega)}\right|^2 \tag{8.13}$$

where

$$|\psi(j\omega)|^2 = |P(j\omega)D(j\omega)|^2 + |M(j\omega)|^2 + \lambda\left[|D(j\omega)|^2 + \left|\frac{M(j\omega)}{P(j\omega)}\right|^2\right] \tag{8.14}$$

Hence, once H(jω) is found, the optimal controller C(s) in Eqn.8.5, or its spectral density $\overline{u^2} = \phi_u(\omega)$ in Eqn.8.9, can be determined.

8.1.3 MODELLING OF SEA SPECTRUM

In order to apply the optimal control theory in practice, the individual transfer functions shown in Fig.8.1. must be known. So far, it is only D(s), the filter for the sea spectrum which remains unknown, whereas P(s) and M(s) are

available from the results of the parameter identification analysis and the manufacturers specification, respectively. To be able to model the sea spectrum appropriately using an equivalent filter D(s), the properties of sea state must be estimated.

It is generally accepted that the occurence of ocean or sea waves are random in nature, requiring the use of statistics to describe their characteristics. A study by Pierson-Moskowitz (77) provides a way to represent the sea state by means of its power spectral density,

$$s(\omega) = \frac{A}{\omega^5} e^{-B/\omega^4} \tag{8.15}$$

where ω is the angular frequency in rad/s,
$A = 4.894$,
$B = 3.1094/h_w^2$, and
h_w is the significant wave height.

An attempt to model this spectrum in the manner

$$s(\omega) = |D(j\omega)|^2 s_i(\omega) \tag{8.16}$$

where $s_i(\omega)=1$ is unit power spectral density, has been reported in (75). The method used is to minimise the error function

$$\Delta s = \min \sqrt{\int_0^{\omega} [\, s(\omega) - |D(j\omega)|^2 \,]\, d\omega} \tag{8.17}$$

for a range of frequencies. As a result, D(s) is found to be

$$D(s) = \frac{K_s s^3}{s^4 + a_1 s^3 + a_2 s^2 + a_3 s + a_4} \tag{8.18}$$

However, a compatible optimisation study (78) shows that a different transfer function is obtained,

$$D(s) = \frac{K_s s^2}{s^4 + a_1 s^3 + a_2 s^2 + a_3 s + a_4} \qquad (8.19)$$

This form is seen to be closely matched to that obtained in (79) of which the Autoregressive moving-average (ARMA) algorithm was employed. For convenience, the results of (78) are used. A table which lists all the coefficients of Eqn.8.19 against Beaufort number as given by (78) is also shown in TABLE 8.1.

8.1.4 OPTIMUM DESIGN OF HEAVE CONTROL SYSTEM

Having acquired the relevant transfer function, the design of the optimal controller C(s) can proceed. As can be seen in Eqn.8.13 and 8.14, the optimum closed-loop transfer function H(s) is primarily governed by $|P(j\omega)|$ $|D(j\omega)|$, and $|M(j\omega)|$. Therefore, if the gain or the modulus of P(s), D(s) and M(s) are obtained for a range of frequency, it is possible to compute $\phi_u(\omega)$ and hence C(s) is determined. Choosing a sea state which associates with Beaufort 4, as shown in TABLE 8.1, for D(s) and using Eqn.7.9 for P(s), then $|D(j\omega)|$ and $|P(j\omega)|$ can be calculated against frequency, as shown in TABLE 8.2. As for $|M(j\omega)|$, the noise level below 1MHz is quoted to be 0.001mV from the transducer specification.

Using the results from TABLE 8.2, $|H(j\omega)|^2$ can thus be calculated as shown in column 4 in TABLE 8.3 where the product of column 2 and 3 is $|\psi(j\omega)|^2$. Eqn.8.9 can be rewritten as

$$\overline{u^2} = \phi_u(\omega) = |H(j\omega)|^2 \{|D(j\omega)|^2 + \left|\frac{M(j\omega)}{P(j\omega)}\right|^2\} \qquad (8.16)$$

where the second term in the right hand side of Eqn.8.16 can be computed as shown in column 5 of TABLE 8.3, whilst $\phi_u(\omega)$ is tabulated in column 6.

It can be seen that $\phi_u(\omega)$ is dependent on λ the Lagrange multiplier. It is shown in (80) that the constraint value of C in Eqn.8.1 can vary from 0 to ∞ corresponding to varying λ from ∞ to 0. Thus a value of λ exists for every positive value of C. In order to demonstrate the technique clearly, λ=0 is chosen which associates with no power constraint on the controller output. Thus the gain of the controller in $dB(20\log_{10}\sqrt{\phi_u(\omega)})$ can be calculated and shown in column 7. By plotting these values against the frequency, ω, a Bode plot, Fig.8.2, is obtained. From this plot the transfer function C(s) can be obtained, approximately, and has the form

$$C(s) = \frac{Ks^2}{(s + 1.4)^4} \qquad (8.17)$$

To be able to justify this controller, the complete system of Fig.8.1 is translated into a computer programme using the Cranfield Advanced-Continuous-Simulation Language(ACSL). The system is then energised by a white noise of unity power density into the sea spectrum filter D(s). Simulation runs were made by setting the total gain K=0.0001 for the controller with the system on/off. The system time responses are shown in Fig.8.3. It can be seen that the controller has little effect in nulling the wave disturbance. This is because, the signal magnitude of the controller is very small as compared to the wave disturbance signal. Thus it is not a surprising result that the open and closed loop responses of g are super-imposed on top of each other. The situation can be improved by increasing the gain to, say, k=1.0. As a result, the closed-loop responses of g are seen to be greatly reduced compared to that of the

open-loop. See Fig.8.4. In Fig.8.5 the situation is improved further when k=100.0. Hence, the design of this controller is proved to be effective and sound. However, the design assumes that the actuator characteristics have no effect on the system performance, but in practice this is not always true. As a matter of fact, the actuation system in this case was approximately identified as a first order system. See Fig.7.4. In order to examine the effect of this time lag on the overall system responses, it was inserted into the system and a simulation run repeated with k=100.0. The time responses obtained are shown in Fig.8.6. It appears that the system responses are influenced by the actuator dynamics, but it is believed that improvement can be made by adjusting k appropriately.

It should be stressed that the present controller was designed for a sea spectrum of wind speed Beaufort 4. If another sea state is to be examined, the design procedure should be repeated. Thus, it is sound practice to design a controller for a worst-case and then use it for a range of sea states including that for a relatively calm sea (75).

However, the technique of adaptive control could be more appropriate in this application. In general, three common basic schemes of parameter adaptive control are used:

A. Gain scheduling

This is a useful technique to reduce the effects of parameter variations. The key problem is to find a set of suitable scheduling variables. This is normally done on a knowledge of the physics of the system. Once a scheduling is obtained, the controller parameters are determined at a number of operating conditions using some suitable design method. This concept is widely used in flight control system design of an aircraft. A general block diagram of the method is shown in Fig.8.7a.

B. Model reference

A reference model is one which can tell how the process output, ideally, should respond to the command signal. It is part of the control system. The controller can be thought of as two loops. The inner loop is an ordinary control loop composed of the process and the controller. The parameters of the controller are adjusted by the outer loop such that the error between the model output and the process output becomes small. The outer loop is thus also a control loop. The key problem of this technique is to determine the adjustment mechanism such that a stable system which brings the error to zero is obtained. This system is shown in Fig.8.7b.

C. Self-tuning

The controller is also composed of two loops. The inner loop consists of the process and an ordinary linear feedback controller. Its parameters are adjusted by the output loop which is composed of a recursive parameter estimator and a design calculation algorithm. A block diagram of this scheme is shown in Fig.8.7c.

An excellent paper (81), gives a full account of the theory and application of adaptive control with particular reference to these three techniques. Maybe, in the future, one of these schemes will be used, and that, the influence on overall drag, range performance and/or the fuel consumption will be beneficial.

Chapter 9

9.0 SYSTEM SYNTHESIS

9.1.1 RIDE QUALITY

When an hovercraft travels in the sea, its ride quality varies with the magnitude of the roughness of the sea, the character of the sea (random or regular), the speed of the craft, the direction and the encounter frequency of the sea, and other physical and environmental characteristics. These key parameters determine the effects on the craft as well as on its crew and passengers. In broad terms, the vertical acceleration and amplitude of the motion are the dominant factors of the ride quality as compared with the lateral or sway and surge accelerations. The other environmental factors such as temperature, noise level, smell and visual reference can also influence the acceptable acceleration level.

In general, the ride quality as it relates to personnel can be divided into two major categories:

1. Motion sickness — which is normally associated with low encounter frequency, less than 1.0Hz, and

2. Working efficiency — which is concerned with the fatigue of personnel. This can occur at all frequencies but is normally associated with the frequencies greater than 1.0Hz.

In both cases, the acceptable level of acceleration depends on the duration, that is, high acceleration can be tolerated for a short period of time, whereas a lower level may be tolerated for a long duration of time. It is also understood that psychological factors must be included when the

acceptable acceleration level is being considered.

9.1.2 CRITERIA

When ride quality is being considered, one is often confronted by the definition, or the form, of the ride quality criteria used. Since the problem of ride quality for hovercraft (amphibious and non-amphibious) is not uniquely defined, applying a criterion to the design procedure of a ride control system must only be on a rational basis.

In ref.(82), three distinct types of criteria were summarised from the Ride Quality Symposium(1), and they were identified and evaluated with regard to attributes and shortcomings, as shown in TABLE 9.1.

The As Good As (AGA) criteria can only be useful when there is sufficient similarity between the new and the comparison craft used as a reference. Therefore, it is difficult to make a realistic specification of a level of ride quality, judging from the degree of 'likeness' to that of the comparison craft.

Unlike the AGA criteria, the Not-to-Exceed criteria (The Absolute Standard) are relatively easy to specify and verify, and can be developed from well documented technology. A typical example for demonstration, is to use the vertical (heave) acceleration responses shown in Fig.6.4, and transfer them into the ISO 2631 chart, see Fig.9.1. From this, the heave control system is able to reduce the acceleration (rms) from a higher level to a lower one, and hence improves the ride quality. In ref.(83), a full description of the criteria is given.

The Output-to-Input criteria, which are a relatively new form of criterion, focus on the craft transfer function and are independent of levels of either the input pertur-

bation to craft or the output ride environment experienced within the craft. The principal difficulty of this criterion centres on specifying the target level of ride comfort. Therefore, a reasonably good definition is required for the expected input environment perturbation to craft transfer function, and of the passenger transfer function which relates the ride environment to passenger ride comfort. Mathematically, this can be defined in terms of spectral density,

$$\phi_q(\omega) = |G(j\omega)|^2 S(\omega) \qquad (9.1)$$

where $\phi_q(\omega)$ = response spectral density,
$S(\omega)$ = sea spectral density,
$G(j\omega)$ = transfer function, and
ω = wave frequency.

If the linear superposition theory is applied, the transfer function, $G(j\omega)$, can be written

$$G(j\omega) = G_1(j\omega) \times G_2(j\omega) \times \ldots\ldots\ldots \times G_n(j\omega)$$

$$= \text{"Cushion to Hull"} \times \text{"Hull to Floor"} \times \ldots\ldots\ldots\ldots\ldots \times \text{"Seat to Person"} \qquad (9.2)$$

That is, each part of the craft has its own mechanical transfer function that can be determined in the design process.

Although the criteria seem to be useful in designing a ride control system as illustrated in Fig.9.2a, in order that the design procedure is completed as shown in Fig.9.2b, then, this criteria must be used in conjunction with the absolute standard. This would provide a guideline for $\phi_q(\omega)$ to be met as the former criteria do not independently specify an acceptable level of ride quality.

9.1.3 RIDE COMFORT SPECIFICATION

Ideally, in order to meet the criteria stated above, a ride comfort specification is required for hovercraft application. This may develop on the same basis as that of aircraft, in which the ride comfort is clearly specified by MIL-A-8892. However, since a similar specification is, so far, not available for hovercraft, it is, perhaps, arguable that the aircraft ride comfort specification may be applicable in the present case, as an amphibious hovercraft is considered to be an airborne vehicle. In (82), a ride discomfort index is given for this specification in rms acceleration terms. An allowance is made for a "human" sensitivity weighting function. This index may be modified from the original form in order to fulfil the application of an hovercraft. Thus, the ride discomfort index is defined as:

$$D_i = \int_{0.1}^{f_t} \{ |W(f)|^2 |G(f)|^2 \phi_u(f) df \}^{\frac{1}{2}} \qquad (9.3)$$

where D_i = ride discomfort index (vertical and lateral),

$W(f)$ = acceleration weighting function (vertical and lateral,

$G(f)$ = transmissibility, at crew station, g/m/sec,

$\phi_u(f)$ = sea spectral density,

f = frequency, Hz, and

f_t = truncation frequency (frequency which no longer significant in sea turbulence).

The acceleration weighting functions are defined for vertical and lateral acceleration as shown in Fig.9.3, and the probability of exceedance versus turbulence intensity is given in TABLE 9.2.

9.2.1 IMPROVEMENT OF FAN (CONTROL-INPUT) SYSTEM

When ride quality is being considered, the important factors which contribute to an acceptable level of passenger comfort are, the technique of designing an active control system, evaluation of external disturbance forces, and the understanding of the craft dynamics. Another important factor which also influences ride quality is the power (spectral density) and efficiency of the "control-input" within the controller. So far it has been assumed that the controller has unlimited power available disregarding the size of the external disturbance forces. In reality, this is not always true and limitation of a controller exists. Therefore, in order to reduce problems to the minimum, a good mechanical design of controller is desirable. In the present case, the design of the fan hub including the fan blade lift profile and the blade angle linkage, are very important (see Fig.4.12).

From the experience of the present research, it was felt that two main shortcomings of the fan hub design were:

1. blade oscillation at low pitch angle setting, and

2. non-linear (stall) characteristics at high pitch angle setting.

These were experienced as a result of the fan speed restriction, in which the speed was limited to 5200rpm. See chapter four. Because of this low speed, as compared with the original design speed of 7000rpm, the air-flow produced by the fan was much less than planned. A typical fan characteristic with speed variation is shown in Fig.9.4 for a direct comparison.

The problem of blade oscillation occurs when the fan blade angle is low (less than 5 degrees). The most likely reason

for this happening, is the loading on each blade through the actuating linkage, being changed to a compressive load from a tensile load as the blade angle decreases. It is at this point of "changeover", the clearance (dead space) of various linkages allow the blades to perform small uncontrollable pitch oscillations. The angular movement was measured statically at 1.5 degrees approximately. This asymmetric loading effect is justified further by mounting a section of fan blade on a strain gauge balance. The wind tunnel speed was 30.5 m/s, corresponding to Reynold number, 10^6 based on chord 0.065m. From the results of the blade profile lift curve, Fig.9.5, it indicates that a rearward shift of the centre of pressure was observed as the blade angle reduced. Thus in order to eliminate this oscillating phenomenon, the following action can be taken:

1. increase the fan speed (if possible) so that the loading on the fan blade is sufficiently high,

2. adjust the linkage "dead space", and

3. enlarge the size of the fan.

The other problem of the fan system is the non-linear (stall) characteristics at high blade angle. Because the fan can no longer produce the air-flow required at a low blade angle setting, as the fan speed is limited at 5200 rpm, the operating point has to be selected at a relatively higher position (10-12 degrees), in order to avoid the fan blade oscillation during the dynamic test. Since the blade angle movement is primarily governed by the feedback signals (cushion pressure and acceleration) it occurs over both the linear and non-linear regions of the cushion pressure versus blade angle characteristics, see Fig.9.6, dependent on the sign changes of the signal. As a result, the absolute magnitude of cushion pressure changes are larger

over the linear region than those over the stall region, even though the blade angle movement may have the same magnitude on either side of the operating point. This phenomenon implies that the fan is to have more capability of decreasing rather than increasing the pressure within the cushion volume. This effect can explicitly reduce the spectral density required by the controller and furthermore, complicates the design of the control law.

Thus, in order to simplify the matter and improve the fan system, either the fan speed control system has to be improved so that the operating point can be shifted into the linear region of the characteristic to avoid the stall region, but maintaining the same cushion pressure threshold level (see the characteristics with broken line in Fig.9.6), or the fan blade aerofoil is replaced with one which has steeper characteristic slope.

9.2.2 FUTURE PROGRAMME

Where from now? This is a question which often arises at the end of a piece of research. Of course, the best possible reply here, is to implement the present system into a full-scale craft and test at sea. However, because of certain practical engineering problems and the large funds required for such a project, this is unlikely. Therefore, in order to improve the present system and obtain realistic results, it is believed that future experiments are still required on a scaled model, but instead of using the Cranfield Whirling Arm Facility, these should be conducted in a "water towing-tank", in conjunction with the Wave Belt facility (14). The results and experience so gained should then lead to the development of an experimental system in a sea-going craft, in which the efficacy of the ride-control technique could be fully explored.

Chapter 10

10.0 CONCLUSIONS

A heave control system, using an active-fan as its control element, for amphibious hovercraft has been developed. Tests on an experimental craft, conducted on the Cranfield Whirling-Arm facility, show that substantial reductions in the heave acceleration experienced over waves are possible and that this is achieved with a simultaneous reduction in craft drag.

The results obtained are not optimum and it is likely that even greater reductions in heave acceleration are possible. To this end, the extensive parameter identification of control sub-systems was used to construct a full mathematical model of the controlled craft to which optimisation procedures were applied. As a result, using the technique of Wiener optimal filtering theory, the results from the computer simulation are encouraging. This technique is capable of being taken further and applied to the specific problem of ride quality and passenger comfort.

It should be stressed that, the present research is confined to the longitudinal motion only. In practice, the system should include the dynamics in full six degrees of freedom, with special attention to pitching effect.

Another feature of the implementation of the present system in a full scale version, is the possible use of compartmentalised cushion. Hence, the cushion is locally pressurised by more than one fan. In order to achieve the required results, in heave acceleration attenuation, synchronization of these fans has to be achieved, or maybe, the whole system configuration has to be modified.

REFERENCES

1. RIDE QUALITY SYMPOSIUM
NASA TM X-3295 DOT-TSC-OST-75-40, 1975.

2. Leatherwood, J.D.
Dempsey, T.K.
PSYCHOPHYSICAL RELATIONSHIPS CHARACTERISING HUMAN RESPONSE TO WHOLE-BODY SINUSOIDAL VERTICAL VIBRATION
NASA TN D-8188, Washington,D.C., June 1976.

3. Leatherwood,J.D.
HEAVE RESPONSE OF A PLENUM AIR CUSHION INCLUDING PASSIVE AND ACTIVE CONTROL CONCEPTS
NASA TND-5202 May 1969, Langley Research Centre, Hampton,Va.

4. Mantle,P.J.
AIR CUSHION CRAFT DEVELOPMENT
DTNSRDC-801012(4727 Revised)
David W.Taylor, Naval Ship Research and Development, Jan.80, Bethesda,MD.

5. Kaplan,P;
Davis,S.
SYSTEM ANALYSIS TECHNIQUES FOR DESIGNING RIDE CONTROL SYSTEM FOR SEA CRAFT IN WAVES
Proc. 5th Ship Control System Symposium, Oct.,78.

6. Amyot,J.R.
COMPUTER STUDIES OF ACV HEAVE PERFORMANCE AS A FUNCTION OF VENTING VALVE PROPORTIONAL CONTROL PARAMETERS
Canadian Aeronautics and Space Journal, Vol.29, No.1, March, 83.

7. Zupanick,J.E. SURFACE EFFECT VEHICLE CONTROL SYSTEM
United States Patent, Sun Oil Co. Dallas, Feb. 1975.

8. Luscher,W.P. SURFACE EFFECTS VEHICLE HAVING VARIABLE GEOMETRY LIFT FAN
United States Patent, Aerojet General Co. El. Monte, Calif. June, 1975.

9. Cox,R. MEASUREMENTS OF THE DYNAMIC RESPONSE OF A HOVERCRAFT MODEL TO WAVES OF VARIOUS LENGTHS USING THE CRANFIELD WHIRLING ARM FACILITY
Aero Report 7803, C.I.T., Cranfield, UK, Nov., 1977.

10. Hinchey,M.J.
Sullivan,P.A. DUCT EFFECT ON THE DYNAMIC FAN CHARACTERISTICS OF AIR CUSHION SYSTEMS
UTIAS Tech Note No.211, June, 1977.

11. Hinchey,M.J. DUCT EFFECT ON THE DYNAMIC FAN CHARACTERISTICS OF AIR CUSHION SYSTEMS
Journal of Hydronautics Vo.13, No.1, Jan.1979.

12. Christopher,P.A.T.
Lim,K.H. HOVERCRAFT RESEARCH AND DEVELOPMENT ON THE CRANFIELD WHIRLING ARM FACILITY
Aero Memo 7905, C.I.T., Cranfield, UK, Nov.,1979.

13. Crewe,P. A REVIEW OF HOVERCRAFT DYNAMIC MOTION WITH PARTICULAR REFERENCE

TO RIDE AND MANOEUVRING CHARACTERISTICS
Symposium on Dynamic Analysis of Vehicle Ride and Manoeuvring characteristics
Inst. of Measurement and Control
pp.97-118, London,1978.

14. Clayton,B.R.
Tuckey,P.R.
DYNAMIC RESPONSE OF HOVERCRAFT TO REGULAR WAVE EXCITATION
Proc. High Speed Surface Craft Conference,
pp.139-159, London,1983.

15. Gustarsson,I.
SURVEY OF APPLICATION OF IDENTIFICATION IN CHEMICAL AND PHYSICAL PROCESS
Automatica, Vol.11,3-24, 1975.

16. Young,P.
PARAMETER ESTIMATION FOR CONTINUOUS TIME MODEL - A SURVEY
Automatica, Vol.17, 23-39, 1981.

17. McCloy,D.
Martin,H.R.
CONTROL OF FLUID POWER AND DESIGN
Ellis Horwood, 1980.

18. Christopher,P.A.T.
Man,K.F.
Osbourn,E.W.
HEAVE CONTROL OF AMPHIBIOUS HOVERCRAFT, AN EXPERIMENT
COA Memo 8204,C.I.T.,Cranfield,UK, March, 1982.

19. Brown,F.T.
THE TRANSIENT RESPONSE OF FLUID LINES
Journal of Basic Engineering,
547-553, Dec.,1962.

20. Schuder,C.
Binder,R.
THE RESPONSE OF PNEUMATIC TRANSMISSION LINES TO STEP INPUTS
A.S.M.E. Paper 58-A-136, Nov.,1958.

21. Rohmann,C.
Grogan,E.
ON THE DYNAMICS OF PNEUMATIC TRANSMISSION LINES
A.S.M.E. Paper 56-8a-1, Dec.,1955.

22. Goodson,R.E.
Leonard,R.G.
A SURVEY OF MODELLING TECHNIQUES FOR FLUID LINE TRANSIENTS
A.S.M.E. Paper 71-WAIFE-9,Nov.,1971.

23. Wheatley,J.H.W.
HEAVE SUSPENSION CHARACTERISTICS AND POWER REQUIREMENTS OF A PLENUM AIR CUSHION
National Physical Lab. Report 9, Dec.,1969.

24. Reynolds,A.J.
RESEARCH NOTE: A LINEAR THEORY FOR THE HEAVING RESPONSE OF A HOVERCRAFT MOVING OVER REGULAR WAVES
Journal Mech.Eng.Sci.,Vol.14, No.2, 1972.

25. Reynolds,A.J.
West,R.P.
Brooks,B.E.
HEAVING AND PITCHING RESPONSE OF A HOVERCRAFT MOVING OVER REGULAR WAVES
Journal Mech.Eng.Sci.,Vol.14,No.5, 1972.

26. Lavis,D.R.
Bartholomew,R.J.
Jones,J.C.
RESPONSE OF AIR CUSHION VEHICLES TO RANDOM SEAWAYS AND THE INHERENT DISTORTION IN SCALE MODELS
Journal Hydronautics, Vol.8,No.3, July,74.

27. Ribich,W.A.
Richardson,H.H.
DYNAMIC ANALYSIS OF HEAVE MOTION FOR A TRANSPORT VEHICLE FLUID SUSPENSION
Report DSR-76110-3,M.I.T.,Jan.,1967.

28. Wormley,D.N.
Garg,D.P.
Richardson,H.H.
A COMPARATIVE STUDY OF THE NON-LINEAR AND LINEAR PERFORMANCE OF VEHICLE AIR CUSHION SUSPENSION USING BOND GRAPH MODELS
Journal of Dynamic System,Measurement, and Control, Sept.,1972.

29. Paynter,H.M.
ANALYSIS AND DESIGN OF ENGINEERING SYSTEMS
M.I.T. Press, Cambridge, Mass.,1961.

30. Karnopp,D.
Rosenberg,R.C.
ANALYSIS AND SIMULATION OF MULTIPORT SYSTEMS
M.I.T. Press, Cambridge, Mass.,1968.

31. Rosenberg,R.C.
STATE-SPACE FORMULATION FOR BOND GRAPH MODEL
Trans. ASME, Series G.Vol.93,No.1, pp35-40, March,1971.

32. Genin,J,
Gineberg,J.H.
Ting,E.C.
FLUID SUSPENSION MODEL FOR AIR CUSHION VEHICLES
Journal of Sound and Vibration, Vol.25, pp83-93, 1972.

33. Astrom,K.J.
Eykhoff,P.
SYSTEM IDENTIFICATION - A SURVEY
Automatica Vol.7, pp123-162,1971.

34. Strejc,V.
TRENDS IN IDENTIFICATION
Automatica Vol.17,No.1, pp7-21,1981.

35. Kay,S.M.
RECURSIVE MAXIMUM LIKELIHOOD ESTIMATION OF AUTOREGRESSIVE PROCESSES
IEEE Trans. on Acoustics, Speech, and Signal Processing, Vol.ASSP-31, No.1, pp51-65, Feb.,1983.

36. Eykhoff,P.
PROCESS PARAMETER ESTIMATION
IEEE TRANS. AC-8, No.4,pp347, 1963.

37.Astrom,K.J.
ON ACHIEVABLE ACCURACY IN IDENTIFICATION PROBLEMS
IFAC Proc. on System Identification, Prague, June,1967.

38. Bohlin,T.
ON THE PROBLEM OF AMBIGUITIES IN MAXIMUM LIKELIHOOD IDENTIFICATION
Automatics Vol.7, pp199-210, 1971.

39. Unbehauen,H.
Gohring,B.
TEST FOR DETERMINING MODEL ORDER IN PARAMETER ESTIMATION
Automatica Vol.10, pp233-244,1974.

40. Van Den Boom,A.J.W.
Van Den Enden,A.W.
THE DETERMINATION OF THE ORDERS OF PROCESS AND NOISE DYNAMICS
Automatica Vol.10, pp245-256,1974.

41. Wellstead,P.E.
MODEL ORDER IDENTIFICATION USING AN AUXILIARY SYSTEM
Proc.IEE Vol.123,No.12, Dec.,1976.

42. Godfrey,K.R.
PRACTICAL ASPECTS OF THE IDENTIFICATION OF PROCESS DYNAMICS
Trans-Inst MC Vol.No.2, April-June, 1979.

43. Godfrey,K.R.
EXPERIMENTAL MODELLING OF PROCESSES IN THE CHEMICAL AND PETROLEUM INDUSTRIES
IEE/ORS Joint Symposium. London, 1971.

44. Iliff,K.W.
Maine,R.E.
PRACTICAL ASPECTS OF USING A MAXIMUM LIKELIHOOD ESTIMATOR
AGARD Flight Mechanics Panel Specialists Meeting, Hampton,VA., Nov.,1974.

45. Christopher,P.A.T.
Cheng,Y.N.
Man,K.F.
PARAMETER IDENTIFICATION WITH A KALMAN FILTER
CoA Report 8328, C.I.T.,Cranfield, Nov.,1983.

46. Chen,C.T.
ANALYSIS AND SYNTHESIS OF LINEAR CONTROL SYSTEMS
Holt, Reinhart and Winston,Inc.1975.

47. Foster,G.W.
A DESCRIPTION OF THE WEIGHTED LEAST SQUARES OUTPUT ERROR METHOD OF PARAMETER IDENTIFICATION
RAE Tech. Memo FS215,1978.

48. Young,P.C.
PROCESS PARAMETER ESTIMATION
J. OF CONTROL VOL.12, No.25, pp931, 1968.

49. Bryson,A.E.
Ho,Y.C.
APPLIED OPTIMAL CONTROL
Waltham, Mass:Blaisdell Publishing Co.,1969.

50. Mehra,R.K.
Lainiotis,D.G.
SYSTEM IDENTIFICATION-ADVANCES AND CASE STUDIES
Academic Press, New York,pp251-282, 1976.

51. Powell,M.J.D. AN EFFICIENT METHOD OF FINDING THE MINIMUM OF A FUNCTION OF SEVERAL VARIABLES WITHOUT CALCULATING DERIVATIVES
Computer J. Vol.7,pp155-162,1964.

52. Powell,M.J.D. A METHOD OF MINIMISING A SUM OF SQUARES OF NONLINEAR FUNCTION WITHOUT CALCULATING DERIVATIVES
Computer J. Vol.7 pp303-307,1965.

53. Coggins,G.F. UNIVARIATE SEARCH METHOD
ICI Central Instr. Lab. Res.
Note 64/11, 1964.

54. Himmelblau,D.M. APPLIED NONLINEAR PROGRAMME
MacGraw Hill, 1972.

55. Davidon,W.C. VARIABLE METRIC METHOD
AEC Research and Development Report
ANL-5990 (rev.), 1959.

56. Fletcher,R.
Powell, M.J.D. RAPIDLY CONVERGENT DESCENT METHOD FOR MINIMISATION
Computer J. Vol.5-6, pp163-168,1964.

57. Cheng,Y.N.
Man,K.F. IDENTIFICATION OF COEFFICIENTS OF AN UNKNOWN TRANSFER FUNCTION OF ELEMENTS IN A CONTROL SYSTEM
CoA Memo 8227, CoA,C.I.T.,
Cranfield, U.K. Jan.,1983.

58. Christopher,P.A.T.
Cheng,Y.N.
Man,K.F.
Osbourn,E.W. A PRACTICAL METHOD FOR IDENTIFICATION OF DYNAMIC PROCESSES
4th IFAC workshop on Application of Nonlinear programming to optimisation and Control, San Francisco, June,1983.

59. Richardson,J.R.
A SCALING TECHNIQUE FOR HOVERCRAFT MODELS
National Physical Lab. Hovercraft Unit, Report, No.1, July,1970.

60. Christopher,P.A.T.
Osbourn,E.W.
HOVERCRAFT RESEARCH AND DEVELOPMENT ON THE CRANFIELD WHIRLING ARM FACILITY
CoA Memo 8009, C.I.T.,Cranfield, 1980.

61. Hinchey,M.J.
HEAVE INSTABILITIES OF AMPHIBIOUS AIR CUSHION SUSPENSION SYSTEM
UTIAS report No.246, CN-ISSN0082-5255, University of Toronto,Nov.,1980.

62. Chaplin,J.B.
"AMPHIBIOUS SURFACE EFFECT VEHICLE TECHNOLOGY - PAST, PRESENT AND FUTURE"
AIAA Conference Proc. on Naval Architects and Marine Engineers Advanced Marine Vehicles, pp74-318, San Diego, Calif. Feb.,1974.

63. Towill,D.R.
Payne,P.A.
LOW ORDER DYNAMIC MODELS FOR ESTIMATING THE IMPULSE RESPONSE OF A COMPLEX ELECTRO-HYDRAULIC SERVO
Tech. Note DAG36, UWIST, Cardiff, Sept.,1970.

64. Payne,P.A.
Towill,D.R.
Baker,K.J.
PREDICTING SERVOMECHANISM DYNAMIC PERFORMANCE VARIATION FROM LIMITED PRODUCTION TEST DATA
IREE Vol.40, No.6, Dec.,1970.

65. Brown,J.M.
Towill,D.R.
Payne,P.A.
PREDICTING SERVOMECHANISM DYNAMIC ERRORS FROM FREQUENCY RESPONSES MEASUREMENT

IREE Vol.42. No.1, Jan.,1972.

66. Richards,R.J. AN INTRODUCTION TO DYNAMICS AND CONTROL
Longman, London, 1979.

67. Hogben,N. ON THE LOSS OF HEIGHT OF A HEAVING HOVERCRAFT DUE TO NON-LINEAR DAMPING
Ship T.M.101, National Physical Lab., Nov.,1965.

68. Dyne,G. AN INVESTIGATION CONCERNING THE MOTIONS OF A HOVERCRAFT IN REGULAR HEAD SEAS
Trans.Inst.of Naval Architecture, Vol.110, pp465-477, 1968.

69. Gornstein,R.J. JETFOIL RIDE SPECIFICATIONS
Boeing Document D320-10050-3,1974.

70. Newton,G.C. COMPENSATION OF FEEDBACK CONTROL SYSTEM SUBJECT TO SATURATION
J.Franklin Inst., Vol.254,pp391-413, Nov.,1952.

71. Fuller,A.T. FEEDBACK CONTROL SYSTEM WITH LOW FREQUENCY STOCHASTIC DISTURBANCE
Int.J.Control, Vol.24,No.2, pp165-207, 1976.

72. Wonham,W.M. ON THE SEPARATION THEOREM OF STOCHASTIC CONTROL
SIAM J.Control & Optimisation, Vol.6, pp312-326, 1968.

73. Kwakernaak,H.
Sivan,R. LINEAR OPTIMAL CONTROL SYSTEMS
Chapter 4-5,John Wiley & Sons,1972.

74. Sage,A.P.
White,C.C.
OPTIMUM SYSTEM CONTROL
Chapter 8-9,Prentice-Hall Inc., 1977.

75. Grimble,M.J.
Patton,R.J.
Wise,D.A.
USE OF KALMAN FILTERING TECHNIQUES IN DYNAMIC SHIP-POSITIONING SYSTEM
Proc.IEE Vol.127, PT.D,No.3, pp93-102, May,1980.

76 Man,K.F.
AIRCRAFT GUST RESPONSE CONTROLLERS
Msc. Thesis, School of ESD, C.I.T., Cranfield, 1978.

77. Pierson,W.J.
Moskowitz,L.
A PROPOSED SPECTRAL FORM FOR FULL DEVELOPMENT WIND SEAS BASED ON SIMILARITY THEORY OF S.A. KITAIGORDSKII
J.Geophys.Res.,Vol.69, pp5181-5190, 1964.

78. Li,C.K.
Leigh,J.R.
S-DOMAIN REALISATION OF SEA SPECTRUM
Engineering Div., The Polytechnic of Central London, U.K., 1983.
(Private communication)

79. Spanos,P.T.D.
ARMA ALGORITHMS FOR OCEAN WAVE MODELLING
Trans.ASME Vol.105, pp300-309, Sept.,1983.

80. Fuller,A.T.
THE REPLACEMENT OF SATURATION CONSTRAINT BY ENERGY CONSTRAINTS IN CONTROL OPTIMISATION THEORY
Int.J.Control, Vol.6,No.3, pp201-227, 1967.

81. Astrom,K.J. THEORY AND APPLICATION OF ADAPTIVE CONTROL - A SURVEY
Automatica, Vol.19,No.5, pp471-486, 1983.

82. Kuhlthau,A.R. WORKSHOP ON VEHICLE RIDE QUALITY
NASA CP-2013 DOT-TSC-OST-77-44, July,1977.

83. Allen,G.R. RIDE QUALITY AND INTERNATIONAL STANDARD ISO 2631('GUIDE FOR THE EVALUATION OF HUMAN EXPOSURE TO WHOLE-BODY VIBRATION')
NASA TM X-3295 DOT-TSC-OST-75-40, pp501-530, 1975.

APPENDIX A

APPENDIX A

1. MULTI-LUMPED-PARAMETER MODEL FOR TRANSFER FUNCTION OF P_c/P_f

The details of this model can be obtained from (17), section 10.6. The model is now applied to the air passage between the fan chamber and cushion via the loop and fingers. It is treated as a series of inter-connected small lumps of flow impedence. As a result the P_c and P_f has the form

$$\frac{\Delta P_c}{\Delta P_f}(s) = [\, L_h C_h s^2 + R_h C_h s + 1\,]^{-1} \qquad A1$$

$$\equiv \frac{\omega_{ni}^2}{s^2 + 2\zeta_i \omega_{ni} s + \omega_{ni}^2}\,, \qquad A2$$

where $\omega_{ni}^2 = (L_h C_h)^{-1}$, and A3

$$\zeta_i = \frac{R_h C_h}{2\omega_{ni}} \qquad A4$$

and ΔP_c, ΔP_f are incremental quantities from equilibrium conditions

2. COEFFICIENT OF R_h

This coefficient can be regarded as analogous to a resistive component in an electrical system. It relates the flow rate Q due to pressure drop in steady conditions. From the pressure vs flow rate characteristics of the present model it is found that

$$\Delta P \propto Q, \qquad A5$$

where $\Delta P = P_f - P_c$

Then, R_h can be obtained from the slope of ΔP_c versus Q characteristics.

3. COEFFICIENT OF C_h

This is a capacitive component in the electrical sense, and when applied to fluid flowing through a chamber of a volume, V, C_h has the form

$$C_h = \frac{V}{\beta_e} , \qquad \text{A6}$$

where β_e is the bulk modulus of elasticity of contained fluid and the walls of the chamber. For the present application, V is the volume of air passage which constitutes the plenum box, loop and fingers and its value is known, approximately. The value of β_e may be expressed in the form

$$\frac{1}{\beta_e} = \frac{1}{\beta_{ef}} + \frac{1}{\beta_{e\ell}} , \qquad \text{A7}$$

where

$$\beta_{ef} \triangleq \gamma P_{mean}$$

$$= \tfrac{1}{2} \gamma (P_f + P_c)$$

$$= 0.7(P_f + P_c) \qquad \text{A8}$$

is the bulk modulus of the air in the loop (assumed undergoing adiabatic variation of pressure) and $\beta_{e\ell}$ is the bulk modulus of the material of the walls of the plenum, loop and fingers. The evaluation of $\beta_{e\ell}$ poses a difficult problem as described in section 2.1.2, one which is not solved.

4. COEFFICIENT OF L_h

This can be interpreted as inductance for the analogous electrical system. When applied to fluid in a pipe of constant cross-sectional area A, and length

$$L_h = \frac{\rho \ell}{A} \quad , \qquad \text{A9}$$

where ρ is the fluid density. In the present application ℓ is known reasonably accurately. But the area A varies considerably and the determination of a mean effective value is complicated, but can be approximated.

NOTATION (Appendix A only)

A	cross sectional area of flow path
C_h	capacitive component of flow impedance
L_h	inductive component of flow impedance
ℓ	length of flow path
P_f	fan pressure
P_c	cushion pressure
Q	rate of air flow
R_h	resistive component of flow impedance
s	Laplace operator
V	Volumn of flow path
γ	ratio of specific heat of fluid
ρ	density of air
Δ	incremental operator
β_e	bulk modulus of electicity
ζ_i	damping ratio
ω_{ni}	natural frequency

APPENDIX B

APPENDIX B

1 DETERMINATION OF TRANSFER-FUNCTION $\Delta P_c/\Delta\alpha$ USING TRANSMISSION LINE SYSTEM

The transmission line between the cushion and the fan can be represented as

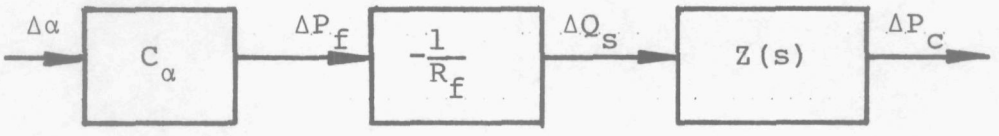

Using the technique of (22), then

$$\frac{\Delta P_c}{\Delta\alpha}(s) = \frac{C_\alpha}{R_f} Z(s)$$

$$= \frac{C_\alpha(R_s+R_L+R_f)}{R_f} \left[\frac{\nu_1 \sinh\tau_c s + \cosh\tau_c s}{\nu_2 \sinh\tau_c s + \cosh\tau_c s}\right], \quad \text{B1}$$

where

$$\nu_1 = \frac{Z_c^2 + R_s R_f + (R_L/2)(R_s+R_f) + (R_L^2/4)}{Z_c(R_s + R_L + R_f)}, \quad \text{B2}$$

$$\nu_2 = (R_f + R_L/2)/Z_c, \quad \text{B3}$$

$$\tau_c = \sqrt{I_d C_d} \equiv L/C \quad \text{B4}$$

$$Z_c = \sqrt{I_d/C_d} \equiv \frac{\rho c}{A_d}, \quad \text{B5}$$

$$c = \sqrt{\gamma(P_c + P_A)/\rho}, \quad \text{B6}$$

$$C_\alpha = \Delta P_f/\Delta\alpha \quad , \qquad \text{B7}$$

$$R_f = -\frac{\Delta P_f}{\Delta Q_s} \equiv \frac{\Delta P_f}{\Delta Q_f} \quad , \qquad \text{B8}$$

$$R_s = \Delta(P_L - P_c)/\Delta Q_s \quad , \qquad \text{B9}$$

$$R_L = \Delta(P_f - P_L)/\Delta Q_f \quad , \qquad \text{B10}$$

$$\gamma = 1.4 \quad ,$$

where I_d = inertance per unit length
and C_d = capacitance

2 FIRST ORDER MODEL

For a first order model, B1 can be approximated by the form

$$\frac{\Delta P_c}{\Delta\alpha}(s) = \frac{C_\alpha(R_s + R_L + R_f)}{R_f}$$

$$= \frac{\nu_1\tau_{c1}s + 1}{\nu_2\tau_{c2}s + 1} \qquad \text{B11}$$

From TABLE A, B11 is,

$$\frac{\Delta P_c}{\Delta\alpha}(s) = \frac{21.2(0.0053s + 1)}{(0.0019s + 1)}$$

3 SECOND ORDER MODEL

For a second order, A1 has the form by expanding B1, thus

$$\frac{\Delta P_c}{\Delta\alpha}(s) = \frac{C_\alpha(R_s+R_L+R_f)}{R_f}\left[\frac{\frac{4}{\pi^2}\tau_c{}^2s^2 + \nu_1\tau_c s + 1}{\frac{4}{\pi^2}\tau_c{}^2s^2 + \nu_2\tau_c s + 1}\right] \qquad \text{B12}$$

Again from TABLE A, B12 is,

$$\frac{\Delta P_c}{\Delta \alpha}(s) = \frac{21.2(7\times10^{-6}s^2 + 5.3\times10^{-3}s + 1)}{7\times10^{-6}s^2 + 1.9\times10^{-3}s + 1}$$

4 SIMPLE LUMPED PARAMETER MODEL

For a simple lumped parameter model,

$$\frac{\Delta P_c}{\Delta \alpha}(s) = \frac{K_s}{\tau_s s + 1}$$

where $K_s = \frac{R_c C_\alpha}{R_f}$ and

$$\tau_s = \frac{V R_{L1}}{\rho c^2}$$

The parameters required by B1-B13 are obtained from an experiment (see chapter five) and results are tabulated in TABLE A in which four different operating conditions are included, whereas the dimensions of the plenum box and loop are estimated and shown in TABLE B.

TABLE A DATA OF TRANSMISSION LINE MODEL

OPERATING P_c CONDITION	P_c 2.24KPa	P_c 1.78KPa	P_c 1.27KPa	P_c 2.55KPa
R_f $Kg/m^2/m^3/sec$	-152.9	-2.4	-285.4	-356.8
R_L "	20.4	10.1	0	76.5
R_{L1} "	173.3	224	285.4	428
R_s "	153	255	306	306
R_c "	357	501	581	714
ν_1	1.67	1.27	1.13	1.04
ν_2	0.33	0.446	0.58	0.8
K_c	20.3	21.2	19.7	19.7
τ_{c1} (sec)	0.007	0.0053	0.0047	0.0044
τ_{c2} (sec)	0.0014	0.0019	0.0042	0.0036
K_s	22.2	22.6	19.4	19
τ_s	0.0015	0.0019	0.0024	0.0036
C_α	9.48	9.48	9.48	9.48
τ_c	0.0042	0.0042	0.0042	0.0042
z_c	491.3	491.3	491.3	491.3

TABLE B DIMENSIONS OF FLOW PATH

NET VOLUME OF PLENUM BOX PLUS LOOP, V, (m^3)	AVERAGE LENGTH OF FLOW PATH, L (m)	AVERAGE CROSS-SECTIONAL AREA OF PATH, $A\alpha$ (m^2)
0.125	1.43	0.087

APPENDIX C

APPENDIX C

HEAVE DYNAMIC MOTION OF AMPHIBIOUS HOVERCRAFT

The following derivations refer to Fig.2.1.

1. CONSERVATION OF MASS

When unsteady compressible flow is considered inside the cushion, the conservation of mass may be expressed by

$$\frac{d}{dt}(\rho V_c) = \dot{m}_i - \dot{m}_o \qquad C1$$

Assuming the changes are in small perturbation form, C1 becomes

$$\rho \Delta Q_i = \rho \Delta Q_o + \Delta \frac{d}{dt}(\rho V_c) \qquad C2$$

or

$$\Delta Q_i = \Delta Q_o + \Delta \dot{V}_c + \frac{V_c}{\rho} \Delta \dot{\rho} \qquad C3$$

2. DERIVATION OF ΔQ_i

Using the Bernoulli relationship between the loop and cushion pressure, then

$$Q_i = C_i A_i [2(P_L - P_c)/\rho]^{\frac{1}{2}}$$

or

$$P_L - P_c = \rho Q_i^2 / 2(A_i C_i)^2$$

then

$$\Delta P_L - \Delta P_c = 2\rho Q_i \Delta Q_i / 2(A_i C_i)^2$$

gives

$$\Delta P_L = \Delta P_c + C_{qi} \Delta Q_i \qquad C4$$

where

$$C_{qi} = \rho Q_i/(A_i C_i)^2$$

But P_L is dependent on the fan characteristics, thus

$$P_L = A + BQ_i + [C - K_D\rho/2A_d^2]Q_i^2 \qquad C5$$

gives

$$\Delta P_L = C_{PL}\Delta Q_i \qquad C6$$

where

$$C_{PL} = B + 2[C - \rho K_D/2A_d^2]Q_i \qquad C7$$

This can be approximated as

$$C_{PL} = B = \frac{dP_L}{dQ_i}\Big|_e$$

Hence C4 can be written as

$$C_{PL}\Delta Q_i = \Delta P_c + C_{qi}\Delta Q_i \qquad C8$$

or

$$\Delta Q_i = \frac{\Delta P_c}{(C_{PL} - C_{qi})} \qquad C9$$

3. DERIVATION OF ΔQ_o

The escape air flow Q can be written as

$$Q_o = C_o V_o A_o \qquad C10$$

$$\Delta Q_o = C_o V_o \Delta A_o + C_o A_o \Delta V_o \qquad C11$$

But

$$V_o = \left(\frac{2P_c}{\rho}\right)^{\frac{1}{2}} \qquad C12$$

gives

$$\Delta V_o = \frac{\Delta P_c}{\rho (2P_c)^{\frac{1}{2}}} \qquad C13$$

and

$$A_o = L(z - h_s) - \int_L \xi dL$$

$$= Lh - \int_L \xi dL \qquad C14$$

where

$$\int_L \xi dL = \int_L h_w \sin [\frac{2\pi x}{\lambda} + \omega_e t] dL \qquad C15$$

and

$$\Delta h_w = h_w \sin\omega_e t \ , \qquad C16$$

$$\omega_e = \omega \pm \frac{\omega^2 v}{g}$$

or

$$\omega_e = (\frac{2\pi g}{\lambda})^{\frac{1}{2}} \pm \frac{2\pi V}{\lambda}$$

As for Whirling Arm

$$\omega_e = \pm \frac{2\pi V}{\lambda}$$

Hence C15 is thus

$$\int_L \xi dL = \int_L h_w [\sin(\frac{2\pi x}{\lambda}) \cos\omega_e t + \cos(\frac{2\pi x}{\lambda}) \sin\omega_e t] dL$$

$$= \int_{-L/2}^{+L/2} \Delta h_w [\{\cos(\frac{2\pi x}{\lambda}) dx\} + 2B_c \cos(\frac{\pi L}{\lambda})]$$

$$= C_{hw1} \Delta h_w$$

where

B_c = cushion width

where the following condilions have been used,

$$\int_L h_w \sin\frac{2\pi x}{\lambda}\cos\omega_e t\,dt = 0 \quad \Rightarrow \sin\frac{2\pi x}{\lambda} = 0$$

and

$$\int_{-L/2}^{L/2} \Delta h_w \cos\left(\frac{2\pi x}{\lambda}\right) dL = 2B_c \cos\left(\frac{\pi L}{\lambda}\right)$$

Thus the perturbation form of C14 is

$$\Delta A_o = L\Delta h - C_{hw1}\,\Delta h_w \qquad C17$$

and

$$\Delta Q_o = C_o V_o (Lh - C_{hw1}\,\Delta h_w) + C_{Pc}\Delta P_c \qquad C18$$

where

$$C_{Pc} = \frac{C_o A_o}{\rho (2P_c)^{\frac{1}{2}}}$$

4. DERIVATION OF $\Delta\dot{V}_c$

The cushion volume

$$V_c = A_e h - B_c \int_{-L/2}^{L/2} \xi\,dx \qquad C19$$

or

$$\Delta V_c = A_e \Delta h - C_{hw2}\Delta h_w \qquad C20$$

where

$$C_{hw2} = \frac{B_c \lambda}{\pi} \sin\left(\frac{\pi L}{\lambda}\right) ,$$

$$\therefore \Delta\dot{V}_c = A_e \Delta\dot{z} - C_{hw2}\dot{\Delta h}_w \qquad C21$$

5. DERIVATION OF $\Delta\dot{p}$

Assuming that the cushion pressure and density changes

are related by a polytropic equation of state

$$\frac{P}{\rho^{\gamma}} = \text{const} \qquad \text{C22}$$

Thus

$$\Delta\dot{\rho} = \frac{1}{c^2}\Delta\dot{P}_c \qquad \text{C23}$$

where

$$c = \gamma\left[(P_c + P_A)/\rho\right]^{\frac{1}{2}}$$

6. TRANSFER FUNCTION OF HEAVE MOTION

Substituting the results of C9, C18, C21 and C23, gives

$$\frac{\Delta P_c}{C_{PL} - C_{qi}} = \{\left[C_o V_o (L\Delta h - C_{hw1}\Delta h_w)\right] + C_{Pc}\Delta P_c\} + \left[A_e\Delta\dot{h} - C_{hw_2}\Delta\dot{h}_w\right] + \frac{V_c}{\rho_c{}^2}\Delta\dot{P}_c \qquad \text{C24}$$

Then rearranging C24 gives

$$\Delta P_c\left[\frac{V_c}{\rho_c{}^2}s + C_{Pc} - \frac{1}{C_{PL}-C_{qi}}\right] = \Delta h_w\left[C_{hw2}s + C_o V_o C_{hw1}\right] - \left[A_e s + C_o V_o L\right]\Delta h \qquad \text{C25}$$

If the assumption of the force produced by cushion pressure acting over an area is valid, then

$$A_e\Delta P_c = \Delta F = m\Delta\ddot{h}$$

Hence C25 can be arranged to produce a transfer function,

$$\frac{\Delta h}{\Delta h_w}(s) = \frac{(C_{hw2}s + C_o V_o C_{hw1})}{\frac{mV_c}{\rho A_e c^2}s^3 + \frac{m}{A_e}(C_{Pc} - \frac{1}{C_{PL}-C_{qi}})s^2 + A_e s + C_o V_o L} \qquad \text{C26}$$

N.B. This transfer function is very similar to that given in ref.(26).

NOTATION (Appendix C only)

A,B,C	fan characteristic cinstants
A_d	duct area
A_i	total area of orifice
A_o	Area of leakage gap
B_c	cushion width
C_i	discharge coefficient of orifice
C_o	discharge coefficient of leakage gap
C_{PL}	constant
C_{qi}	constant
c	speed of sound
d	differential operator
g	acceleration due to gravity
h	hover gap
h	heave displacement
h_s	skirt height
h_w	wave amplitude
K_D	loss in the duct
L	cushion length
m_i	mass of input air flow
m_o	mass of output air flow
P_c	cushion pressure
P_L	loop pressure
Q_i	input air flow rate
Q_o	output air flow rate
s	Laplace operator
t	time
V	craft forward velocity
V_c	cushion volumn
x	direction of motion
ρ	air density
ξ	wave surface height
λ	wavelength of wave
ω	wave frequency
ω_e	encounter frequency

APPENDIX D

APPENDIX D

1.0 FREQUENCY TO TIME DOMAIN TRANSFORMATION OF A GENERAL TRANSFER FUNCTION

There are two ways of producing a step or impulse transient response from a transfer function. The use of Runge-Kutta Integration Method requires that the transfer function is realizable by a set of linear time-invariant dynamical equations. These dynamical equations may have the same dimensions as the degree of the transfer function matrix. The other one is Inverse Laplace Transformation (ILT) which requires a subroutine for factorization of the denominator of the transfer function, i.e. finding roots of a characteristics equation. In this way, the transfer function can then be separated into a partial fraction form for ILT to take place.

1.1 REALIZATION OF PROPER RATIONAL TRANSFER FUNCTION

In general, every proper rational transfer function can be written in the form as

$$G(s) = \frac{Y(s)}{U(s)} = d' + \frac{\beta_1 s^{n-1} + \beta_2 s^{n-2} + \ldots\ldots + \beta_n}{s^n + \alpha_1 s^{n-1} + \ldots\ldots\ldots + \alpha_n} \qquad (D.1)$$

$$\equiv d' + \frac{N(s)}{D(s)}$$

Following Chen, Ref (46), the transfer function is realizable by a linear time-invariant dynamical equation of the form

$$\dot{\underline{X}} = A\,\underline{X} + B\,u \qquad (D.2)$$

$$y = C\,\underline{X} + d\,u$$

Then

$$G'(s) = C(sI-A)^{-1}B + d$$

$$= d' + \frac{N(s)}{D(s)} \qquad (D.3)$$

If $d' = d$, the matter is simplified to the form

$$\dot{\underline{X}} = A\,\underline{X} + Bu$$

$$y = C\,\underline{X} \qquad (D.4)$$

Thus

$$G(s) = \frac{Y(s)}{U(s)} = \frac{N(s)}{D(s)}$$

$$= \frac{\beta_1 s^{n-1} + \beta_2 s^{n-2} + \cdots\cdots + \beta_n}{s^n + \alpha_1 s^{n-1} + \cdots\cdots + \alpha_n} \qquad (D.5)$$

Let the state-variable as follows:

$$X_n(t) = y(t)$$

$$X_{n-1}(t) = y'(t) + \alpha_1 y(t) - \beta_1 u(t)$$

$$X_{n-2}(t) = y''(t) + \alpha_1 y'(t) - \beta_1 u'(t) + \alpha_2 y(t) - \beta_2 u(t)$$

$$\vdots$$

$$X_1(t) = y^{(n-1)}(t) + \alpha_1 y^{(n-2)}(t) - \beta_1 u^{(n-2)} + \cdots\cdots + \alpha_{n-1} y(t) - \beta_{n-1} u(t) \qquad (D.6)$$

Then $X = (X_1\ X_2\ \ldots\ldots\ X_n)^T$ is the state vector and thus

$$\begin{aligned} y &= X_n \\ \dot{X}_{n-1} &= \dot{X}_n + \alpha_1 X_n - \beta_1 u \\ \dot{X}_{n-2} &= \dot{X}_{n-1} + \alpha_2 X_n - \beta_2 u \\ &\vdots \\ \dot{X}_1 &= \dot{X}_2 + \alpha_{n-1} X_n - \beta_{n-1} u \end{aligned} \qquad (D.7)$$

Differentiating X_1 in (D.6) gives

$$\dot{X}_1(t) = y^{(n)}(t) + \alpha_1 y^{(n-1)}(t) - \beta_1 u^{(n-1)} + \ldots\ldots + \alpha_{n-1} y'(t) - \beta_{n-1} u(t)$$

so that the derivative of X_1 is

$$\dot{X}_1(t) = -\alpha_n X_n + \beta_n u \qquad (D.8)$$

The foregoing equation can be arranged in matrix form

$$\begin{bmatrix} \dot{X}_1 \\ \dot{X}_2 \\ \vdots \\ \dot{X}_n \end{bmatrix} = \begin{bmatrix} 0 & 0 & \ldots\ldots & 0 & -\alpha_n \\ 1 & 0 & \ldots\ldots & 0 & -\alpha_{n-1} \\ \vdots & & & \vdots & \vdots \\ 0 & 0 & \ldots\ldots & 1 & -\alpha_1 \end{bmatrix} \begin{bmatrix} X_1 \\ X_2 \\ \vdots \\ X_n \end{bmatrix} + \begin{bmatrix} \beta_n \\ \beta_{n-1} \\ \vdots \\ \beta_1 \end{bmatrix} [u] \qquad (D.9)$$

$$y = [0\ 0\ \ldots\ldots\ 0\ \ 1\ ]\ \underline{X}$$

1.2 RUNGE-KUTTA METHOD

If the input signal is a step function, then

$$u(t) = \begin{cases} 1 & (t>0) \\ 0 & (t\leq 0) \end{cases} \qquad \text{(D.10)}$$

The Runge-Kutta Method is employed to integrate equation (D.9) when the step function is applied to the input. Hence, the output y = Xn is the transient response of the transfer function stated in (D.5). In this programme, the integration step is automatically changed in size to ensure the desirable accuracy.

As for an impulse transient response, it can be found from the output time derivative of step response, i.e. the value of $\dot{X}n$ in (D.7).

In the case of inproper transfer function, (D.1), the step transient response will be

$$y' = [0 \quad 0 \ldots\ldots 0 \quad 1][\underline{X}] + d'u \qquad \text{(D.11)}$$

The impulse transient response can be obtained in the same manner as above.

1.3 INVERSE LAPLACE TRANSFORMATION (ILT)

The use of ILT to obtain a transient response from a transfer function can be made. Recall (D.5), the output

$$Y(s) = \frac{N(s)}{D(s)} U(s) \qquad \text{(D.12)}$$

$$= \frac{P(s)}{Q(s)} ,$$

where U(s) is the input in the Laplace form.
When ILT takes place the output becomes

$$y(t) = \mathcal{L}^{-1} Y(s)$$
$$= \mathcal{L}^{-1} \frac{P(s)}{Q(s)} \qquad (D.13)$$

Since P(s) and Q(s) are generally more than first order, application of ILT on (D.12) requires factorization of Q(s). In other words, finding roots from the characteristics equation. The properties of the roots are dependent on the coefficient values of Q(s). The roots may be real, repeated real, complex or even repeated complex. Classification of these roots requires a special subroutine for the operation.

1.4 TRANSIENT RESPONSE OF A TRANSFER FUNCTION WITH REAL ROOTS

If Q(s) is of order n, the characteristic equation (Q(s) = 0) may have n distinct roots, $s_1, s_2, s_3, \ldots\ldots s_n$
Thus

$$Y(s) = \frac{P(s)}{Q(s)}$$
$$= \frac{P(s)}{(s-s_1)(s-s_2)\ldots\ldots(s-s_n)} \qquad (D.14)$$

This may be arranged in the form

$$Y(s) = \frac{A_1}{(s-s_1)} + \frac{A_2}{(s-s_2)} + \ldots\ldots + \frac{A_k}{(s-s_k)} \qquad (D.15)$$
$$+ \ldots\ldots + \frac{A_n}{(s-s_n)}$$

Where the coefficients $A_1, A_2, \ldots\ldots A_n$ are the residues of Y(s) at the corresponding poles, such that

$$A_k = \left|\frac{P(s)}{Q(s)}(s-s_k)\right|_{s=s_k} \qquad (D.16)$$

When ILT is applied to each individual root and summing them together, the output Y(s) becomes in time variant form,

$$y(t) = \sum_{i=1}^{n} A_i e^{s_i t} \qquad \text{for all} \quad t>0 \qquad (D.17)$$

Hence, the transient response is obtained.

1.5 TRANSIENT RESPONSE OF A TRANSFER FUNCTION WITH REPEATED REAL ROOTS

For a polynomial Q(s) which has repeated real roots, the output Y(s) may have the form as

$$Y(s) = \frac{P(s)}{Q(s)} = \frac{P(s)}{(s-s_q)^{\gamma}(s-s_1)(s-s_2)\ldots(s-s_{n-\gamma})}$$

$$= \frac{A_{q\gamma}}{(s-s_q)^{\gamma}} + \frac{A_{q(\gamma-1)}}{(s-s_q)^{\gamma-1}} + \ldots\ldots + \frac{A_{q1}}{(s-s_q)} \qquad (D.18)$$

$$+\frac{A_{\gamma+1}}{(s-s_{\gamma+1})} + \ldots\ldots + \frac{A_n}{(s-s_n)}$$

Where

$$A_{q(\gamma-k)} = \frac{1}{k!}\frac{d^k}{ds^k}\left|(s-s_q)^{\gamma}\frac{P(s)}{Q(s)}\right|_{s=s_q} \qquad (D.19)$$

for $k = 0, 1, \ldots\ldots \gamma-1$

and $$A_k = \left|(s-s_k)\frac{P(s)}{Q(s)}\right|_{s=s_k} \qquad (D.20)$$

for $k = (\gamma+1, \gamma+2, \ldots\ldots n)$

Thus the output Y(s) after ILT becomes

$$y(t) = \left(\sum_{i=1}^{\gamma} \frac{t^{i-1}}{(i-1)!} Aqi \right) e^{s_q t} + \sum_{i=\gamma+1}^{n} A_i e^{s_i t} \qquad (D.21)$$

1.6 TRANSIENT RESPONSE OF A TRANSFER FUNCTION WITH COMPLEX ROOTS

It is quite often that the polynomial Q(s) has complex conjugate roots, i.e. the output Y(s) has the form

$$Y(s) = \frac{A_1 s + A_2}{(s-s_1)(s-s_2)} + \frac{A_3}{s-s_3} + \ldots\ldots + \frac{A_n}{s-s_n} \qquad (D.22)$$

where

$$(A_1 s + A_2)_{s=s_1} = \left| \frac{P(s)}{Q(s)} (s-s_1)(s-s_2) \right|_{s=s_1} \qquad (D.23)$$

and let

$$\frac{A_1 s + A_2}{(s-s_1)(s-s_2)} = \frac{A_1 (s+a)}{(s+a)^2 + \omega^2} \qquad (D.24)$$

Then the output Y(s), after inversion, is

$$y(t) = A_1 e^{-at} \cos\omega t + \sum_{i=3}^{n} A_i e^{s_i t} \qquad (D.25)$$

When $A_1 = 0$, (D.24) may have the form

$$\frac{A_2}{(s-s_1)(s-s_2)} = \frac{A\omega}{(s+a)^2 + \omega^2} \qquad \text{(D.26)}$$

and (2.25) becomes

$$y(t) = Ae^{-at}\sin\omega t + \sum_{i=3}^{n} A_i e^{s_i t} \qquad \text{(D.27)}$$

The possibility of the polynomial having repeated complex conjugate roots is not considered. This is beyond the scope of the report, in fact, it rarely happens in an actual dynamic system.

NOTATION (Appendix D only)

A,B,C	matrices
$A_1, A_2 \ldots A_n$	residues of poles
D(s)	polynomial of denominator
d,d'	constant
e	exponential factor
G'(s)	transfer function
k	number of roots
N(s)	polynomial of numerator
n	integer
s	Laplace operator
$s_1, s_2 \ldots s_n$	roots of characteristic equation
t	time
U(s)	input in Laplace form
$\underline{x}$	state vectors
Y'(s)	output in Laplace form
y	ouyput
$\alpha_1 \ldots\ldots \alpha_n$	coefficient of denominator
$\beta_1 \ldots\ldots \beta_n$	coefficient of numerator
$\mathcal{L}^{-1}$	Inverse Laplace operator
γ	order of multiple roots
ω	natural frequency

APPENDIX E

APPENDIX E

POWELL OPTIMISATION PROCEDURE

STEP 1:

A. Determine $\lambda_1^{(K)}$ by unidimensional search from $z_o^{(K)}$, so that $f[z_o^{(K)} + \lambda_1 s_1^{(K)}]$ is a minimum.

B. Let $z_1^{(K)} = z_o^{(K)} + \lambda_1^{(K)} s_1^{(K)}$

C. Repeat A and B sequentially in each direction, starting always from the last immediate point in the sequence until all the $\lambda_i^{(K)}$, i=1,.....n are determined.

D. The search for $\lambda_o^{(K)}$ to minimise J(z) in the direction $s_n^{(K-1)}$ is taken into account in step 4.

STEP 2:

A. After minimising J(z) in each of the n directions as described in step 1, one additional step of size $[z_K^{(K)} - z_o^{(K)}]$ is taken corresponding to the total progress on the k(th) stage to yield the point $[2z_n^{(K)} - z_o^{(K)}]$

B. A test is then made (see step 3) to ascertain whether or not adding the new direction and dropping an old one decreases the determinant of the search directions.

STEP 3:

A. Let the largest reduction in J(z) in any search direction on the k(th) stage be denoted by

$$\Delta^{(K)} = \text{Max}\,[\,J(z_{i-1}^{(K)}) - Jz_i^{(K)}\,], \text{ for } i=1....n$$

B. Let

$$J_1 = J(z_o^{(K)}) \ ,$$

$$J_2 = J(z_n^{(K)}) \ , \text{ and}$$

$$J_3 = J(2z_n^{(K)} - z_o^{(K)})$$

where

$$z_o^{(K)} = Z_n^{(K-1)} \ ,$$

$$z_n^{(K)} = z_{n-1}^{(K)} + \lambda_n^{(K)} s_n^{(K)}$$

$$= z_o^{(K)} + \sum_{i=1}^{n} \lambda_i^{(K)} s_i^{(K)}$$

C. Test

$$J_3 \geqslant J_1 \qquad \text{and/or}$$

$$[J_1 - 2J_2 + J_3][J_1 - J_2 - \Delta^{(K)}] \geqslant 0.5\Delta^{(K)}[J_1 - J_3]^2$$

STEP 4:

A. If step 3 not satisfied, the direction $s^{(K)}$ from $z_o^{(K)}$ to $z_n^{(K)}$ is searched for the minimum of $J(z)$ which will be used as the starting point for the next stage, (k+1).

B. At (k+1) stage, the directions to be used are

$$[s_1^{(k+1)}, s_2^{(k+1)} .....s_n^{(k+1)}] = [s_1^{(k)}, s_2^{(k)} .... \\ ...s_{m-1}^{(k)}, s_{m+1}^{(k)}, s_n^{(k)}]$$

STEP 5:

A. A satisfactory convergence criterion for the Powell method is to terminate the search at the end of any stage in which the change in each independent variable is less than the required accuracy,

$$\frac{z_i^{(k+1)} - z_i^{(k)}}{z_i^{(k)}} < \varepsilon \qquad \text{for } i=1,\ldots.n$$

or for

$$||z_n^{(k)} - z_o^{(k)}|| \leq 0.1\varepsilon$$

B. If A is satisfied, programme stop at this point, minimum of J(z) is obtained, otherwise return to step 1 to repeat the process.

APPENDIX F

APPENDIX F

A MODIFIED VERSION OF HEAVE DYNAMIC MODEL. REF.(26)

In (26), the transfer-function $(h/h_w)(s)$ includes the pitching effect of the model craft. Since its effect is, in this case, being ignored the $(h/h_w)(s)$ is thus modified to

$$\frac{h}{h_w}(s) = \frac{(A_e s + G)}{\frac{m}{C_B A_e}s^3 - \frac{mR}{A_e}s^2 + A_e s + G} \qquad (F.1)$$

where C_B is the adiabatic stiffness $(P_c+P_A)\gamma/V_c$,

A_e is the cushion area,

m is the craft mass,

G is the heave dependent leakage parameter, discharge coefficient,

R is the fan conductance.

APPENDIX G

APPENDIX G

WIENER OPTIMAL FILTERING THEORY, REF(71)

Suppose a signal p(t) is added to a noise q(t) to produce a process r(t), i.e.

$$r(t) = p(t) + q(t) \qquad G1$$

Here p(t) and q(t) are statistically independent, stationary, stochastic processes with zero mean and rational spectral densities. Suppose r(t) is fed into a linear, time-invariant, filter with transfer function H(s) and output f(t). The filtering problem is to find the physically realisable filter which minimises the mean-square-error,

$$\overline{e^2} = \overline{(f - p)^2} \qquad G2$$

between filter output f(t) and signal p(t) when the system is in stochastic steady state.

The problem can be formulated in the frequency domain as follows. Let the spectral densities of signal, noise and error be $\phi_p(\omega)$, $\phi_q(\omega)$, and $\phi_e(\omega)$, then

$$\overline{e^2} = \frac{1}{2\pi}\int_{-\infty}^{\infty} \phi_e(\omega)\,d\omega \qquad G3$$

$$= \frac{1}{2\pi}\int_{-\infty}^{\infty} [\,|1 - H(j\omega)|^2 \phi_p(\omega) + |H(j\omega)|^2 \phi_q(\omega)]\,d\omega \qquad G4$$

The problem reduces to finding the transfer function H(s) which minimises in G4, subject to the restriction that H(s) has all its poles in the left hand half-plane.

$$R_e s < 0 \qquad \text{G5}$$

Wiener's solution is to let the spectral densities of the signal plus noise be

$$\phi_r(\omega) = \phi_p(\omega) + \phi_q(\omega) \qquad \text{G6}$$

This can be factorised into the form

$$\phi_r(\omega) = |\psi(j\omega)|^2 = \psi(j\omega)\psi(-j\omega) \quad , \qquad \text{G7}$$

where $\psi(s)$ has all its poles and zeros in the left hand plane. Then the optimal transfer function is

$$H(s) = \frac{\phi_p(s)}{\psi(s)\psi(-s)} \qquad \text{G8}$$

Table 5.1 Experimental data

h_n	$\alpha = 0^0$					$\alpha = 5^0$					$\alpha = 10^0$					$\alpha = 15^0$					$\alpha = 20^0$				
	P_f	P_L	P_c	Q	L	P_f	P_L	P_c	Q	L	P_f	P_L	P_c	Q	L	P_f	P_L	P_c	Q	L	P_f	P_L	P_c	Q	L
Cm	KPa	KPa	KPa	m^3/s	KN	KPa	KPa	KPa	m^3/s	KN	KPa	KPa	KPa	m^3/s	KN	KPA	KPa	KPa	m^3/s	KN	KPa	KPa	KPa	m^3/s	KN
+7	0.57	0.49	0.05	0.32	0.06	1.06	0.94	0.1	0.45	0.15	1.55	1.31	0.14	0.524	0.25	1.87	1.58	0.17	0.58	0.29	2.04	1.78	0.19	0.61	0.35
+6	0.62	0.49	0.16	0.28	0.2	1.09	0.95	0.26	0.4	0.37	1.58	1.34	0.35	0.48	0.52	1.89	1.6	0.43	0.52	0.60	2.07	1.79	0.47	0.56	0.68
+5	0.66	0.59	0.33	0.25	0.3	1.09	1.0	0.48	0.35	0.51	1.61	1.51	0.71	0.43	0.74	1.92	1.79	0.83	0.48	0.88	2.01	1.9	0.9	0.185	0.91
+4	0.85	0.7	0.45	0.24	0.6	1.45	1.25	0.5	0.42	0.97	2.0	1.6	0.85	0.42	1.12	2.3	2.0	1.05	0.47	1.25	2.42	2.25	1.21	0.49	1.51
+3	0.86	0.75	0.52	0.23	0.76	1.44	1.31	0.98	0.28	1.21	1.87	1.75	1.21	0.36	1.43	2.3	2.13	1.47	0.39	1.78	2.44	2.31	1.56	0.42	1.96
+2	0.92	0.9	0.78	0.17	0.87	1.49	1.31	1.12	0.21	1.27	2.0	2.0	1.73	0.25	1.87	2.35	2.38	1.99	0.3	2.18	2.64	2.63	2.16	0.33	2.41
+1	1.0	0.94	0.87	0.13	1.02	1.58	1.38	1.3	0.14	1.29	2.15	2.06	1.9	0.19	2.18	2.44	2.38	2.16	0.23	2.54	2.73	2.68	2.42	0.24	2.67
0	1.15	1.0	0.9	0.15	1.16	1.7	1.65	1.4	0.24	1.61	2.3	2.15	2.1	0.11	2.41	2.6	2.5	2.4	0.15	2.81	2.85	2.7	2.7	0	3.07
-1	1.03	1.06	1.0	0.12	1.25	1.81	1.9	1.85	0.11	2.22	2.3	2.38	2.25	0.17	2.58	2.64	2.63	2.48	0.19	3.03	2.87	2.94	2.85	0.15	3.34
-2	1.09	1.06	1.04	0.069	1.34	1.87	1.94	1.9	0.097	2.28	2.35	2.38	2.28	0.15	2.72	2.73	2.69	2.6	0.145	3.21	3.01	3.0	2.89	0.16	3.56
-3	1.15	1.13	1.12	0.048	1.43	1.95	1.98	1.85	0.17	2.36	2.44	2.5	2.34	0.19	2.76	2.85	2.75	2.68	0.14	3.34	3.16	3.13	2.94	0.21	3.70
-4	1.3	1.25	1.15	0.15	1.32	2.0	2.0	1.9	0.15	2.18	2.6	2.5	2.4	0.15	2.81	2.85	2.8	2.75	0.11	3.25	3.65	3.5	3.1	0.31	3.65

Table 8.1 Optimum filter coefficients as a function of different Beaufort numbers

Beaufort number	wave height	K_s	a_1	a_2	a_3	a_4
4	1.1	0.553	1.364	4.698	2.353	3.766
5	2.0	0.824	1.237	2.865	1.200	1.300
6	3.1	0.965	1.041	1.893	0.653	0.558
7	4.5	1.117	0.911	1.322	0.394	0.268
8	6.7	1.223	0.741	0.889	0.215	0.121
9	9.2	1.341	0.641	0.648	0.135	0.064
10	12.3	1.473	0.569	0.484	0.0895	0.0354
11	15.5	1.338	0.439	0.3566	0.0538	0.0202

Table 8.2 Modulus of transfer functions as a function of frequency

ω rad/s	$\lvert D(j\omega)\rvert$	$\lvert P(j\omega)\rvert$
0.1	1.483×10^{-3}	1.0
0.25	9.12×10^{-3}	1.0
0.5	4.901×10^{-2}	1.0
1.0	0.558	1.0
2.5	0.166	1.009
5.0	2.568×10^{-2}	1.17
10.0	5.743×10^{-3}	1.17
26.0	8.226×10^{-4}	3.3
50.0	2.204×10^{-4}	0.421

Table 8.3 Numerical data for $\phi_u(\omega)$ calculation

ω rad/s	A $\lvert P(j\omega)D(j\omega)\rvert^2$	B $\lvert M(j\omega)\rvert^2\left[1+\frac{\lambda}{\lvert P(j\omega)\rvert^2}\right]$	C $\lvert H(j\omega)\rvert^2=\frac{A}{A+B}$	D $\lvert D(j\omega)\rvert+\lvert\frac{M(j\omega)}{P(j\omega)}\rvert^2$	$\phi_u(\omega)$ = C.D	λ = 0.0 $20\log_{10}\sqrt{\phi_u(\omega)}$
0.1	2.2×10^{-6}	$0.001+0.001\lambda$	$\frac{2.2\times10^{-6}}{0.001+0.001\lambda}$	0.001	$\frac{2.2\times10^{-9}}{0.001+0.001\lambda}$	-56
0.25	9.8×10^{-5}	$0.001+0.001\lambda$	$\frac{9.8\times10^{-5}}{0.001+0.001\lambda}$	0.001	$\frac{9.8\times10^{-5}}{0.001+0.001\lambda}$	-40
0.5	2.4×10^{-3}	$0.001+0.001\lambda$	$\frac{2.4\times10^{-3}}{0.0034+0.001\lambda}$	3.4×10^{-3}	$\frac{8.6\times10^{-6}}{0.0034+0.001\lambda}$	-26
1.0	0.311	$0.001+0.001\lambda$	$\frac{0.0311}{0.311+0.001\lambda}$	0.311	$\frac{0.097}{0.311+0.001\lambda}$	-5.0
2.5	0.0275	$0.001+0.001\lambda$	$\frac{0.0275}{0.0285+0.001\lambda}$	0.285	$\frac{7.8\times10^{-4}}{0.0285+0.001\lambda}$	-15.6
5.0	6.59×10^{-4}	$0.001+0.001\lambda$	$\frac{6.59\times10^{-4}}{0.001+0.001\lambda}$	0.026	$\frac{1.7\times10^{-5}}{0.001+0.001\lambda}$	-30.0
10.0	4.44×10^{-5}	$0.001+7.3\times10^{-4}\lambda$	$\frac{4.44\times10^{-5}}{0.001+7.3\times10^{-4}\lambda}$	9.57×10^{-4}	$\frac{4.25\times10^{-8}}{0.001+7.3\times10^{-4}\lambda}$	-43.7
26.0	7.36×10^{-6}	$0.001+9.18\times10^{-5}\lambda$	$\frac{7.36\times10^{-6}}{0.001+9.18\times10^{-5}\lambda}$	1.09×10^{-3}	$\frac{8.0\times10^{-9}}{0.001+9.18\times10^{-5}\lambda}$	-61.0
50.0	8.53×10^{-9}	$0.001+5.66\times10^{-3}\lambda$	$\frac{8.53\times10^{-9}}{0.001+5.66\times10^{-3}\lambda}$	5.66×10^{-3}	$\frac{4.83\times10^{-11}}{0.001+5.6\times10^{-3}\lambda}$	-73.0

Table 9.1 Criteria attributes and shortcomings

Criteria	Attributes	Shortcomings
As good As (AGA)	Related to known vehicles and response of passengers to rides of these vehicles Easy to specify Covers all factors of enviroment	Determination of compliance difficult Uncertain Application to new vehicle types Cost/Benefit trade difficult
Not-to-Exceed (1974 ISO-2631 standards)	Easy to specify values Frequency vs. acceleration curve shape not arbitrary Easy to verify compliance	Go/No-Go limits Limited to vibration Applies to linear degrees of freedom only>1.0Hz Frequency vs. acceleration curve level arbitrary
Output-to-Input Relationship	Easy to express vehicle specifications Easy to verify compliance	Specifications not directly related to ride comfort

Table 9.2 Ride discomfort index limits

Ride Discomfort Index, D_i		Flight Phase Duration (exposure Time)	Probability of Exceeding rms Turbulence Intensity
Long Term Requirement	0.10	Over 3 Hours	0.20
	0.13	From 1.5 to 3 Hours	0.20
	0.20	From 0.5 to 1.5 Hours	0.20
Short Term Requirement	0.28	Less than 0.5 Hour	0.01

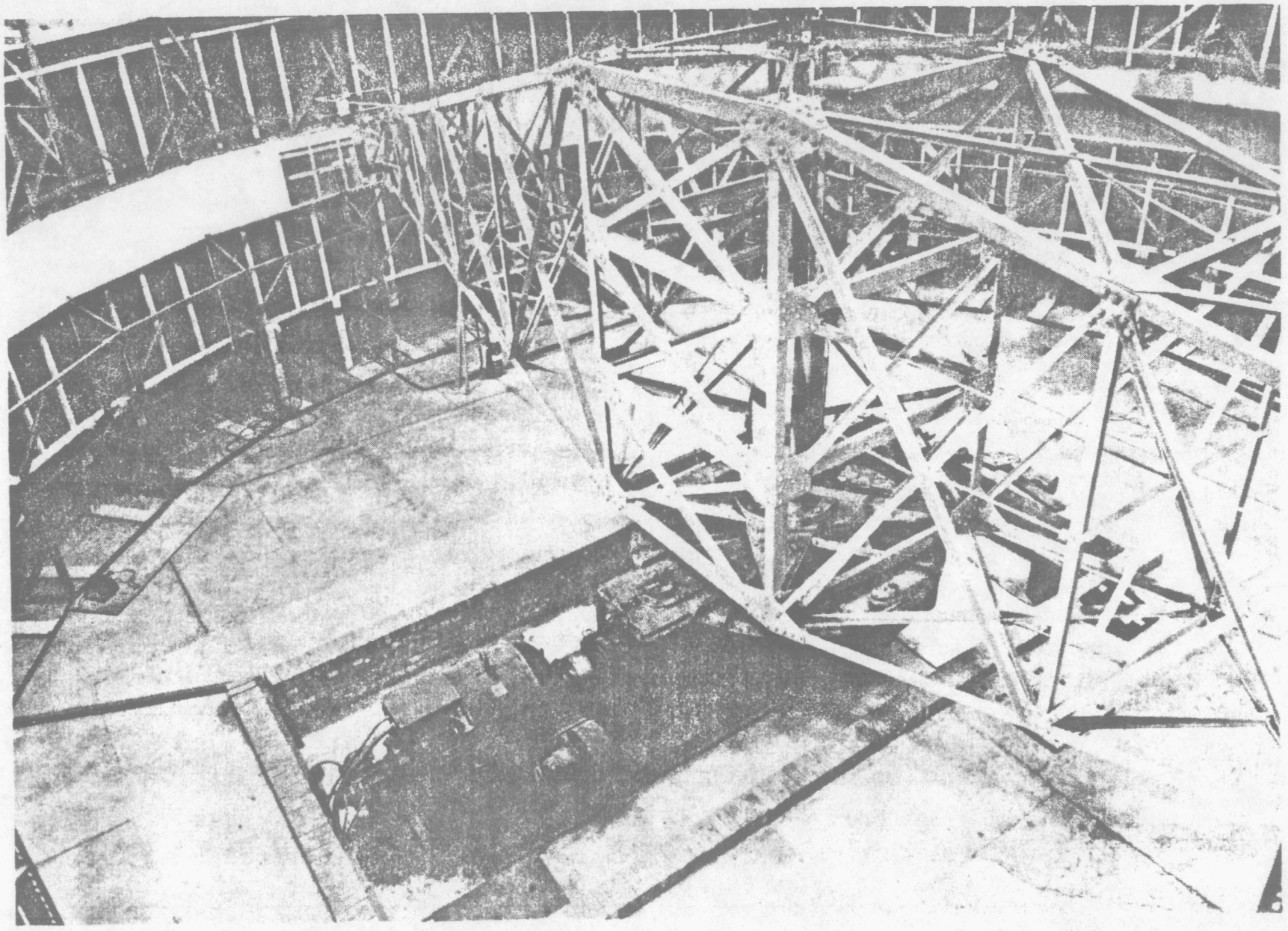

Fig.1.1 General view of the Whirling Arm facility.

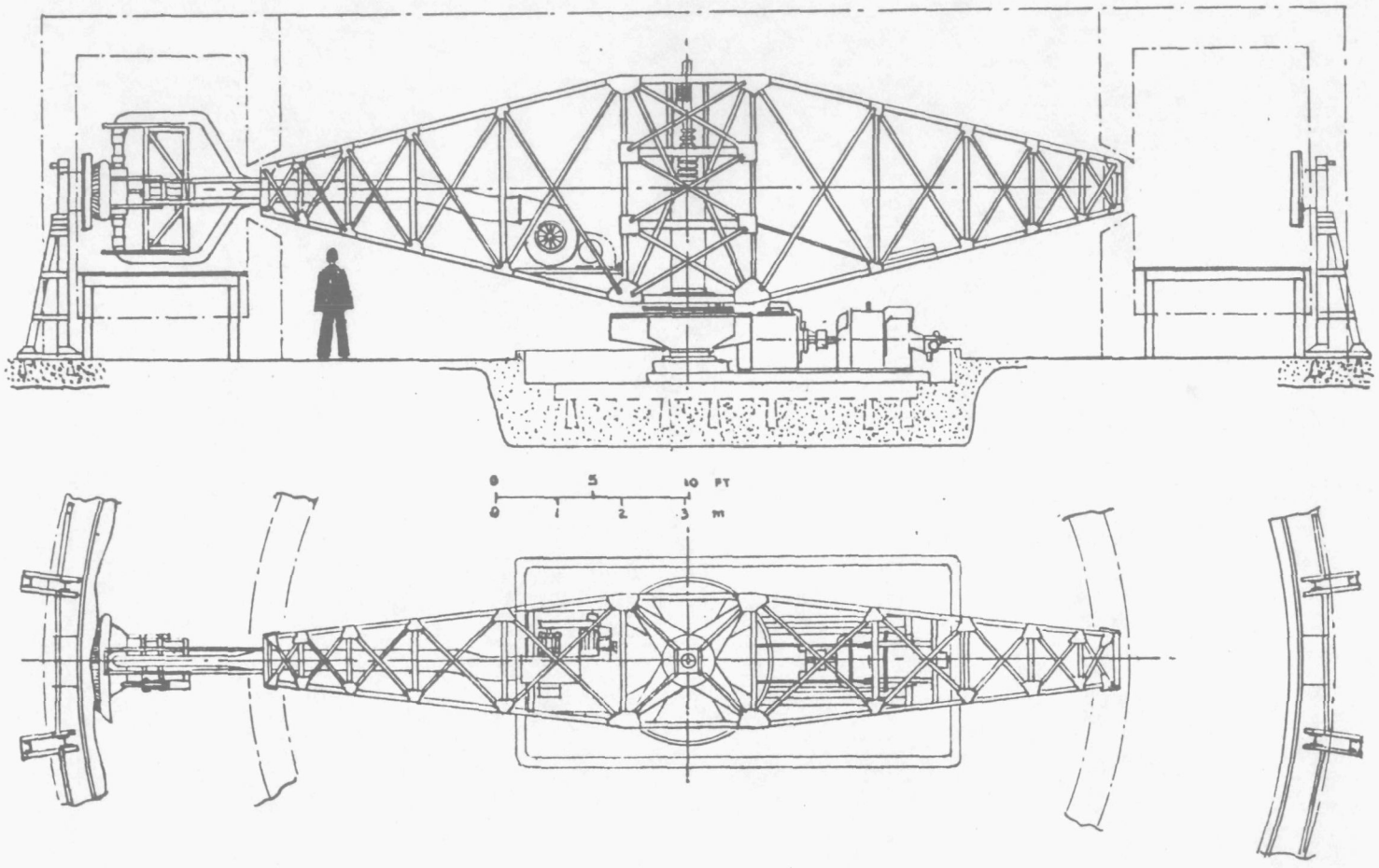

Fig.1.2 General veiw of Whirling-Arm for hovercraft research

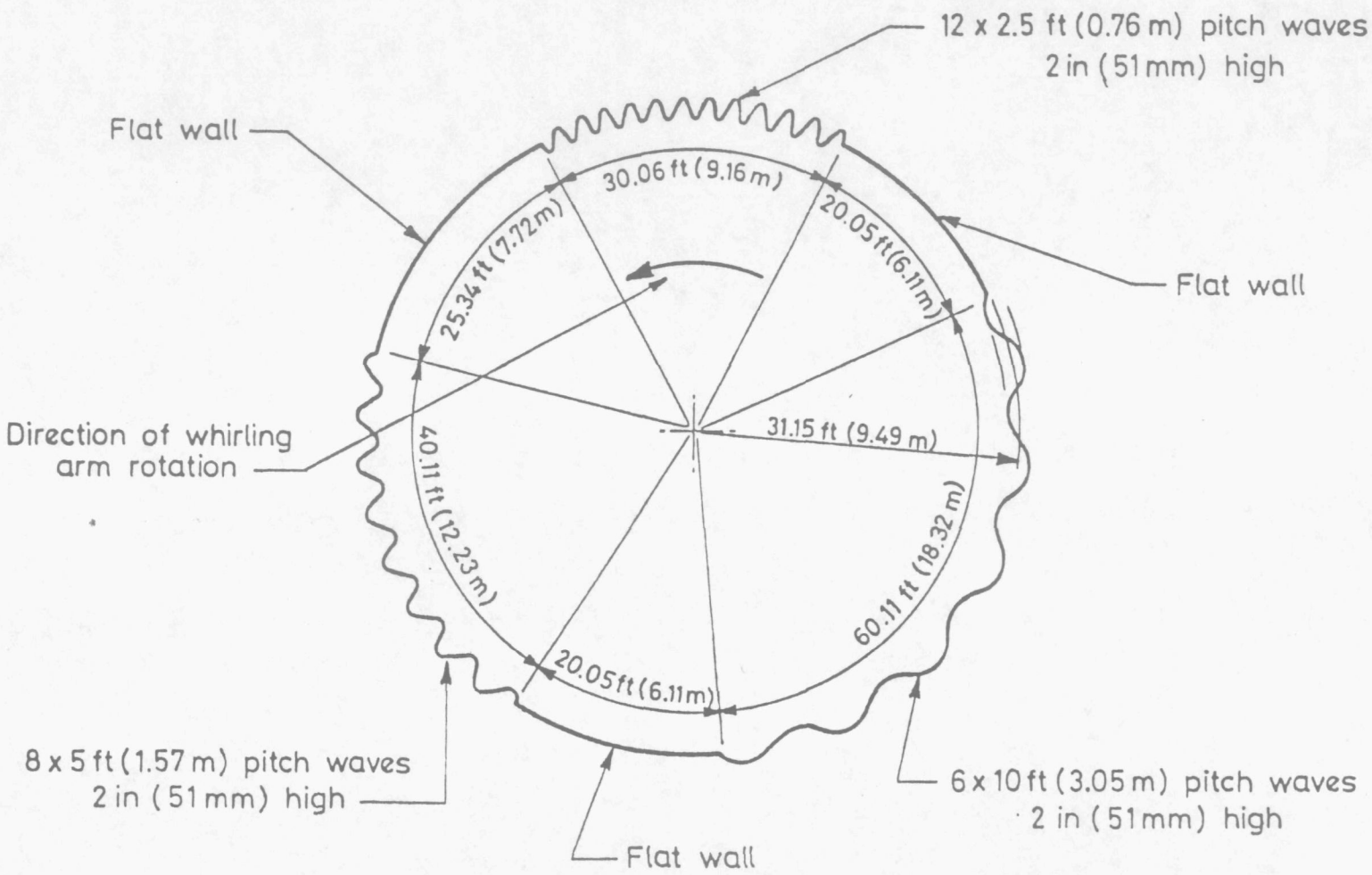

Fig.1.3 Disposition of waves.

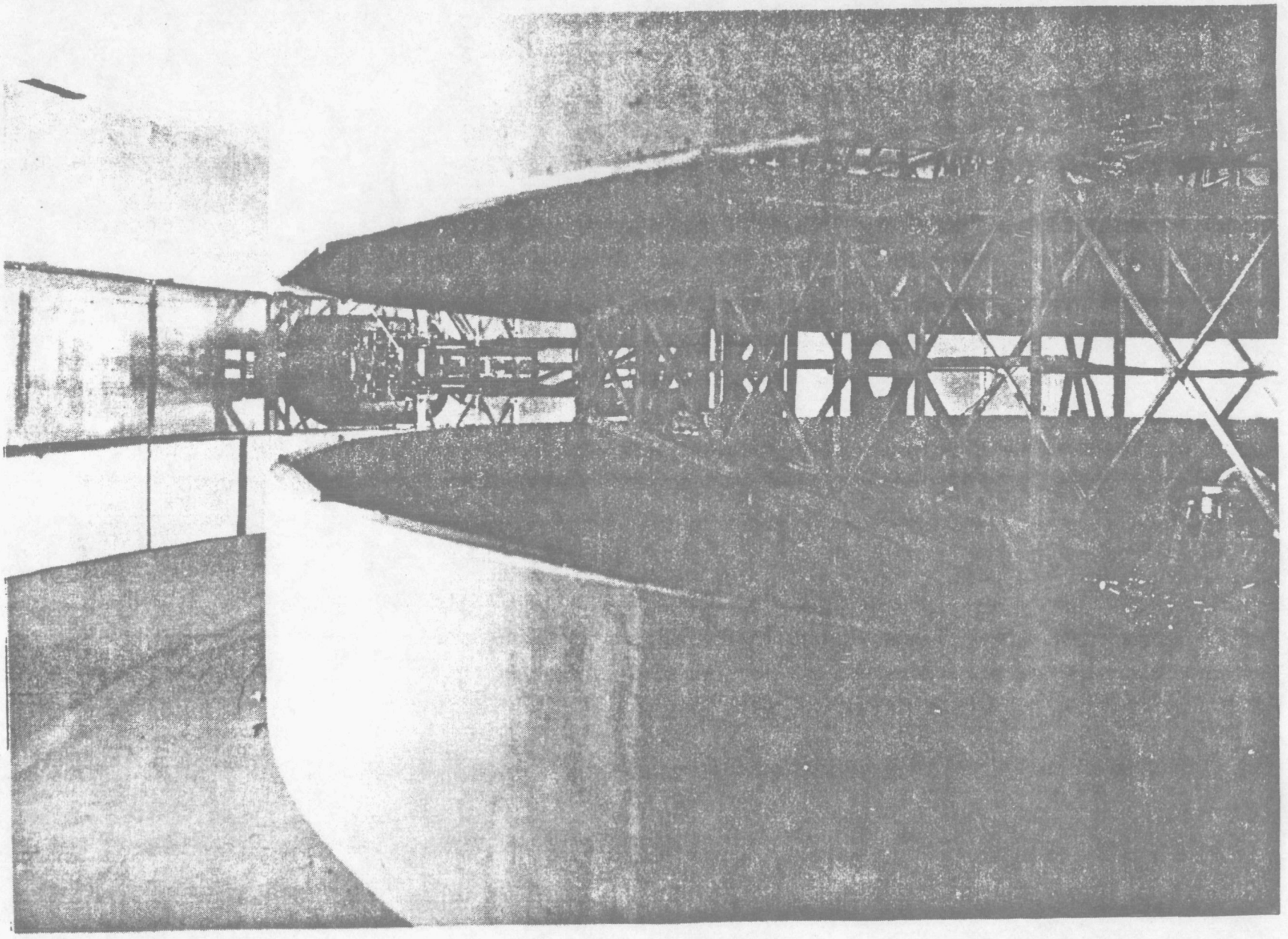

Fig. 1.4 General view of the modified whirling arm.

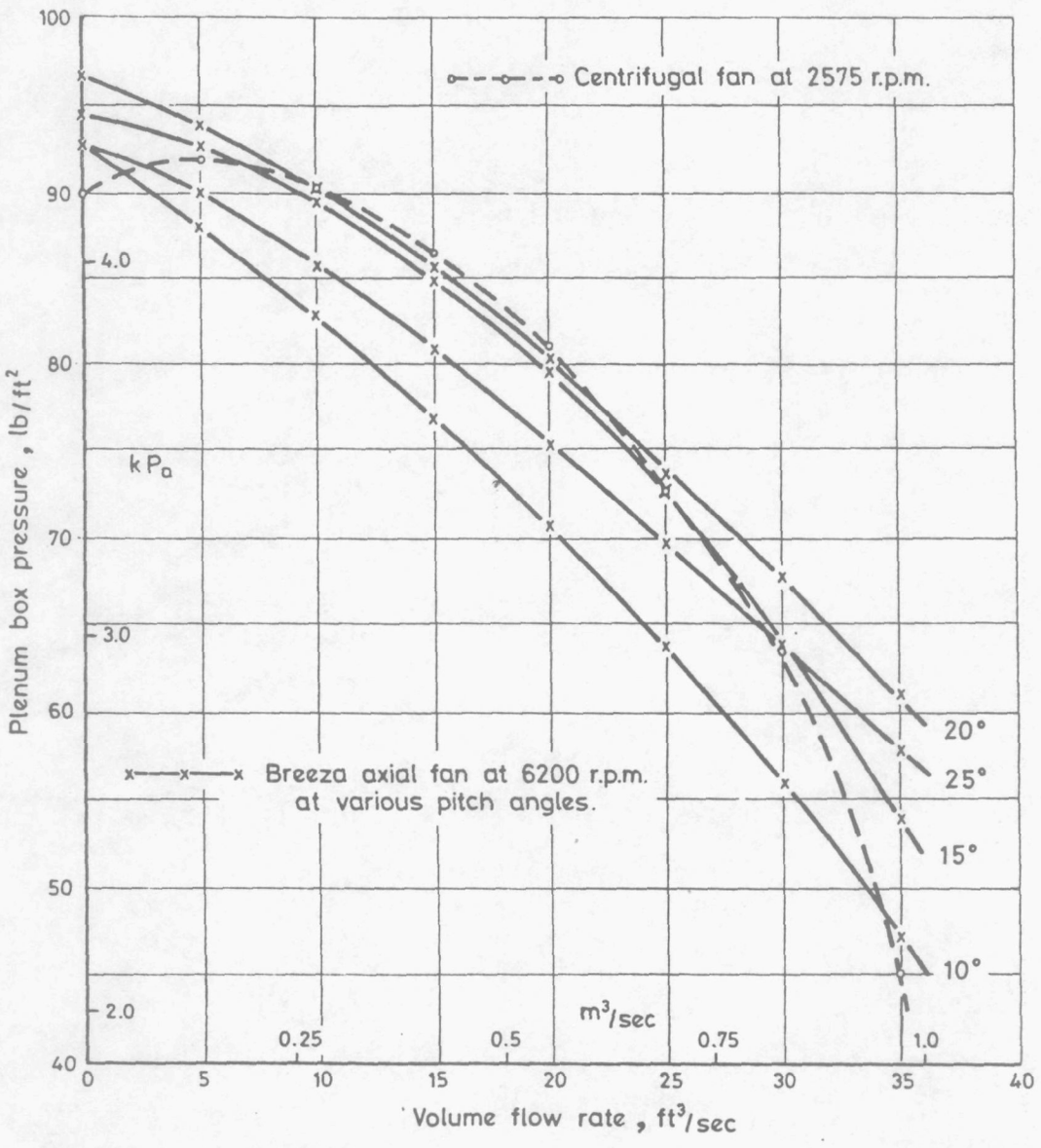

Fig.1.5 Comparison of the former static fan characteristics to that of the present rig

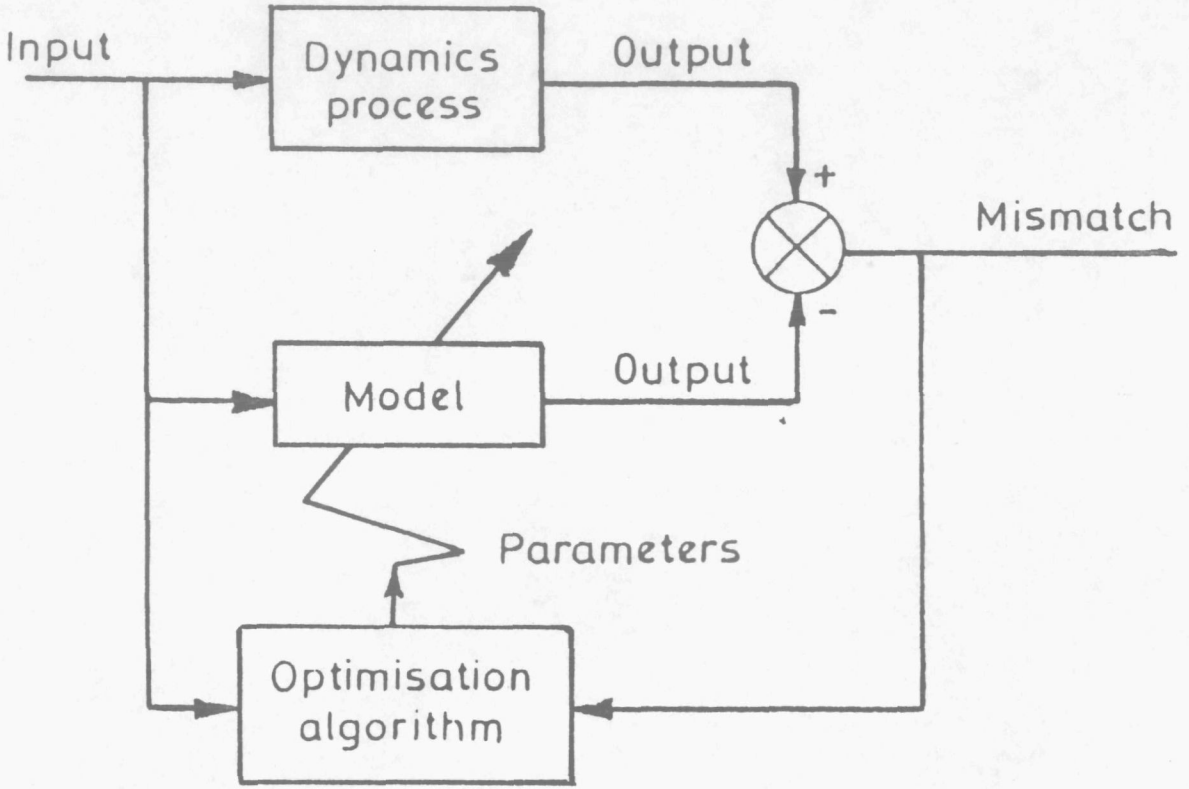

Fig. 1.6 Identification of dynamic process

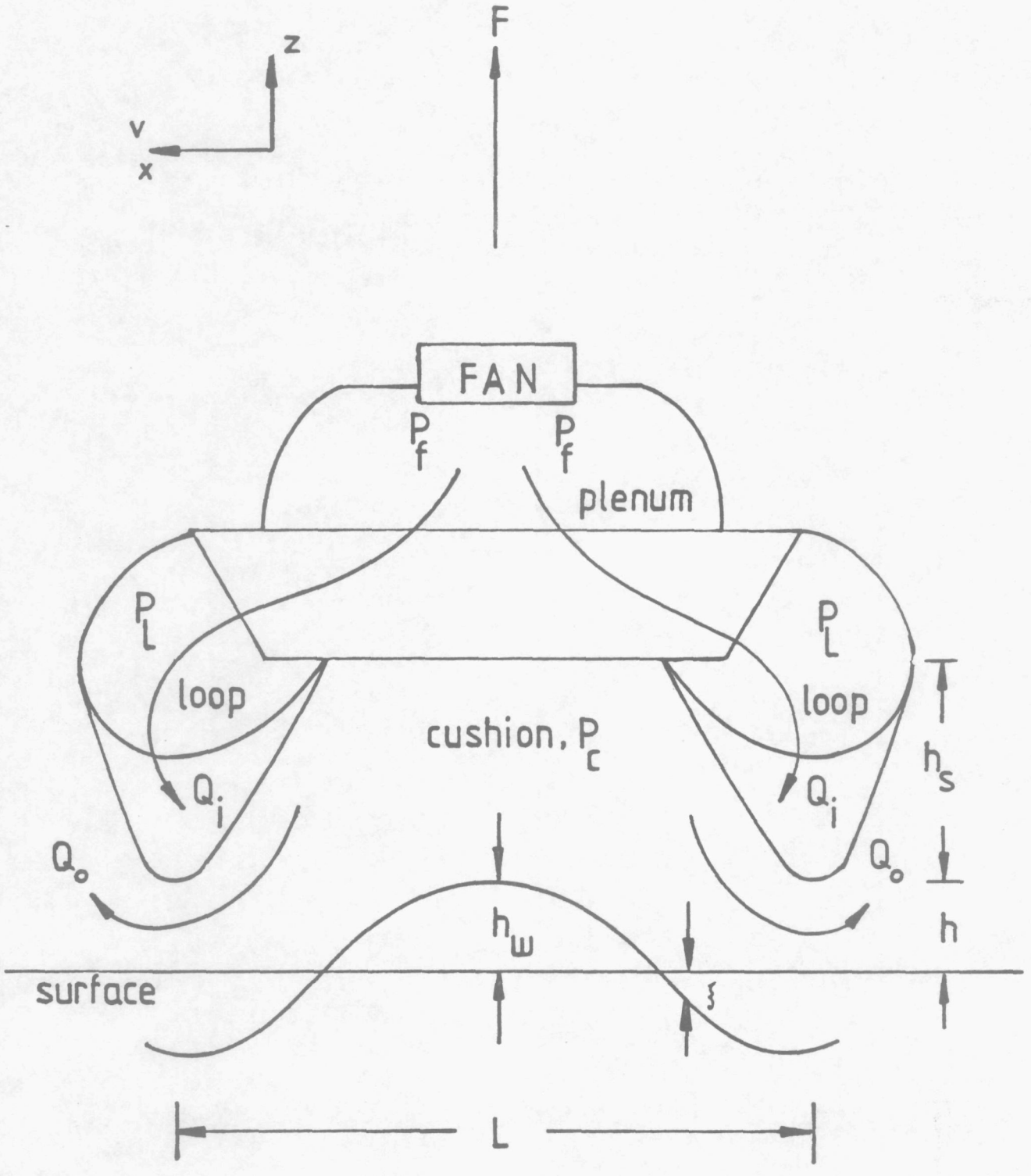

Fig. 2.1 Pressurised flexible skirt

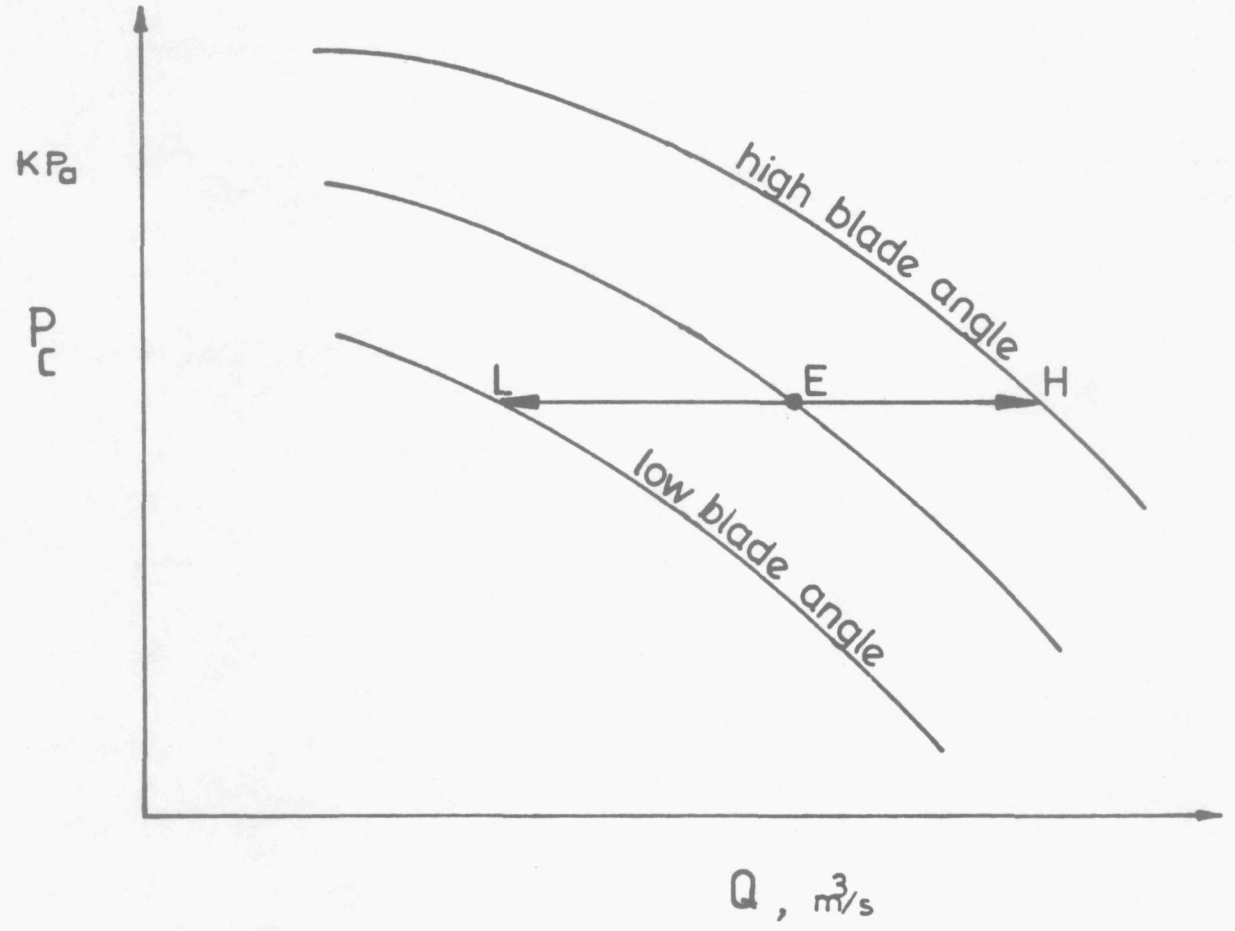

Fig. 2.2 Cushion pressure and flow rate variation due to blade angle changes

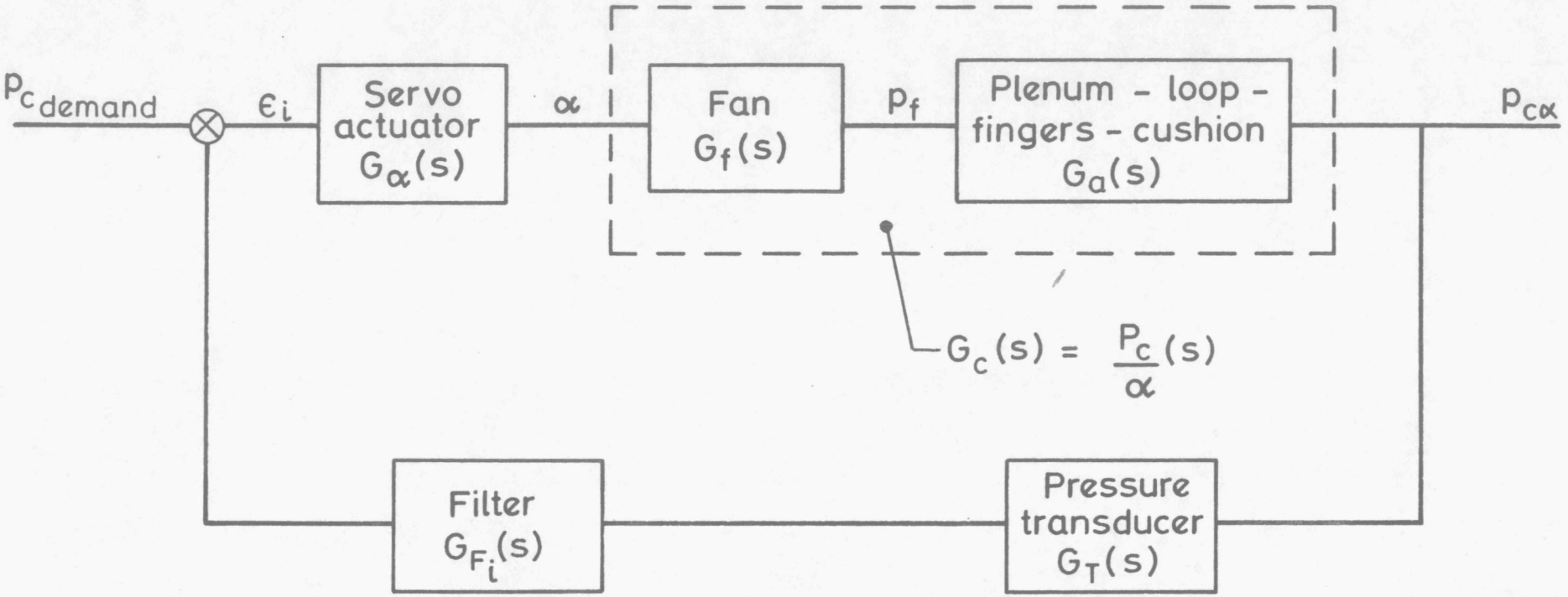

Fig. 2.3 Inner loop

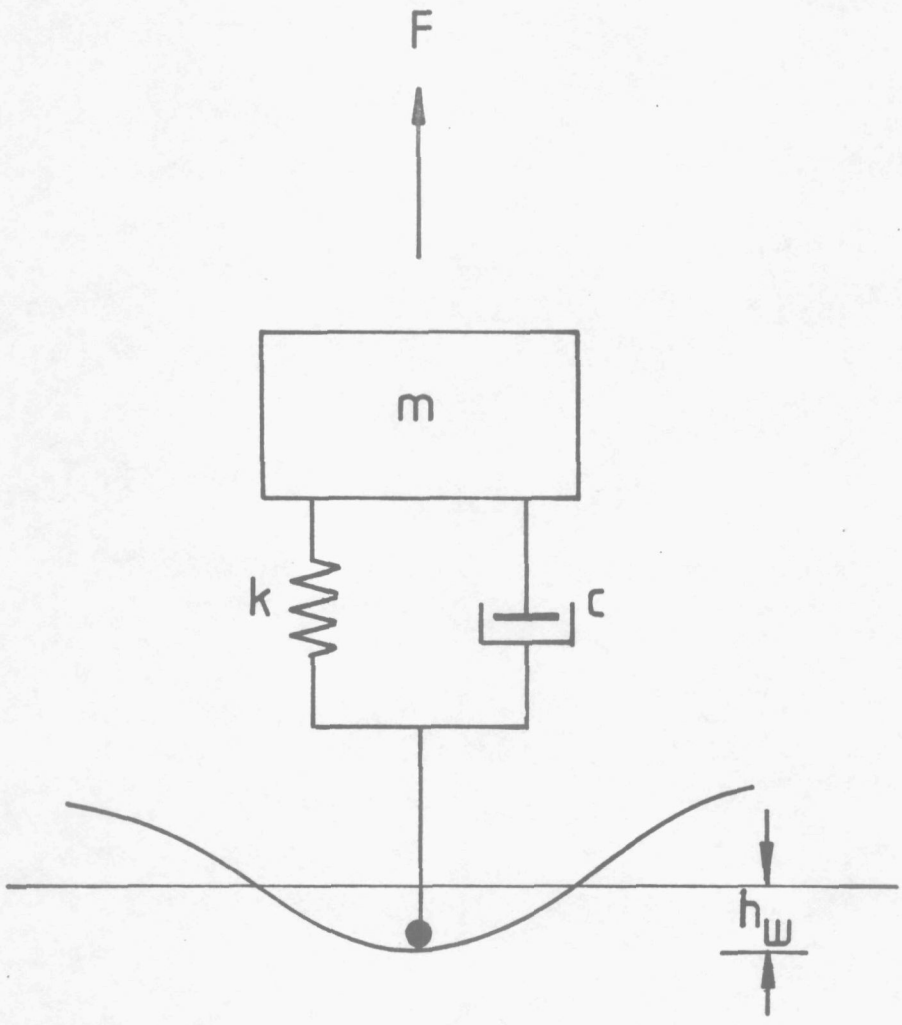

Fig. 2.4 Point mass floating on a surface

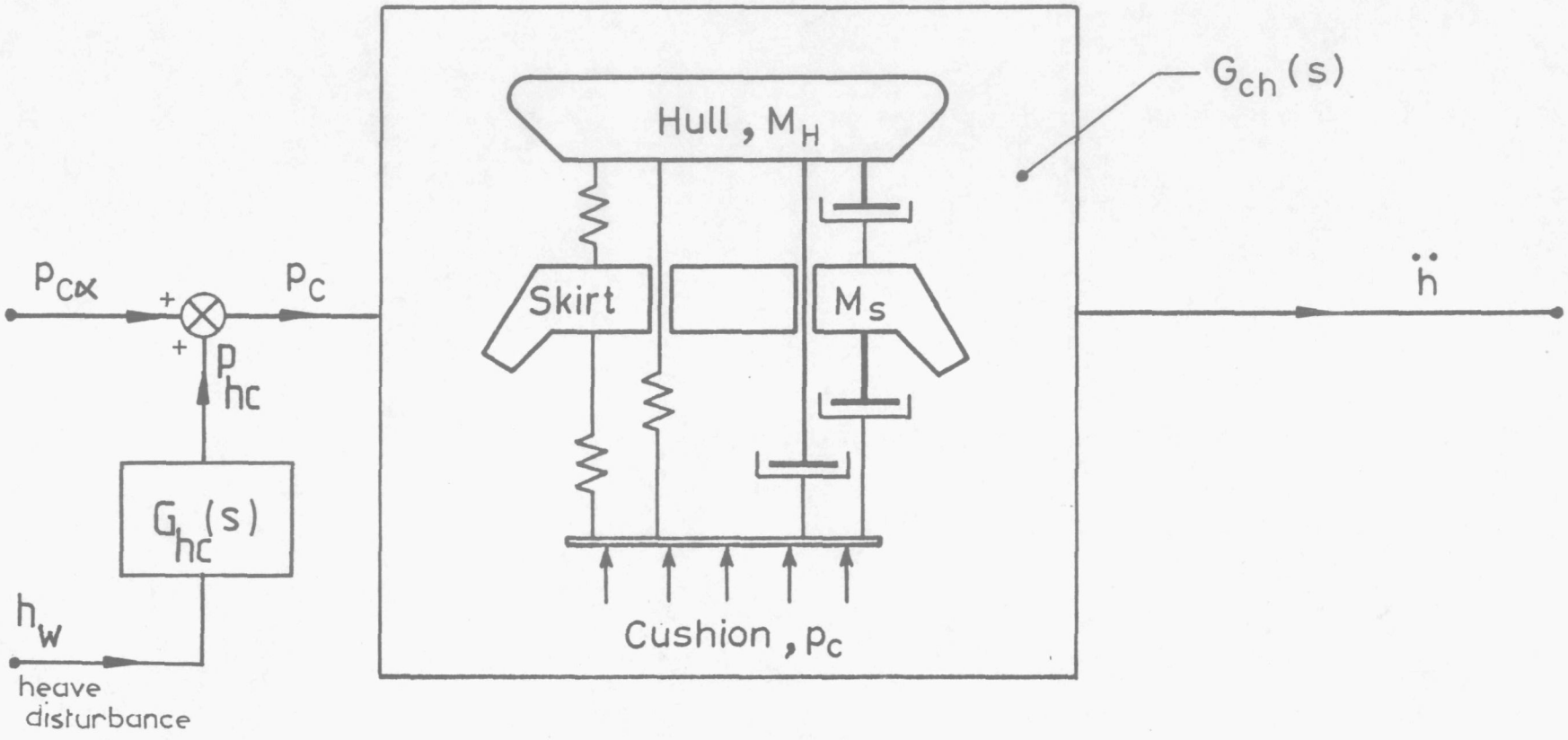

Fig. 2.5 Craft - cushion dynamics

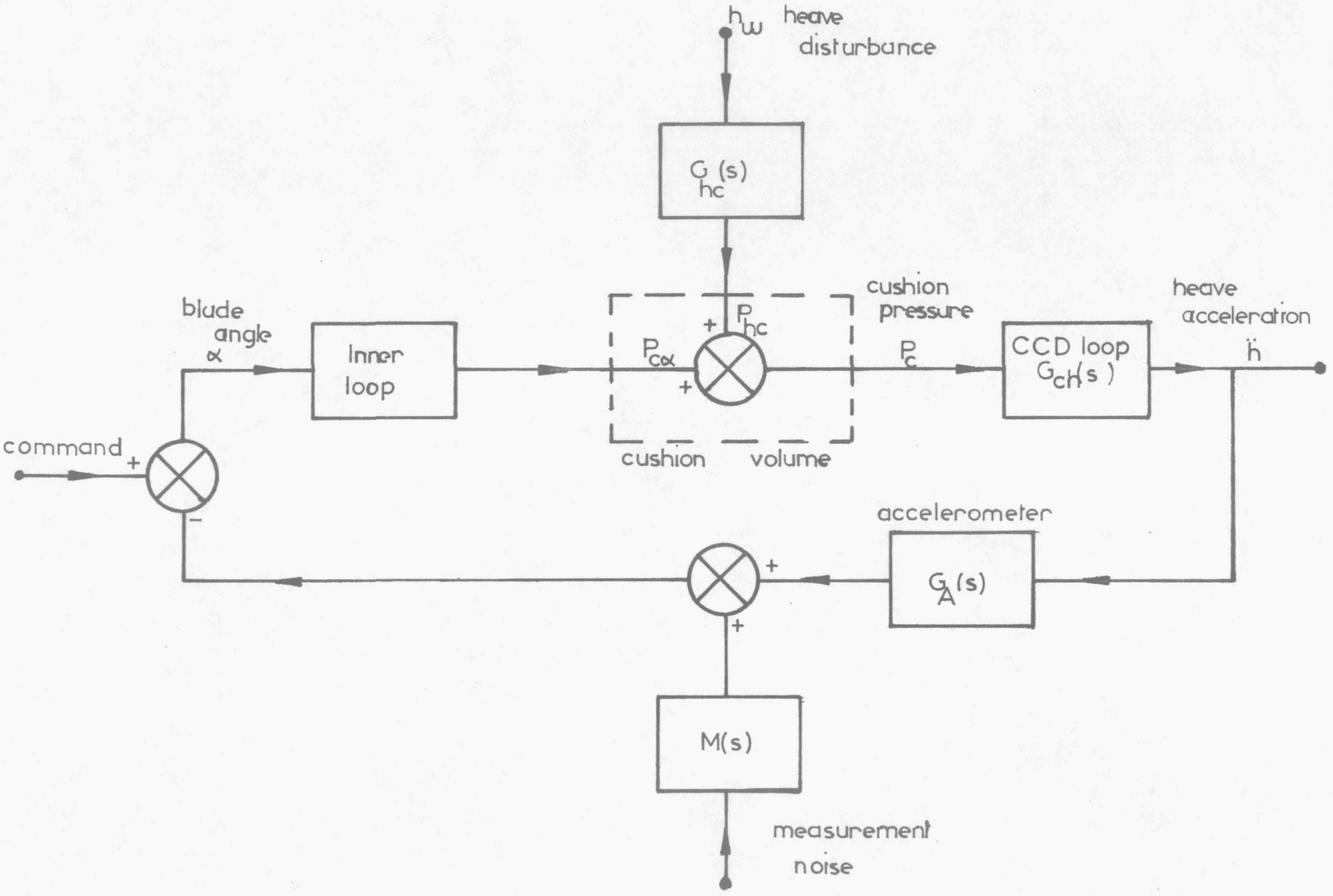

Fig. 2.6 Overall heave control system

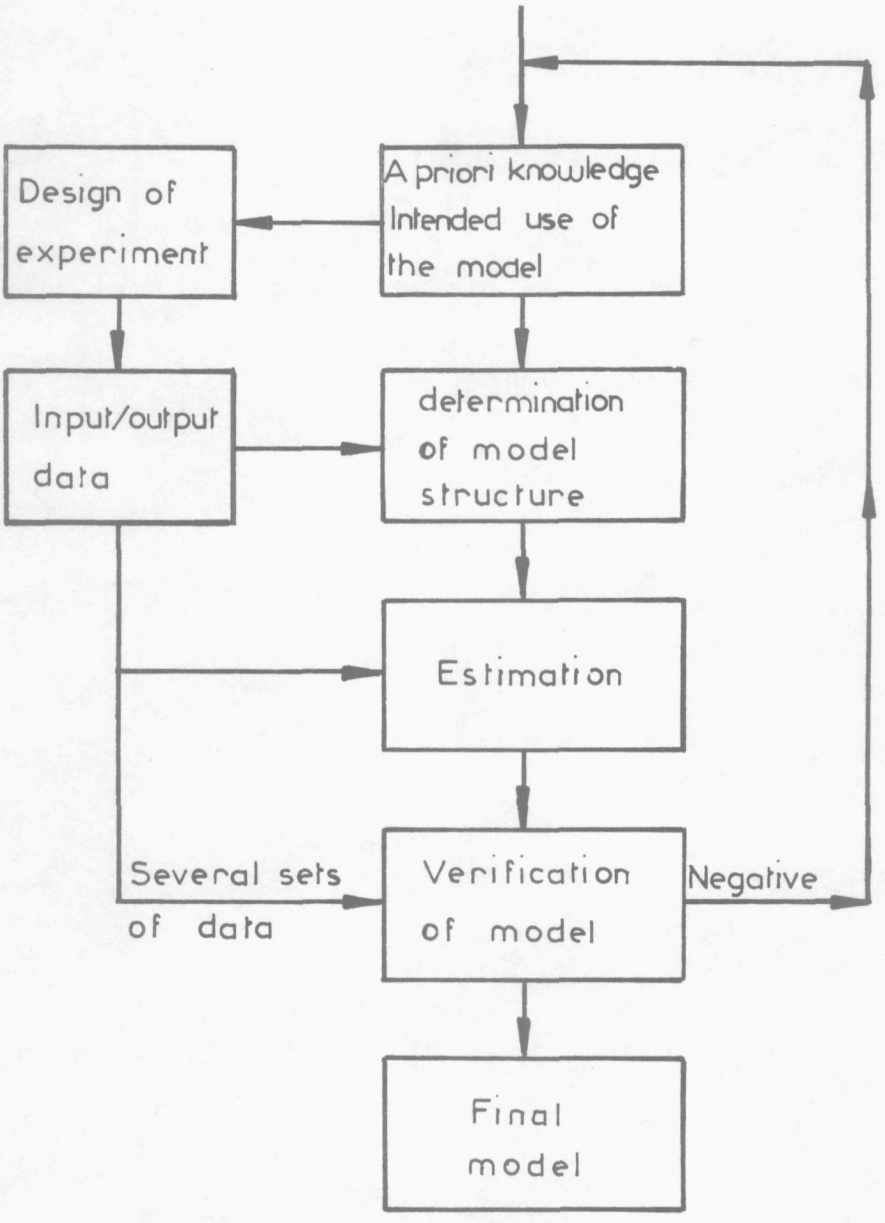

Fig. 3.1 Parameter identification procedures

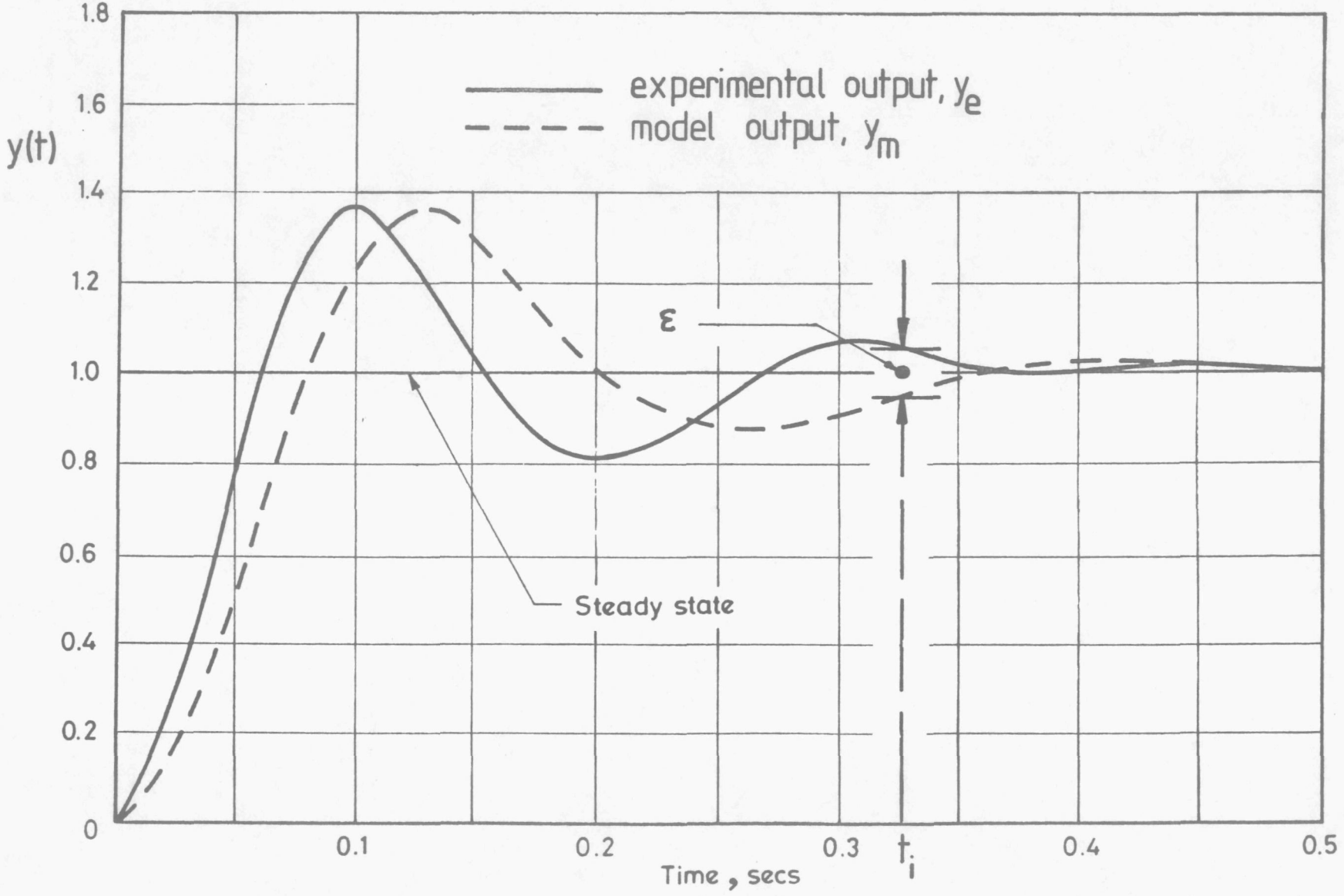

Fig. 3.2 Cost function development

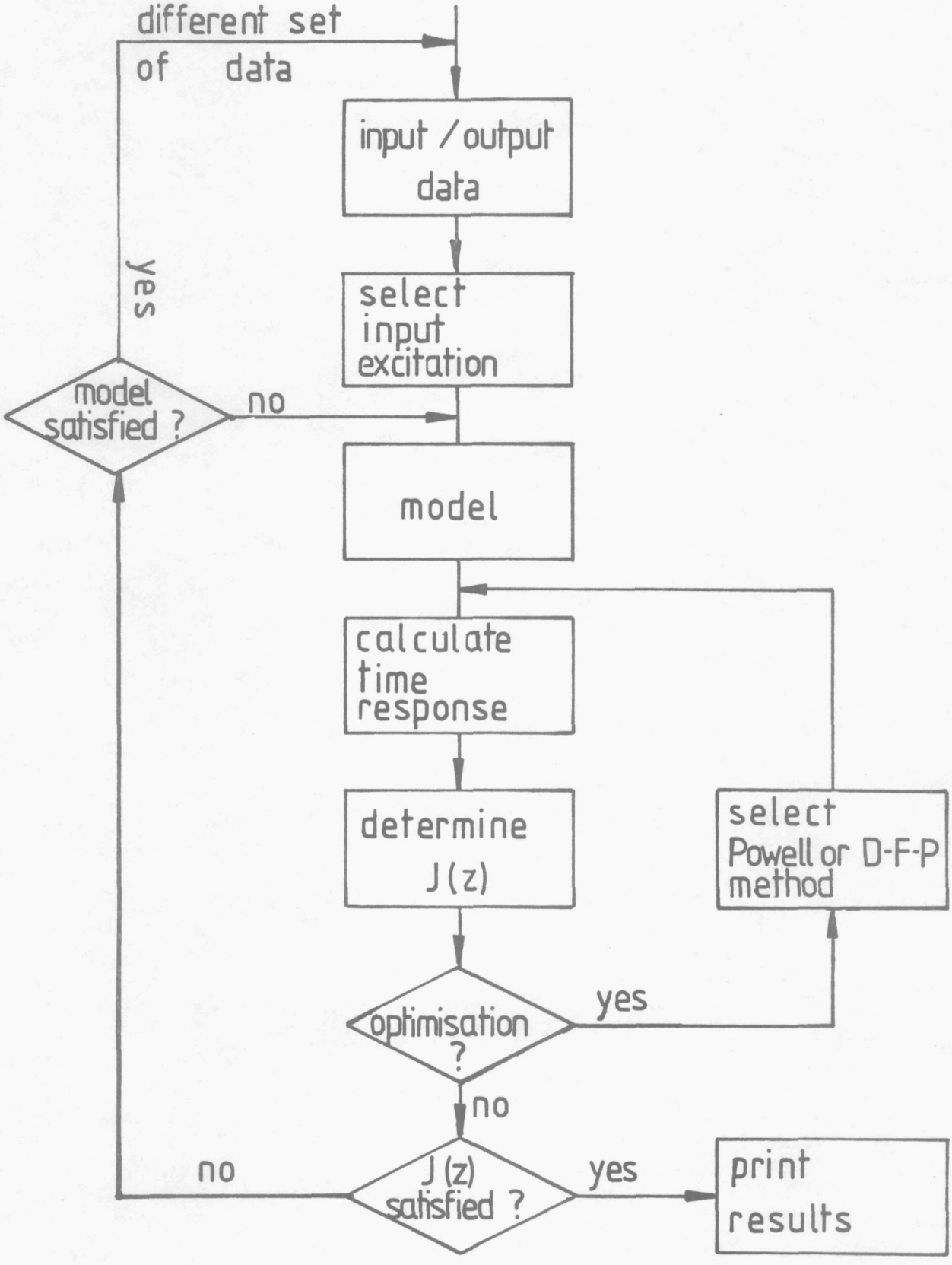

Fig. 3.3 Flow chart diagram for parameter identification procedures

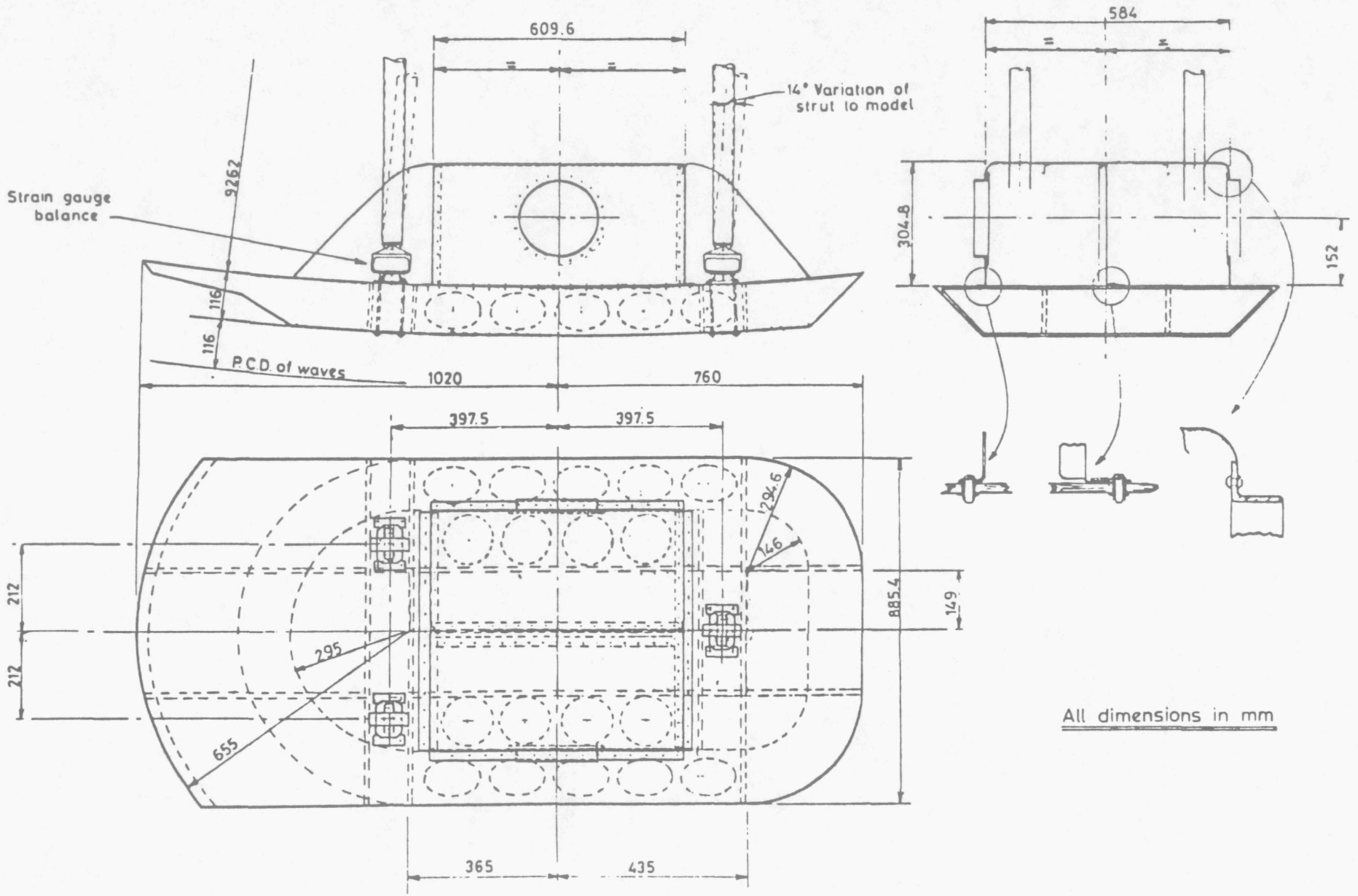

Fig. 4.1 Geometry of model.

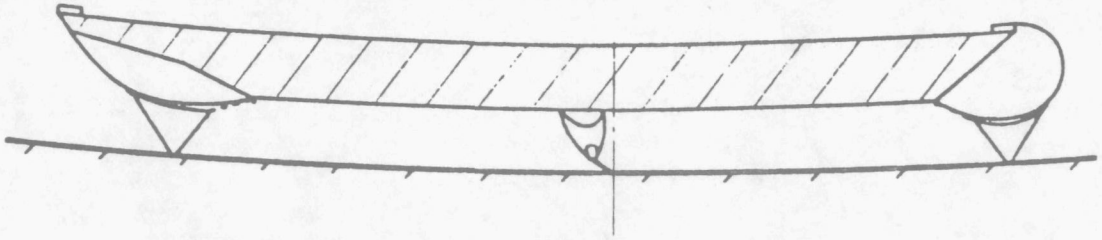

Half section on model ℄

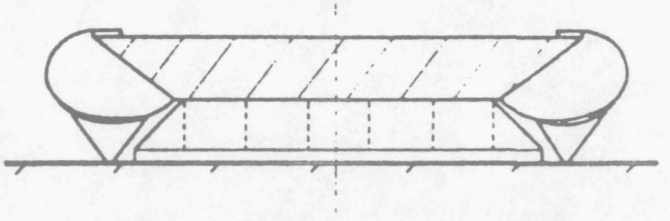

Half section on datum line

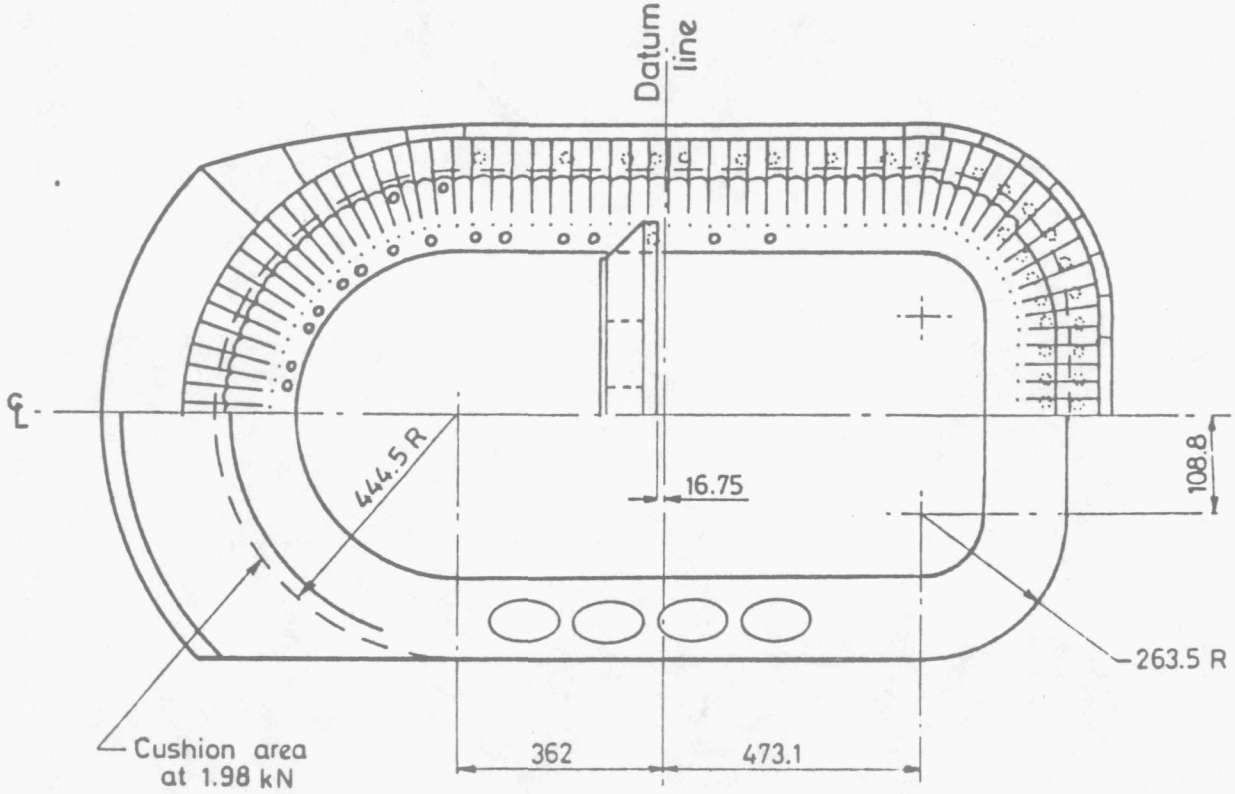

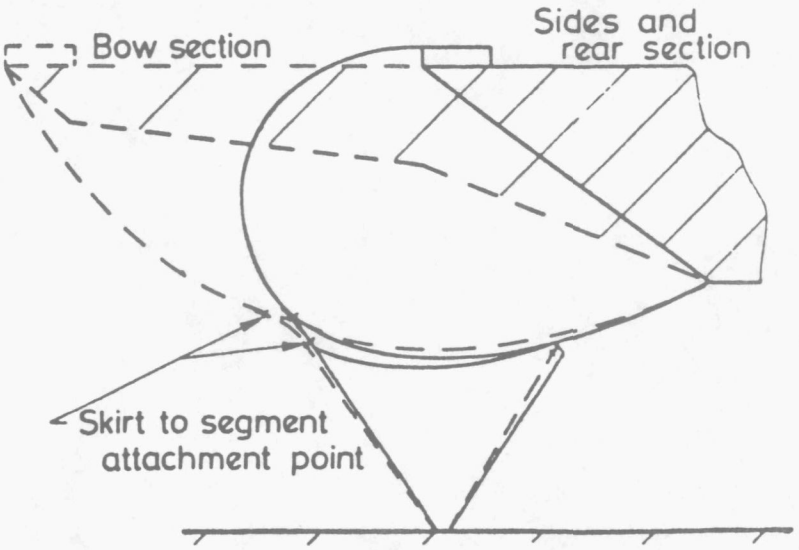

All dimensions in mm

Fig. 4.2 General arrangement of skirt configuration.

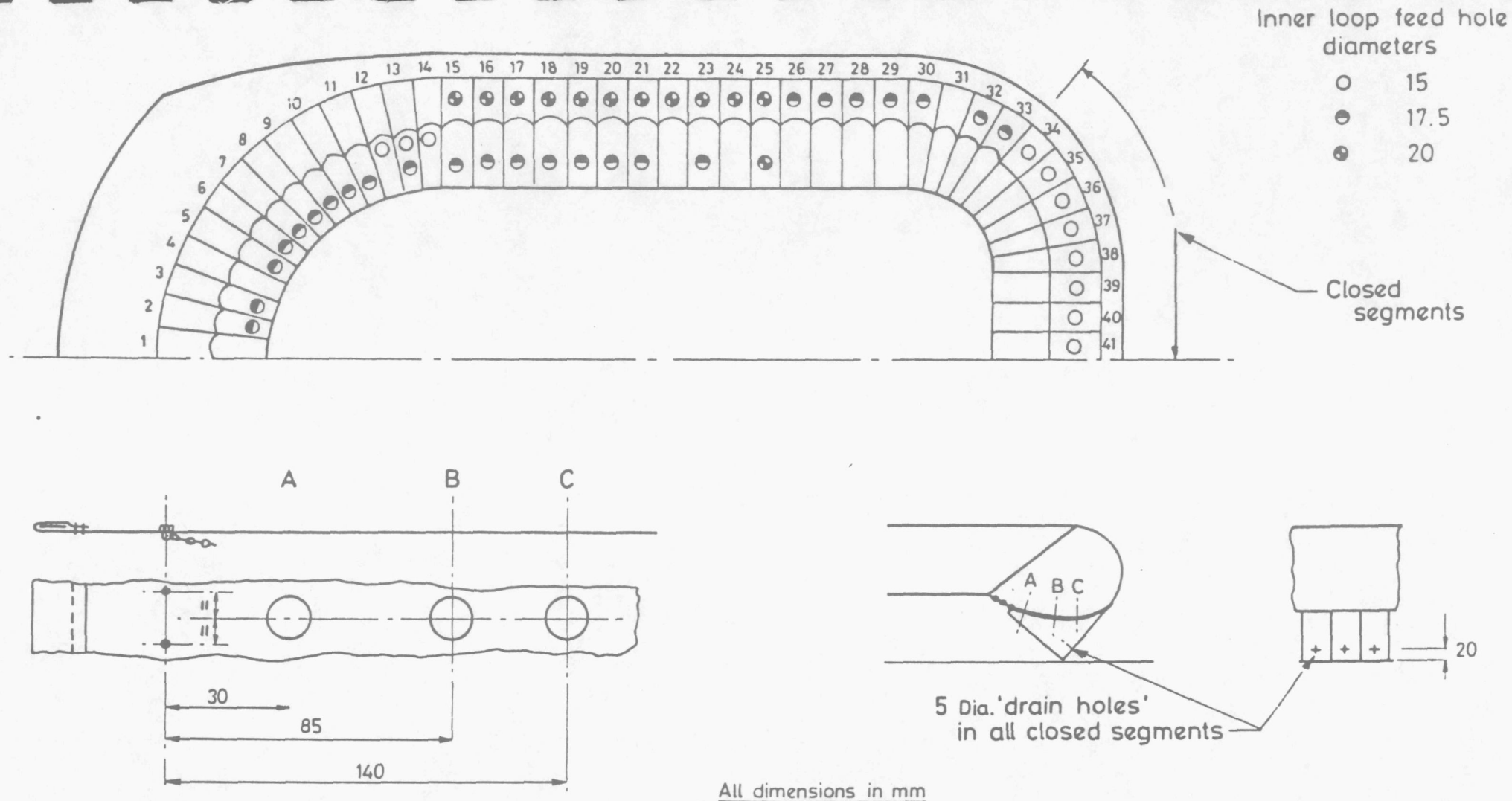

Fig. 4.3 Skirt feed arrangement.

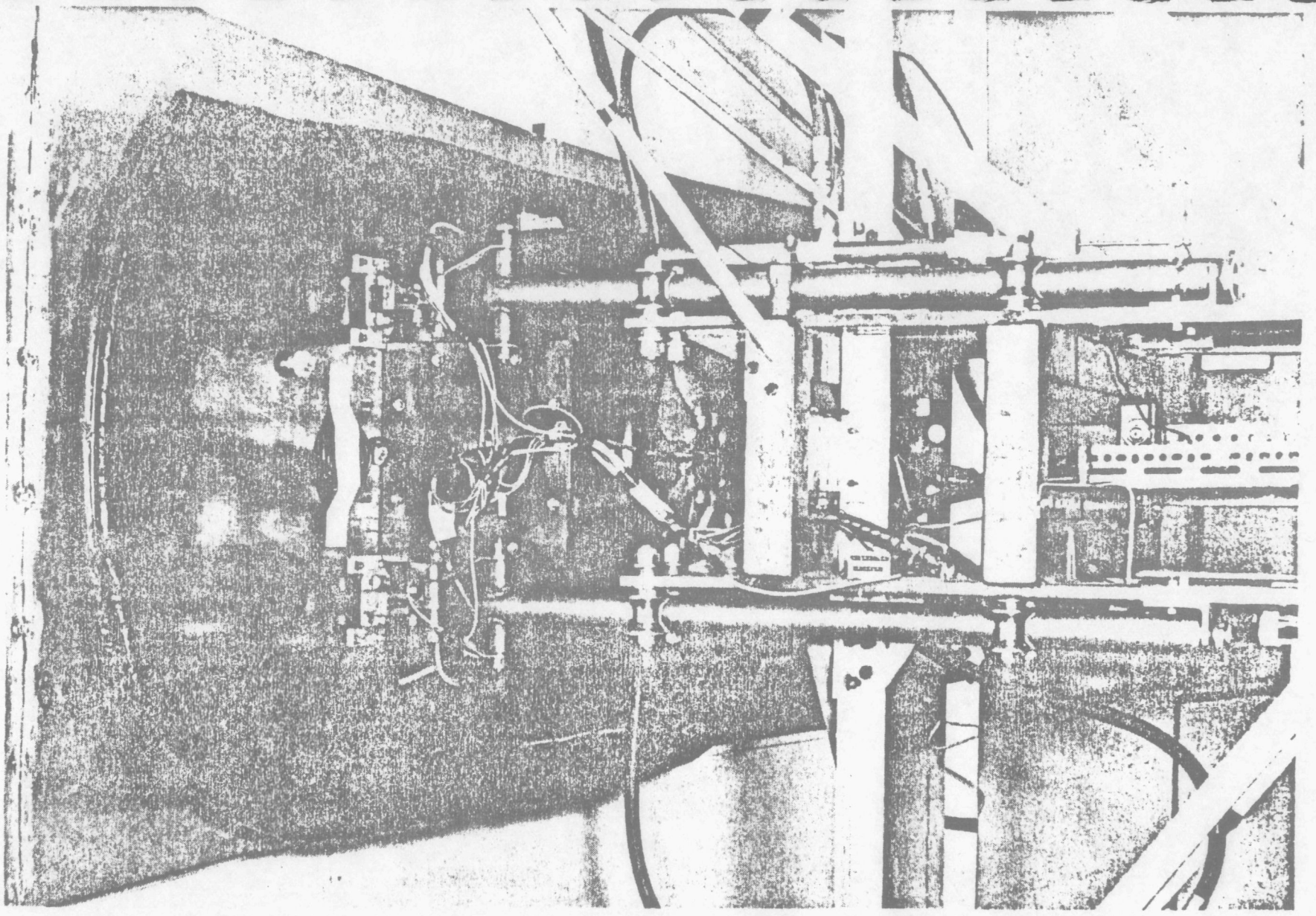

Fig. 4.4 Detailed view of model installation.

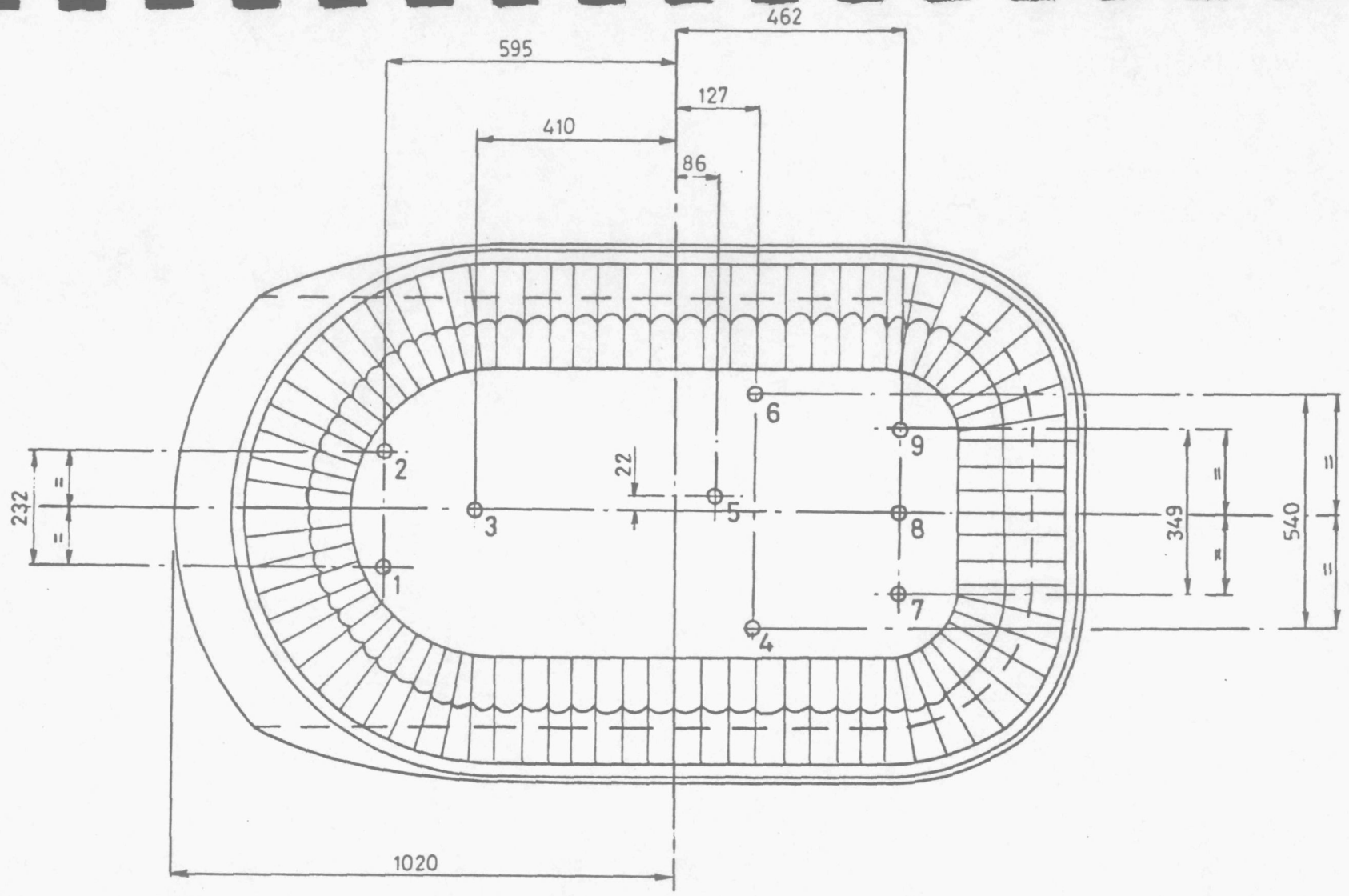

All dimensions in mm.

View from underside of model.

Fig. 4.5 Pressure transducer locations.

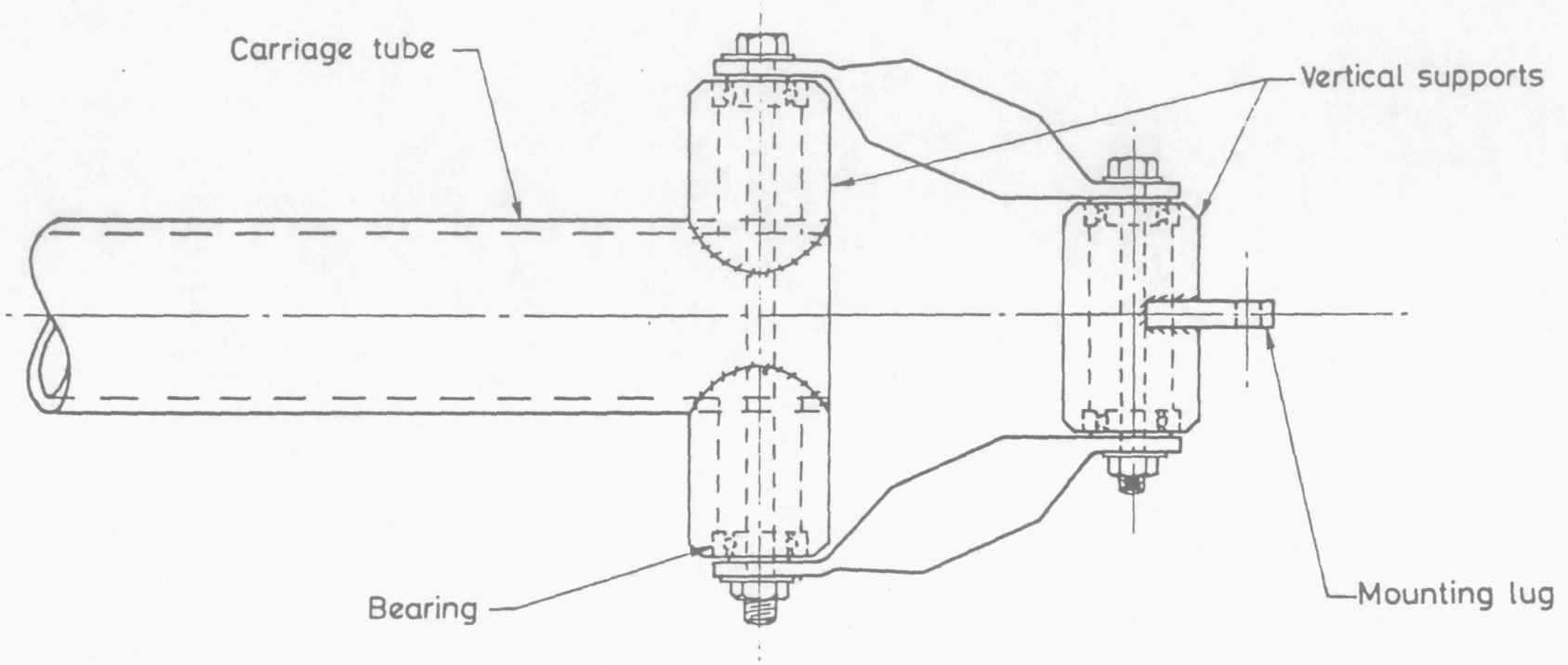

Fig. 4.6 General assembly of model support links.

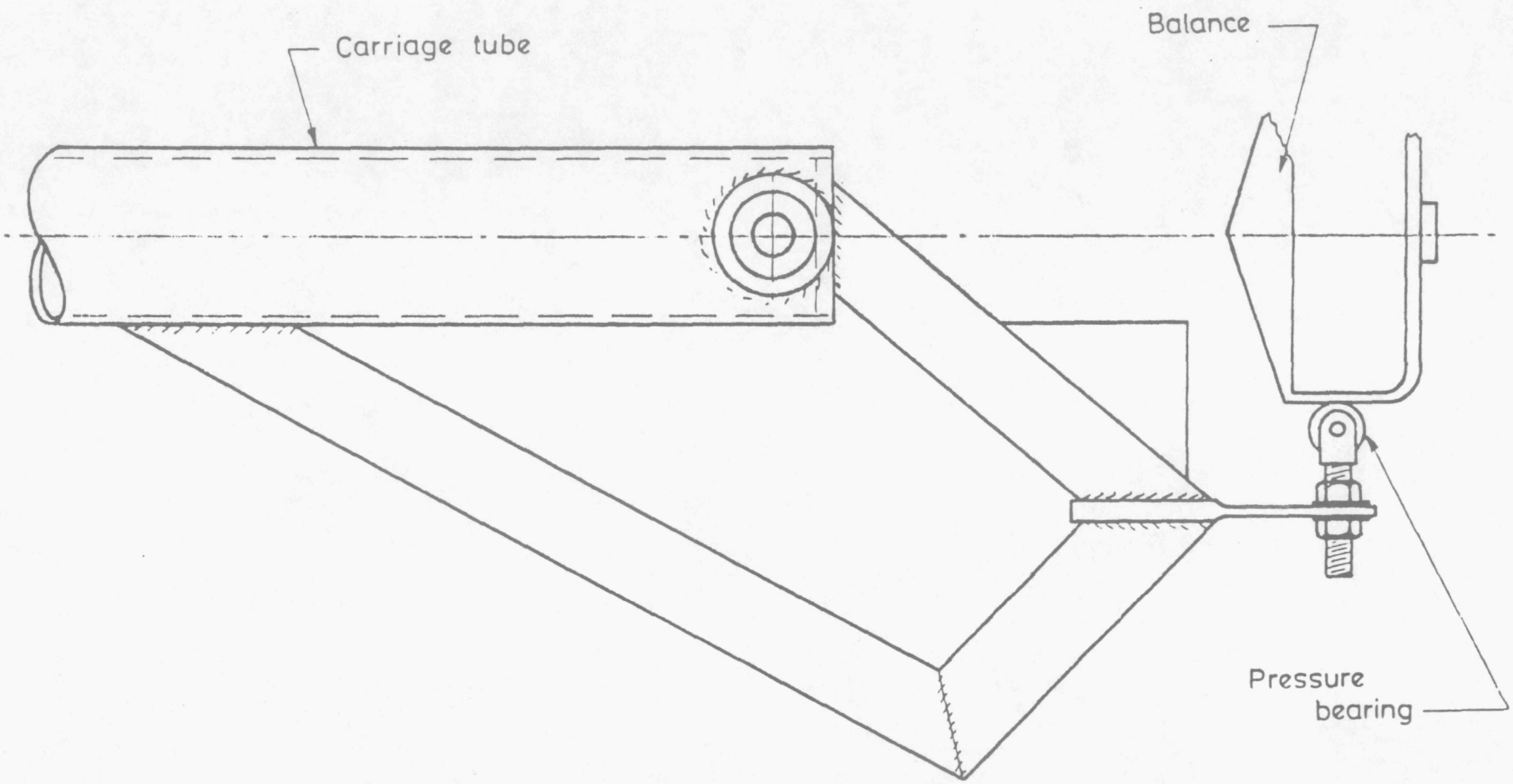

Fig. 4.7 Modified drag balance.

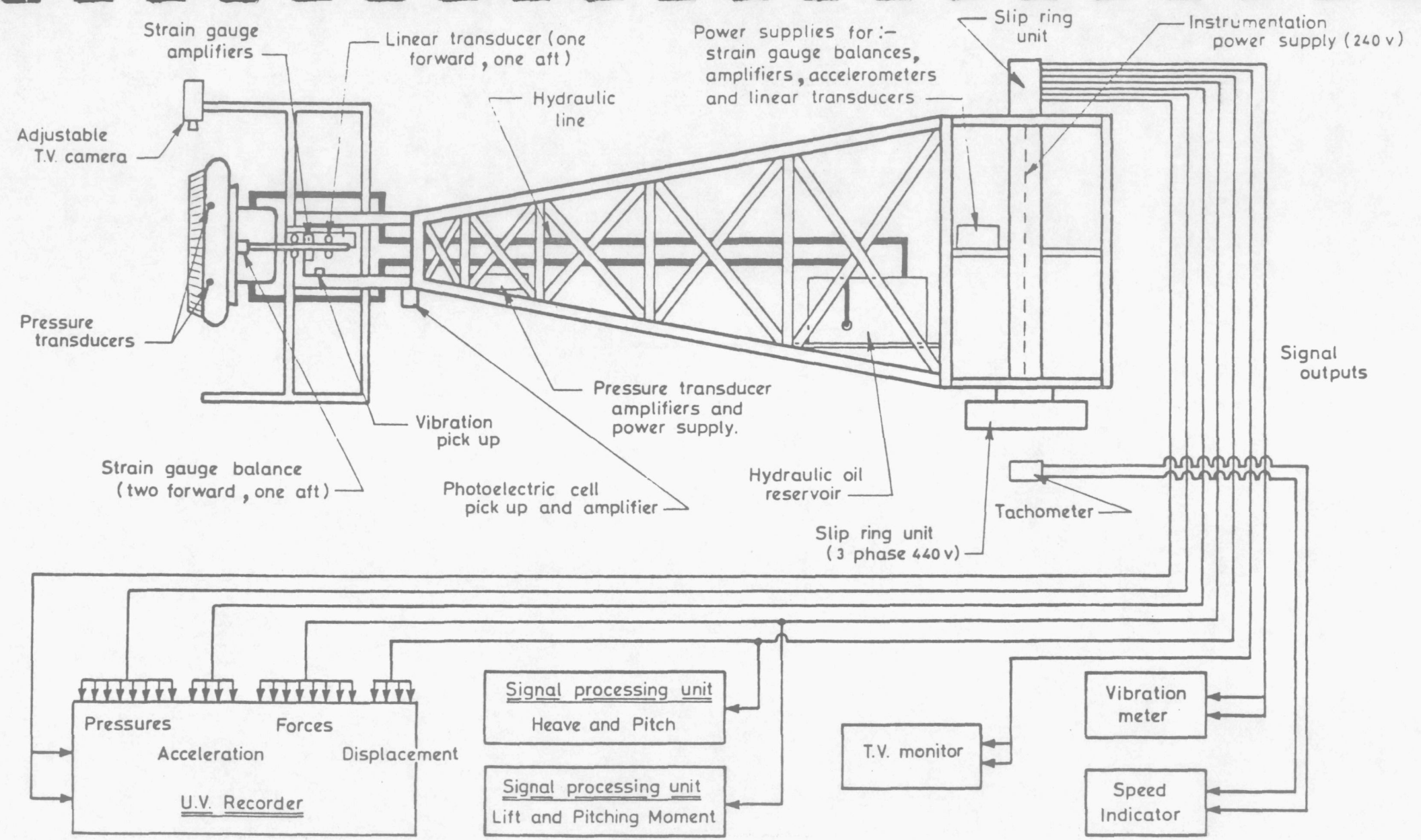

Fig. 4.8 Data acquisition.

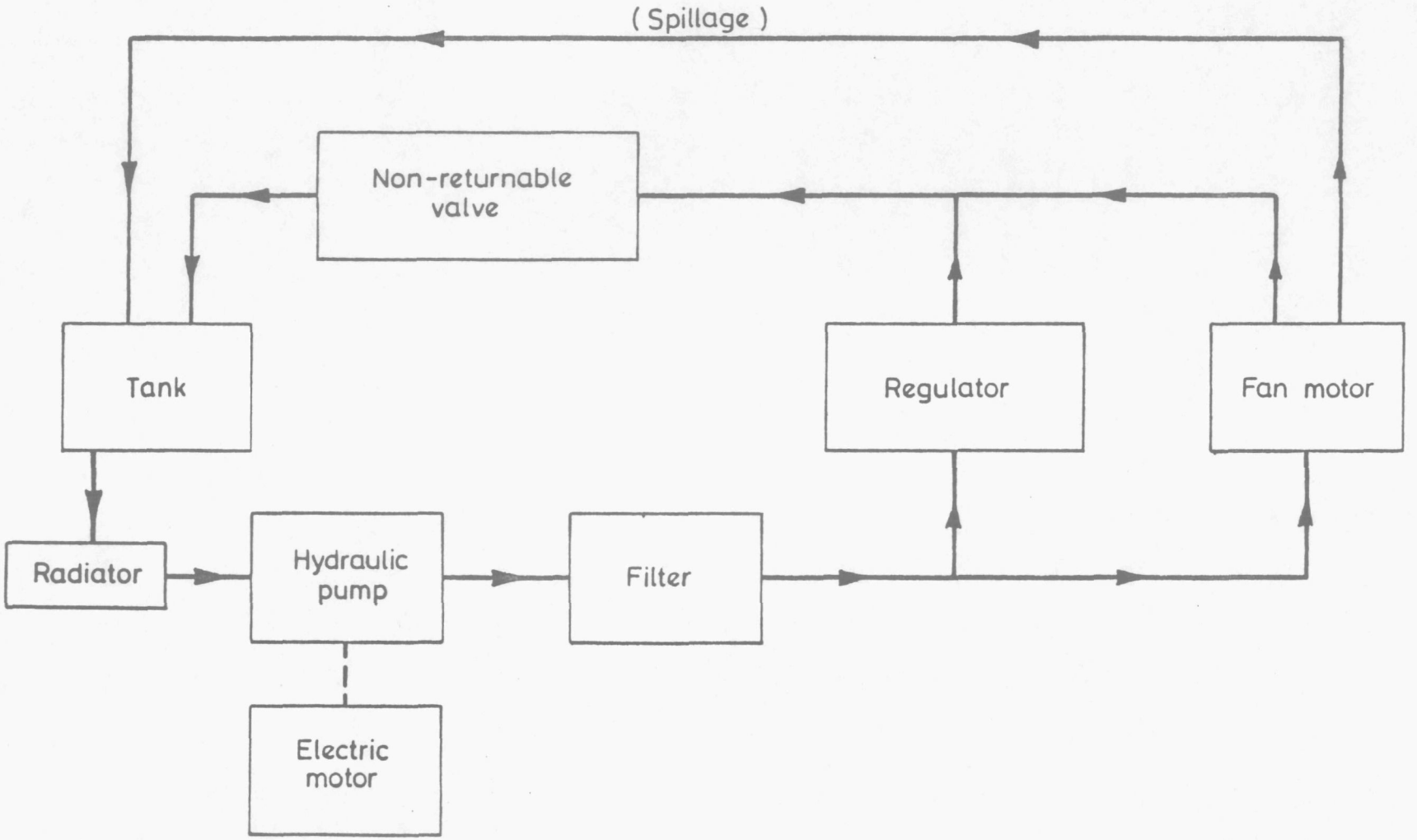

Fig. 4.9 Layout of the original hydraulic drive system

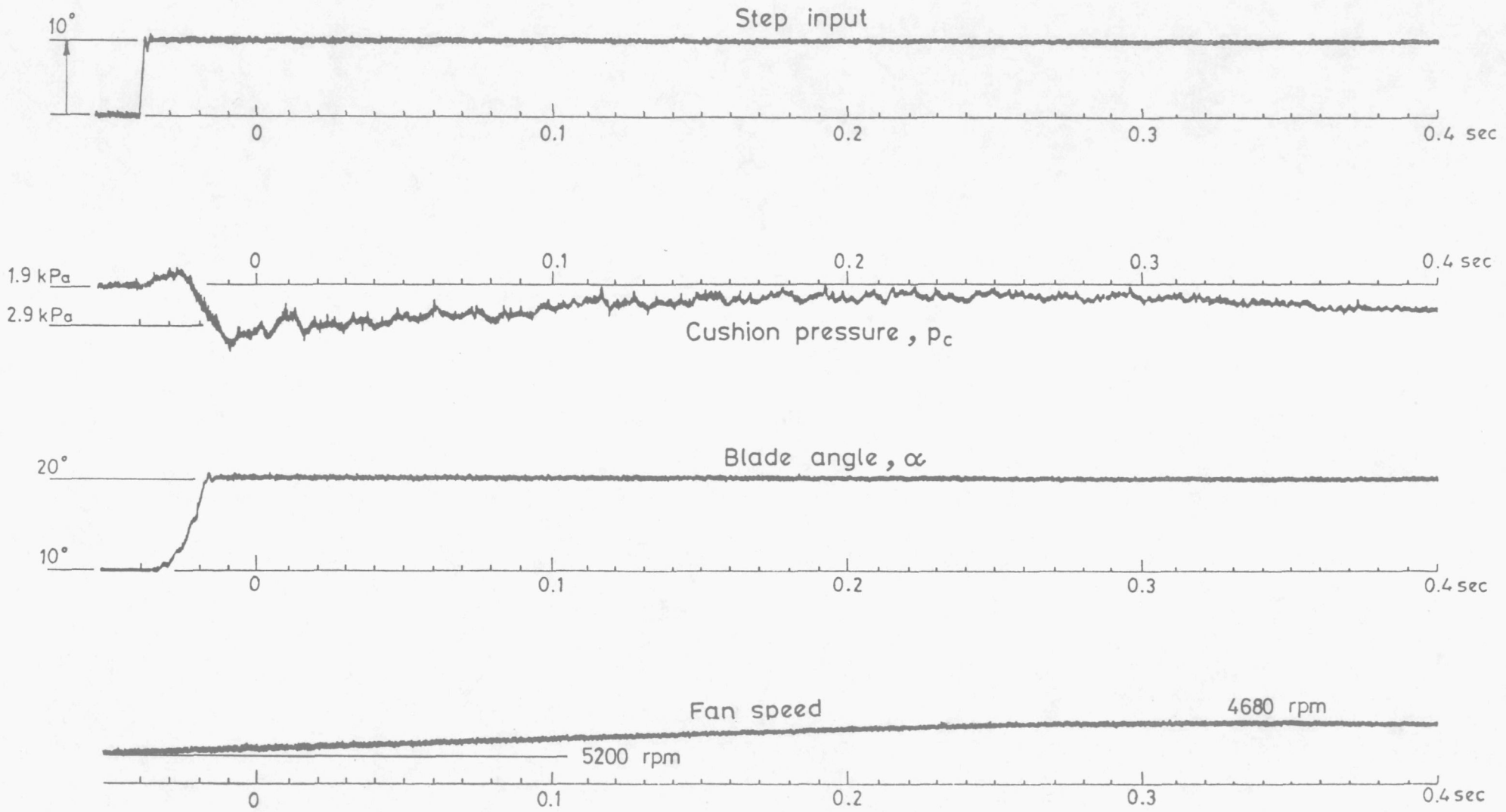

Fig. 4.10 Influence of fan blade transient on fan speed.

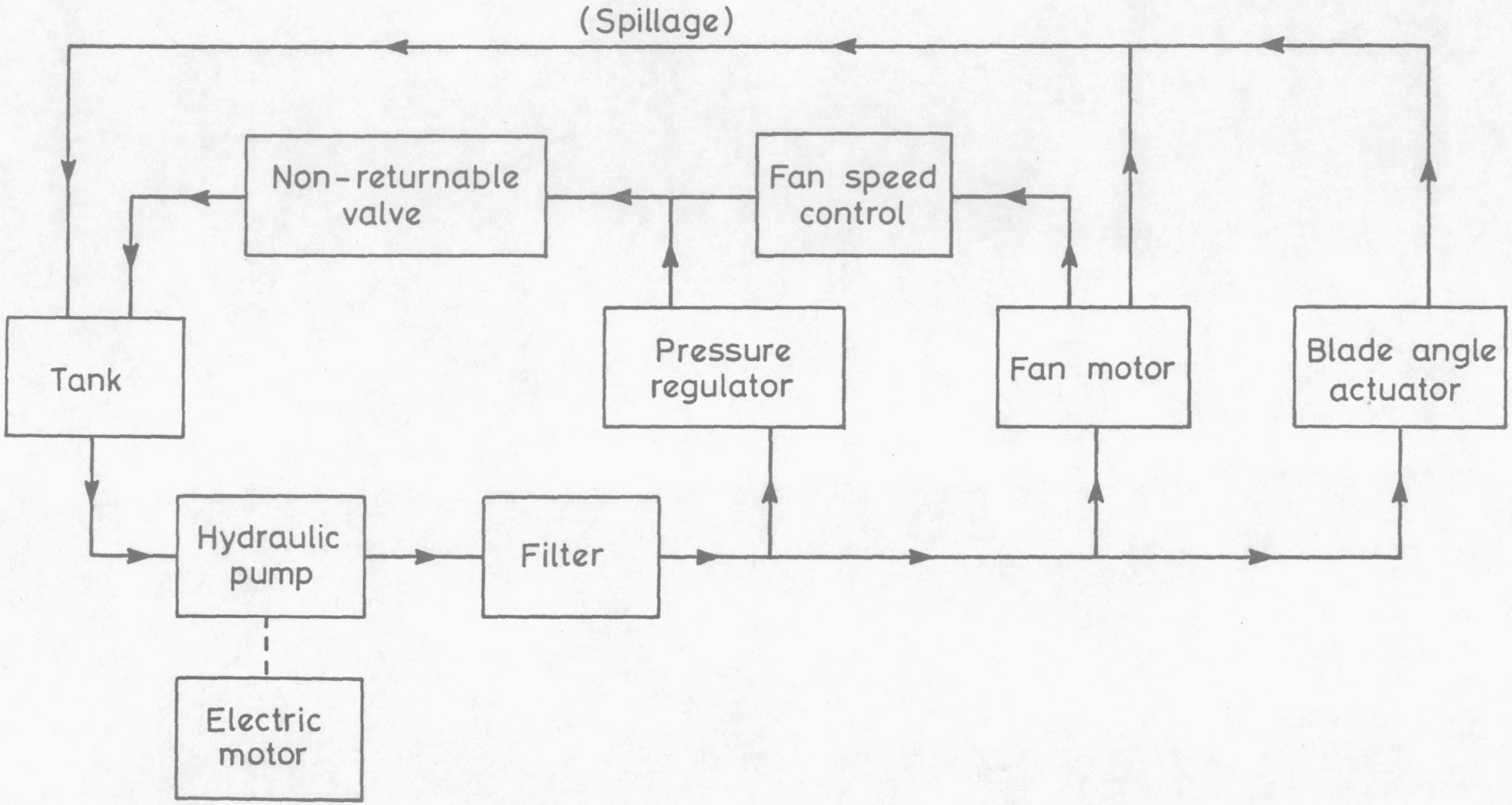

Fig. 4.11 The hydraulic drive system and line.

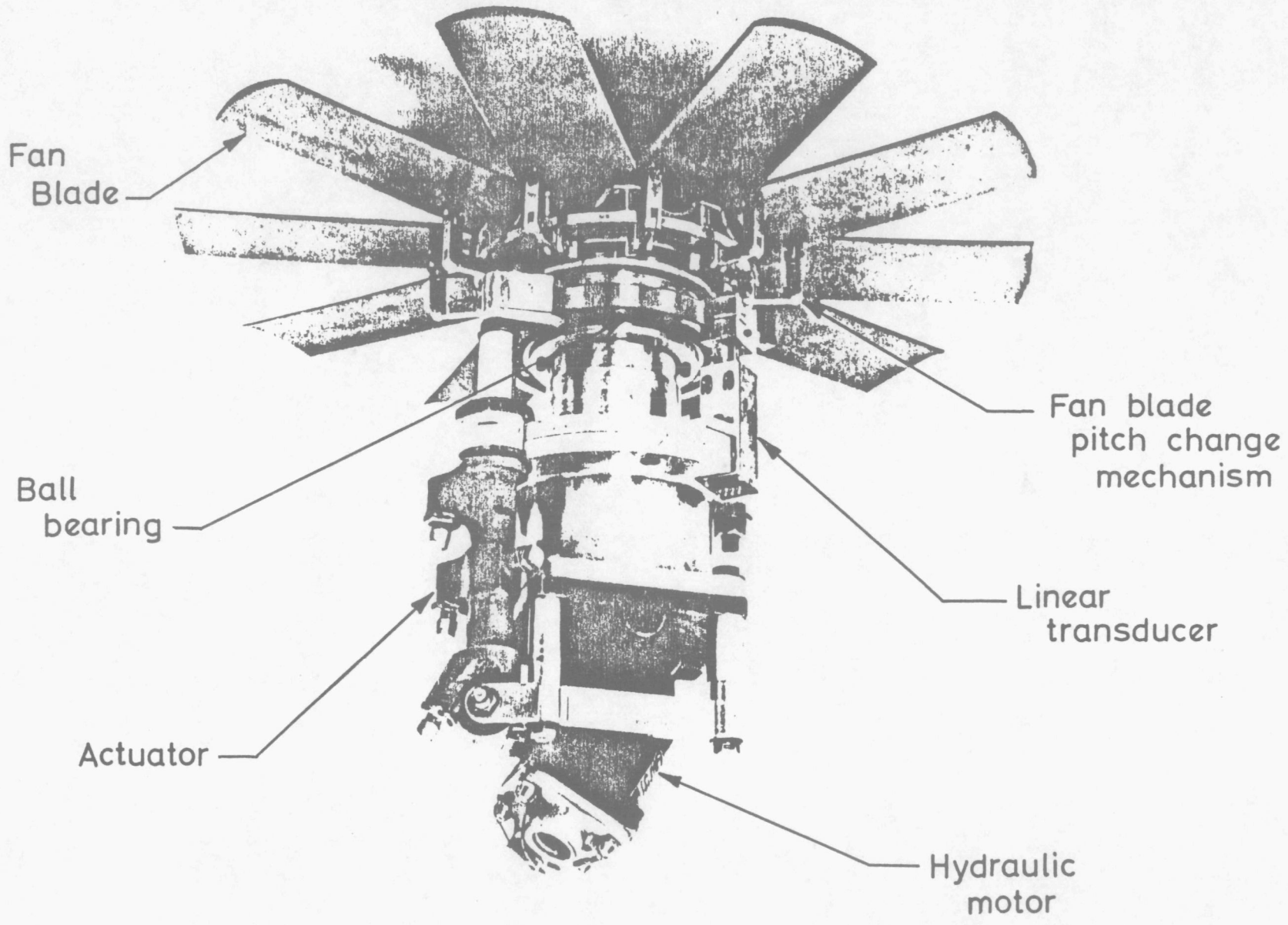

Fig. 4.12 Fan and actuating system assembly

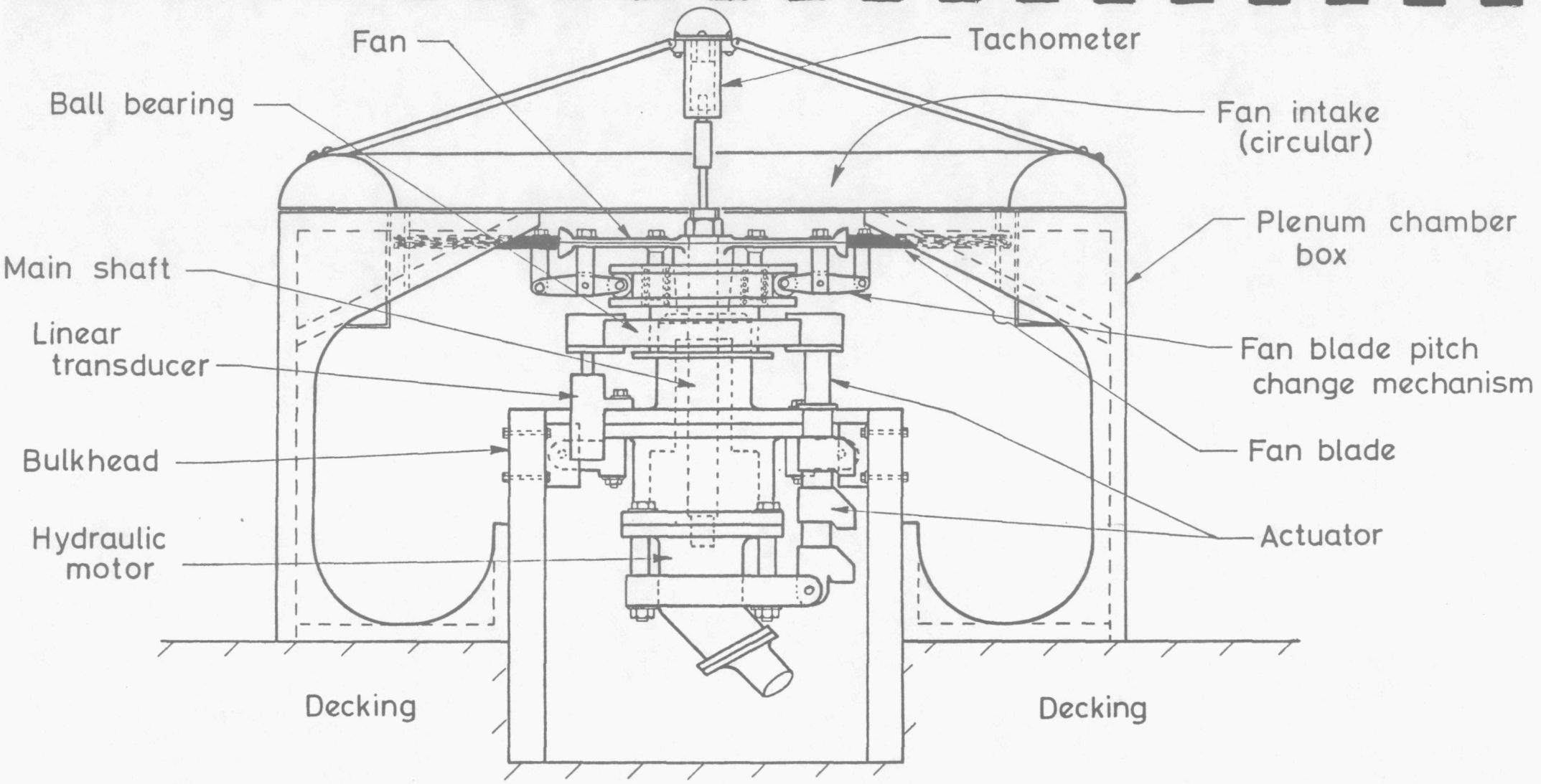

View with front bulkheads and attachments removed

Fig. 4.13 Modified model fan and hydraulic motor installation.

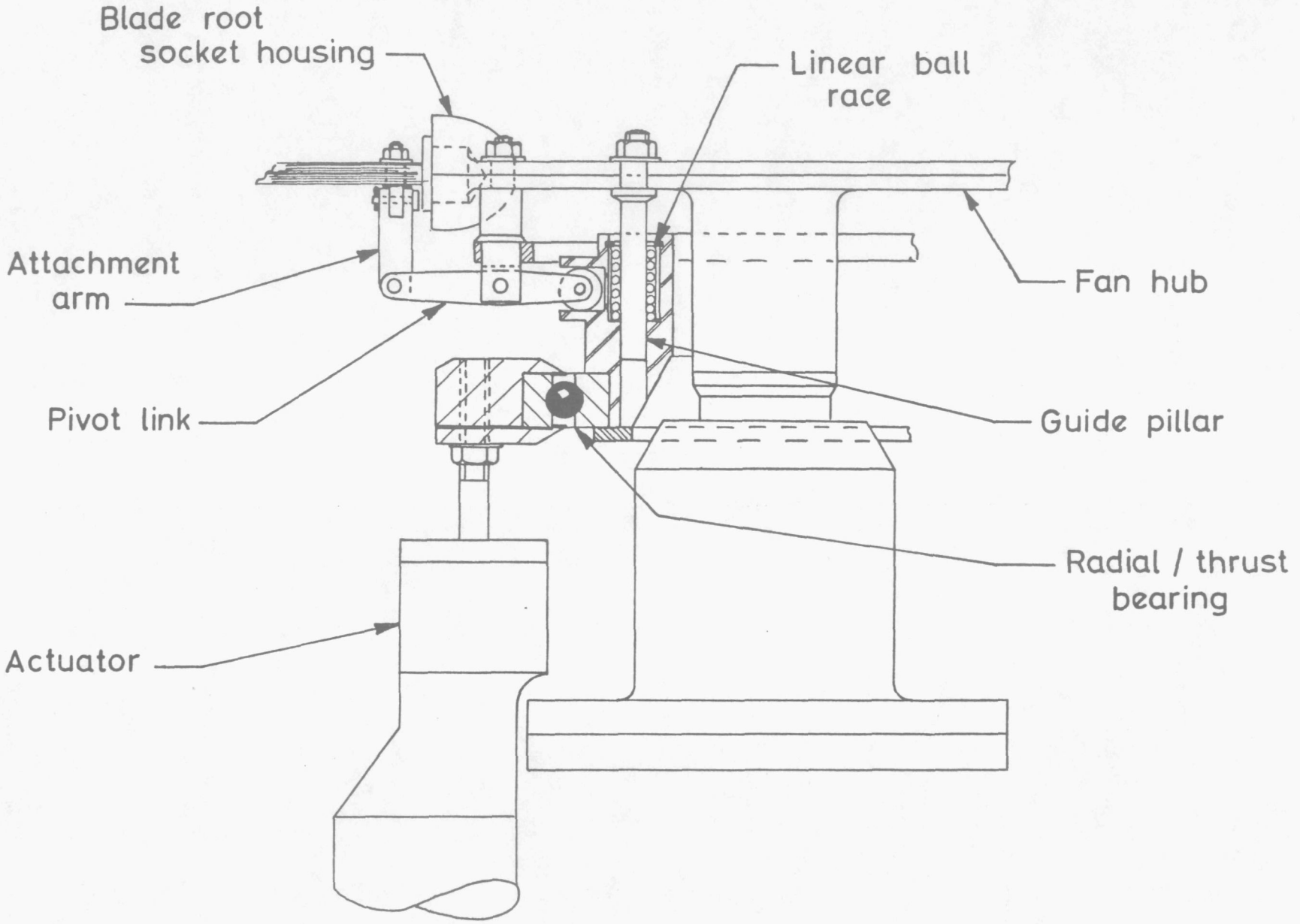

Fig. 4.14 Linkage mechanism

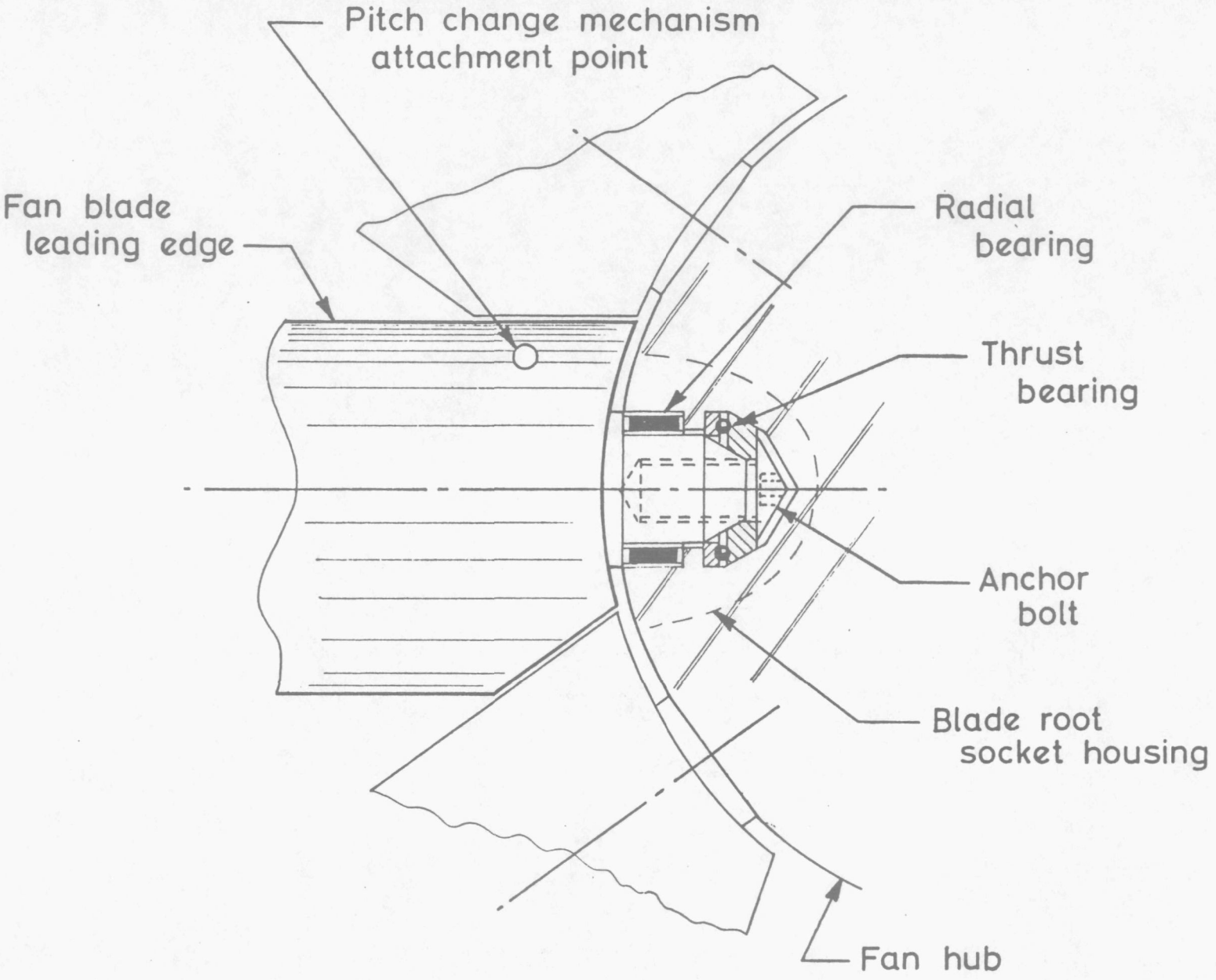

Fig. 4.15 Detailed view of the blade attachment

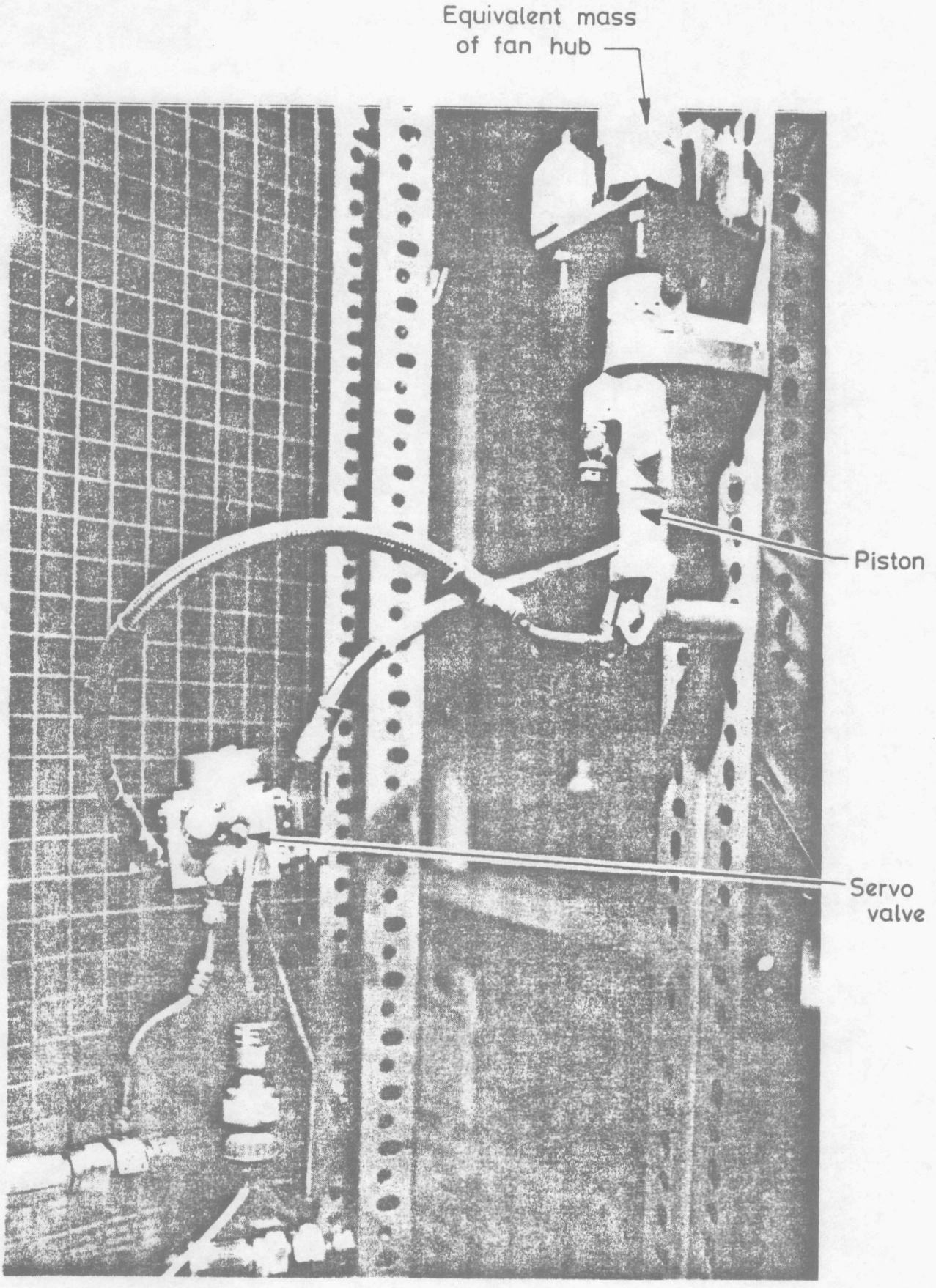

Fig. 4.16 Actuator bench rig.

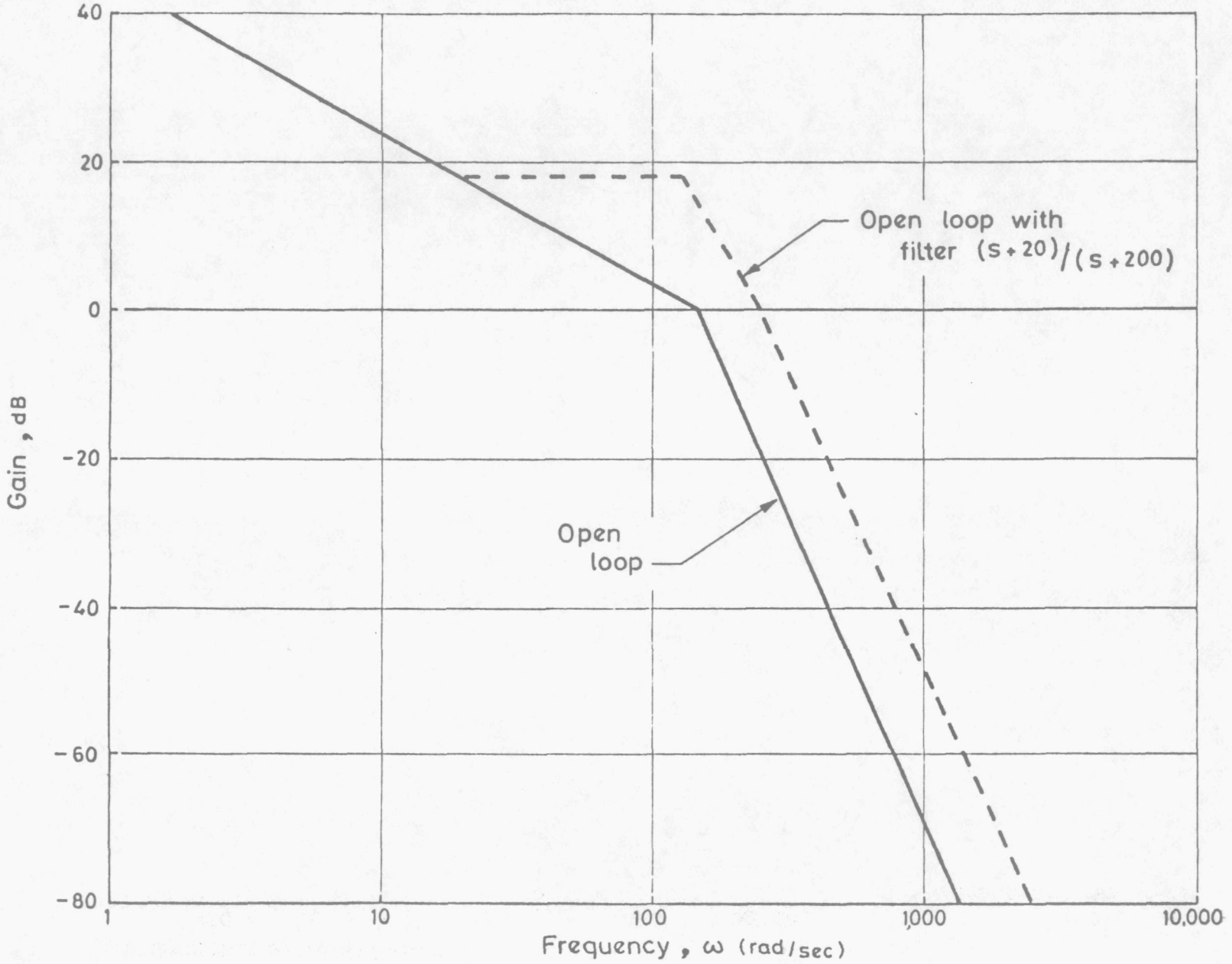

Fig. 4.17 Bode plot for servo actuation system, (open loop).

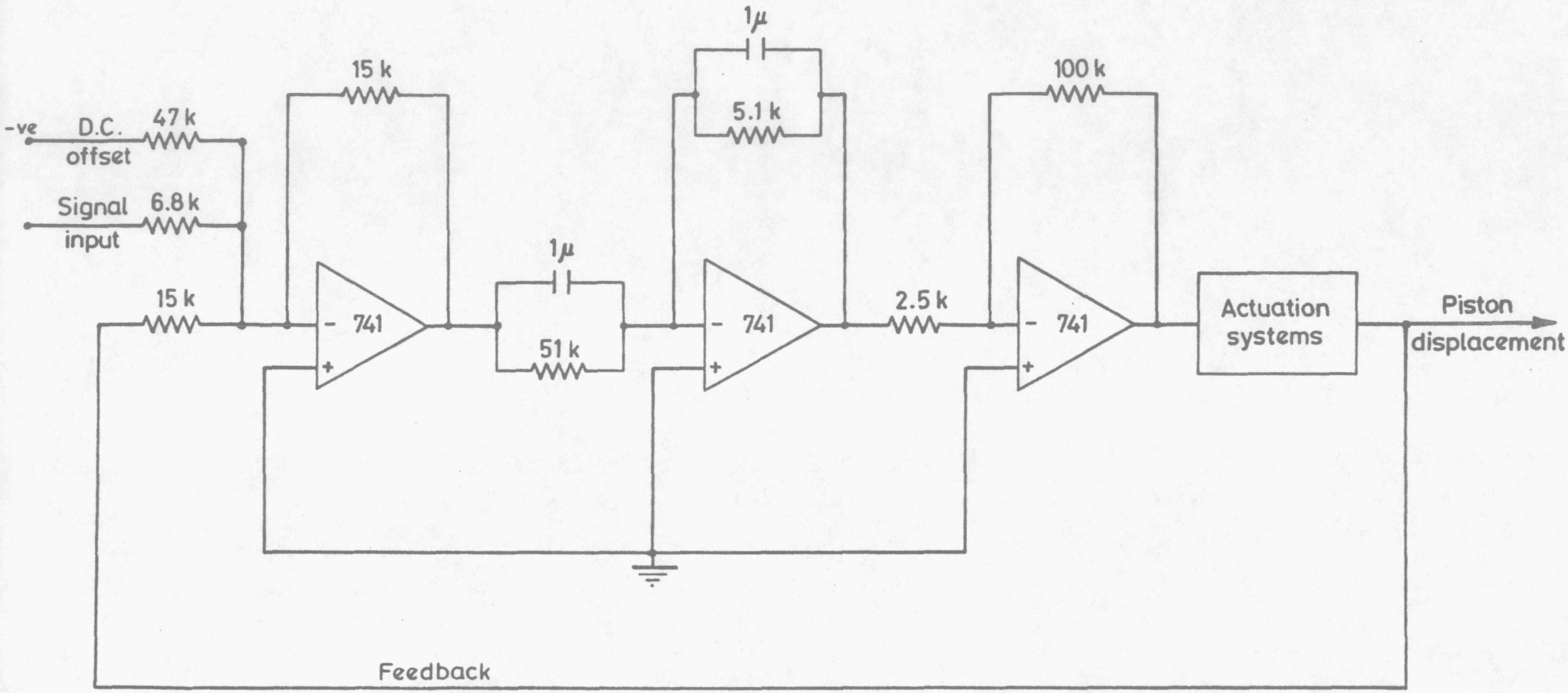

Fig. 4.18 Circuit diagram for closed-loop servo actuation system.

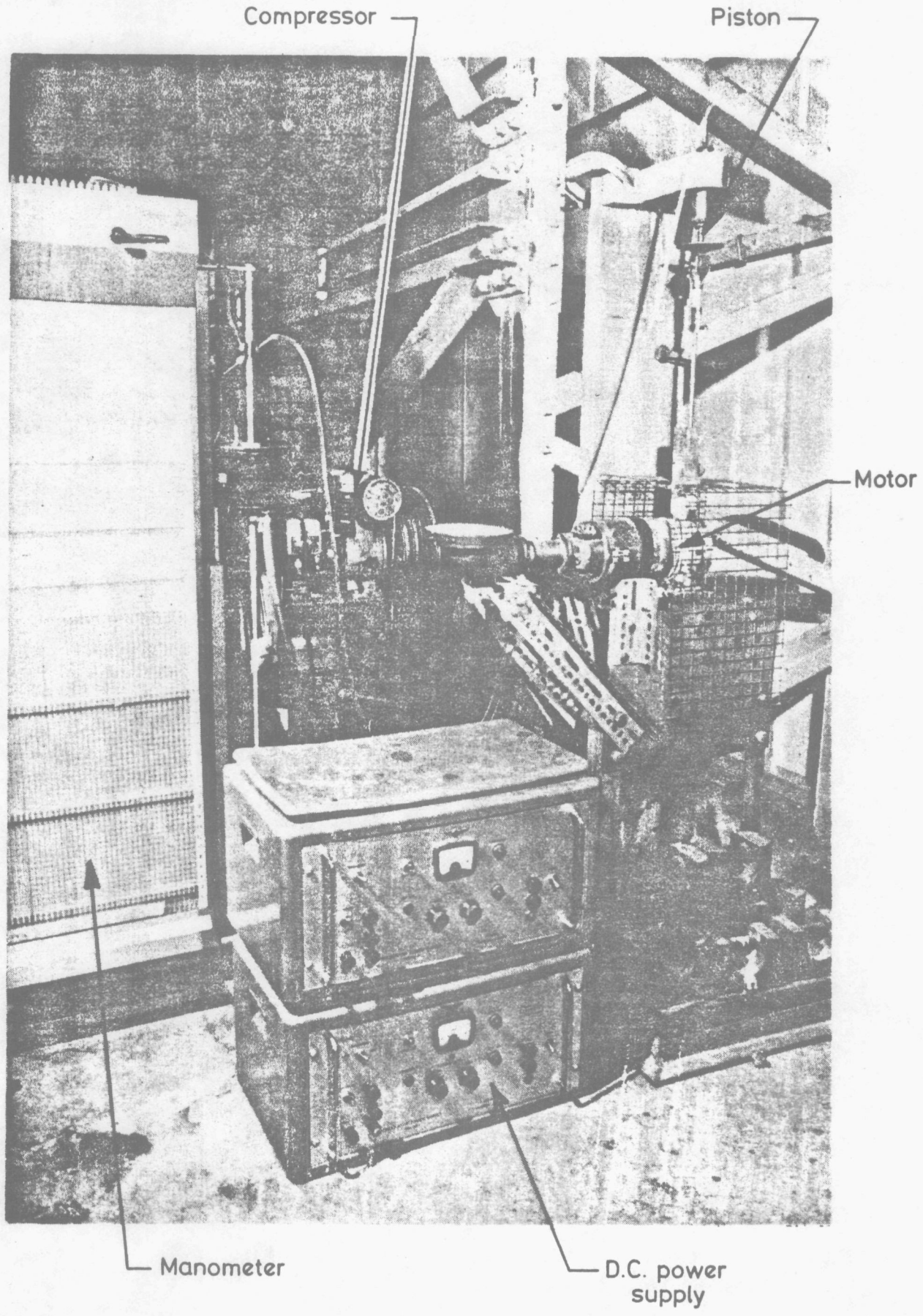

Fig. 4.19 Cushion pressure simulator.

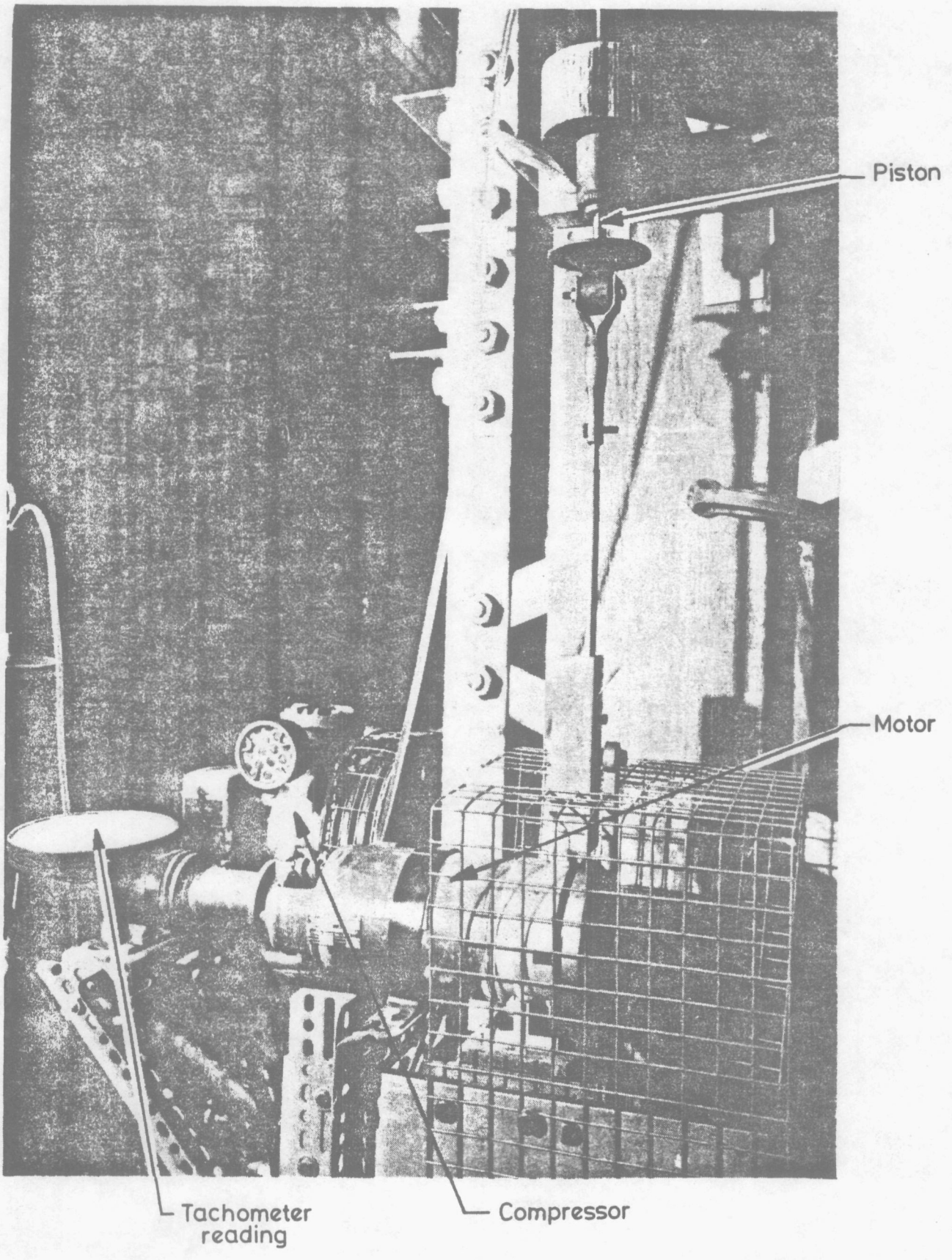

Fig. 4.20 Cushion pressure simulator, (close up).

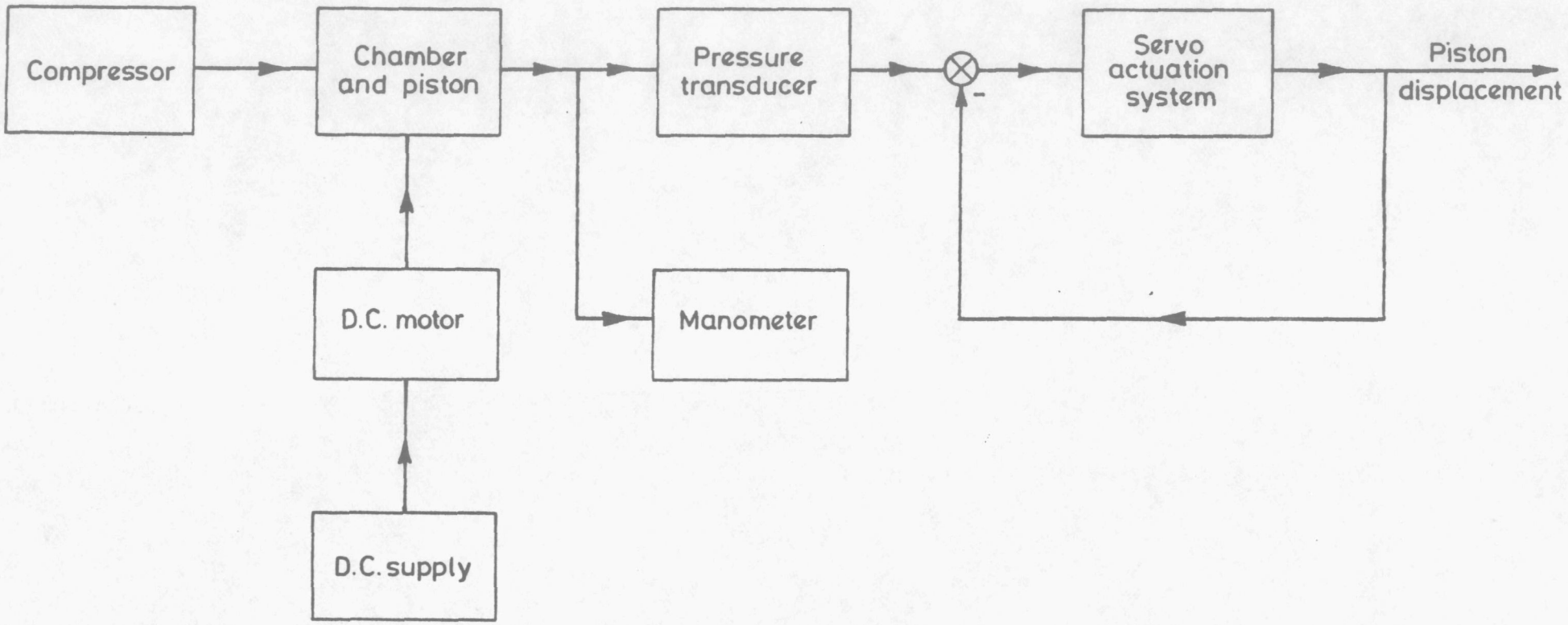

Fig. 4.21 Cushion pressure simulator, (general arrangement).

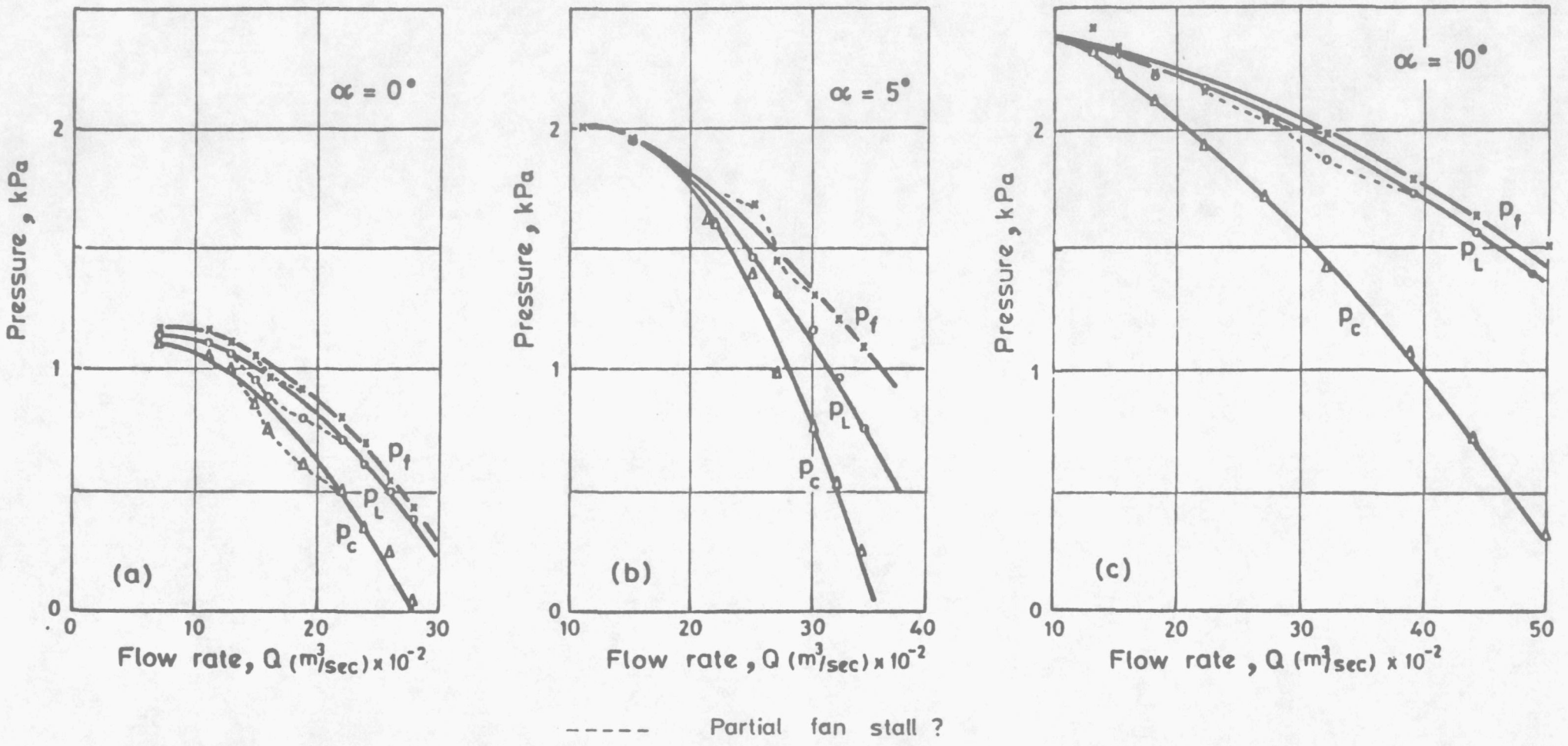

Fig. 5.1 Pressure - flow rate characteristics at fan speed 5200 r.p.m.

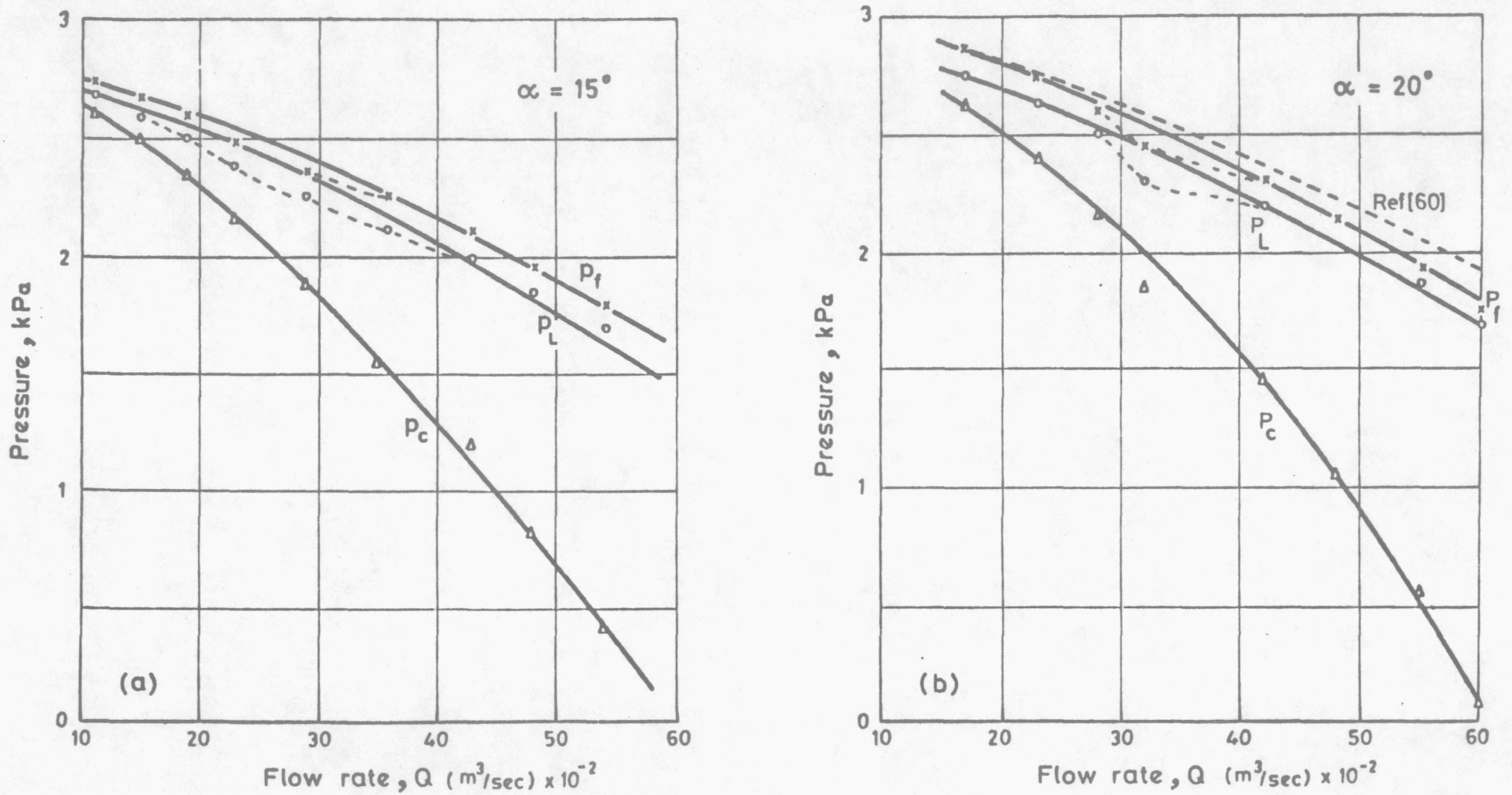

---- Partial fan stall ?

Fig. 5.2 Pressure - flow rate characteristics at fan speed 5200 r.p.m.

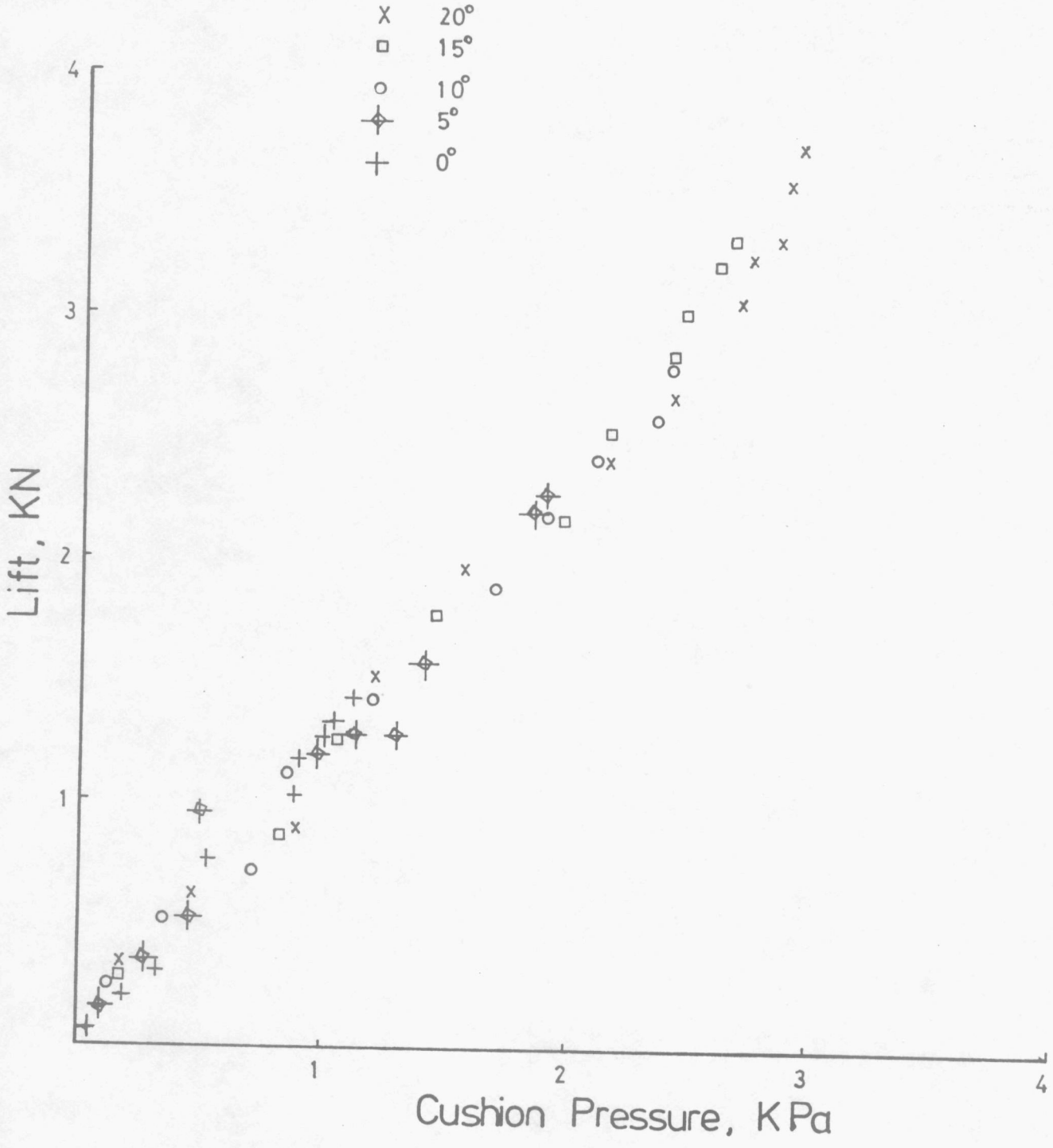

Fig.5.3a Lift Vs cushion pressure characteristics

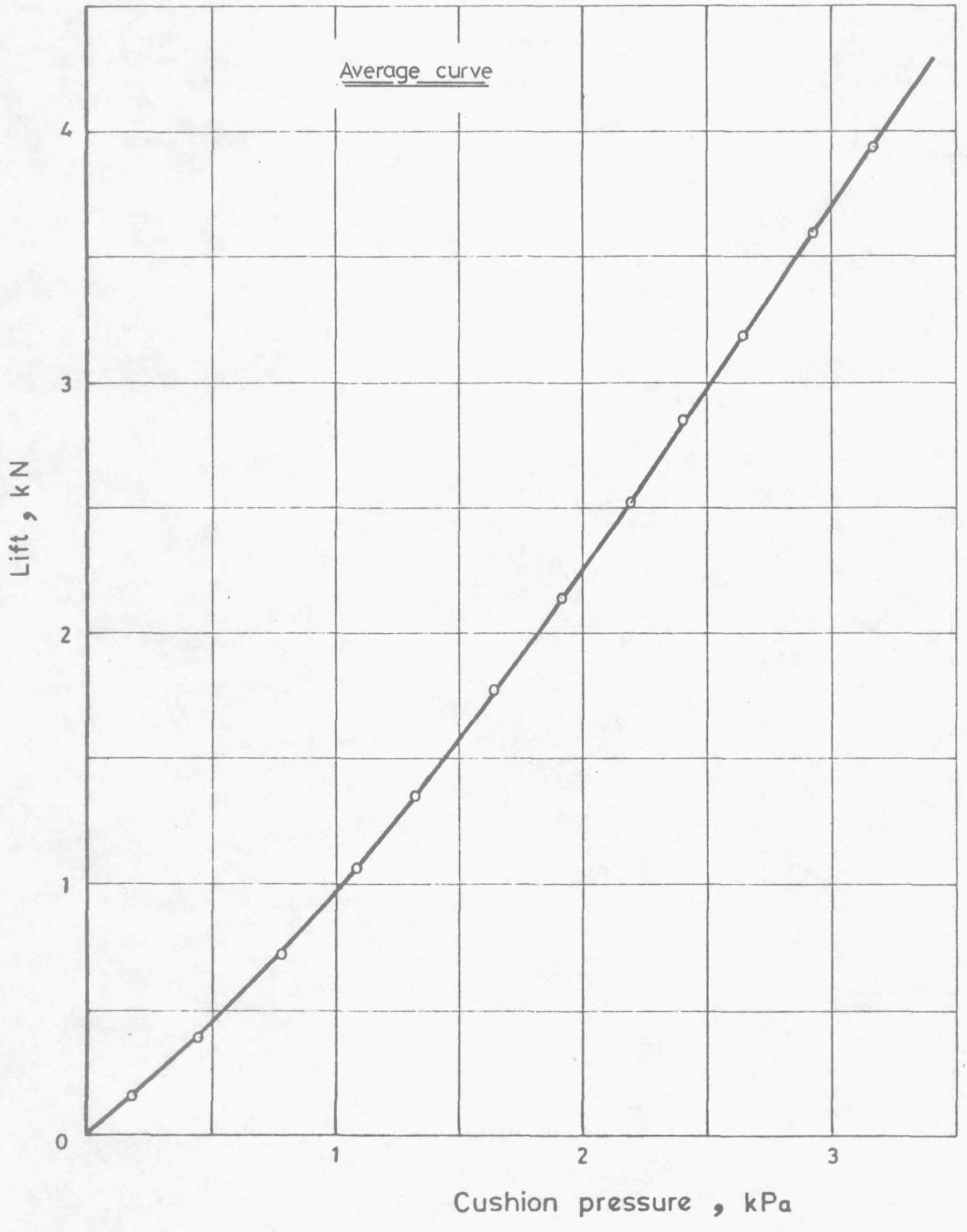

Fig. 5.3b Lift vs cushion pressure characteristics.

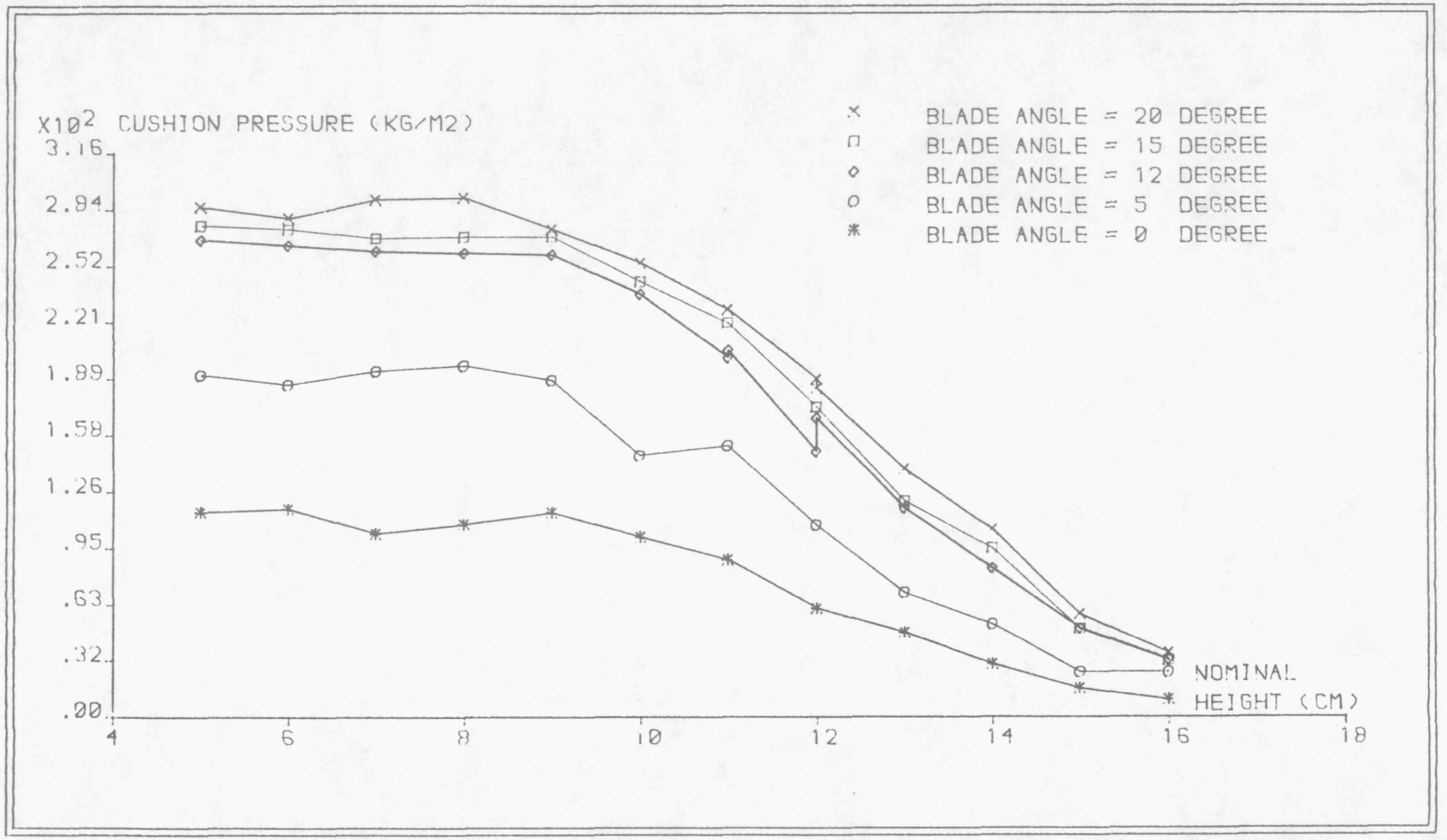

Fig. 5.4 Nominal height and cushion pressure characteristics

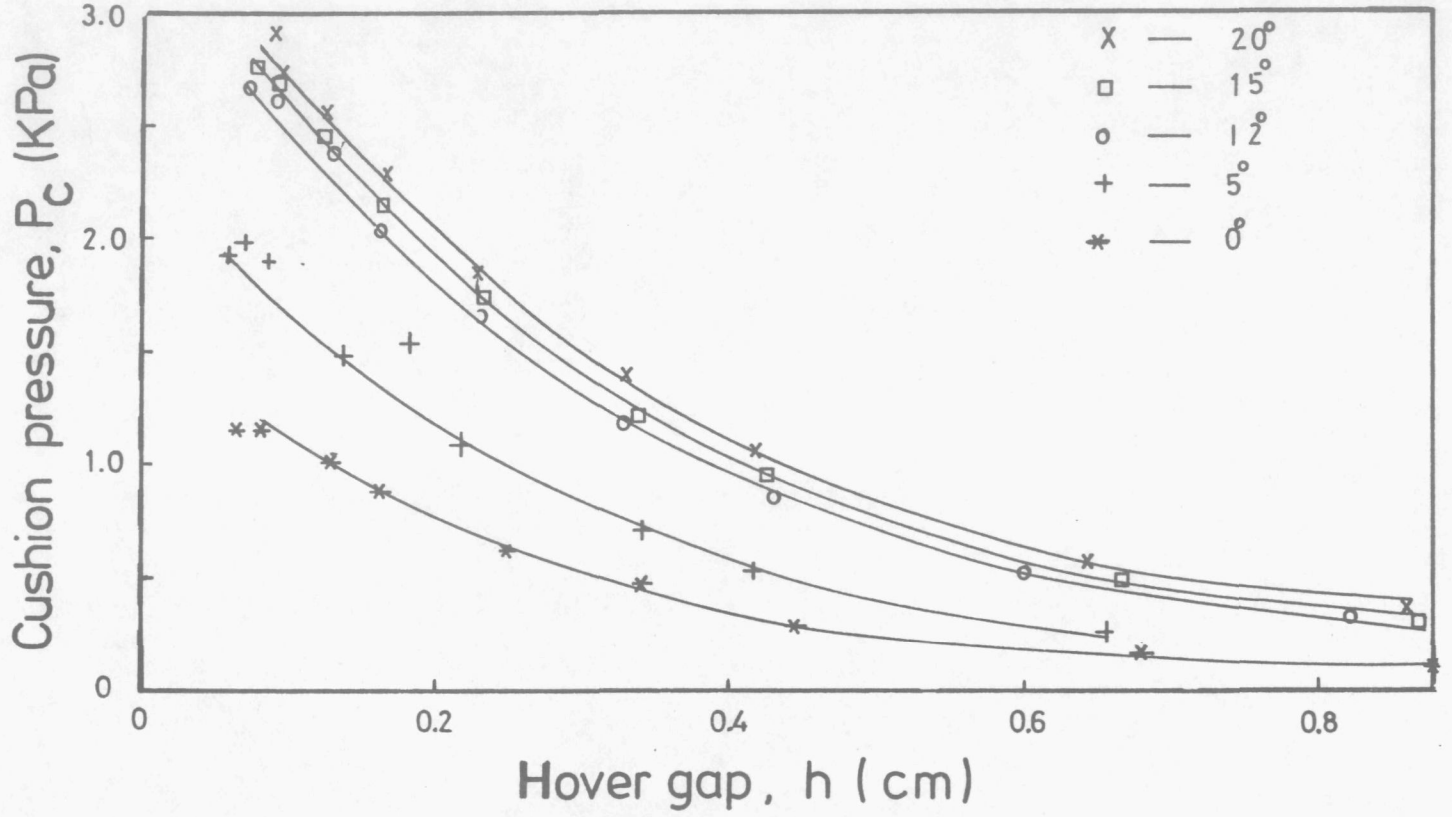

Fig.5.5 Relationship between cushion pressure and hover gap

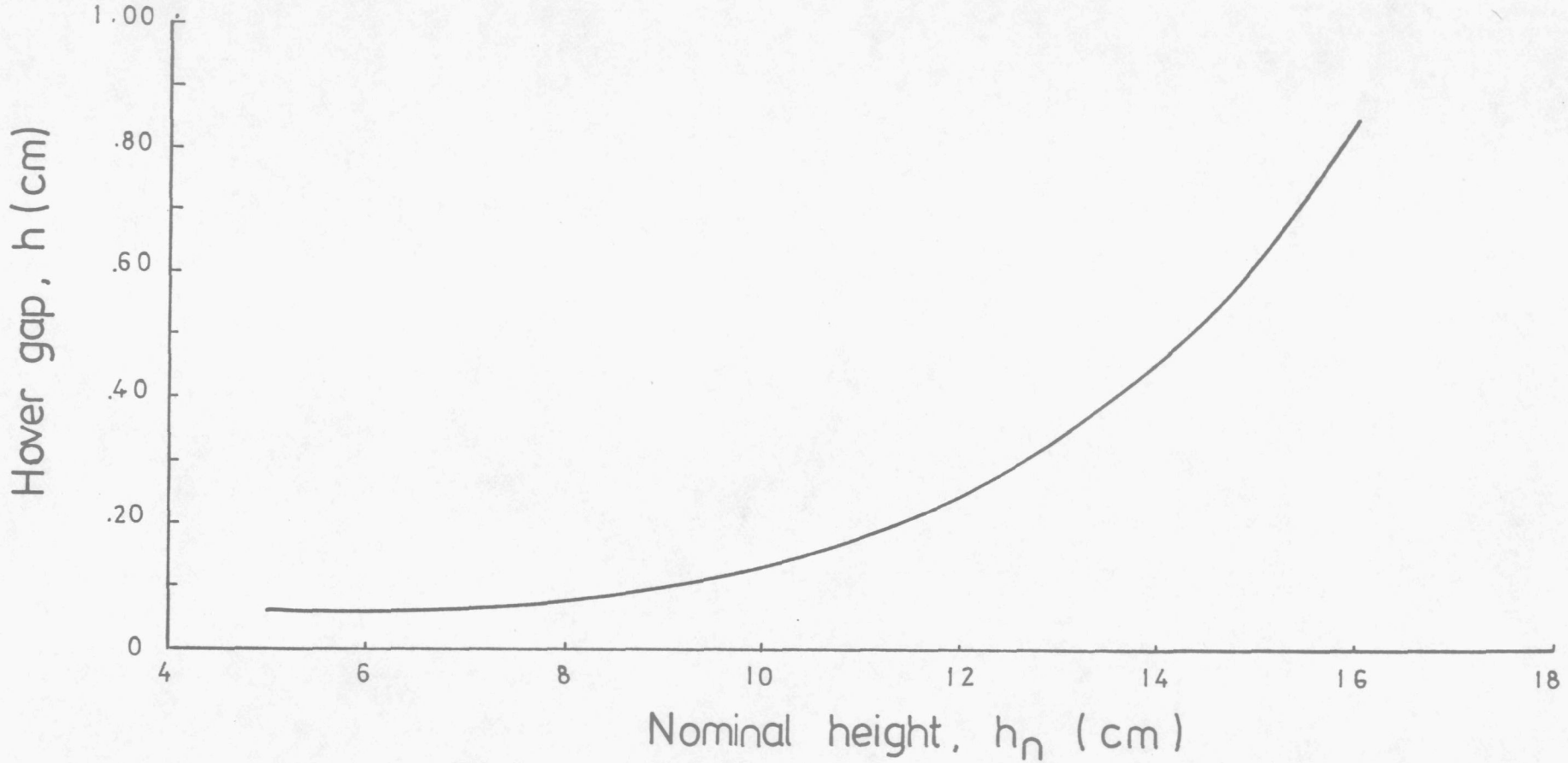

Fig.5.6 Relationship between hover gap and nominal height

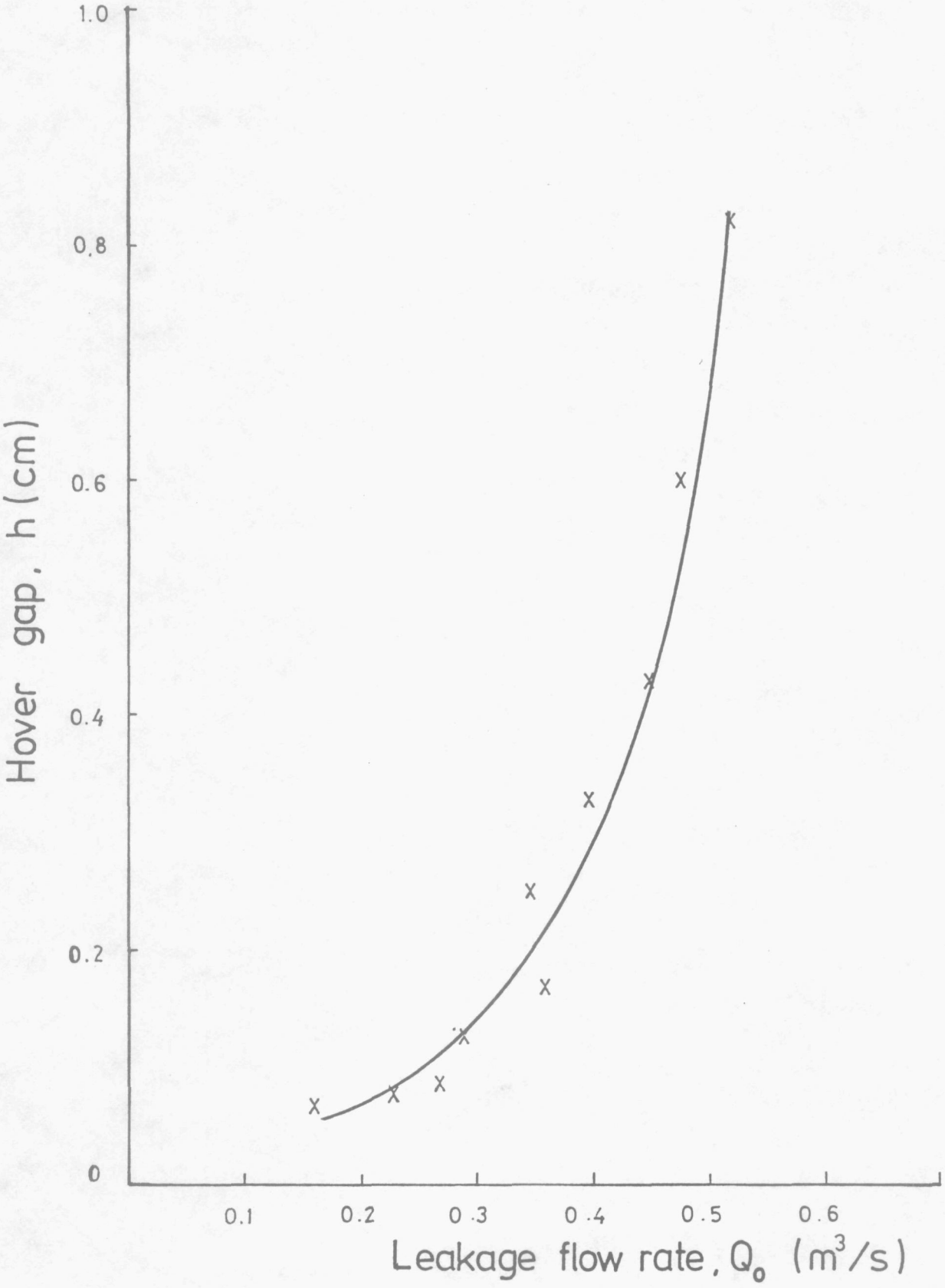

Fig.5.7 Relationship between leakage flow rate and hover gap

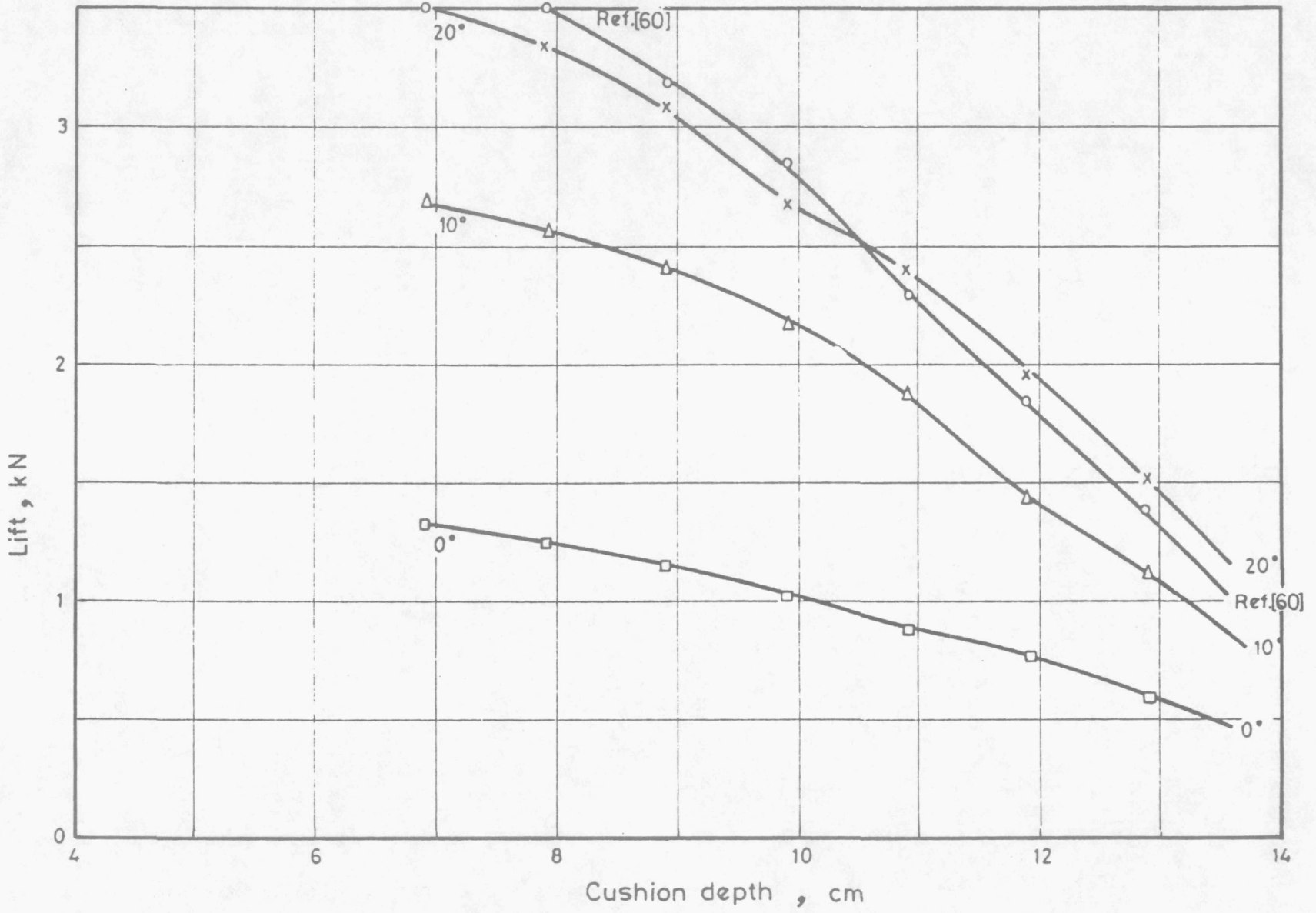

Fig.5.8a Heave characteristics.

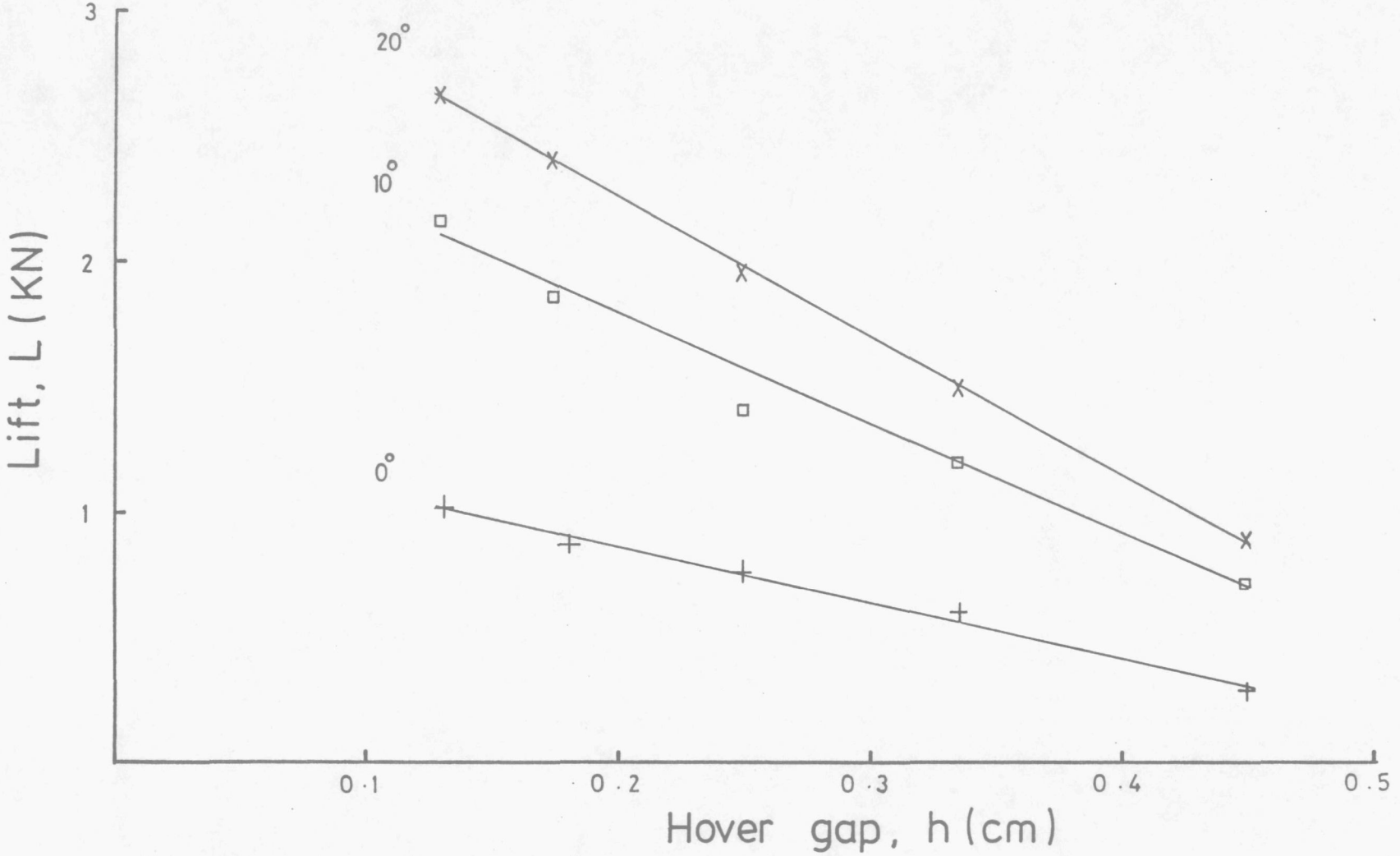

Fig.5.8b Heave characteristics

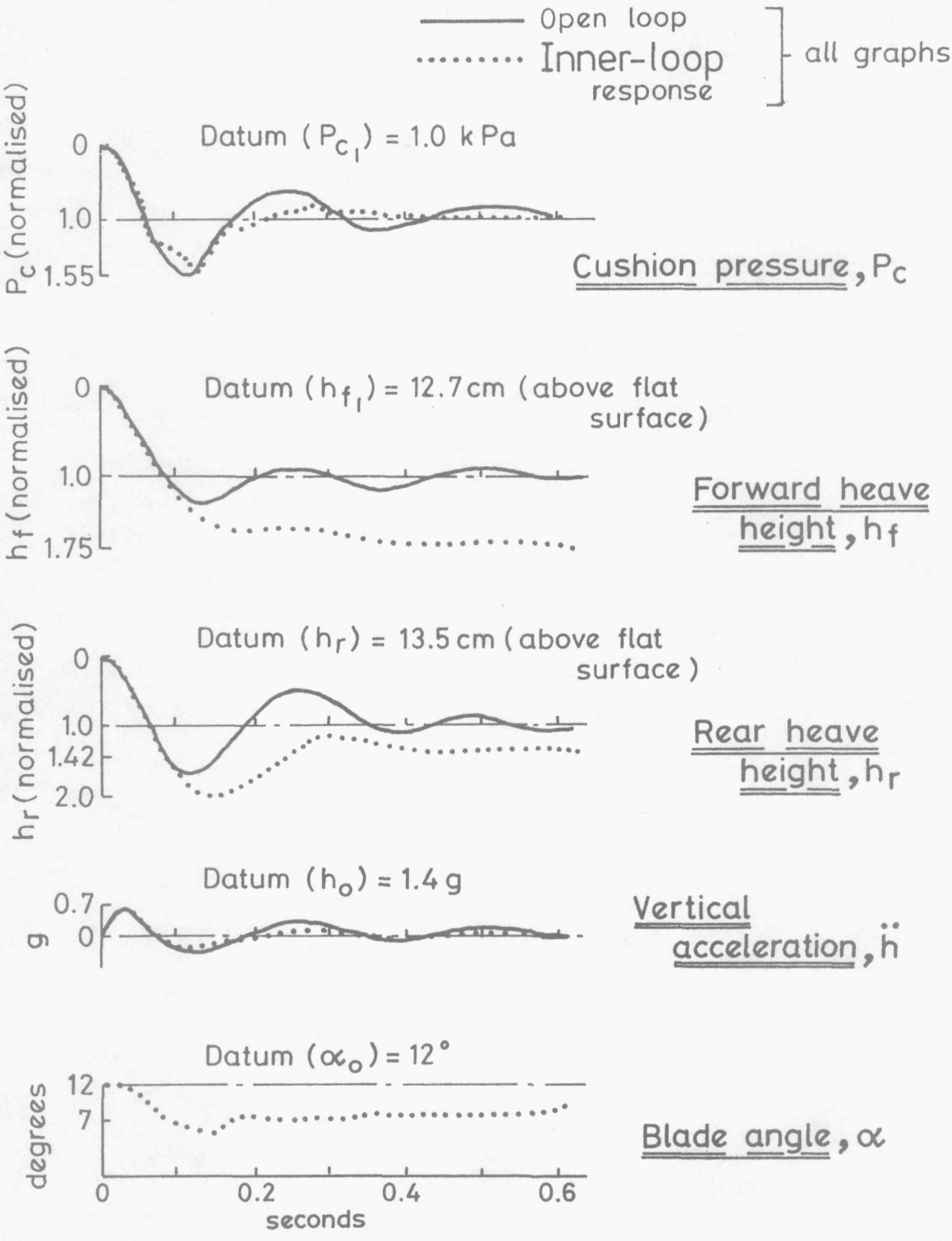

Fig. 6.1 **Inner loop transient response**

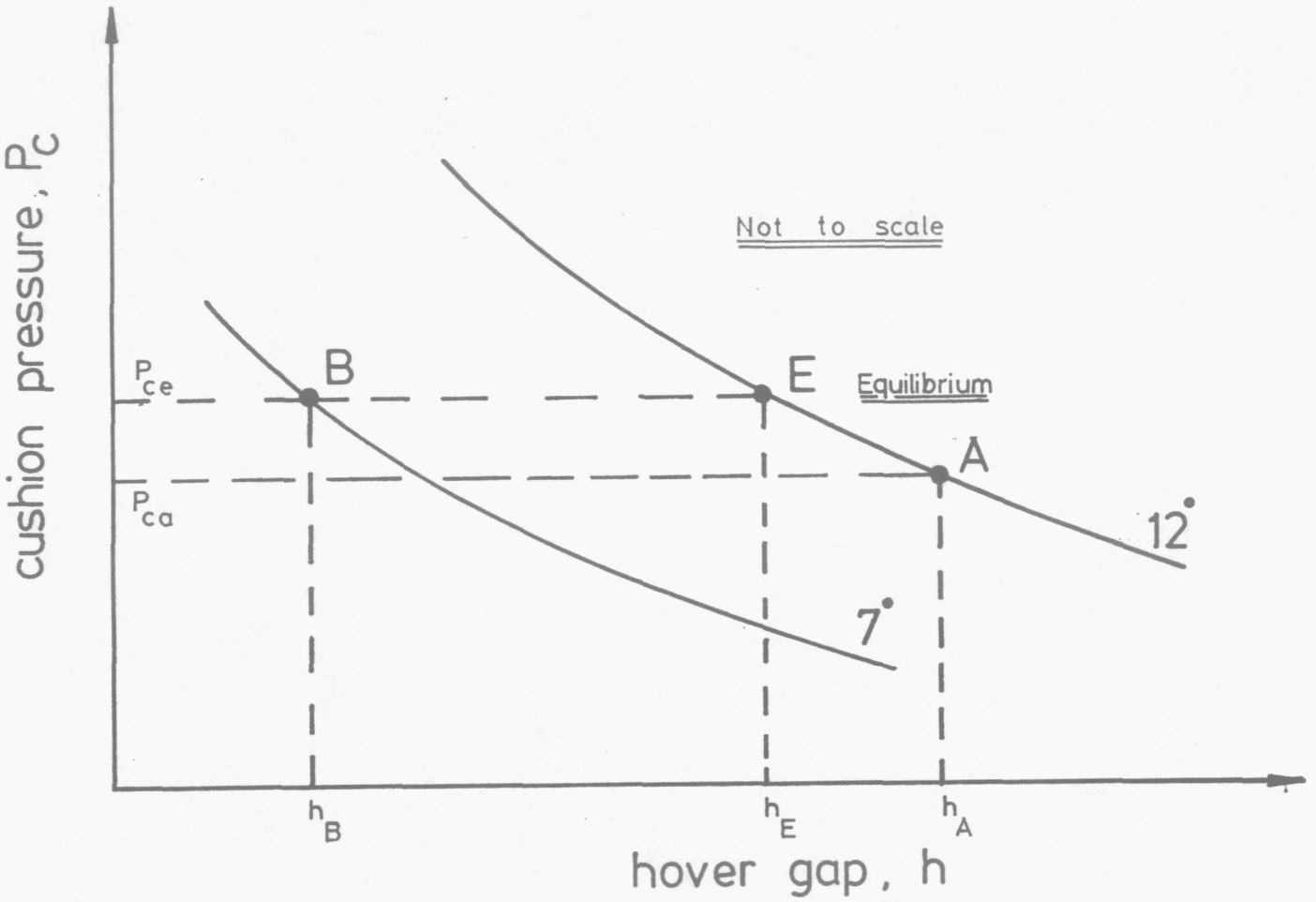

Fig. 6.2 Inner-loop behaviour due to step heave height changes

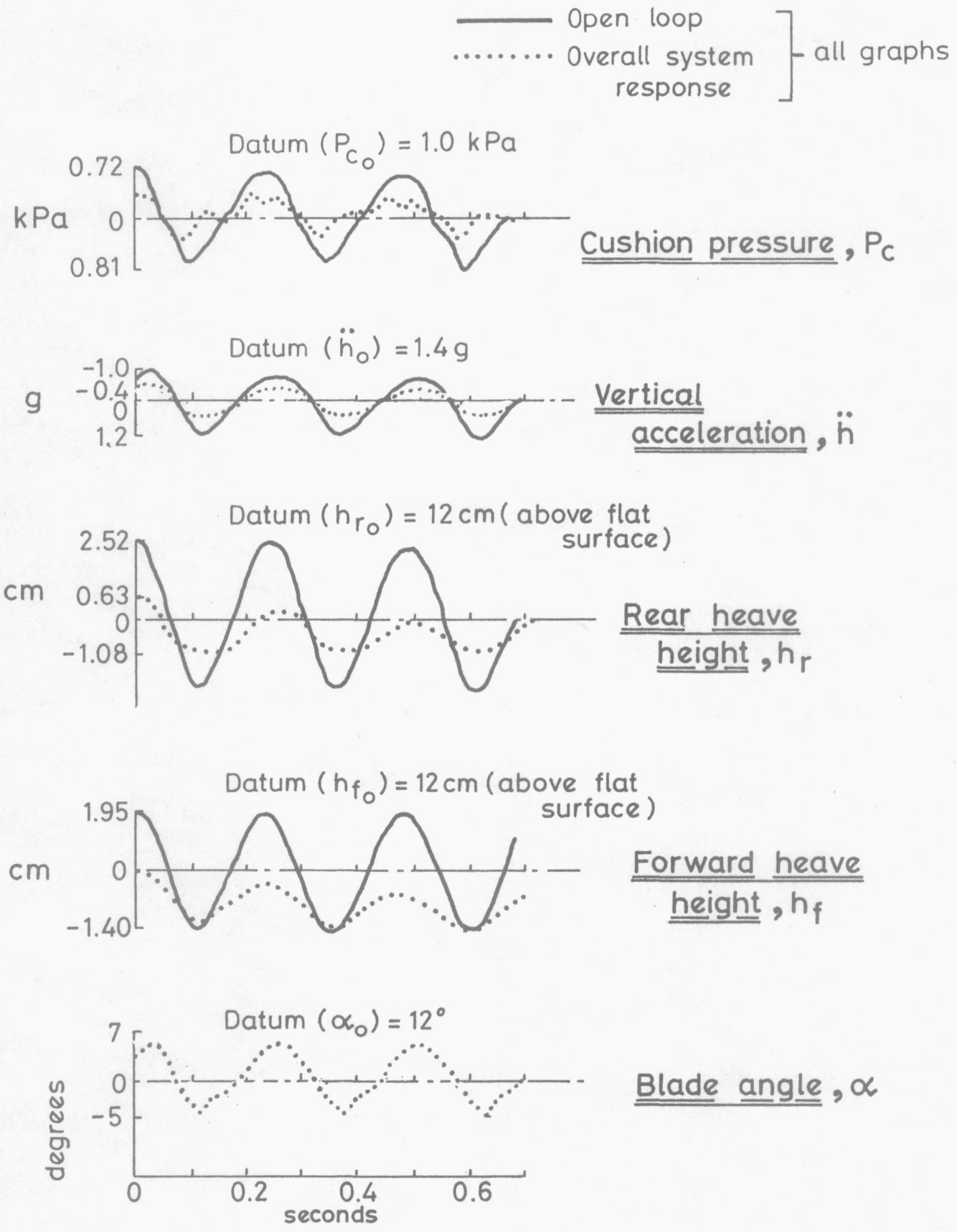

Fig. 6.3 Responses over 10 ft waves

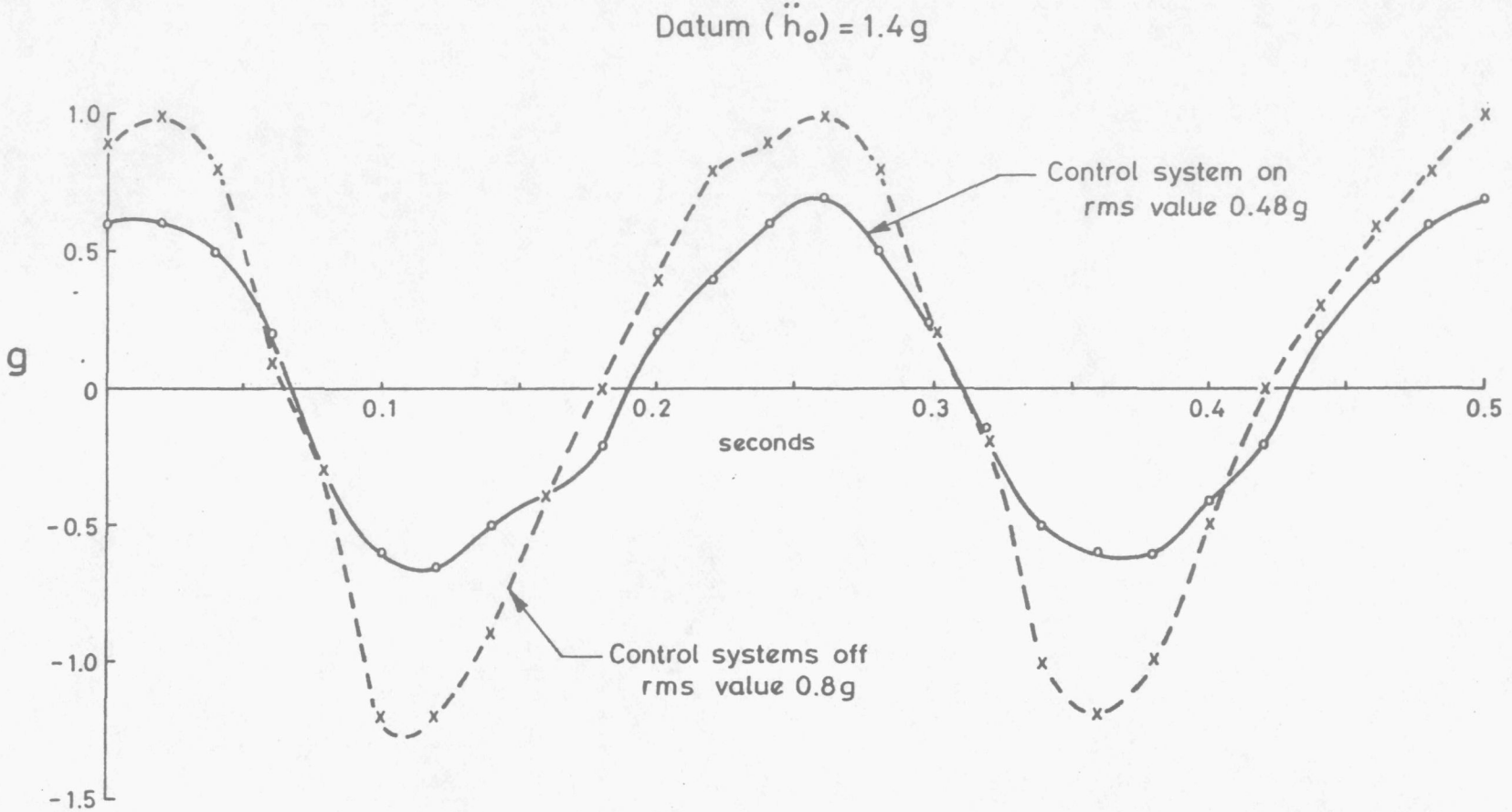

Fig. 6.4 Comparison of vertical acceleration between control systems on and off over 10ft waves

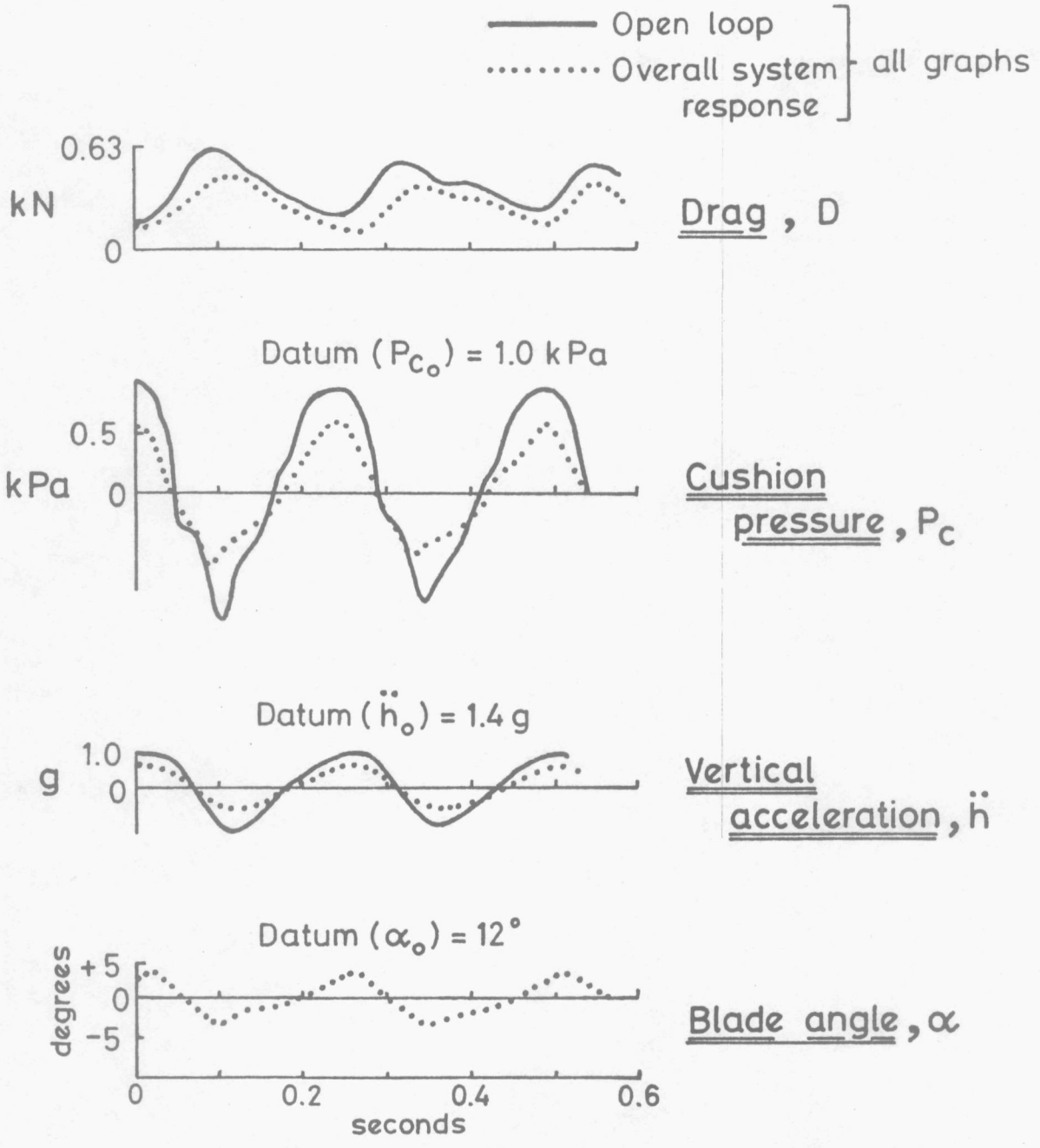

Fig. 6.5 Response over 10 ft waves with drag measurement

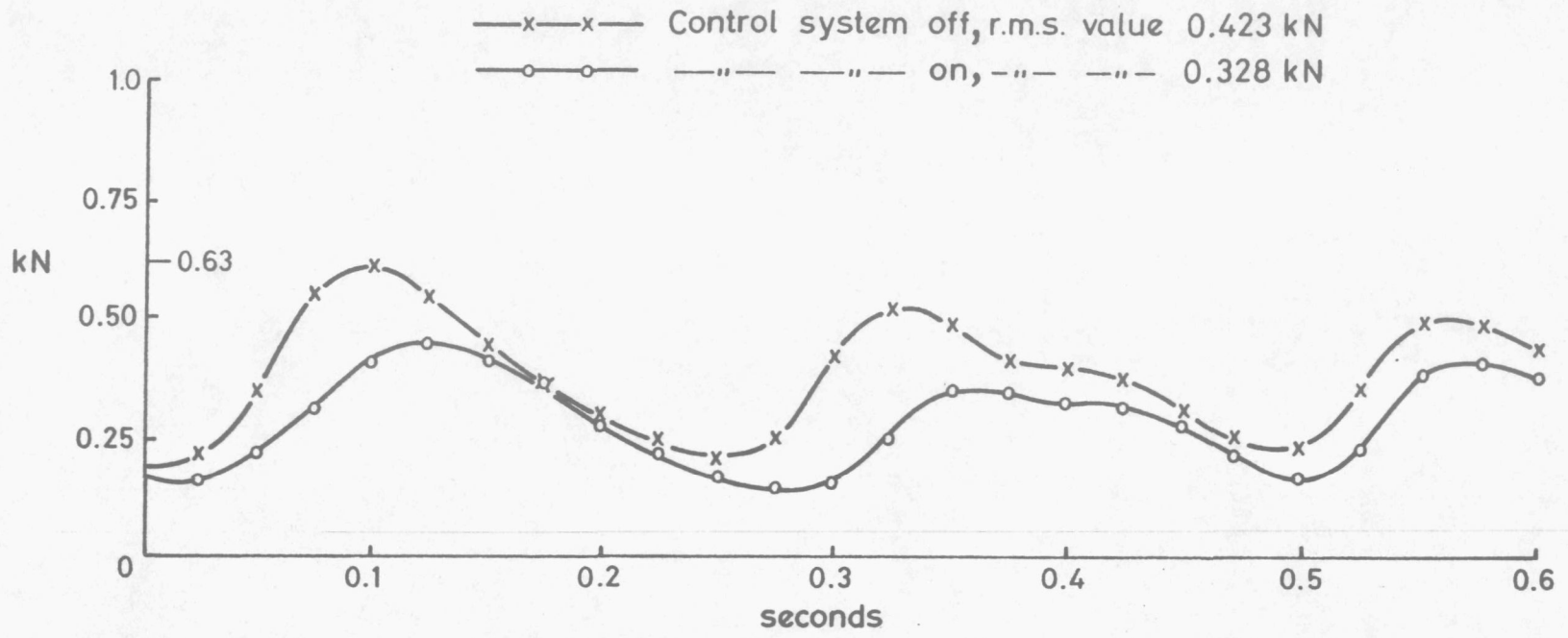

Fig. 6.6 Comparison of drag measurement between control systems on and off over 10ft waves

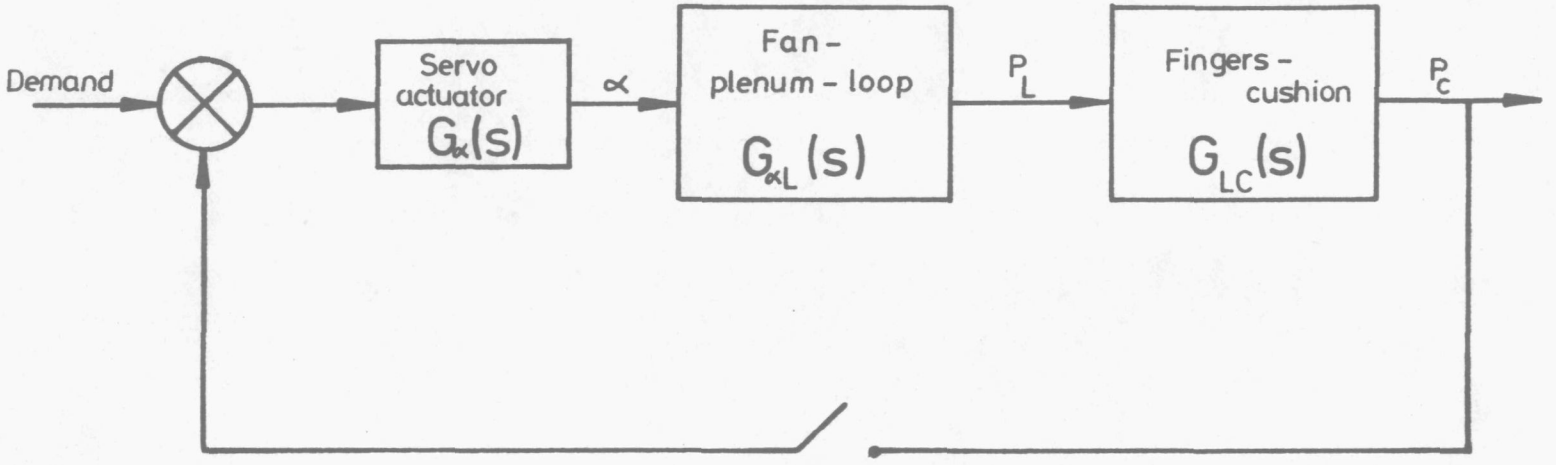

Fig. 7.1 Inner loop(open) system

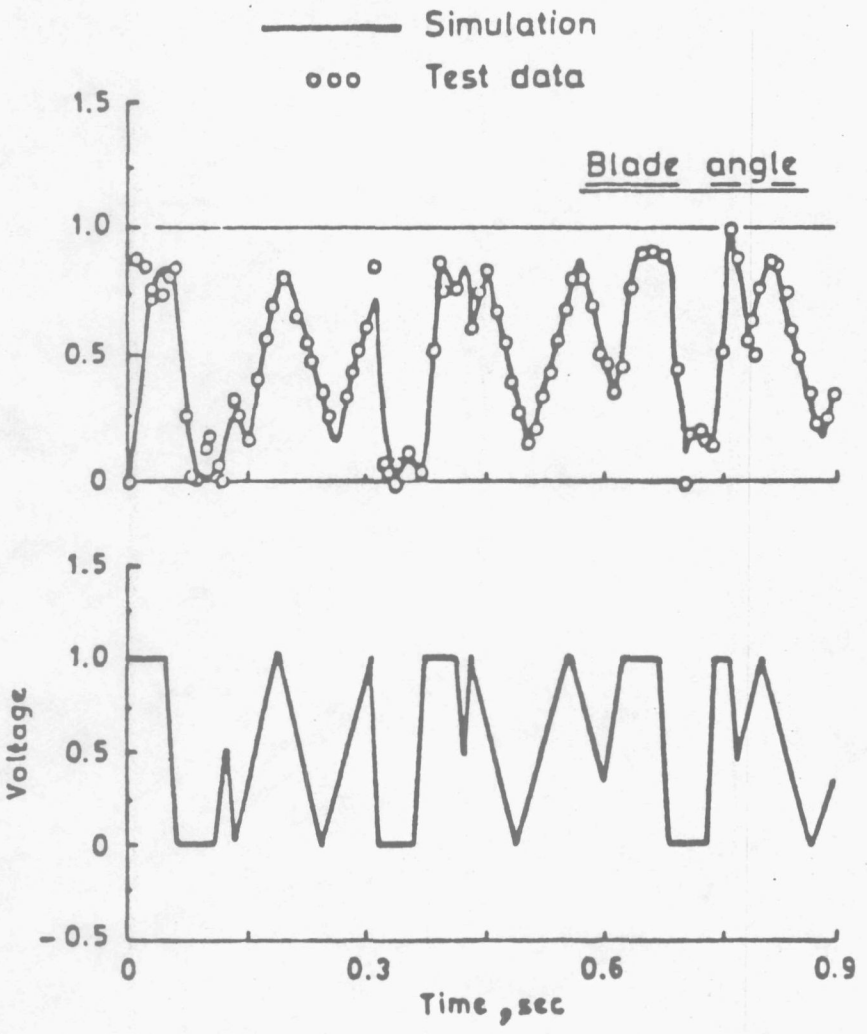

(Normalized)

Fig. 7.2 Blade angle response to random input

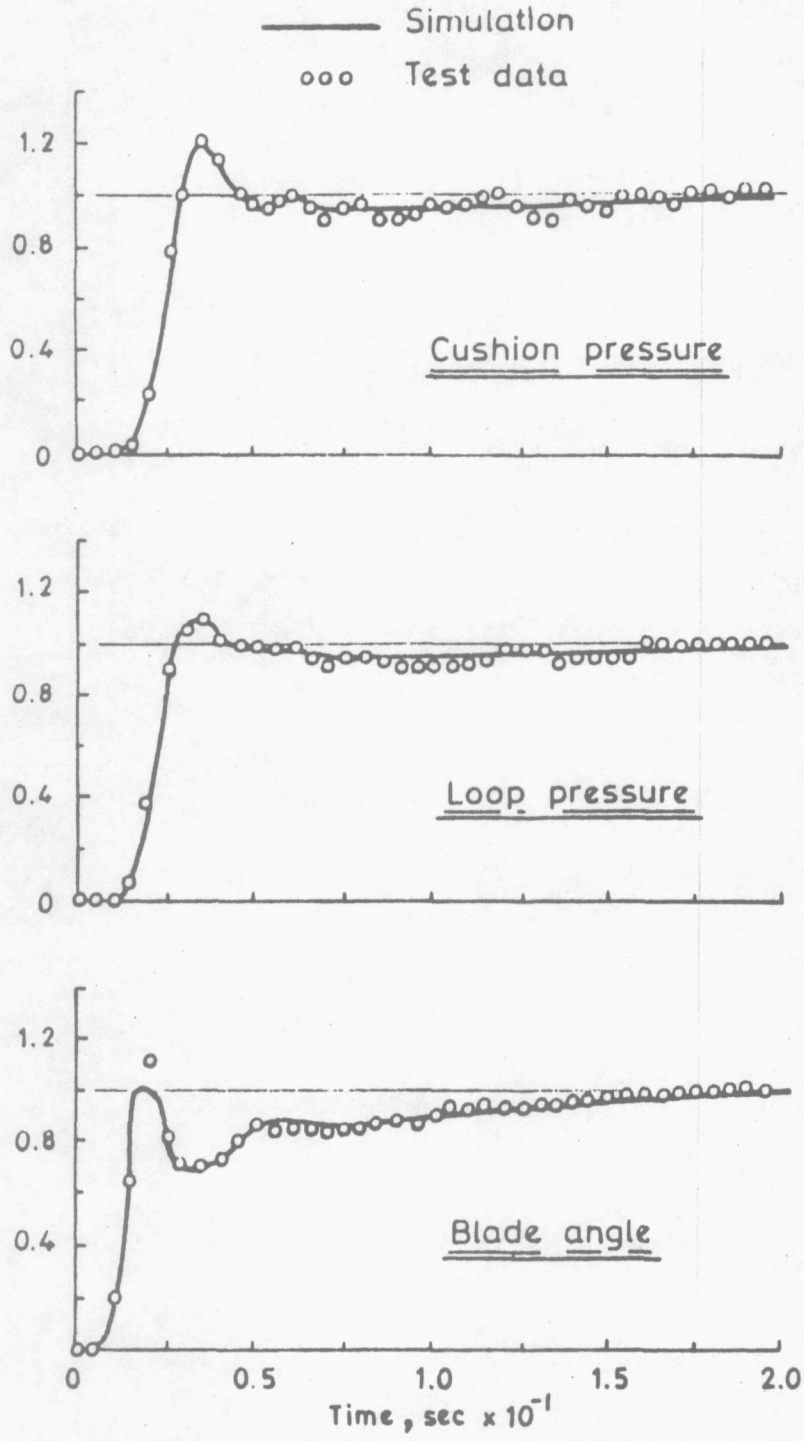

Fig. 7.3 Normalized step response to voltage input

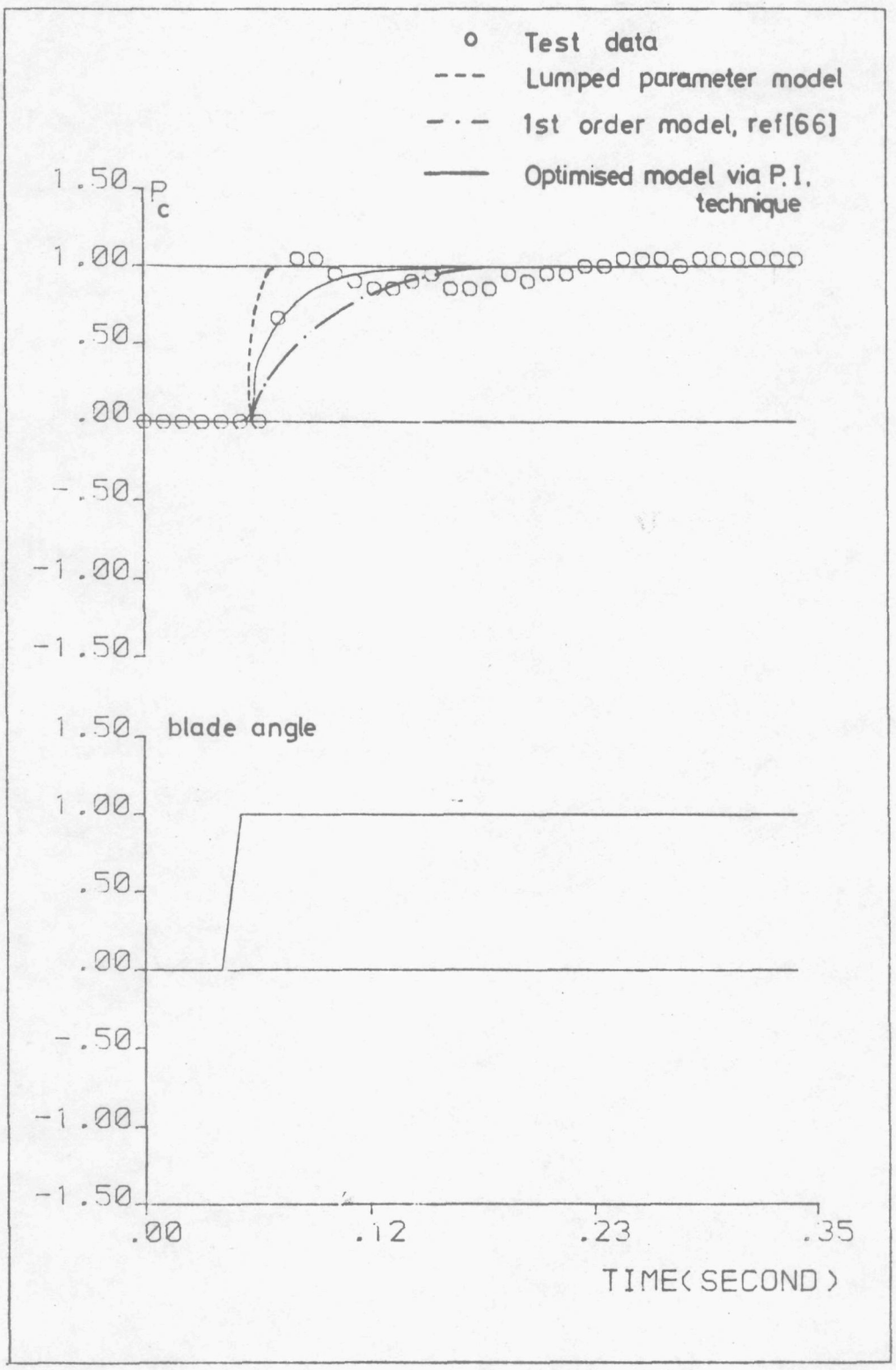

Fig. 7.4 Cushion pressure transient response due to blade angle changes

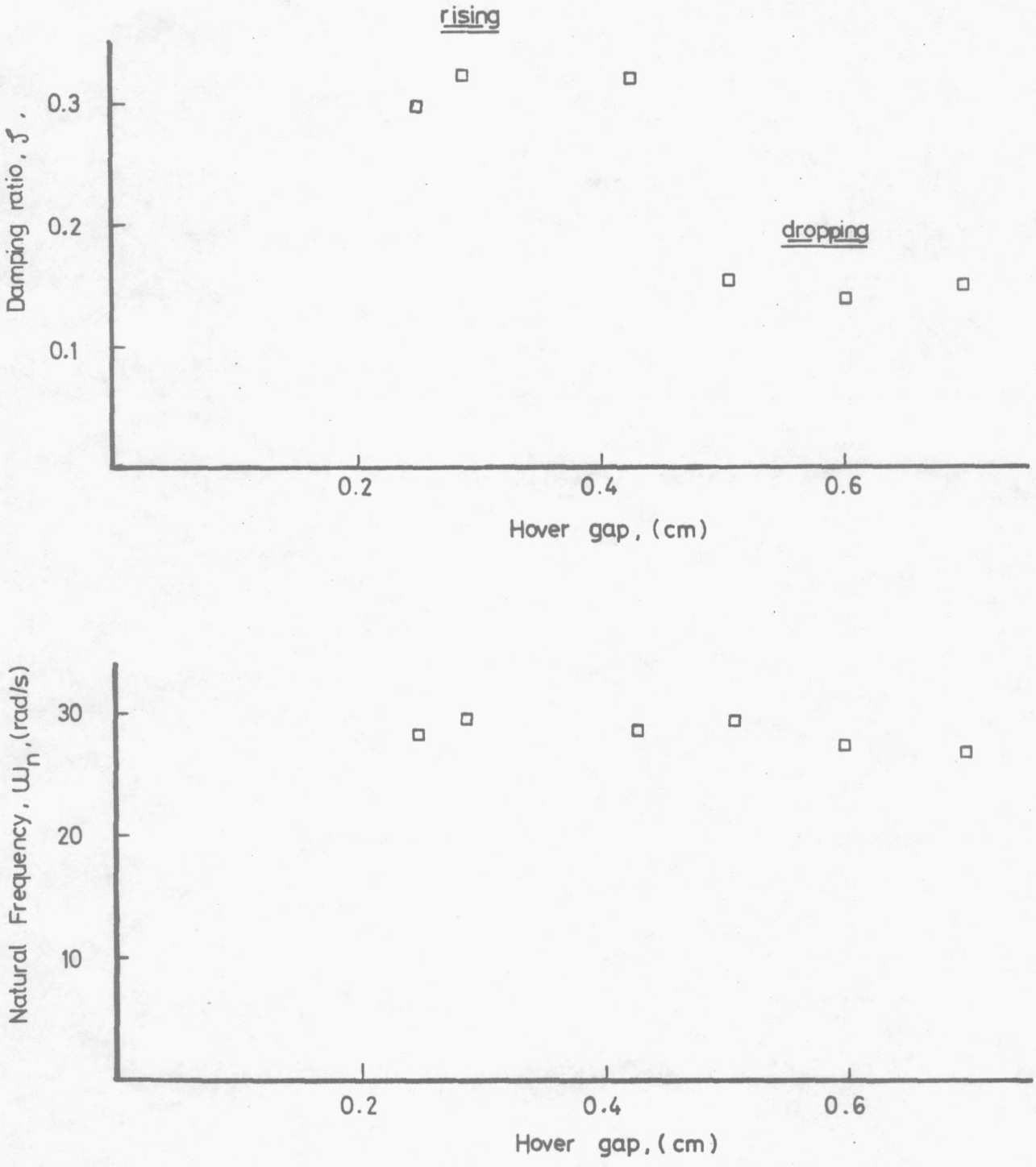

Fig. 7.5 Variation of damping ratio and natural frequency over a range of hover gaps

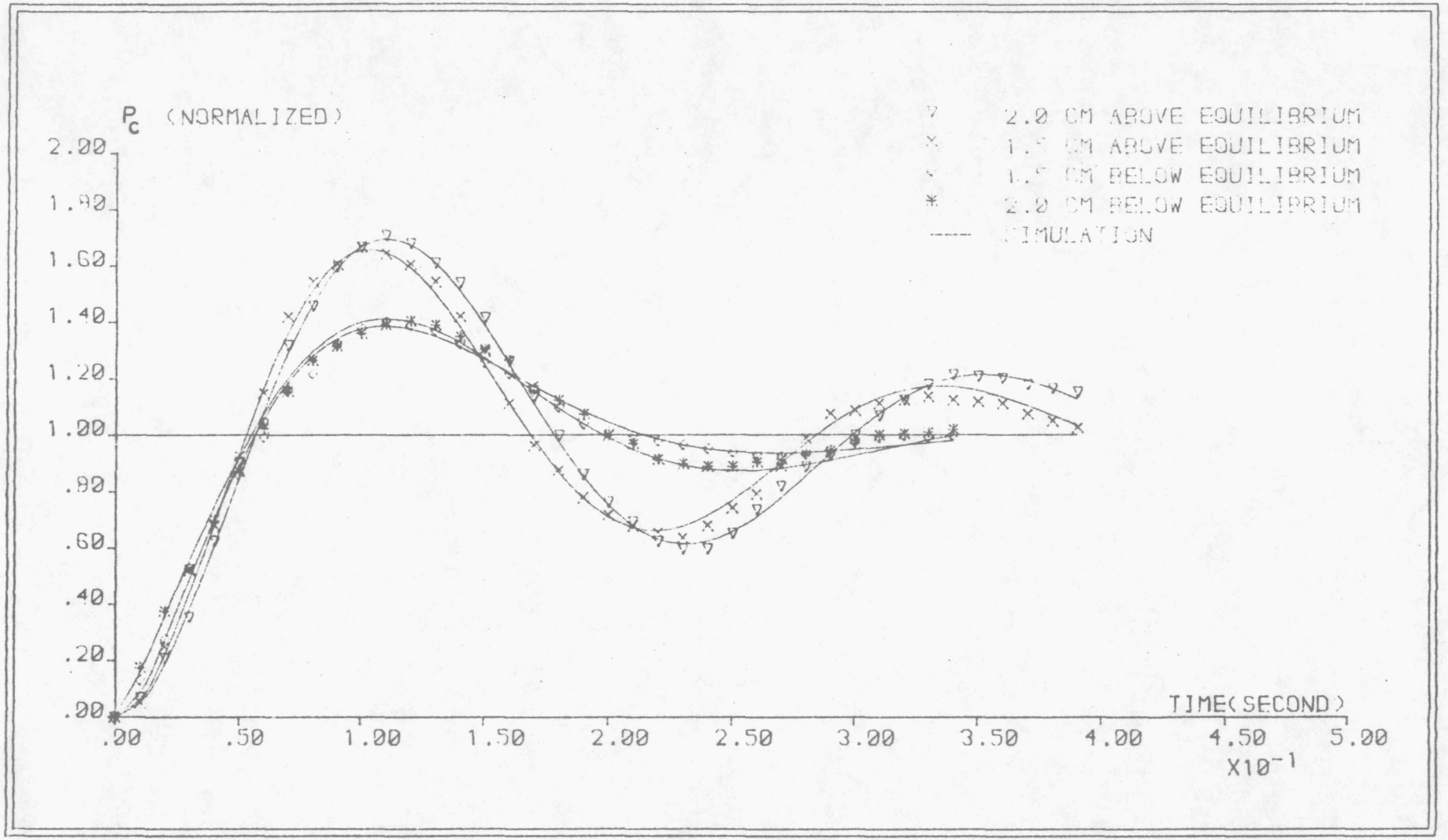

Fig. 7.6 Cushion pressure response to step input of heave height

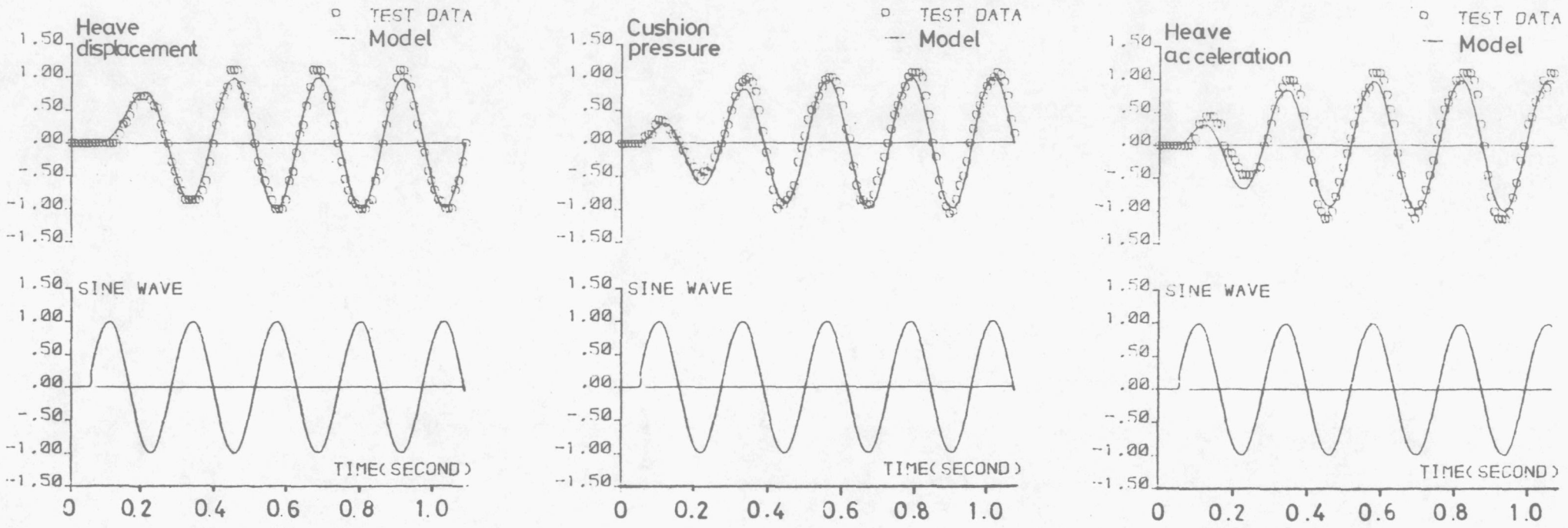

— All graphs are normalised —

Fig. 7.7 Application of a 3rd order model to the responses over 10 ft waves

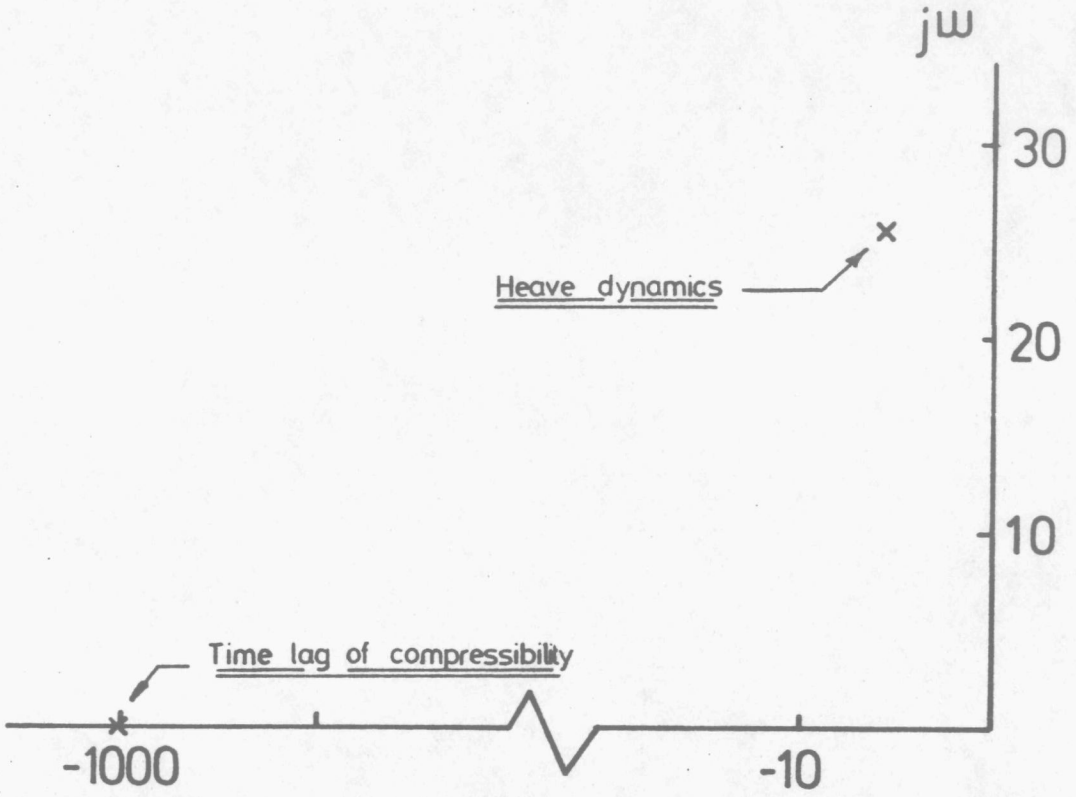

Fig. 7.8 The effect of compressibility in s-plane

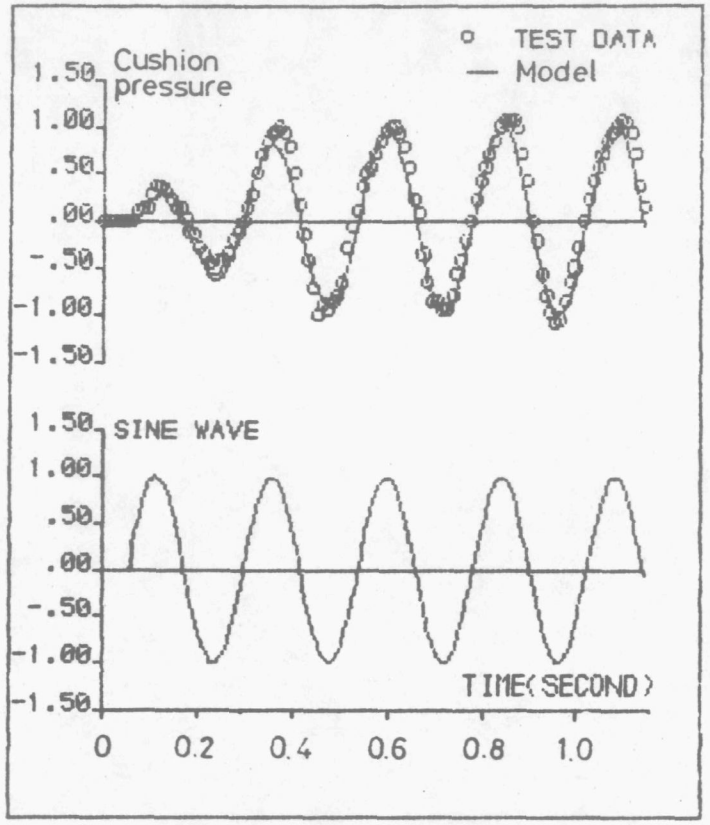

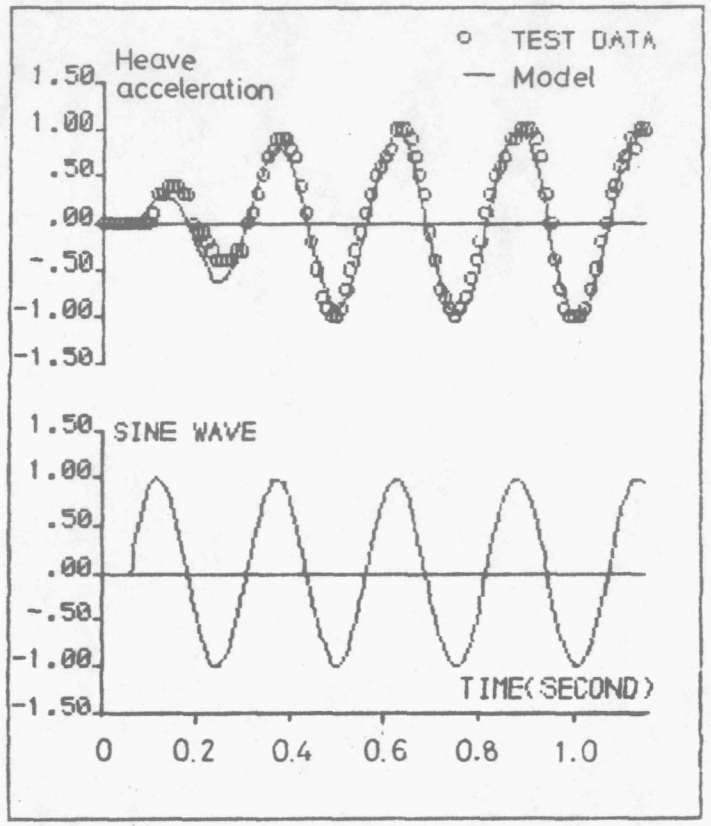

– All graphs are normalised –

Fig. 7.9 Application of a 2nd order model to the responses over the 10 ft waves

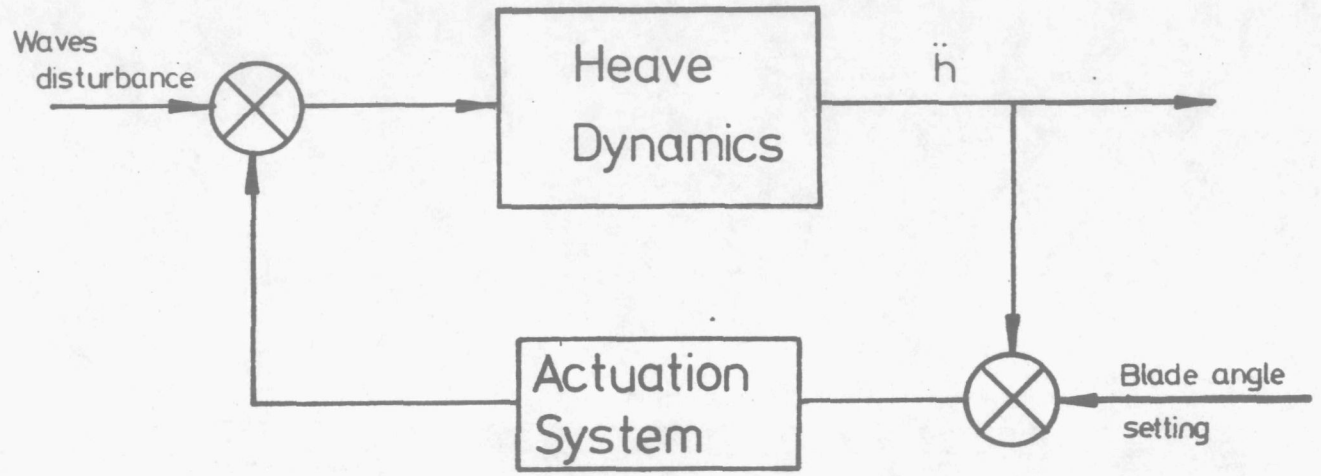

Fig. 7.10 The simplified heave control system

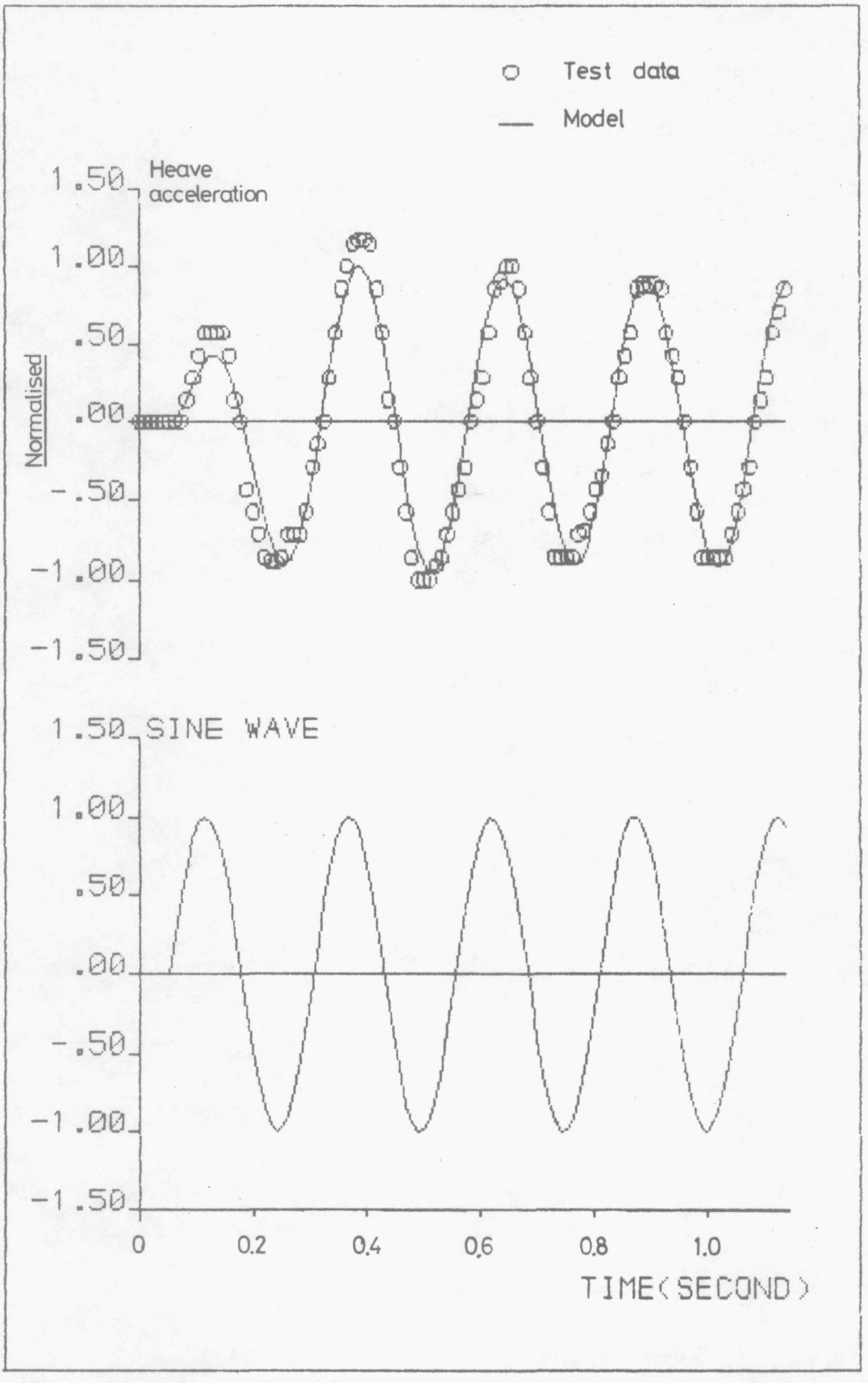

Fig. 7.11 Heave control system responses with 1st order actuation time-lag

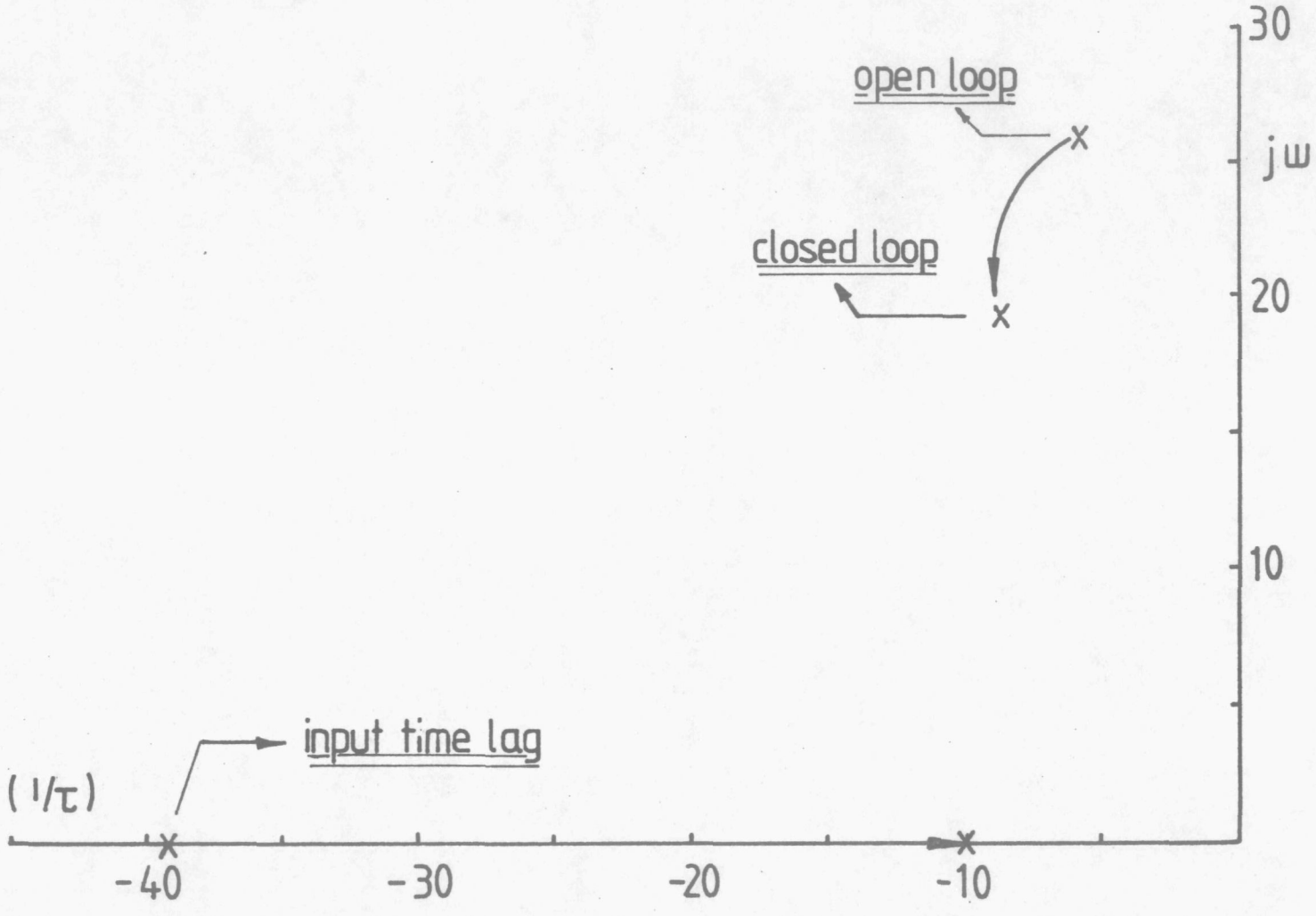

Fig. 7.12 Root locus plot of heave control system

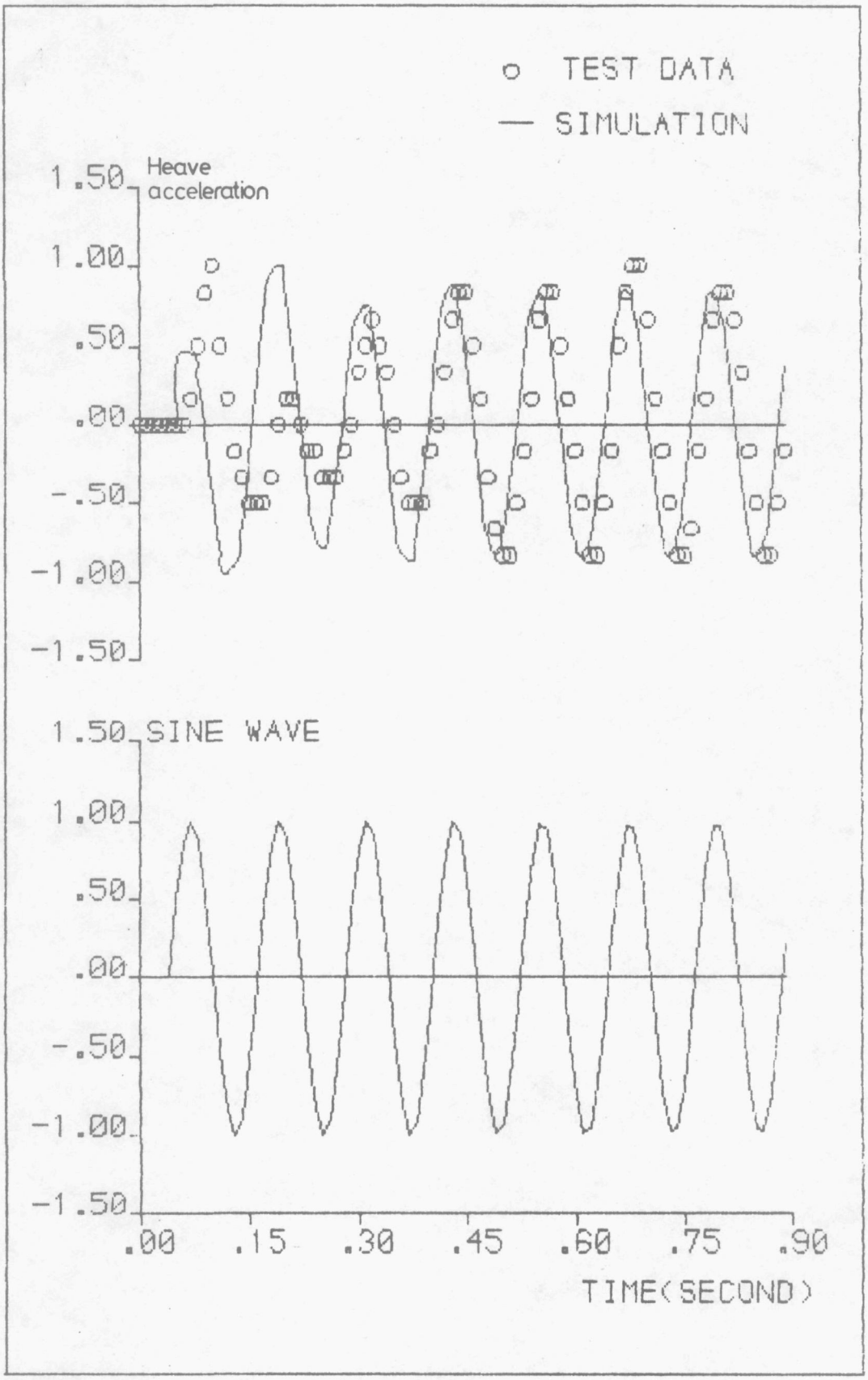

Fig. 7.13 Sampling of heave acceleration responses at the beginning of 3.3ft waves excitation

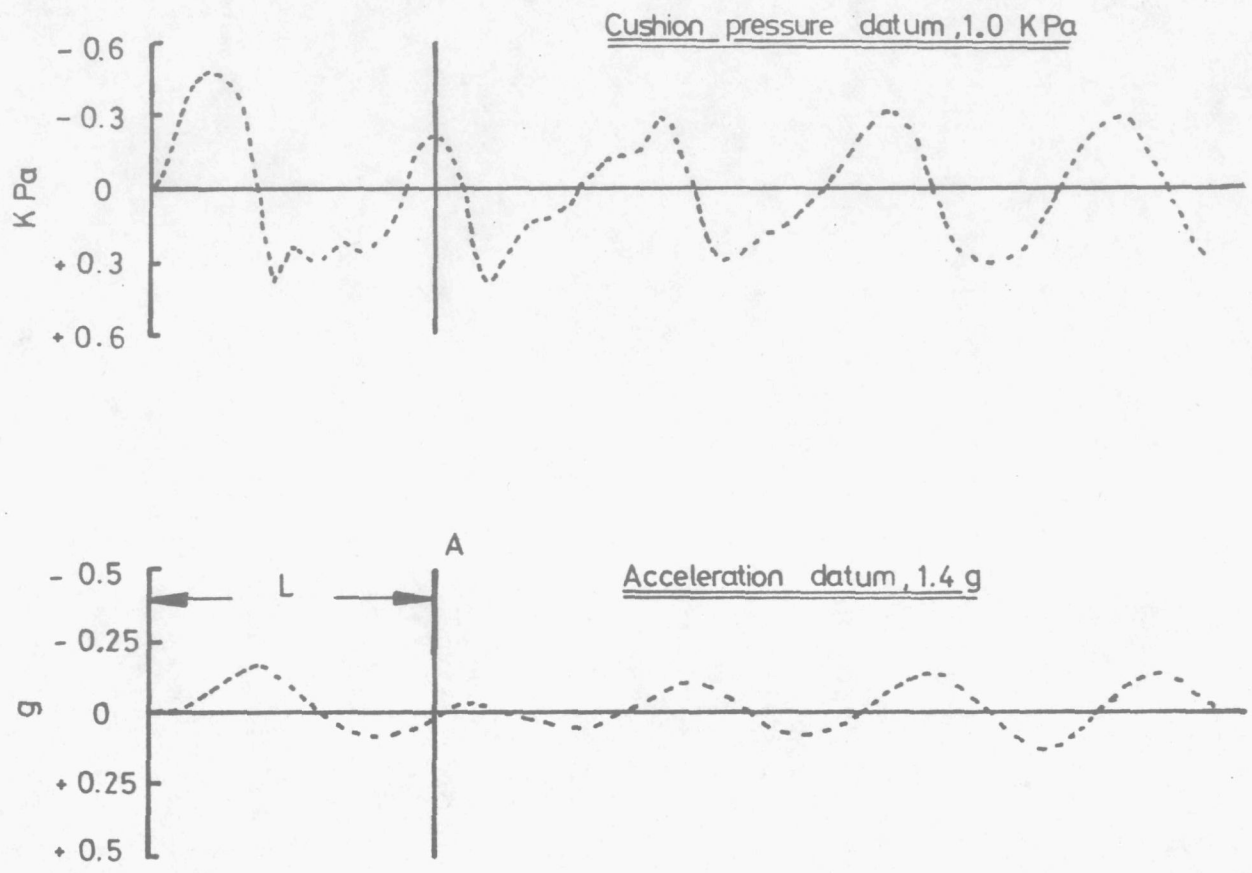

Fig. 7.14 Responses over the 3.3ft waves

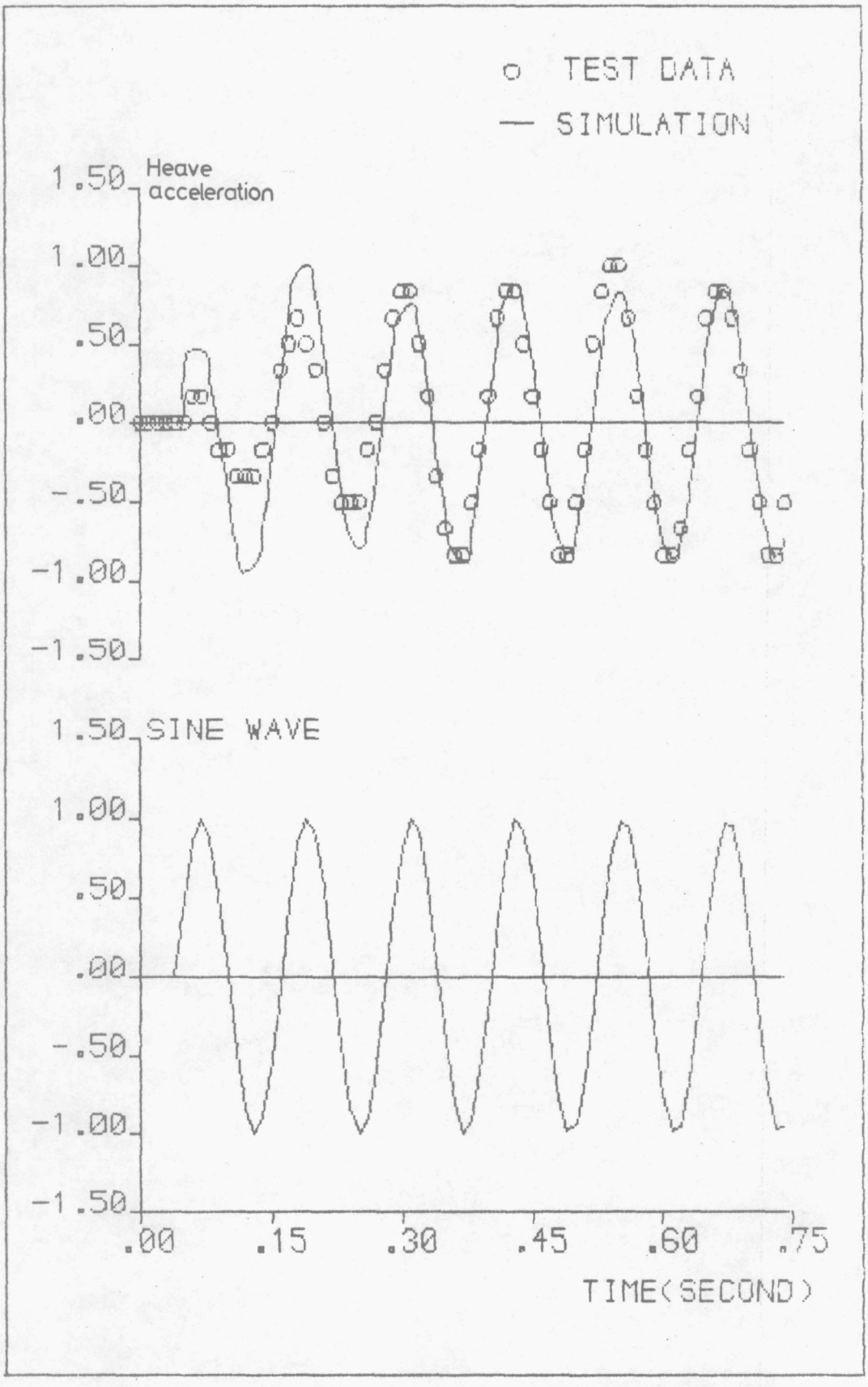

Fig. 7.15 Sampling of heave acceleration responses after the initial transient period of the 3.3ft waves

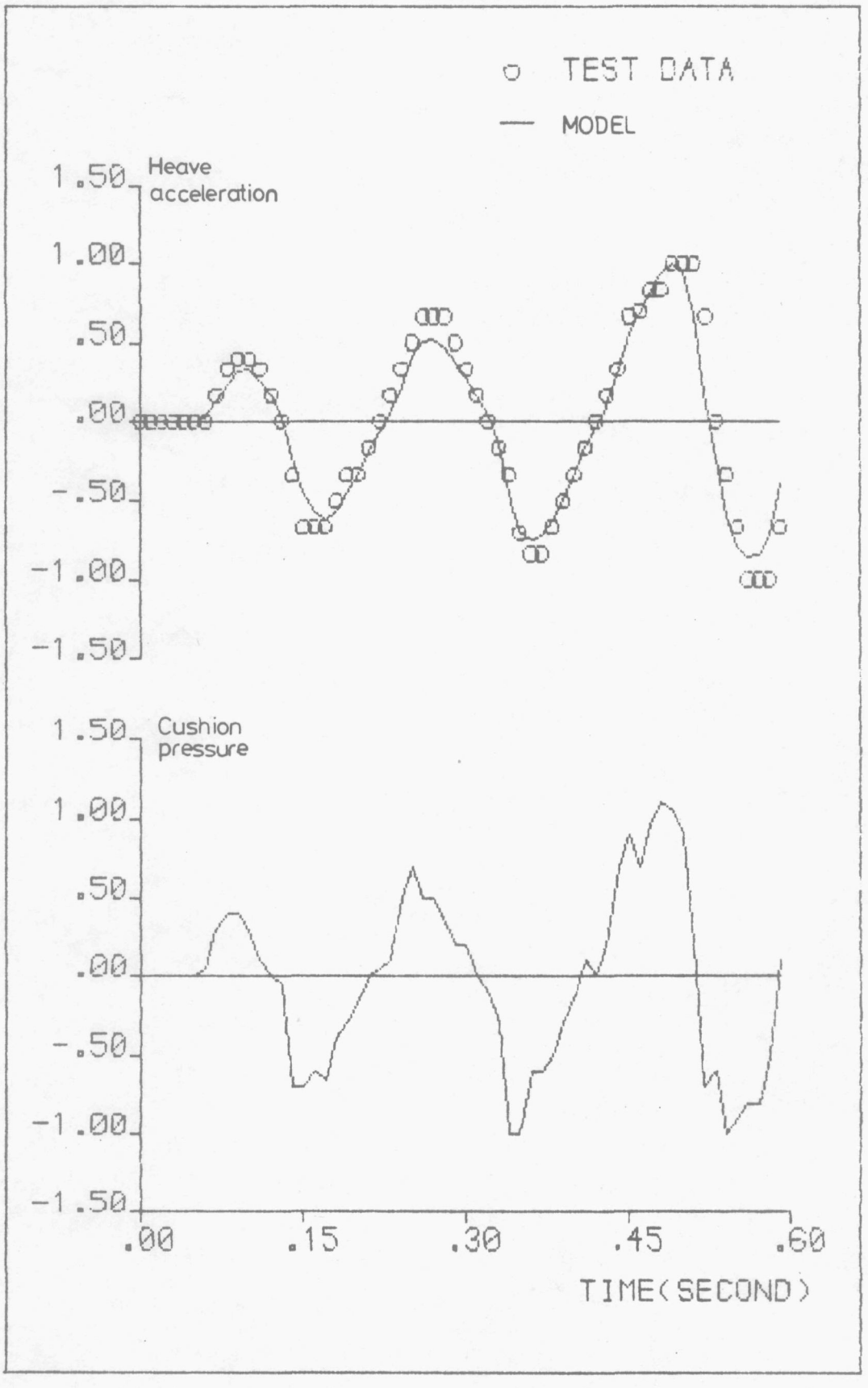

Fig. 7.16 Modelling of cushion-craft dynamics using responses from blade angle excitation

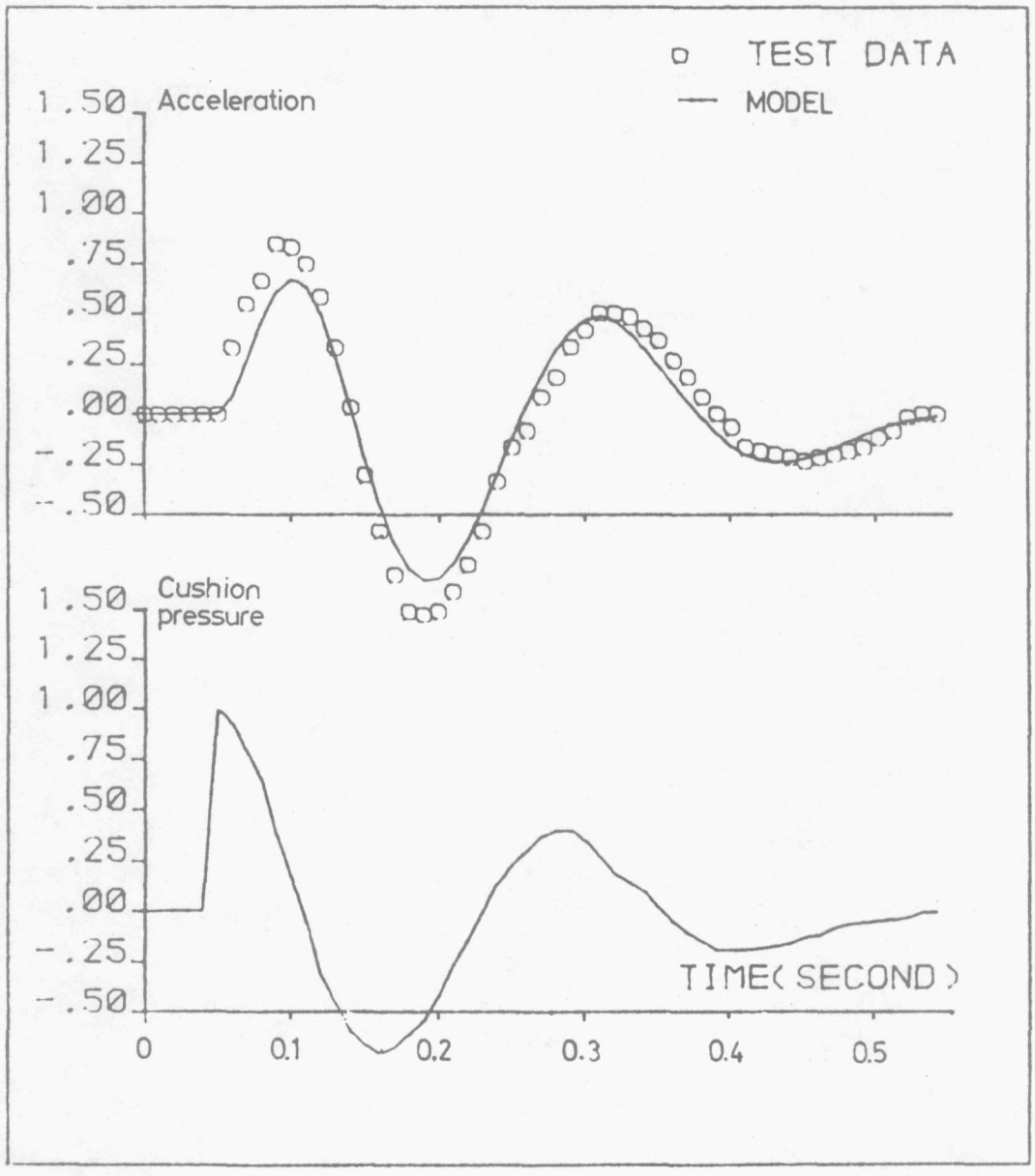

Fig. 7.17 Modelling of cushion-craft dynamics using responses from step heave height experiment

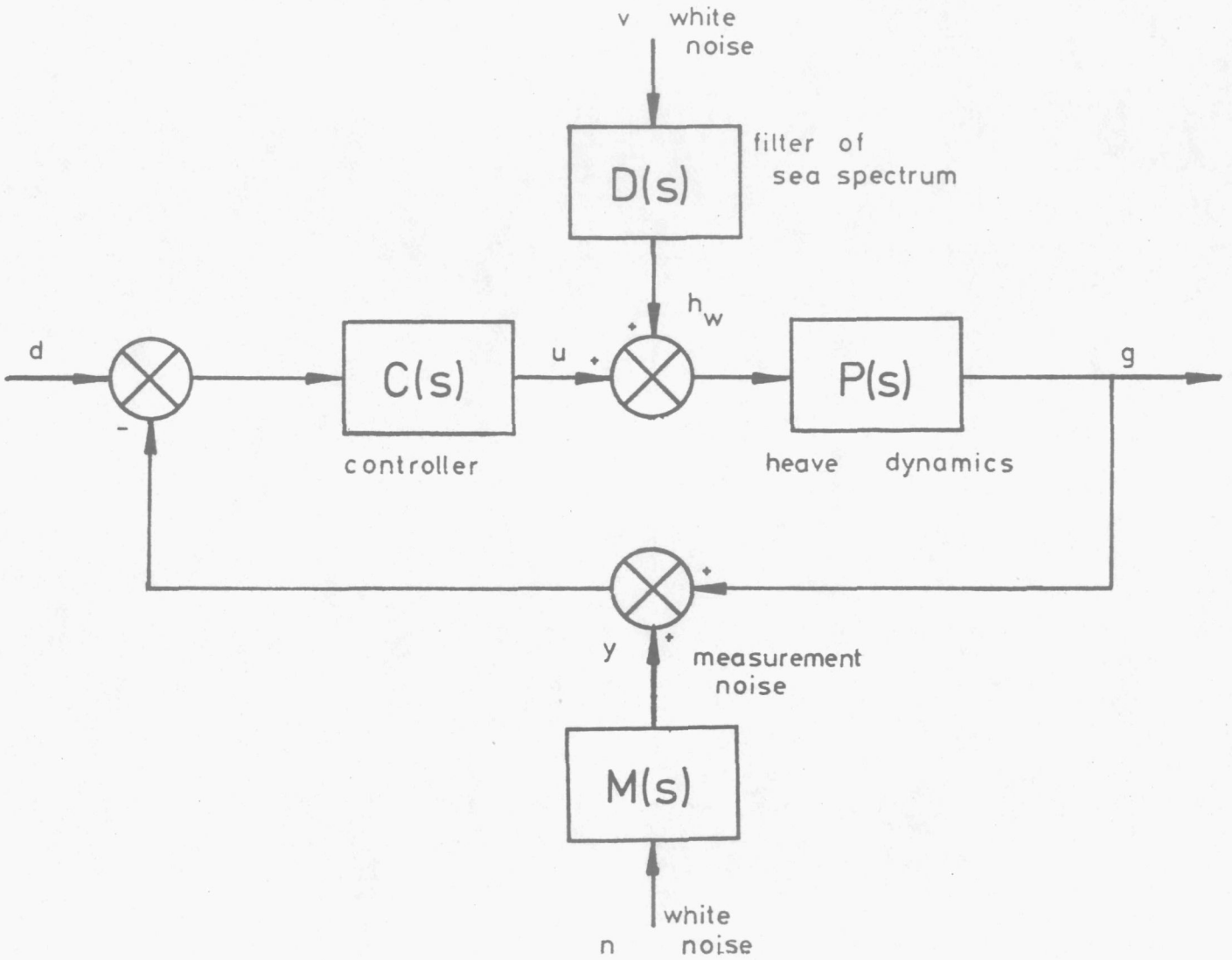

Fig. 8.1 Feedback control system

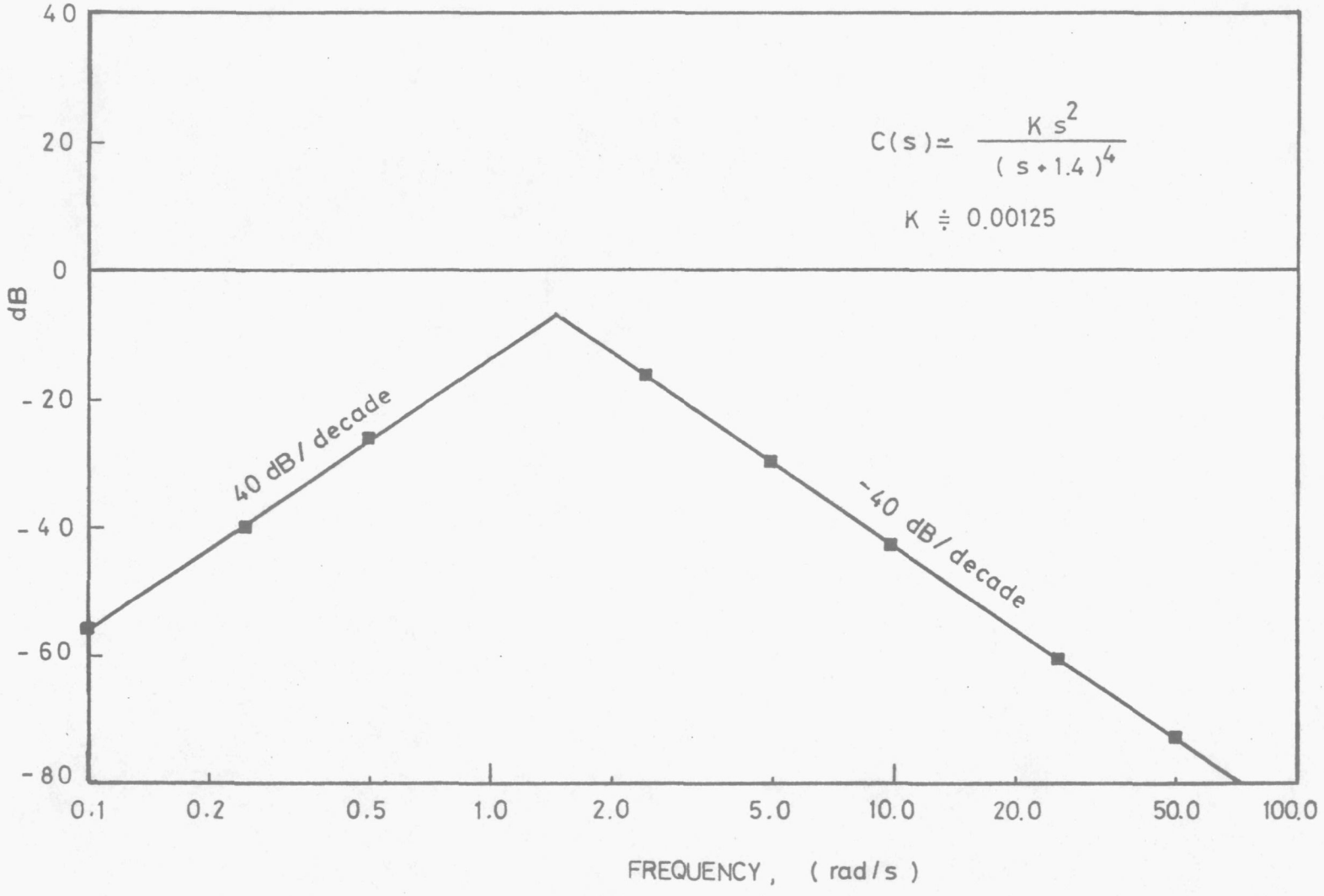

Fig. 8.2 Transfer-function of the controller from a Bode plot

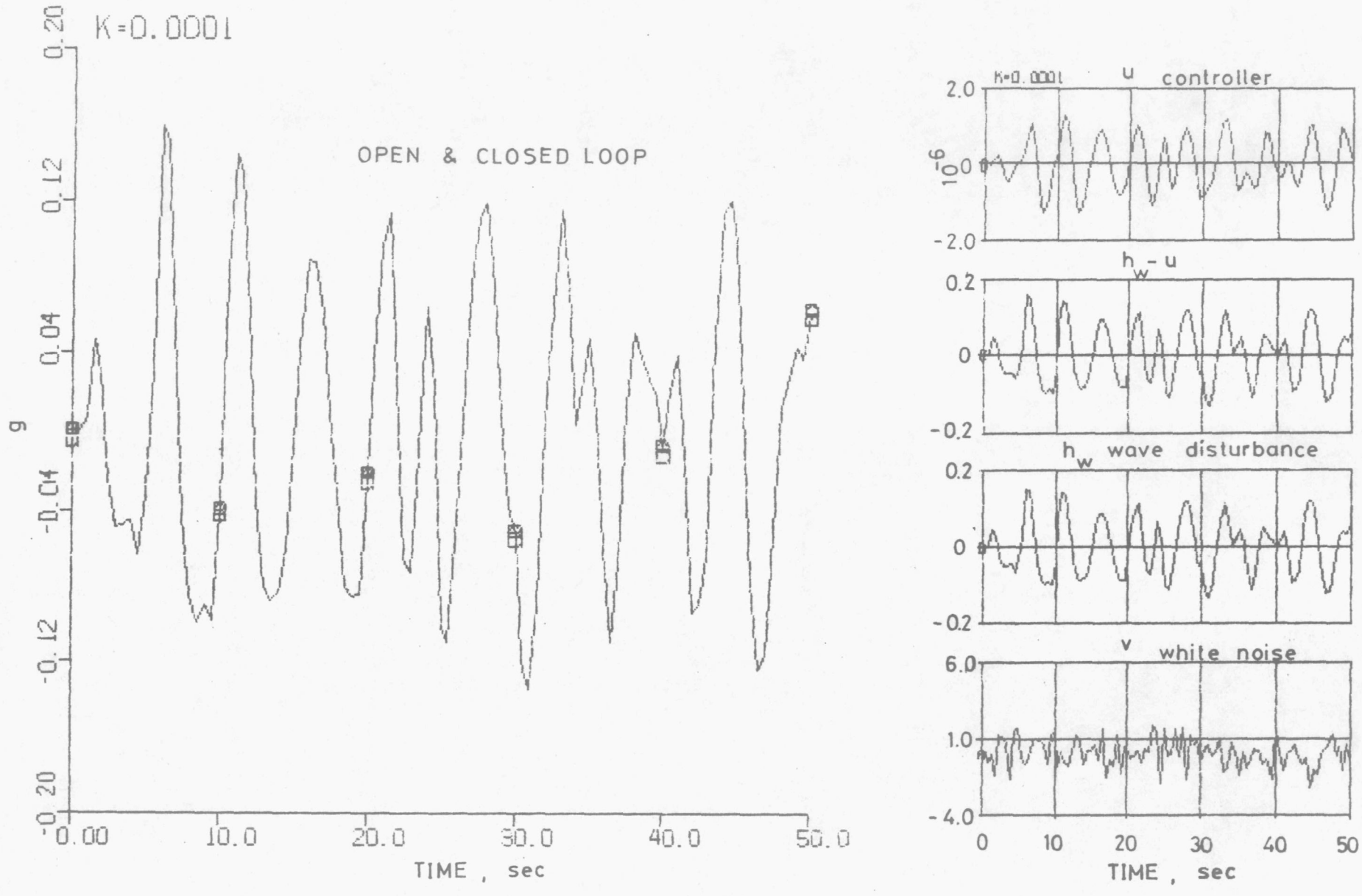

Fig. 8.3 Control system responses at K = 0.0001

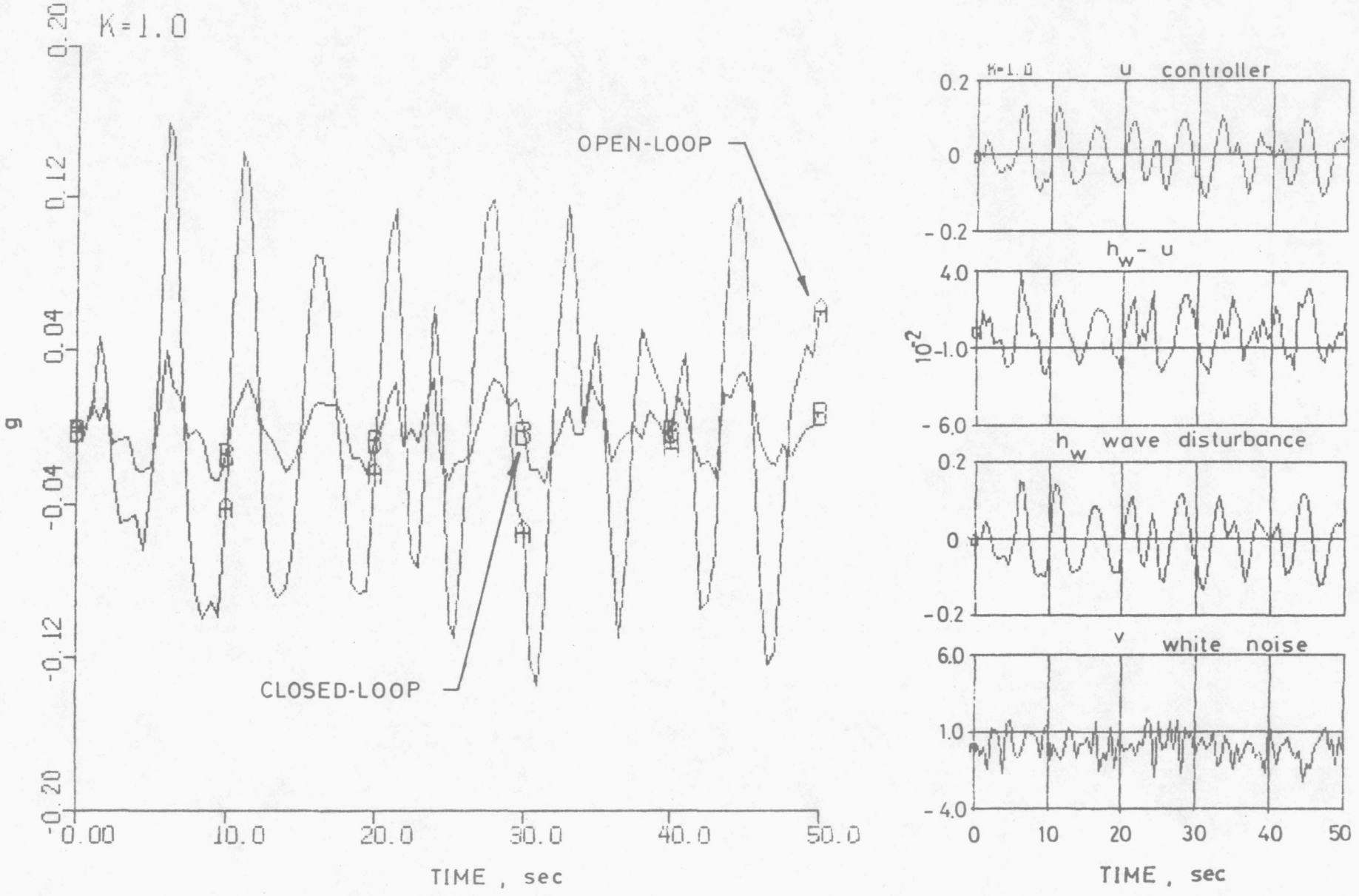

Fig. 8.4 Control system responses at K = 1.0

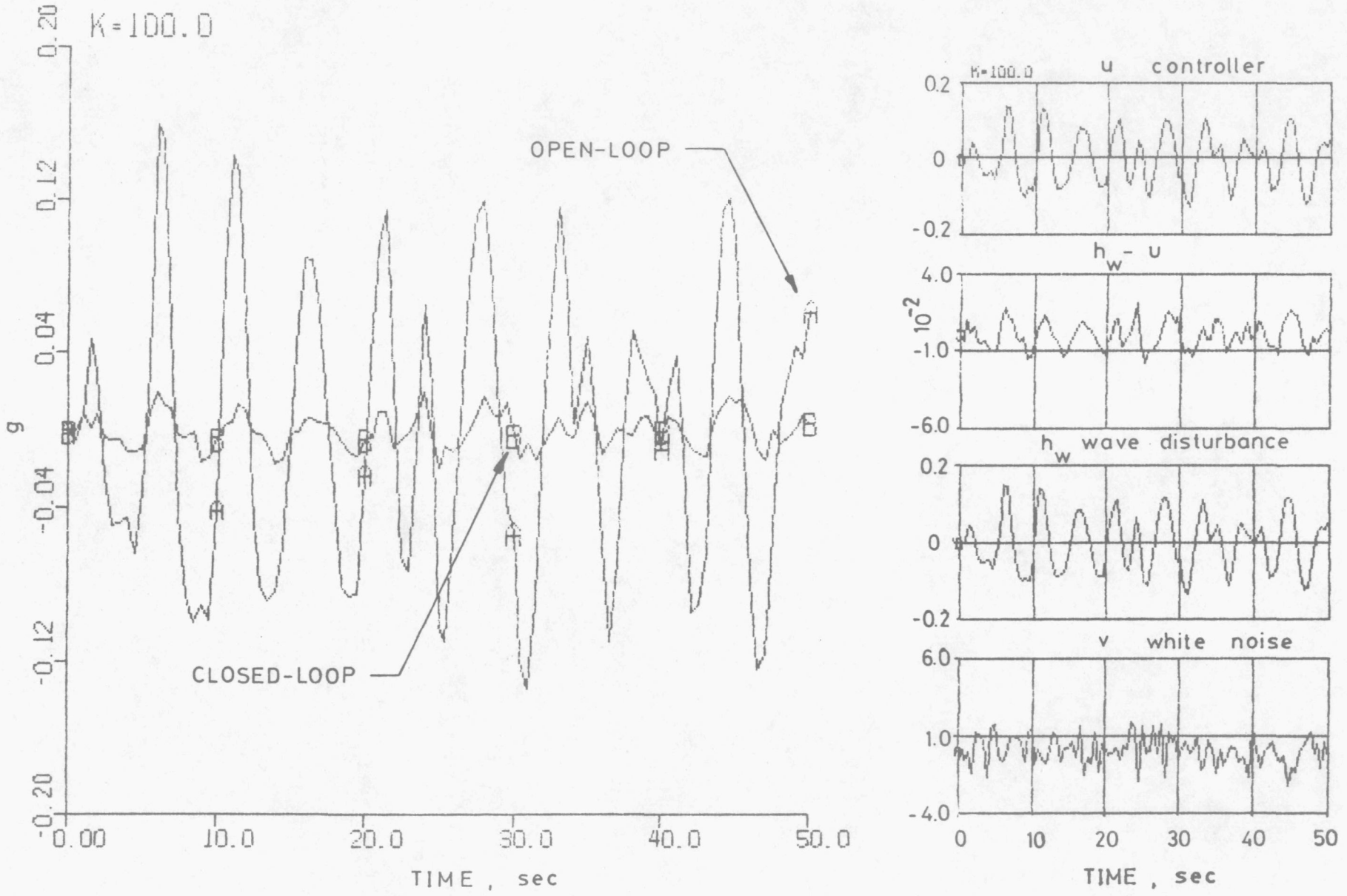

Fig. 8.5 Control system responses at K = 100.0

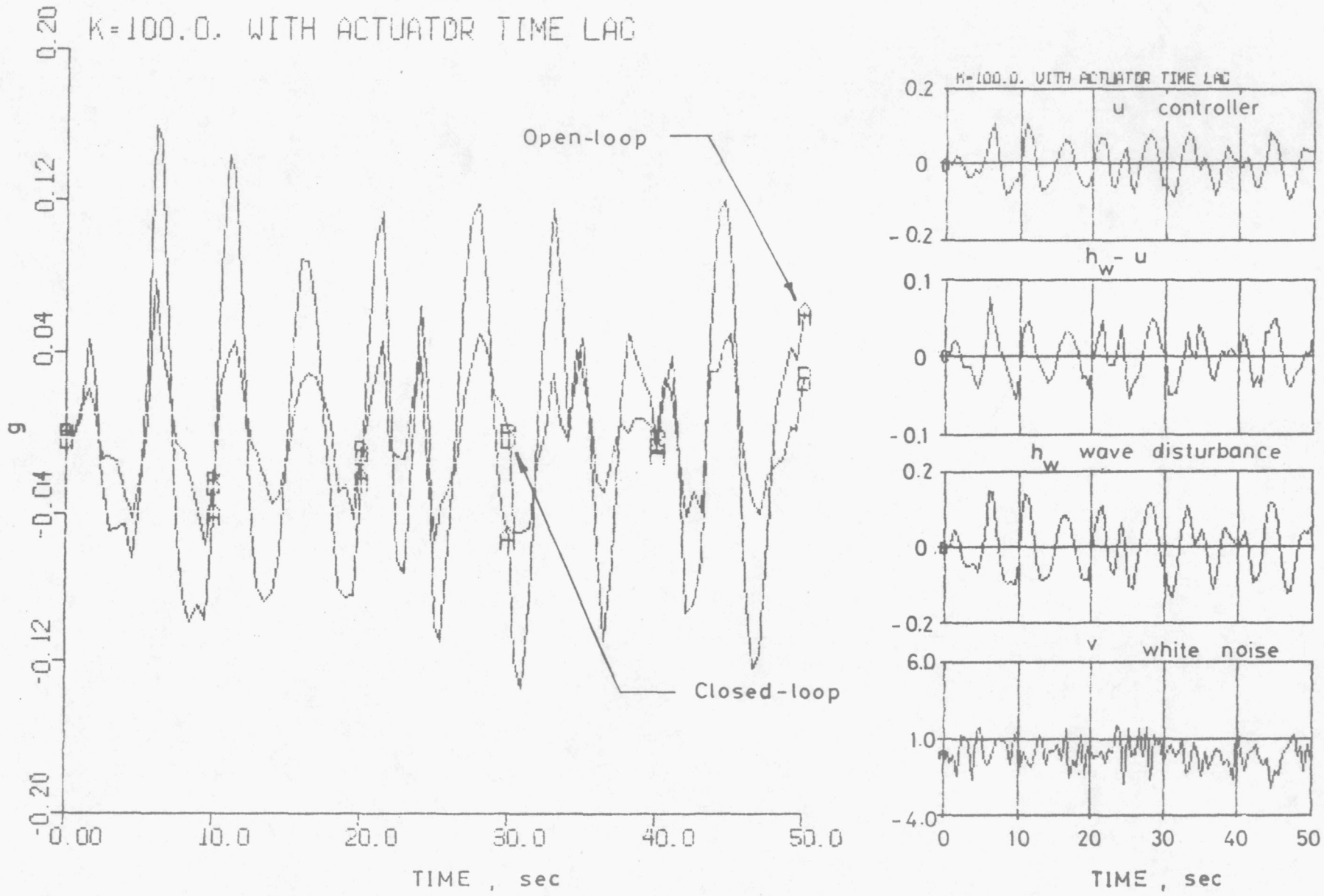

Fig. 8.6 Control system responses at K =100.0, including actuator time lag

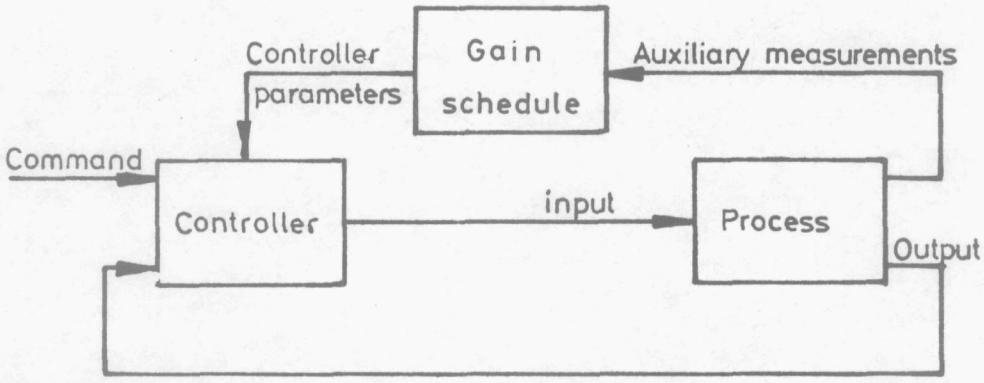

(a) Gain scheduling

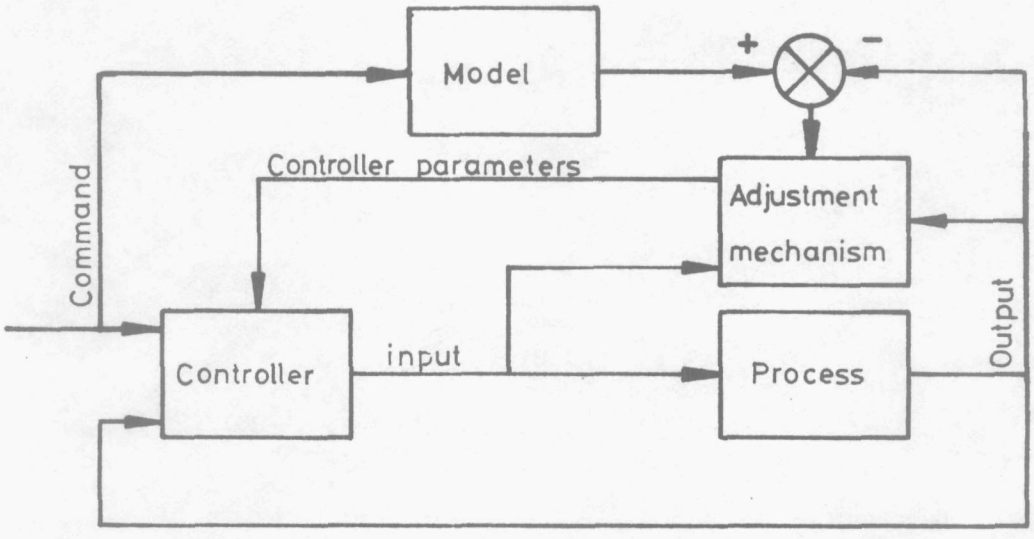

(b) Model reference

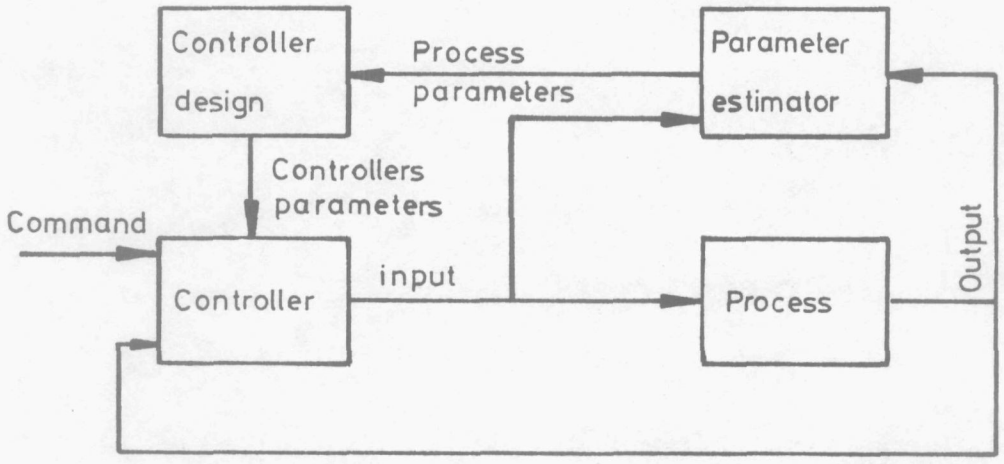

(c) Self - tuning

Fig. 8.7 Block diagram of adaptive control techniques

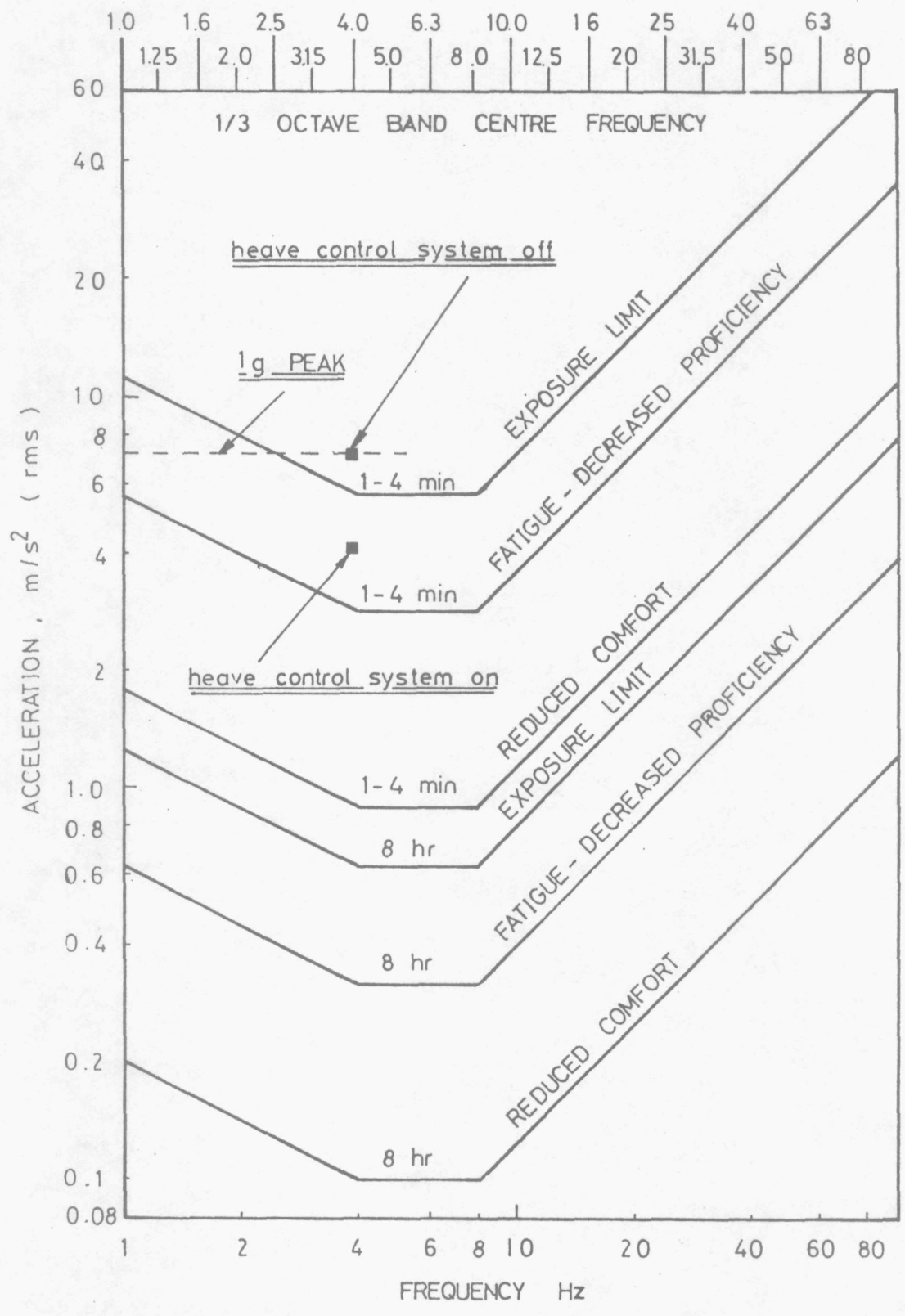

Fig.9.1 ISO 2631: Acceleration/frequency curves for longitudinal, a_z axis

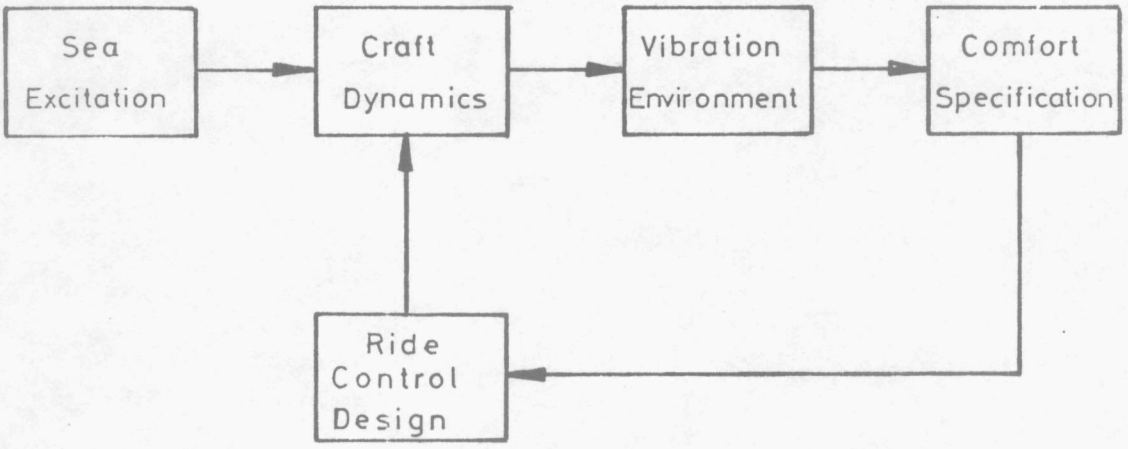

Fig. 9.2a Ride control system design

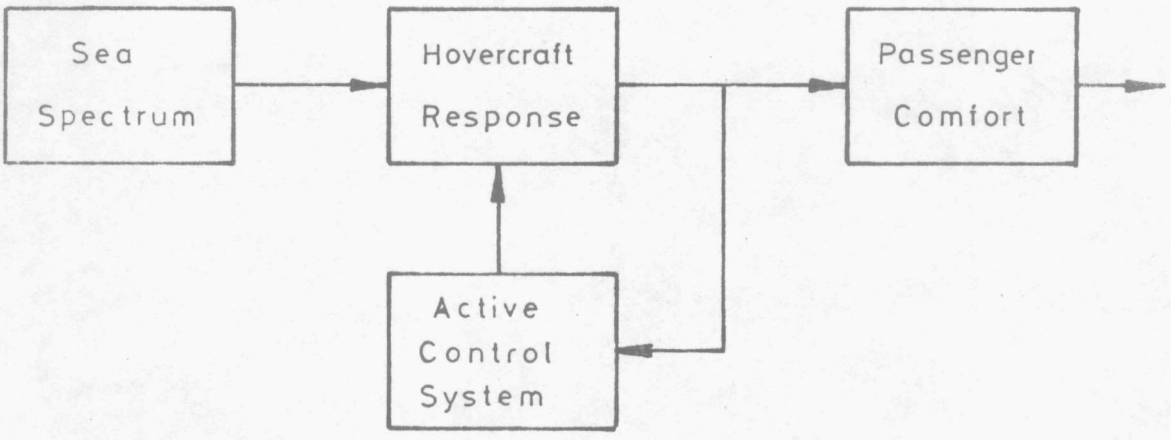

Fig. 9.2b Hovercraft ride control

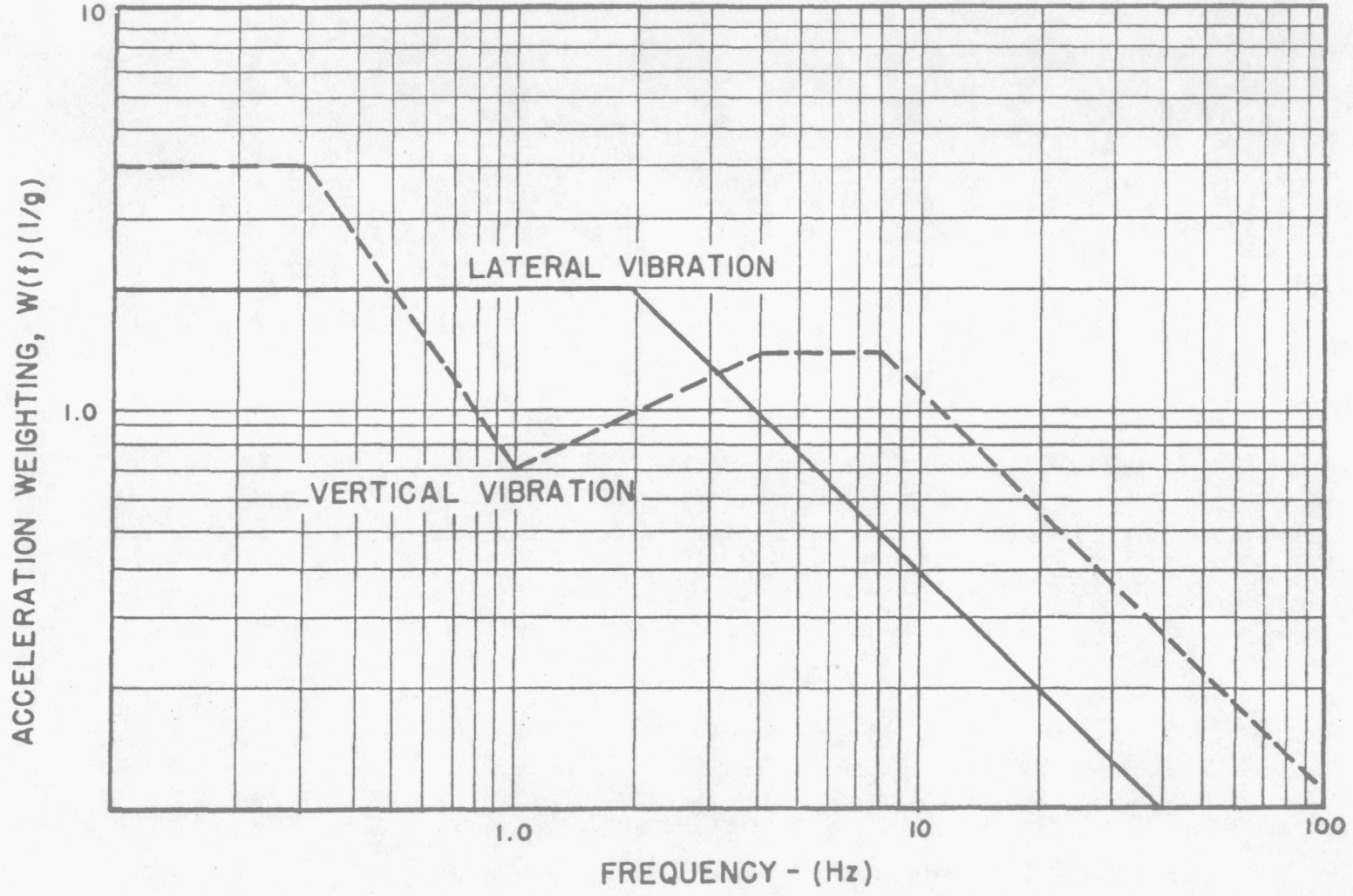

Fig. 9.3 Acceleration weighting function, ref.[82]

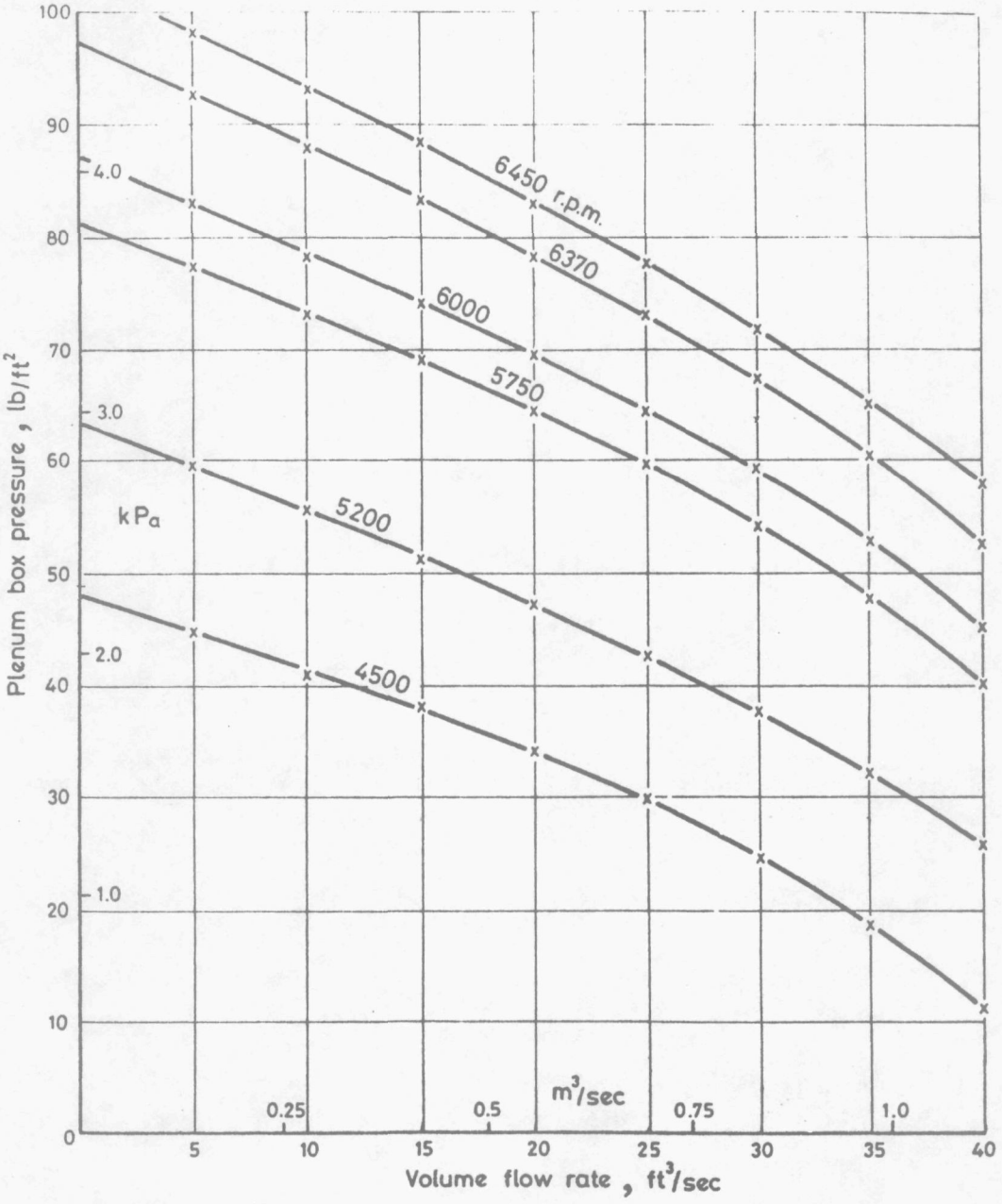

Fig. 9.4 Static fan characteristics of the Breeza axial fan fixed at 20° pitch , speed varied.

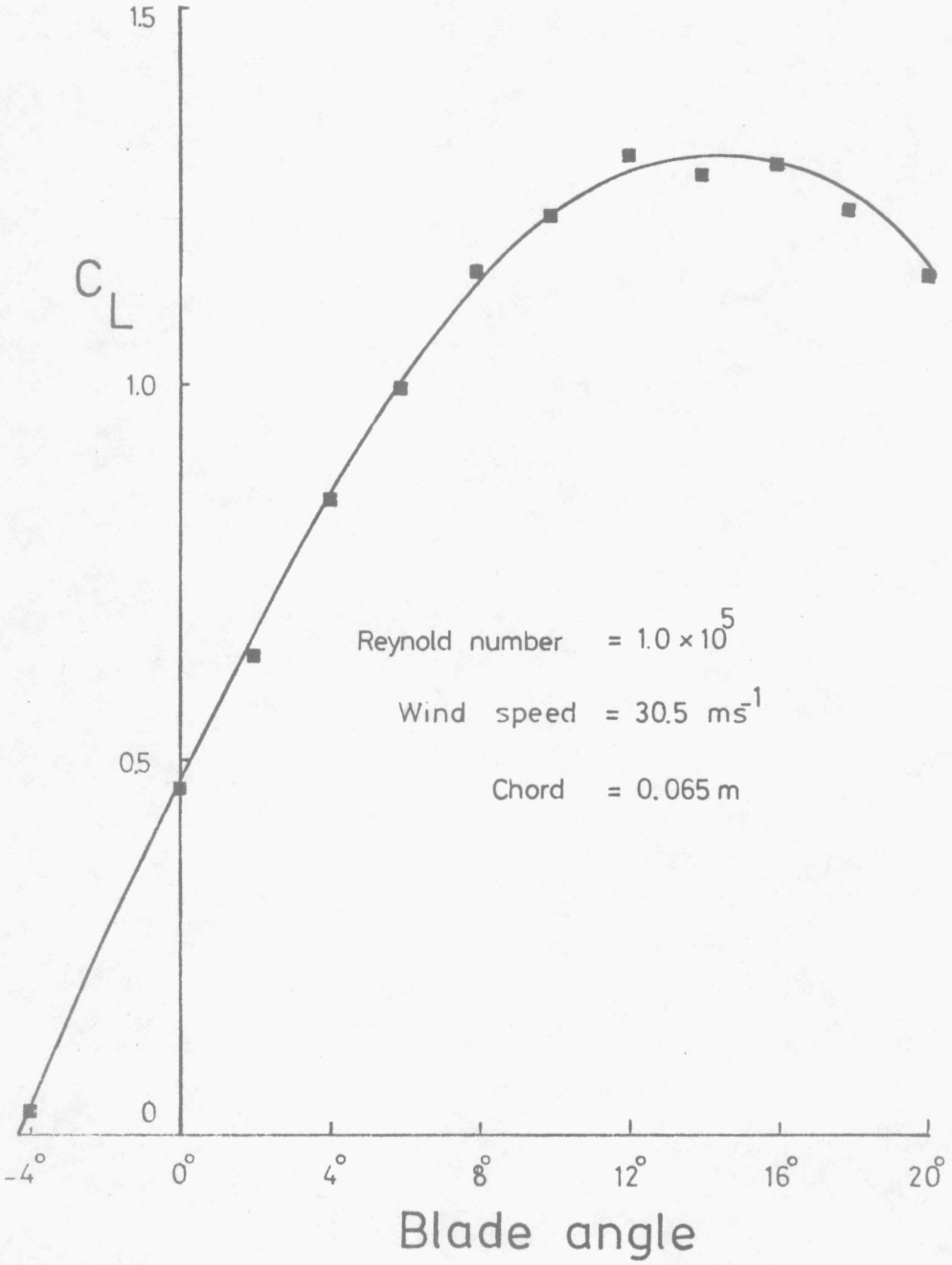

Fig. 9.5 Blade profile lift curve

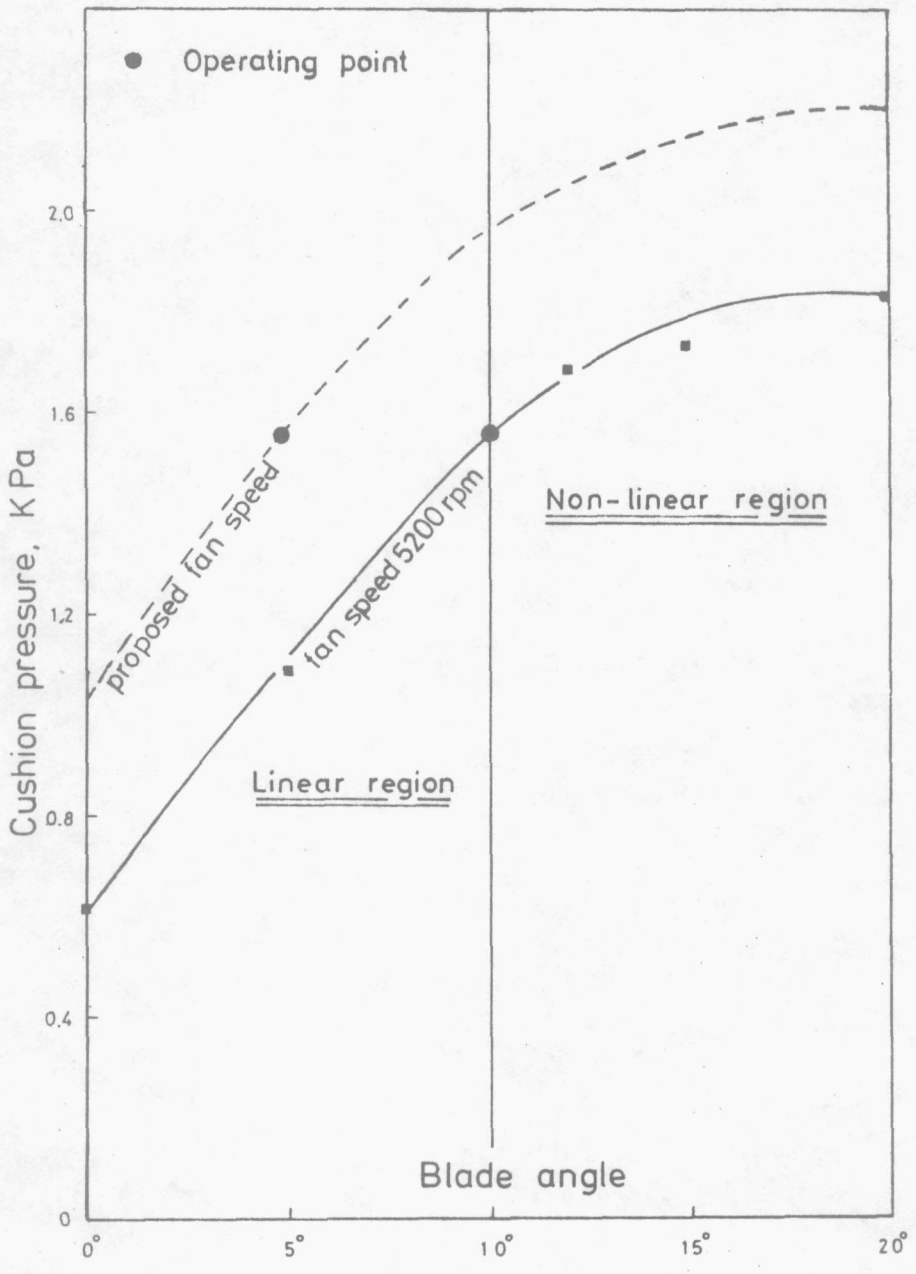

Fig. 9.6 Cushion pressure and blade angle characteristics